Signatures of Primordial Magnetic Fields from Phase Transitions

Dissertation zur Erlangung des Doktorgrades
an der Fakultät für Mathematik, Informatik und Naturwissenschaften
der Universität Hamburg

vorgelegt von

Peter Niksa

aus Gütersloh, Deutschland

Hamburg, 2019

Gutachter der Dissertation:

Prof. Dr. Günter Sigl

Prof. Dr. Robi Banerjee

Gutachter der Disputation:

Prof. Dr. Robi Banerjee

Prof. Dr. Thomas Konstandin

Prof. Dr. Jochen Liske

Prof. Dr. Géraldine Servant

Prof. Dr. Günter Sigl

Datum der Disputation: 10. 12. 2019

Vorsitzender des Prüfungsausschusses:

Prof. Dr. Jochen Liske

Vorsitzender des Promotionsausschusses:

Prof. Dr. Günter Sigl

Dekan der Fakultät für Mathematik,

Informatik und Naturwissenschaften:

Prof. Dr. Heinrich Graener

Wir müssen wissen.

Wir werden wissen.

David Hilbert, *Königsberg, 1930*

Zusammenfassung

Wir untersuchen die Entwicklung kausal erzeugter Magnetfelder, die während und nach einem kosmologischen Phasenübergang erster Ordnung erzeugt wurden, in der strahlungsdominierten Phase des Universums. Zusätzlich untersuchen wir das Gravitationswellensignal, das durch magnetohydrodynamische (MHD) Turbulenz generiert würde. Der Hauptfokus ist dabei ein elektroschwacher Phasenübergang erster Ordnung, da er das Problem der Baryogenese lösen könnte, von dunkler Materie ausgelöst sein könnte und primordiale Magnetfelder erzeugen kann, die als Quelle für die heutigen galaktischen und intergalak-tischen Magnetfelder dienen können.

Bei der Untersuchung des von MHD Turbulenz generierten Gravitationswellen (GW) Spektrum verbessern wir frühere Schätzungen des GW Spektrums, indem wir die Wahl der Dekorrelationsrate turbulenter Fluktuationen sinnvoll anpassen. Dabei finden wir, dass das GW Spektrum einen steileren Hochfrequenz-"Schwanz" hat als vorher vermutet und die Amplitude des Spektrums insgesamt um bis zu mehrere Größenordnungen reduziert wird. Insgesamt finden wir, dass das Spektrum einen f^3 Niederfrequenz-"Schwanz" und einen $f^{-8/3}$ bis $f^{-5/3}$ Hochfrequenz-"Schwanz" hat, wobei letzterer Fall nur bei sehr starken Phasenübergängen auftritt. Darüber hinaus zeigen wir, dass eine Ausrichtung des elektromagnetischen Vektorpotenzials mit dem Magnetfeld bei nahezu maximaler magnetischer Helizität zu einem flacheren niederfrequenten Heck mit f^2 führt. Weiterhin untersuchen wir den Einfluss von Wirbeln und Magnetfeldern auf das Gravitationswellenspektrum, welches von Schallwellen erzeugt wird, und stellen fest, dass jenes Signal ebenfalls teilweise stark reduziert wird, beispielsweise um eine Größenordnung.

Zusätzlich untersuchen wir die Entwicklung der MHD Turbulenz unter Anwendung der Eddy-Damped Quasi-Normal Markovian (EDQNM) Näherung und entwickeln einen Code zur Lösung der resultierenden Gleichungen für den Grenzfall eines inkompressiblen Plasmas. Von besonderem Interesse sind für uns MHD Kreuzkorrelationen, also relative Ausrichtungen zwischen Magnet- und Geschwindigkeits- (Kreuz-Helizität) bzw. dem Wirbelfeld (Kreuzskalar) und kinetischer Helizität (Ausrichtung von Geschwindigkeit- und Wirbelfeld), da diese in diesem Zusammenhang kaum studiert wurden. Im Rahmen der inkompressiblen MHD Turbulenz stellen wir fest, dass keine dieser drei Größen einen nachhaltigen Einfluss auf das heutige verbliebene primordiale MHD-Spektrums hat. Dennoch kann die Kreuzhelizität die Evolution vor der Neutrino-Entkopplung beeinflussen, da sie in dieser Phase zu einem Einfrieren der Turbulenz führen kann. Darüber hinaus argumentieren wir, dass die Kreuzhelizität im Rahmen kompressibler MHD Turbulenz sogar einen nachhaltigen Einfluss auf ein möglicherweise beobachtbares Magnetfeld und das damit verbundene GW Spektrum haben kann.

Abstract

We study the evolution of causally generated magnetic fields, by a cosmological first order phase transition, in the radiation dominated phase and essentially towards the present day. Additionally, we study the gravitational wave signal associated with primordial MHD turbulence. An electroweak first order phase transition is of particular interest as it could resolve the baryogenesis problem, may be driven by dark matter and can act seed sufficient primordial magnetic fields that may act as a source of the present day galactic and intergalactic magnetic fields.

Specifically, we investigate the gravitational wave (GW) spectrum sourced by magnetohydrodynamic (MHD) turbulence, during and after a phase transition, based on MHD scaling solutions. Therein we improve earlier estimates of the GW spectrum by adjusting the choice of the rate of decorrelation of turbulent fluctuations in a meaningful manner. This leads to an overall steeper high-frequency tail, compared to previous studies, in the GW spectrum and a severe reduction of the GW power spectrum by up to several orders of magnitudes depending on the basic properties of the turbulence with an f^3 low frequency tail and an $f^{-8/3}$ to $f^{-5/3}$ high frequency scaling, where the latter case appears in very strong phase transitions. Moreover, we show that a near maximal magnetic helicity, an alignment of the electromagnetic vector potential with the magnetic field, leads to a shallower f^2 low frequency tail. Furthermore, we investigate the impact of vorticity and magnetic fields on the gravitational wave spectrum produced by acoustic waves and find a significant reduction of the expected signal e.g. by an order of magnitude depending on the precise properties of the turbulence.

Next, we study the evolution of MHD turbulence primarily in the context of the eddy-damped quasi-normal Markovian (EDQNM) approximation and develop a code to solve the resulting equation in the incompressible limit. Of key interest to us are MHD cross correlations i.e. alignments between the magnetic field and velocity (cross helicity) or vorticity (cross scalar) and the kinetic helicity (alignment of velocity and vorticity), as these have received barely any attention in this context. In incompressible MHD turbulence we find that none of these three quantities leads to a lasting effect on the modern-day MHD spectrum. Nonetheless, the cross helicity can affect the evolution prior to neutrino decoupling, as it leads to a freeze-out of turbulence. Moreover, for compressible turbulence we anticipate and expect that cross helicity may even have a lasting influence on a potentially observable magnetic field and associated GW spectrum today. Lastly, even though kinetic helicity does not lead to an overall change in the evolution we find that it can produce a substantial magnetic helicity spectrum with a net zero total or integrated magnetic helicity, that never leads to an inverse cascade in contrast to MHD turbulence with a significant net total magnetic helicity.

List of Publications

This thesis is in part based on the following publication:

(Niksa et al. 2018) Peter Niksa, Martin Schlederer and Günter Sigl, *Gravitational waves produced by compressible MHD turbulence from cosmological phase transitions*, Classical and Quantum Gravity 35(14), 144001

Acronym	**Name**
GR	General Relativity
GW	Gravitational Wave
HD	Hydrodynamics
MHD	Magnetohydrodynamics
EMHD	Electro-Magnetohydrodynamics
UTC	Unequal Time Correlation
QN	Quasi-Normal
EDQNM	Eddy-Damped Quasi-Normal
EWPT	Electroweak Phase Transition
FOPT	First Order Phase Transition
CMB	Cosmic Microwave Background
QCD	Quantum Chromodynamics
BSM	Beyond the Standard Model
GUT	Grand Unified Theory
PTA	Pulsar Timing Array
DIA	Direct Interaction Approximation
ISM	Interstellar Medium
IGM	Intergalactic Medium
IGMF	Intergalactic Magnetic Field
AGN	Active Galactic Nuclei

Contents

1 Introduction **1**

2 Basics of GRMHD **7**

2.1 GREMHD equations 7

2.1.1 Stress energy tensors 8

2.1.2 Perturbative treatment 8

2.2 Gravitational Wave equation 10

2.3 MHD equations in an expanding universe 13

2.3.1 Maxwell equations in a flat expanding background 13

2.3.2 Dissipative stress energy tensor 15

2.3.3 Fluid equations in a flat expanding background 16

2.3.4 MHD equations 21

2.4 Basic magnetic and velocity field measures in GWMHD 23

2.4.1 Kinetic, magnetic and gravitational wave energy 23

2.4.2 Kinetic helicity 25

2.4.3 Cross helicity 26

2.4.4 Magnetic helicity 28

2.4.5 Cross scalar 29

3 MHD turbulence and GW **31**

3.1 Spectral correlation functions 31

3.1.1 Interdependencies 34

3.2 MHD turbulence 37
3.2.1 Incompressible MHD equations 39
3.2.2 Compressible MHD 43
3.3 Unequal Time Correlations 45
3.3.1 Random sweeping approximation 47
3.3.2 UTCs in MHD 51
3.3.3 Decorrelation due to forcing 53
3.3.4 Decorrelation of dilatational fluctuations 53
3.3.5 Summary of the different UTC functions 54
3.4 EDQNM approximation 55
3.4.1 Incompressible spectral two point evolution functions 56
3.4.2 Schematic of the EDQNM approximation 58
3.4.3 Incompressible MHD EDQNM equations 61
3.4.4 Large scale behavior of the EDQNM equations 64
3.4.5 Self-similar Evolution 67
3.4.6 Compressible contributions 70
3.4.7 Compressible Large Scale Behavior 76
3.5 Quasi-normal GW equation 78
3.5.1 Gravitational wave energy density 78
3.5.2 Scaling behavior of the MHD-GW-equation 82

4 Magnetogenesis and Dissipation in the Early Universe 87

4.1 Magnetogenesis 88
4.1.1 Cosmological Phase Transitions 91
4.1.2 MHD topology from a FOPT 96
4.2 Viscous and Resistive Damping in Radiation Dominated Universe 98
4.2.1 Viscous damping by neutrinos 99
4.2.2 Viscous damping by photons 100
4.2.3 Viscous damping above the electroweak scale 101
4.2.4 Resistive damping 102

4.2.5 Cosmological Reynolds numbers 103
4.3 Impacts of matter dominated phase on the Evolution of primordial magnetic fields 107
4.4 Constraints 108
4.4.1 Zeeman Effect 110
4.4.2 Faraday-Rotation 111
4.4.3 CMB 113
4.4.4 Gamma Rays 114
4.4.5 Potential future constraints 115

5 Evolution of primordial magnetic fields and associated gravitational waves 117
5.1 Solutions to the EDQNM equations 117
5.1.1 Reflectional-Symmetric MHD 118
5.1.2 Helical MHD 124
5.2 Solutions to the GW equation 132
5.2.1 Different Unequal Time Correlations 133
5.2.2 Parametric Dependence of GW spectrum 134
5.2.3 GWs from compressible MHD turbulence 137

6 Summary, Conclusions and Outlook 142
6.1 Summary 142
6.2 Conclusions and Outlook 146

A Supplement to EDQNM derivation 150
A.1 Example on Calculation of the EDQNM equations 150
A.2 Nonlinear compressible functions 152

B Numerical Treatment of EDQNM equations 155
B.1 Discretization and Symmetrization scheme 155
B.2 Time integration 159
B.3 Cleaning, hyper-viscosity and hyper-resistivity 160

C Assumptions in Solving the GWMHD equations **163**

Bibliography **165**

Acknowledgements **182**

List of Figures

3.1 Eddy Turnover Times . . . 52

4.1 Phase Transition Example . . . 92
4.2 Efficiency Parameter . . . 95
4.3 Reynolds Numbers . . . 105

5.1 Parity Invariant EDQNM Simulation S1 . . . 121
5.2 Parity Invariant EDQNM Simulation S2 and S3 . . . 122
5.3 Temporal Scaling of Parity Invariant EDQNM Simulations . . . 124
5.4 Helical EDQNM Simulation H2 . . . 127
5.5 Helical EDQNM Simulation H7 . . . 128
5.6 Helical EDQNM Simulation H5 . . . 129
5.7 Temporal Scaling in Parity Violating EDQNM Simulations . . . 130
5.8 Evolution of total magnetic and cross helicity . . . 131
5.9 GW spectrum from MHD turbulence (Higgsportal) . . . 133
5.10 Non-helical GW Scaling . . . 135
5.11 Helical GW Scaling . . . 136
5.12 GW from compressible MHD for $\Omega_{\rm tot} = 0.2$ . . . 139
5.13 GW from compressible MHD for $\Omega_{\rm tot} = 0.1$ . . . 141

1 Introduction

Magnetic fields are present in the universe, from magnetars with field strength of $B \sim 10^{15}$ G (Kaspi & Beloborodov 2017, e.g.) to planets, galaxies and even in intergalactic voids potentially with field strengths of up to $B \gtrsim 10^{-16}$ G (Neronov & Vovk 2010, Taylor et al. 2011). Curiosity drives us to explore the origin of these large scale magnetic fields and to try to learn as much as possible about the underlying processes to complement or even extend our overall understanding of fundamental processes in nature. There are two types of processes that may produce sufficiently strong void magnetic fields. On the one hand, magnetic fields may be sourced by astrophysical processes after recombination ($z \lesssim 1100$, $T \lesssim 0.3$ eV) e.g. by galaxies that amplify seed fields, which are produced by a battery mechanism (Biermann 1950). The amplification of those seed fields is supported by a dynamo mechanism in these galaxies (Kulsrud 1999*a*, Brandenburg & Subramanian 2005, e.g.). On the other hand, the magnetic fields may have a primordial origin (Turner & Widrow 1988, Vachaspati 1991). The latter class is of particular interest as it points to new physics. Also, a sufficient dynamo amplification of astrophysically sourced magnetic fields might be insufficient to explain sufficiently strong void magnetic fields (Furlanetto & Loeb 2001). Primordial magnetogenesis can also be split into two classes, a production related to first order phase transitions (Vachaspati 1991) and inflation (Starobinskiǐ 1979, Turner & Widrow 1988). Usually, two particular phase transitions are of interest, the QCD chiral and deconfinement transition at $T \sim 200$ MeV (Polyakov 1978, Susskind 1979) and the electroweak transition at $T \sim 100$ GeV (Kirzhnits & Linde 1976). Both the standard model electroweak (Buchmuller et al. 1994, Chatrchyan et al. 2012) and the

QCD transition (Stephanov 2004) are suspected to be either a second-order or cross-over transition. A strong magnetogenesis at a phase transition requires the transition to be a first order phase transition (FOPT). Consequently, magnetogenesis at a FOPT implies beyond the standard model (BSM) physics. In principle, BSM phase transitions at the GUT scale or e.g. dark sector phase transitions at $T \gtrsim$ TeV may exist and be of first order (Schwaller 2015, e.g.). Also, for sufficiently large neutrino chemical potentials the QCD phase transition may be of first order (Schwarz & Stuke 2009). Furthermore, for the electroweak phase transition there are many possible modifications of the standard model that can lead to a first order electroweak phase transition (Pietroni 1993, Espinosa et al. 2012, Caprini et al. 2016) that have not been ruled out and are compatible with constraints by present experiments (Arcadi et al. 2019, e.g.). A first order electroweak phase transition is particularly attractive as a solution to the baryogenesis problem, i.e. the appearance of more baryons than anti-baryons (Kuzmin et al. 1985, Morrissey & Ramsey-Musolf 2012). Inflationary scenarios may provide sufficiently strong magnetic fields, as long as the conformal symmetry is violated during inflation, otherwise only small scale magnetogenesis during inflation would be possible (Turner & Widrow 1988, Subramanian 2010). Magnetogenesis during a conformal symmetry breaking phase of inflation would differ significantly from magnetogenesis at e.g. the electroweak phase transition, since during such a phase of inflation magnetic fields may occur with seemingly acausal correlation lengths, which is not possible for thermal phase transitions. Unlike for the anticipated production of inflationary primordial density fluctuations, these magnetic fields are typically not scale / nearly-scale invariant (Subramanian 2010). Magnetic field spectra produced during inflation will have initially either a red or a blue-tilted spectrum, depending on the mechanism.

Here, we will focus mostly on causal primordial magnetic fields sourced around the electroweak scale by a first order electroweak phase transition (EWPT) (Vachaspati 1991, Kamionkowski et al. 1994, Sigl et al. 1997). Typically for most scenarios of interest, these magnetic fields will be turbulent and the magnetic energy cascades towards smaller scales (Brandenburg et al. 1996, Jedamzik & Sigl 2011, Saveliev et al. 2012).

The transport to smaller scales leads to a loss of magnetic and kinetic energy that is primarily due to viscous damping and hence a production of heat, which quickly thermalizes at very high redshifts $z \gtrsim 10^6$ ($T \gtrsim$ keV) (Chluba & Sunyaev 2012). This type of turbulence is also known as magneto-hydro-dynamic (MHD) turbulence. In a barotropic plasma, i.e. a plasma for which the pressure is only a function of the density $p = p(\rho)$, in which no dissipative effects are present, like resistive and viscous damping, the total kinetic and magnetic energy, as well as the so-called magnetic helicity, i.e. the alignment of the magnetic field with its vector potential, and the cross helicity, i.e. the alignment between the plasma velocity and the magnetic field, are conserved (Biskamp 1993). Of particular interest is a non-vanishing magnetic helicity as its conservation leads to a transfer of magnetic energy from smaller to larger scales, a so-called inverse cascade (Frisch et al. 1975, Meneguzzi et al. 1981, Cornwall 1997, Saveliev et al. 2013). It is generally believed that magnetogenesis at the electroweak scale requires substantial helical magnetic fields in order to explain the potentially present void magnetic fields with $B \gtrsim 10^{-16}$ G (Wagstaff & Banerjee 2016). In the radiation dominated universe turbulence can be possible prior to the decoupling of neutrinos and afterwards and prior to photon decoupling. Any causally generated kinetic perturbation sourced prior to neutrino decoupling should have decayed after neutrino decoupling and one expects that the only type of sub-horizon perturbation that may survive neutrino decoupling are magnetic fields with or without magnetic helicity. Therefore, most studies focus on the impact of the magnetic fields with or without magnetic helicity. However, recent simulations find that an inverse transfer without magnetic helicity is possible (Kahniashvili et al. 2013, Brandenburg et al. 2015, Brandenburg & Kahniashvili 2017), which increases the interest in the study of other factors. Particularly, prior to neutrino decoupling cross-alignments like an alignment between the vorticity and the magnetic field and the cross helicity, as well as any initial kinetic helicity may affect the evolution of the magnetic field. Here, we look at the impact of kinetic, magnetic and cross helicity and the cross scalar on the evolution of primordial MHD turbulence. Furthermore, we study the evolution of magnetic fields using a semi-analytical equation to calculate the evolution of spectral correlation function that describe the evolution of primordial magnetic fields, similarly to previous calculations of incompressible (solenoidal velocity field $\nabla \cdot \mathbf{v} = 0$) MHD turbulence without (Saveliev et al. 2012) and with magnetic helicity (Saveliev et al. 2013, Saveliev 2014). In contrast to these calculations, we self-consistently treat the assumption of incompressibility, account for viscous and resistive effects in the early universe and include the kinetic and cross helicity and the cross scalar. Additionally, we discuss compressible effects and show how these have to be included in the subsonic limit, but we do not include compressible effects when studying the evolution of primordial magnetic fields in the present computations, which represents one of the major drawbacks of the present study.

Recently, the first detection of gravitational waves in 2015 (Abbott et al. 2016) opened another exciting and promising new window beyond cosmic rays, neutrinos and photons to study the universe. Gravitational waves from the early universe could be detected in the future and open up another avenue to observe as of yet unobservable but potentially existing processes in the early universe, e.g. first order phase transitions or inflation (Starobinskiǐ 1979, Witten 1984, Hogan 1986, Kamionkowski et al. 1994, Huber & Konstandin 2008, Caprini & Figueroa 2018). Here of particular interest are gravitational waves that are sourced by potential electroweak phase transitions that can also provide substantial seed magnetic fields. In these thermal phase transition the most important source of gravitational waves is compressible MHD turbulence, i.e. sound-waves (Hindmarsh et al. 2014, Hindmarsh et al. 2015), vorticity (Kamionkowski et al. 1994, Kosowsky et al. 2002) and magnetic fields (Caprini & Durrer 2002, Caprini et al. 2009). The electroweak phase or TeV phase transitions are of particular interest as future space-based gravitational wave observatories like the planned detector LISA (Caprini et al. 2016, Amaro-Seoane et al. 2017) are able to observe the relevant frequency range 10^{-4} to 10^{-1} Hz. In principle, a QCD phase transition can produce signatures that may be observable by pulsar timing arrays (PTAs) (Caprini et al. 2010), yet even if these exist they may be obscured by the expected, but still unobserved, gravitational wave background produced by supermassive black hole inspirals (Sesana 2013, Bonetti et al. 2018). Here we discuss the production of gravitational waves during and after a phase transition due to compressible MHD turbulence, particularly by looking at incompressible MHD turbulence with and without magnetic helicity and compressible hydrodynamic turbulence (for simplicity) in a simplified picture (Niksa et al. 2018). One key factor of importance in studying the generation of gravitational waves from velocity and magnetic fields are the turbulent unequal time correlation (UTC) functions (Caprini et al. 2009), i.e. different ansatze for the decorrelation function lead to vastly different gravitational wave spectra. In turbulence, there are two critical time scales, for once the Eulerian eddy turnover time, which dictates the rate of decorrelation of Eulerian fluctuations, and the Lagrangian eddy turnover time, that dictates the rate of energy transfer and the decorrelation rate for Lagrangian fluctuations, i.e. from the perspective of individual particle trajectories. The Lagrangian eddy turnover time is generally more well known, as it allows us to understand the energy transfer of equal time correlations of velocity and magnetic field fluctuations. It has also been unknowingly ill-applied in the treatment of the rate of decorrelation of MHD turbulence in studies regarding the generation of gravitational waves from turbulence (e.g. Kosowsky et al. 2002, Caprini & Durrer 2006, Kahniashvili, Campanelli, Gogoberidze, Maravin & Ratra 2008*a*, Kahniashvili, Gogoberidze & Ratra 2008). Therefore, here we look at the differences between the different choices of the timescale for the unequal time correlation function.

The thesis is structured in the following manner. In the next chapter titled Basics of GRMHD, chapter 2, we discuss the basic equations that allow us to study MHD turbulence and the generation of gravitational waves by MHD, and we introduce several key quantities of MHD, the kinetic, magnetic and cross helicity and the cross scalar. Next, in chapter 3, titled MHD turbulence and GW, we discuss the stochastic quantities that are the key focus of this study, we discuss the basic equations that govern MHD turbulence and the defining properties of turbulence. In that chapter, we also discuss the unequal time correlations, the eddy damped quasi normal equations that forms the basis of our discussion on the evolution of the primordial MHD turbulence and the generation of a stochastic gravitational wave background by MHD turbulence. Thereafter, in chapter 4 we briefly discuss how magnetic fields can appear and be amplified during a phase transition, we also discuss viscous and resistive dissipation of kinetic and magnetic fluctuations in the radiation dominated phase. Additionally, we briefly discuss the evolution of primordial MHD turbulence in the matter dominated phase, and present constraints on large scale magnetic fields. In the penultimate chapter, chapter 5 we discuss the evolution of the MHD equations and the solution of the GW equation for different initial conditions. Finally in chapter 6 we summarize and discuss our findings and results. Throughout, this thesis we use natural Gauss units i.e. $c = \hbar = k_B = 1$.

2 | Basics of GRMHD

Here, we begin by reviewing magnetohydrodynamics in a weakly curved space-time (GRMHD). First we start with an overview of the relevant equation governing electromagnetic fields in a plasma with perturbative deviations from a flat space-time.

2.1 GREMHD equations

A general relativistic electro-magnetic hydro-dynamic (GREMHD) system is described by the Einstein equation

$$R_{\mu\nu} = 8\pi G \left(T_{\mathrm{tot},\mu\nu} - \frac{1}{2} g_{\mu\nu} T_{\mathrm{tot}} \right) , \tag{2.1}$$

where G is Newton's gravitational constant, $R_{\mu\nu}$ is the Ricci tensor, $T_{\mathrm{tot},\mu\nu}$ is the total stress energy tensor, while $T_{\mathrm{tot}} = g_{\mu\nu} T^{\mu\nu}_{\mathrm{tot}}$ is the trace of the total energy momentum tensor, which contains electromagnetic and the gas/ fluid component. For the metric signature convention we use $(-, +, +, +)$. The total stress energy tensor is given by

$$T^{\mu\nu}_{\mathrm{tot}} = T^{\mu\nu}_{\mathrm{kin}} + T^{\mu\nu}_{\mathrm{em}}, \tag{2.2}$$

where the subscript kin stands for kinetic and em for electromagnetic. The relevant equations of motion are then given by

$$\nabla_\mu T^{\mu\nu}_{\mathrm{tot}} = 0 \tag{2.3}$$

Then, the evolution of the magnetic field is governed by Maxwell's equations, where the derivatives are replaced by their covariant counterparts

$$\nabla_\mu F^{\mu\nu} = 0 \tag{2.4}$$

and

$$\epsilon_{\alpha\beta\nu\mu} \nabla^\beta F^{\mu\nu} = \mu_0 J_\alpha, \tag{2.5}$$

where $F^{\mu\nu}$ is the electromagnetic field strength tensor and J_α is the electromagnetic 4 current density and $\mu_0 = 4\pi$. In this section, we follow mostly the approach by e.g. (Ellis 1973, Brandenburg et al. 1996, Banerjee & Jedamzik 2004, Durrer & Neronov 2013, Subramanian 2016, Weinberg 2008).

2.1.1 Stress energy tensors

We model the fluid as a perfect fluid given by the stress energy tensor

$$T^{\mu\nu}_{\mathrm{kin}} = (\rho + p)\, u^\mu u^\nu + p g^{\mu\nu}, \tag{2.6}$$

where ρ is the energy density of the fluid, p is its pressure, u^μ is the four velocity of the flow. In the presence of electromagnetic fields one also needs to take the electromagnetic stress energy tensor into account

$$T^{\mu\nu}_{\mathrm{em}} = \frac{1}{\mu_0} \left(F^{\mu\alpha} g_{\alpha\beta} F^{\nu\beta} - \frac{1}{4} g^{\mu\nu} F_{\gamma\delta} F^{\delta\gamma} \right), \tag{2.7}$$

where $F^{\mu\nu}$ is the electromagnetic field strength tensor.

2.1.2 Perturbative treatment

In the following we will split the metric into a background and perturbative component $g_{\mu\nu} = g^b_{\mu\nu} + h_{\mu\nu}$, where $q_{\mu\nu}$ is the Friedmann-Robertson-Walker metric

$$g^b_{\mu\nu} = a^2 \mathrm{diag}\,(-1, 1, 1, 1)\,, \tag{2.8}$$

where a is the scale factor and $h_{\mu\nu}$ is the perturbation. Also, up to first order in h, one has $g^{\mu\nu} = g_b^{\mu\nu} - h^{\mu\nu}$, since $g^{\mu\alpha} g_{\alpha\nu} = \delta^\mu_\nu$. Here, the zeroth component corresponds to the conformal time τ given by dτ=dt/a, where t is the physical time. Similarly, the four velocity is split as $u_\mu = u_\mu^b + u_\mu^h$, where the superscript again b denotes the background value and the superscript h denotes the perturbation. For an observer at rest with respect to the expanding background, we have $u_\mu^b = (-a, \mathbf{0})$ and we set $u_0^h = -h_{00}/(2a^2)$ at first order in h. Similarly, the kinetic stress energy tensor can be split into a background

$$T_{\mu\nu}^{\mathrm{kin},b} = \left(\rho^b + p^b\right) a^2 \delta_\mu^0 \delta_\nu^0 + p^b g_{\mu\nu}^b \tag{2.9}$$

and a perturbative component

$$T_{\mu\nu}^{\mathrm{kin},h} = \left(\rho^h + p^h\right) u_\mu^b u_\nu^b + p^h g_{\mu\nu}^b + \left(\rho^b + p^b\right) \left(u_\mu^h u_\nu^b + u_\mu^b u_\nu^h\right) + \left(\rho^b + p^b\right) u_\mu^h u_\nu^h + p^b h_{\mu\nu}, \tag{2.10}$$

where we also take into account seemingly second order terms like $u_\mu^h u_\nu^h$, as these are of the same order as the perturbation of the energy itself. Note that δ_μ^ν is the Kronecker delta symbol, which is 1 for $\mu = \nu$ and 0 otherwise. Moreover, we neglect a background electromagnetic field strength tensor and take only a perturbative electromagnetic field strength tensor given by

$$T_{\mu\nu}^{\mathrm{em},h} = \frac{1}{\mu_0} \left(F_{\mu\alpha} g_b^{\alpha\beta} F_{\nu\beta} - \frac{1}{4} g_{\mu\nu}^b F_{\gamma\delta} F^{\delta\gamma} \right) \tag{2.11}$$

into account. When solving for the evolution of the electromagnetic fields and the change in thermal and kinetic energy, we neglect the impact of the metric perturbation, as it is a higher order term. Here, we are only interest in the production of metric perturbations from kinetic and magnetic perturbations, as it is in general an observable of interest in itself.

2.2 Gravitational Wave equation

First, we discuss the appearance of metric perturbations due to perturbations in the stress energy tensor. The Ricci-tensor is given as

$$R_{\mu\nu} = \Gamma^{\lambda}_{\mu\nu,\lambda} - \Gamma^{\lambda}_{\mu\lambda,\nu} + \Gamma^{\delta}_{\mu\nu}\Gamma^{\lambda}_{\lambda\delta} - \Gamma^{\delta}_{\mu\lambda}\Gamma^{\lambda}_{\nu\delta}, \tag{2.12}$$

where $\Gamma^{\lambda}_{\mu\nu}$ are the Christoffel symbols given by

$$\Gamma^{\lambda}_{\mu\nu} = \frac{1}{2} g^{\lambda\delta} \left(g_{\delta\nu,\mu} + g_{\mu\delta,\nu} - g_{\mu\nu,\delta} \right), \tag{2.13}$$

where $X_{,\alpha} = \partial_\alpha X$. Here, we only require the Ricci-tensor at order $\mathcal{O}(h)$ denoted as $R^h_{\mu\nu}$. The evolution of the background is governed by the Friedmann equations for a flat space, which is the solution of the Einstein equation for a perfect fluid at rest with respect to the background expansion and with purely time-dependent density. Then, the Einstein equations read

$$R^h_{00} = \frac{\mathcal{H}}{a^2}\left[\frac{3}{2}h_{kk,0} - \frac{3}{2}h_{00,0} + 3\mathcal{H}h_{00} - h_{kk,k}\right] + \left[2h_{0k,k0} - h_{00,kk} - h_{kk,00}\right] + h_{kk}\left(\frac{a_{,00}}{a^3} - \frac{\mathcal{H}^2}{a^2}\right) \tag{2.14}$$

$$R^h_{0i} = \frac{\mathcal{H}}{a^2}\left[h_{kk,i} - h_{00,i} - h_{ki,k}\right] + \left[h_{ik,k0} + h_{k0,ik} - h_{kk,i0} - h_{i0,kk}\right] + h_{i0}\left(\frac{a_{,00}}{a^3} + 2\frac{\mathcal{H}^2}{a^2}\right) \tag{2.15}$$

$$\begin{aligned} R_{ij} =& \delta_{ij}\left[\frac{1}{2}\frac{\mathcal{H}}{a^2}\left(h_{00,0} - 2h_{k0,k}\right) + h_{00}\left(\frac{a_{,00}}{a^3} - \frac{\mathcal{H}^2}{a^2}\right) - \frac{\mathcal{H}^2}{a^2}h_{kk}\right] + \frac{\mathcal{H}}{a^2}\left[h_{i0,j} - h_{0j,i} - h_{ij,0}\right] \\ &+ 2\frac{\mathcal{H}^2}{a^2}h_{ij} + \frac{1}{2a^2}\left[h_{ik,jk} + h_{jk,ik} - h_{ij,kk} - h_{i0,j0} - h_{j0,i0} + h_{ij,00} + h_{00,ij} - h_{kk,ij}\right] \end{aligned} \tag{2.16}$$

where $\mathcal{H} = a_{,0}/a$ is the conformal Hubble parameter and the indices i and j can have the values $1, 2, 3$, while the index is summed over the values $k = 1, 2, 3$. In the following it is useful to split the curvature perturbation as follows

$$h_{00} = -A \tag{2.17}$$

$$h_{0i} = B_i + C_{,i} \tag{2.18}$$

$$h_{ij} = \delta_{ij} D + E_{i,j} + E_{j,i} + F_{,ij} + H_{ij}, \tag{2.19}$$

where A, C, D, G are scalars, B, E, F are vectors and H is the only non-reducible two dimensional tensor. These quantities are chosen to fulfill the following conditions $E_{i,i} = B_{i,i} = H_{ij,i} = H_{ii} = 0$. In particular of interest is (2.16) and the terms involving H_{ij}

$$R^H_{ij} = -\frac{1}{2a^2}\left[H_{ij,00} - H_{ij,kk}\right] - \frac{\mathcal{H}}{a^2} H_{ij,0} + 2\frac{\mathcal{H}^2}{a^2} H_{ij}. \tag{2.20}$$

Thus the left side of the Einstein equation for pure perturbative tensor modes is a simple wave equation. The tensor R^H_{ij} can be derived from R_{ij} by the transformation

$$R^H_{ij} = P_{ijlm}(\nabla) R_{ij}, \tag{2.21}$$

where

$$P_{ijlm}(\nabla) = P_{il}(\nabla) P_{jm}(\nabla) - \frac{1}{2} P_{ij}(\nabla) P_{lm}(\nabla) \tag{2.22}$$

is a projection operator and

$$P_{ij}(\nabla) = \delta_{ij} - D_{ij}(\nabla) = \delta_{ij} - \frac{\partial_i \partial_j}{\nabla^2}. \tag{2.23}$$

is the solenoidal projection operator, while D_{ij} is the dilatational projection operator. The spatial Fourier transformation of (2.20) is

$$R^H_{ij}(\mathbf{k}) = \frac{1}{2a^2}\Big[H_{ij,00}(\mathbf{k}) + k^2 H_{ij}(\mathbf{k})\Big] - \frac{\mathcal{H}}{a^2} H_{ij,0}(\mathbf{k}) + 2\frac{\mathcal{H}^2}{a^2} H_{ij}(\mathbf{k}). \tag{2.24}$$

Furthermore, the Fourier transform of the projection operator P_{ij} is

$$P_{ij}(\mathbf{k}) = \delta_{ij} - D_{ij}(\mathbf{k}) = \delta_{ij} - \frac{k_i k_j}{k^2}. \tag{2.25}$$

Moreover, the right hand side of(2.1), i.e. the stress energy contribution, also involves terms which are directly proportional to H_{ij}, due to the appearance of a background density and pressure term, while this is not the case for the electromagnetic component as we do not consider background fields. The right hand side of the Einstein equation at first order in the perturbation for the off-diagonal spatial components ($i \neq j$) reads

$$8\pi G\left(T^h_{ij} - g^b_{ij}T^h - h_{ij}T^b\right) = 8\pi G\left(p_b h_{ij} + (\rho^b + p^b)u^h_i u^h_j - \frac{h_{ij}}{2}\left(3p^b - \rho^b\right)\right), \quad (2.26)$$

where we have neglected the electromagnetic component. Using the Friedmann equations

$$\mathcal{H}^2 = \frac{8\pi G}{3}a^2\rho^b \quad (2.27)$$

$$\frac{a_{,00}}{a} = \frac{4\pi G}{3}a^2\left(\rho^b - 3p^b\right) \quad (2.28)$$

one finds

$$\frac{1}{2a^2}\left[H_{ij,00} + k^2 H_{ij}\right] - \frac{\mathcal{H}}{a^2}H_{ij,0} + \left(\frac{\mathcal{H}^2}{a^2} - \frac{a_{,00}}{a}\right)H_{ij} = 8\pi G a^2\left(\rho^b + p^b\right)P_{ijlm}\pi_{lm}, \quad (2.29)$$

where

$$\pi_{lm}(\mathbf{k}) = \int \frac{\mathrm{d}^3\mathbf{q}}{(2\pi)^3}\, u^h_l(\mathbf{p})u^h_m(\mathbf{q}), \quad (2.30)$$

with $\mathbf{p} = \mathbf{k} - \mathbf{q}$. Lastly, we introduce the conformal strain tensor $H_{ij} = a^2\tilde{H}_{ij}$ and include the magnetic contributions to find

$$\tilde{H}_{ij,00}(\mathbf{k},\tau) + 2\mathcal{H}\tilde{H}_{ij,0}(\mathbf{k},\tau) + k^2\tilde{H}_{ij}(\mathbf{k},\tau) = 16\pi G a^2\left(\rho^b + p^b\right)P_{ijlm}\left[\pi_{lm}(\mathbf{k}) + \pi^{\mathrm{em}}_{lm}(\mathbf{k})\right], \quad (2.31)$$

where

$$\pi^{\mathrm{em}}_{lm}(\mathbf{k}) = \frac{1}{\mu_0 a^2(\rho^b + p^b)}\int \frac{\mathrm{d}^3\mathbf{q}}{(2\pi)^3}\, F_{ln}(\mathbf{p})F_{mn}(\mathbf{q}). \quad (2.32)$$

The resulting wave equation then describes the evolution of the conformal strain tensor. In the following we take a look at the relevant evolution equation for the magnetic and kinetic contributions.

2.3 MHD equations in an expanding universe

Here, we describe and discuss the basic equations governing the evolution of magnetic fields and fluid turbulence in an expanding universe, while we neglect the impact of back-reaction from metric perturbations seeded by the MHD flow and the impact of metric perturbations on the flow in general. In particular, gravitational potential fluctuations can be neglected as the pressure generally dominates on all scales below the sound-horizon $d_s \sim d_H$ and we assume that density perturbations $\delta \ll 1$ can be treated as sound waves in the radiation dominated phase without any relevant growing modes. Also, we will discuss interactions between sound waves and solenoidal fluctuations only in superficial detail without performing numerical simulations. We primarily focus on the radiation dominated universe and only comment on the evolution after matter-radiation equality without a numerical study. First, we look at the Maxwell equations for an expanding universe, then we look at the dissipative stress energy tensor and afterwards at the fluid equations.

2.3.1 Maxwell equations in a flat expanding background

In order to study the Maxwell equations we use the field strength tensor in the following form

$$F_{\mu\nu} = w_\mu \bar{E}_\nu - w_\nu \bar{E}_\mu + \epsilon_{\mu\nu\alpha\beta} \bar{B}^\alpha w^\beta, \tag{2.33}$$

where $\bar{E}_\mu$ and $\bar{B}_\mu$ are generalized four vectors of the magnetic and electric fields with

$$\bar{E}_\mu = F_{\mu\nu} w^\nu, \quad \bar{B}_\mu = \frac{1}{2} \epsilon_{\mu\nu\rho\lambda} w^\nu F^{\rho\lambda}, \tag{2.34}$$

while $\epsilon_{\mu\nu\rho\lambda} = \frac{E_{\mu\nu\rho\lambda}}{\sqrt{-g}}$ with $E_{\mu\nu\rho\lambda}$ being the fully antisymmetric symbol with $E_{0123} = -a^8$ and g is the metric determinant. The vector w^ν denotes a specific observer. Here, we choose an observer with $w^\mu = (a^{-1}, \mathbf{0})$. As shown before, (2.4) and (2.5) together with

(2.33) govern the evolution of electromagnetic fields. Note, that the four magnetic and electric fields do not directly correspond to the conventional electric and magnetic fields. However, these are found by evaluating the fields in the basis of a fundamental observer with basis e^{μ}_{ν}

$$g_{\mu\nu} e^{\mu}_{(a)} e^{\nu}_{(b)} = \eta_{ab}, \quad \eta^{ab} e^{\mu}_{(a)} e^{\nu}_{(b)} = g^{\mu\nu}, \tag{2.35}$$

where $\eta = \mathrm{diag}(-1, 1, 1, 1)$ is the Minkoswski metric. Thus, one finds $e^{\mu}_{(\nu)} = a^{-1}\delta^{\mu}_{(\nu)}$. Then, along such a fundamental observer the magnetic and electric fields are given by

$$B^i = e^{(i)}_{\mu} \bar{B}^{\mu} = a\bar{B}^i, \quad E^i = e^{(i)}_{\mu} \bar{E}^{\mu} = a\bar{E}^i. \tag{2.36}$$

Analogously, the charge density is $\rho_c = -J^{\mu} w_{\mu}$ and the current density is $j_i = J_{\mu} e^{\mu}_{(i)}$ The generalized Maxwell equations (2.4) and (2.5) in the fundamental frame of reference read

$$\nabla \cdot \mathbf{B} = 0, \tag{2.37}$$

$$\nabla \cdot \mathbf{E} = 4\pi a \rho_c, \tag{2.38}$$

$$\nabla \times \mathbf{E} = -\, 2\mathcal{H}\mathbf{B} - \partial_{\tau}\mathbf{B}, \tag{2.39}$$

$$\nabla \times \mathbf{B} = 4\pi a \mathbf{j} + 2\mathcal{H}\mathbf{E} + \partial_{\tau}\mathbf{E}, \tag{2.40}$$

where ρ_c is the electric charge density. For convenience, it is useful to express these quantities by their comoving counterparts. Therefore, we introduce the following transformation

$$\tilde{\mathbf{B}} = a^2\mathbf{B}, \quad \tilde{\mathbf{E}} = a^2\mathbf{E}, \quad \tilde{\mathbf{j}} = a^3\mathbf{j}, \quad \tilde{\rho}_c = a^3\rho_c. \tag{2.41}$$

The comoving and conformal Maxwell equation for an expanding space are then the same as for flat non-expanding background

$$\nabla \cdot \tilde{\mathbf{B}} = 0, \tag{2.42}$$

$$\nabla \cdot \tilde{\mathbf{E}} = 4\pi \tilde{\rho}_c, \tag{2.43}$$

$$\nabla \times \tilde{\mathbf{E}} = -\partial_\tau \tilde{\mathbf{B}}, \tag{2.44}$$

$$\nabla \times \tilde{\mathbf{B}} = 4\pi \tilde{\mathbf{j}} + \partial_\tau \tilde{\mathbf{E}}. \tag{2.45}$$

Moreover, we require Ohm's law which in the non-relativistic limit $v \ll 1$ reads

$$\tilde{\mathbf{j}} = \tilde{\rho}_c \mathbf{v} + \tilde{\sigma} \left(\tilde{\mathbf{E}} + \mathbf{v} \times \tilde{\mathbf{B}} \right), \tag{2.46}$$

where $\tilde{\sigma} = a\sigma$ with σ being the electric conductivity of the fluid. Note, that the physical peculiar velocities $\mathbf{v}$ are the same as the comoving peculiar velocities. In the following, we apply the MHD approximation, which is reasonable for non-relativistic flows, and it allows to neglect the displacement current $\partial_\tau \tilde{\mathbf{E}}$. Thus, we have

$$\nabla \times \tilde{\mathbf{B}} = 4\pi \tilde{\mathbf{j}}. \tag{2.47}$$

Also, it follows from Ohm's law that

$$\tilde{\mathbf{E}} = \frac{1}{\tilde{\sigma}} \tilde{\mathbf{j}} - \frac{\tilde{\rho}_c}{\tilde{\sigma}} \mathbf{v} - \mathbf{v} \times \tilde{\mathbf{B}}. \tag{2.48}$$

Next we look at the dissipative stress energy tensor.

2.3.2 Dissipative stress energy tensor

In the presence of viscous forces one needs to add additionally contributions to the stress energy tensor, which model the viscous decay i.e. the production of thermal energy by the decay of ordered kinetic flow. Hence we introduce the following dissipative stress tensor (Weinberg 2008)

$$T^{\alpha\beta}_{\rm vis} = -\left(\rho + p\right)\nu A^{\alpha\gamma} A^{\beta\delta} W_{\gamma\delta}, \tag{2.49}$$

where we have neglected heat conduction and bulk viscosity, while ν is the kinematic shear viscosity, and

$$A^{\alpha\beta} = g^{\alpha\beta} + u^\alpha u^\beta, \quad W_{\alpha\beta} = u_{\alpha;\beta} + u_{\beta;\alpha} - \frac{2}{3} g_{\alpha\beta} u^{\gamma}_{;\gamma}, \tag{2.50}$$

where the subscript ";" denotes a covariant derivative. Note that the above expression for the viscous stress tensor is a simple generalization of the flat space stress tensor presented in (Weinberg 2008). However, the presented viscosity tensor can lead to acausal behavior for relativistic flows. A proper description of a relativistic viscous fluid in curved space time requires a first principle calculation of a viscous stress tensor rather than a simple Lorentz-invariant traceless extension of non-relativistic results. Since, we are primarily working in the non-relativistic bulk flow limit and with comparably weak magnetic fields, we do not anticipate that different or more complicated dissipation stress tensors will change our results in any manner, even if the fluid itself is relativistic.

Together with the dissipation stress tensor the equations of motion of the fluid are given by

$$\nabla_\mu T^{\mu\nu}_{\rm tot} = \nabla_\mu \left(T^{\mu\nu}_{\rm kin} + T^{\mu\nu}_{\rm em} + T^{\mu\nu}_{\rm vis}\right) = 0, \tag{2.51}$$

where ∇_μ is the covariant derivative. Note that the dissipative stress energy technically also appears in the gravitational wave equation, yet we neglect it here, as the scales at the time scales of interest to us are not relevant for this discussion. Next, we look at the fluid equations.

2.3.3 Fluid equations in a flat expanding background

Now, we look at the fluid equations governing the evolution of a fluid. The fluid approximation is generally useful for systems, where the mean free path of the particles constituting the fluid is smaller than the scales of interest $\lambda_{\mathrm{mfp}} \ll L$ and the particles constituting the fluid are tightly coupled. In the context of the fluid equations, the evolution of the fluid is governed by (2.51). As we later discuss in full, there are several phases where the fluid approximation can technically not be applied, these are phases where some component of the fluid begins to decouple or has decoupled. In particular in the context of the radiation dominated phase, the density ρ as discussed here only constitutes of the tightly coupled relativistic component i.e. neutrinos do not contribute to the relativistic energy component as defined here after neutrino decoupling. Moreover, here we only discuss the fluid equations for the radiation dominated phase, where $p = \rho/3$. For convenience, we introduce the enthalpy density

$$h = \rho + p. \tag{2.52}$$

Analogously, to the previous section we introduce the comoving density $\tilde{\rho} = a^4\rho$, comoving pressure $\tilde{p} = a^4 p$ and comoving viscosity $\tilde{\nu} = \nu/a$. Here, we primarily assume non-relativistic bulk flows $v \ll c$. The 0 component of (2.51) gives the equation for the change of energy

$$\partial_\tau \tilde{\rho} + \nabla \cdot \left(\tilde{h}\mathbf{v}\right) = \tilde{\mathbf{E}} \cdot \tilde{\mathbf{j}} + \tilde{h}\tilde{\nu}\nabla \cdot \left(\nabla \frac{v^2}{2} - \frac{2}{3}\mathbf{v}\nabla \cdot \mathbf{v}\right), \tag{2.53}$$

where the evolution equations for the magnetic field have been applied and we have chosen the four velocity vector as $u = a\gamma(1, \mathbf{v})$ with $\gamma = (1-v^2)^{-1/2}$. In (2.53) the terms involving ν and σ, which implicitly appear due to Ohm's law, denote contributions where magnetic and bulk kinetic energy is transformed into radiation energy and perturbations are damped.

Furthermore, the $\nu = i$ components of (2.51) describe the evolution of the velocity fluctuations

$$\partial_\tau \mathbf{v} + \frac{\mathbf{v}\cdot\nabla\left(\tilde{h}\mathbf{v}\right)}{\tilde{h}} = -\frac{\mathbf{v}}{\tilde{h}}\partial_\tau \tilde{p} - \frac{\nabla\tilde{p}}{\tilde{h}} + \frac{\tilde{\mathbf{j}}\times\tilde{\mathbf{B}}}{\tilde{h}} - \mathbf{v}\frac{\tilde{\mathbf{j}}\cdot\tilde{\mathbf{B}}}{\tilde{h}} - \mathbf{v}\tilde{\nu}\nabla\cdot\left(\nabla\frac{v^2}{2} - \frac{2}{3}\mathbf{v}\left(\nabla\cdot\mathbf{v}\right)\right) + \tilde{\nu}\left(\nabla^2\mathbf{v} + \frac{1}{3}\nabla\left[\nabla\cdot\mathbf{v}\right]\right), \tag{2.54}$$

where we also applied (2.53). Moreover, we separate the pressure contribution into an adiabatic and a non-adiabatic component

$$\mathrm{d}p = \mathrm{d}p_{\mathrm{ad}} + \mathrm{d}p_{\mathrm{nad}} = c_s^2\mathrm{d}\rho + \mathrm{d}p_{\mathrm{nad}}, \tag{2.55}$$

where $c_s^2 = \mathrm{d}p/\mathrm{d}\rho$ is the sound speed, which for a radiation dominated gas is $c_s^2 = 1/3$. Consequently, one can approximate the enthalpy as

$$h = \rho_b + p_b + (1 + c_s^2)\delta\rho + \delta p_{\mathrm{nad}}, \tag{2.56}$$

where the δ marks a small fluctuation, e.g. $\delta\rho \ll \rho_b$ around a constant background, which is denoted by the subscript b. The non-adiabatic component of the pressure is typically split into two parts (Kodama & Sasaki 1984)

$$p_{\mathrm{nad}} = p_{\mathrm{int}} + p_{\mathrm{rel}}, \tag{2.57}$$

where p_{int} is the intrinsic non-adiabatic pressure from individual components, e.g. due to some fluctuating net particle production, while p_{rel} is the non-adiabatic pressure due to entropy fluctuations between different species. The relative pressure fluctuation corresponds to

$$\mathrm{d}p_{\mathrm{rel}} = \frac{1}{2\partial_\tau\rho}\sum_{i,j}\left[\left(c_i^2 - c_j^2\right)\left(\partial_\tau\rho_j\mathrm{d}\rho_i - \partial_\tau\rho_i\mathrm{d}\rho_j\right)\right], \tag{2.58}$$

where c_i is the sound speed of species i. Obviously, relative non-adiabatic pressure fluctuations from relativistic species are negligible in a strongly radiation dominated universe. In particular, at high energies, e.g. as long as e^+-e^- pair production is effective, we expect that the energy from dissipation quickly thermalizes (Burigana et al. 1991). Therefore, the entropy production from dissipation is effectively uniform and related temperature fluctuations are suppressed due to dissipation itself. In principle, we only expect non-adiabatic terms to be of interest at low temperatures $T \lesssim 1$keV (Chluba & Sunyaev 2012) or in non-trivial phases of the evolution of the cosmological fluid e.g. a first order phase transitions or some epoch of inflation and reheating. This term should be in general only of interest at later times e.g. around matter-radiation equality (Brown et al. 2012). The most interesting source in the primordial radiation dominated setting are intrinsic non-adiabatic pressure fluctuations, which one might expect to occur e.g. in baryogenesis or leptogenesis scenarios, due to a net-production of particles, or around the end of inflation.

Taking the curl of (2.54) leads us to the rate of change of the vorticity $\tilde{\boldsymbol{\omega}}$. For simplicity, we generally neglect terms involving fluctuations at third order e.g. terms like $\partial_\tau \tilde{p}(\mathbf{v} \times \nabla \tilde{h})$ and viscous contributions. Then we find

$$\begin{aligned}\partial_\tau \tilde{\boldsymbol{\omega}} = &- \tilde{\boldsymbol{\omega}} \nabla \cdot \mathbf{v} - \mathbf{v} \cdot \nabla \tilde{\boldsymbol{\omega}} + \tilde{\boldsymbol{\omega}} \cdot \nabla \mathbf{v} - \tilde{\boldsymbol{\omega}} \frac{\partial_\tau \tilde{p}}{\tilde{h}} - \frac{\mathbf{v} \times \nabla \partial_\tau \tilde{p}}{\tilde{h}} + \frac{\nabla \tilde{h} \times \nabla \tilde{p}}{h^2} \\ &+ \frac{\tilde{\mathbf{j}} \cdot \nabla \tilde{\mathbf{B}}}{\tilde{h}} - \frac{\tilde{\mathbf{B}} \cdot \nabla \tilde{\mathbf{j}}}{\tilde{h}}. \end{aligned} \tag{2.59}$$

Note, that most of the terms are only non-vanishing if the initial vorticity is nonzero. The first term on the right hand side describes the enhancement of vorticity in the presence of dilatational motion (e.g. acoustic modes), the second term describes the advection of vorticity and the third term effectively describes a change of vorticity due to an "advection" of the flow along the vorticity vector. Furthermore, there are several more terms of interest involving the pressure, the first two terms that involve the pressure do not appear in the classical vorticity equation, while the third term is the baroclinic vector which describes the production of vorticity in a non-adiabatic flow, even if the initial vorticity is zero. Besides, the neglected higher order terms that involve spatial derivatives of h also lead to terms which can, in the context of non-adiabatic and adiabatically perturbed flows, produce vorticity even if none is present before. The first two terms involving the pressure can be understood as follows, for a purely adiabatically evolving fluid the first term will lead to an increase in the effectiveness of enhancing initial vorticity by compressible motion

$$-\tilde{\boldsymbol{\omega}}\frac{\partial_\tau \tilde{p}}{\tilde{h}} + \tilde{\boldsymbol{\omega}}\nabla\cdot\mathbf{v} \approx \left(1+c_s^2\right)\tilde{\boldsymbol{\omega}}\nabla\cdot\mathbf{v}, \tag{2.60}$$

where the $\approx$ is due to the negligence of the advection term in the energy equation. The second term is also of interest, as it can modify the efficiency of baroclinic production. In order to see this, we briefly model a purely dilatational velocity field as having the following property, assuming a reasonable smooth flow,

$$\mathbf{v} = \frac{\nabla}{\nabla^2}\nabla\cdot\mathbf{v} + \mathbf{v}_0, \tag{2.61}$$

where $\mathbf{v}_0$ describes some constant background flow. In general the dilatational fluid component is found by contracting the dilatational projection operator D_{ij}, as defined in (2.23), with the velocity field. Analogously, the solenoidal component is found by contracting the solenoidal projection operator P_{ij} as defined in (2.23) with the velocity field. If the fluctuations in h are only due to acoustic modes and adiabatic, we anticipate at second order

$$\mathbf{v}\times\nabla\partial_\tau p \approx hc_s^2\mathbf{v}\times\nabla\nabla\cdot\mathbf{v} = hc_s^2\mathbf{v}\times\nabla^2\mathbf{v} = 0, \tag{2.62}$$

since $\nabla^2\mathbf{v} \parallel \mathbf{v}$ for a purely dilatational flow. However in the case of a non-adiabatic pressure perturbation we expect this to give a production term for vorticity, even if the vorticity is zero initially, similar to the baroclinic vector. Moreover, this term also leads to a non-linear enhancement of the vorticity in case that the initial vorticity is nonzero. Technically, the relativistic $\partial_\tau p$ term corrects for the appearance of h and makes certain that the frequency remains $c_s k$, whereas in the case that $p \ll \rho$ this term is negligible. The last two terms involve the magnetic field and the current and generally describe the production of vorticity due to the advection of a magnetic field along the current and the advection of the current along the magnetic field. Thus, magnetic fields generate bulk vorticity within a plasma, even if no bulk motion is present before. As, we discuss later on in more detail, the relativistic term is not expected to alter the evolution of an incompressible or near incompressible flow. Overall, the behavior of non-relativistic fluid turbulence is expected to be similar to that of a relativistic fluid in the context of non-relativistic bulk-flows.

Analogously to taking the curl of (2.54), one can also look at its divergence to find

$$\begin{aligned}\partial_\tau \nabla \cdot \mathbf{v} =& -\mathbf{v} \cdot \nabla\nabla \cdot \mathbf{v} - \sum_{ij} (\partial_i v_j)\partial_j v_i + \frac{\nabla\tilde{p} \cdot \nabla\tilde{h}}{\tilde{h}^2} - \frac{\nabla^2 \tilde{p}}{\tilde{h}} - \frac{\partial_\tau \nabla\tilde{p}}{\tilde{h}} \nabla \cdot \mathbf{v} - \frac{\mathbf{v} \cdot \partial_\tau \nabla\tilde{p}}{\tilde{h}} \\ & + \frac{\tilde{\mathbf{B}} \cdot (\nabla \times \tilde{\mathbf{j}})}{\tilde{h}} - + \frac{\tilde{\mathbf{j}} \cdot (\nabla \times \tilde{\mathbf{B}})}{\tilde{h}},\end{aligned} \tag{2.63}$$

where we have again neglected terms which are at least of third order in the fluctuating quantities like the velocity field and or variations of the density and viscous terms. All terms on the right hand side except for the second term vanish when $\nabla \cdot \mathbf{v} = 0$ and $\nabla p = 0$. Hence, the second term consequently describes the generation of dilatational motion from solenoidal motion. An incompressible flow is a flow for which $\nabla \cdot \mathbf{v} = 0$, yet due to the second term, this can at most only be satisfied approximately in adiabatic systems. As is well known, acoustic waves correspond to the linearized solution of the above equation with an adiabatic equation of state. We will discuss the non-linear effects later on in more detail, including magnetic effects. Next, we focus on the overall MHD equations.

2.3.4 MHD equations

Now, we briefly discuss the complete set of equation governing the evolution of a magnetized plasma in the fluid and MHD approximation.

The evolution of the magnetic field is described by (2.47) in the MHD approximation and together with Ohm' law (2.48) one finds

$$\partial_\tau \tilde{\mathbf{B}} = \frac{\tilde{\rho}_c}{\tilde{\sigma}}\boldsymbol{\omega} + \frac{\mathbf{v}}{\tilde{\sigma}} \times \nabla\tilde{\rho}_c - \frac{1}{4\pi\tilde{\sigma}}\nabla \times \left(\nabla \times \tilde{\mathbf{B}}\right) + \nabla \times \left(\mathbf{v} \times \tilde{\mathbf{B}}\right). \tag{2.64}$$

Here we set $\rho_c = 0$, in accordance with constraints on the net charge of the universe at photon decoupling (Caprini & Ferreira 2005). However, net currents might appear during certain processes. Also, net charge flows can play a role after recombination and even prior to reionization due to ambipolar diffusion (Banerjee & Jedamzik 2004) since the universe has only a slight fractional ionization i.e. electrons will not be strongly trapped by protons and can diffuse over sufficiently longer length-scales than protons due to their smaller mass. Furthermore, by applying 2.47 on 2.54 we find for the evolution of the velocity field in the MHD approximation

$$\partial_\tau \mathbf{v} + \frac{\mathbf{v}\cdot\nabla\left(\tilde{h}\mathbf{v}\right)}{\tilde{h}} = -\frac{\mathbf{v}}{\tilde{h}}\partial_\tau\tilde{p} - \frac{\nabla\tilde{p}}{\tilde{h}} + \frac{\left(\nabla\times\tilde{\mathbf{B}}\right)\times\tilde{\mathbf{B}}}{4\pi\tilde{h}} + \tilde{\nu}\left(\nabla^2\mathbf{v} + \frac{1}{3}\nabla\left[\nabla\cdot\mathbf{v}\right]\right). \tag{2.65}$$

and for the energy density one has

$$\partial_\tau\tilde{\rho} + \nabla\cdot\left(\tilde{h}\mathbf{v}\right) = \frac{\left(\nabla\times\tilde{\mathbf{B}}\right)^2}{(4\pi)^2\tilde{\sigma}} - \frac{\tilde{\rho}_c}{4\pi\tilde{\sigma}}\mathbf{v}\cdot(\nabla\times\tilde{\mathbf{B}}) + \tilde{h}\tilde{\nu}\nabla\cdot\left(\nabla\frac{v^2}{2} - \frac{2}{3}\mathbf{v}\nabla\cdot\mathbf{v}\right), \tag{2.66}$$

where third order terms in fluctuating quantities like $\mathbf{vB}\nabla p$ have been neglected. Lastly, a general equation of state for the pressure needs to be specified e.g. for a barotropic cosmological fluid one has $p = c_s^2\rho$. Alternatively, other conditions can be applied, like only solenoidal bulk motion $\nabla\cdot\mathbf{v} = 0$, which also fixes the pressure and is a common approximation for sub-sonic systems. Such a flow is also known as a incompressible flow. Ultimately, the equations (2.64), (2.54) and (2.55) describe MHD turbulence.

Note that in general other modifications to the fluid equations can be of interest in particular when similar to a net charge different particle species are affected differently by the magnetic field. In that case further modification to Ohm's law (2.48) appear, which modify the overall evolution of magnetic fields. One particular class of modifications are imbalances in the handedness of e.g. left and right handed particles, e.g.

the so-called chiral magnetic effect (Boyarsky et al. 2012, Pavlović et al. 2017). These imbalances can in the presence of magnetic fields grow and affect the evolution of the magnetic fields in particular by an additional source term for magnetic helicity, which is an important topological measure as we discuss below. In general these class of imbalances are of relevance for temperatures 10TeV $\gtrsim T \gtrsim$ 100MeV, at lower temperatures other processes that reduce the imbalance become increasingly important. Here, we do not include this particular effect, however we will also study the impact of magnetic helicity. For relevant numerical studies on this effect, see (Schober et al. 2019, Brandenburg et al. 2017)

In the next section, we will briefly discuss the kinetic, magnetic and gravitational wave energy density and thereafter we discuss four relevant topological measures of MHD flows, the kinetic helicity, cross helicity, magnetic helicity and the cross scalar. For MHD systems of particular interest is the cross helicity and magnetic helicity, since these are conserved if the system is ideal and barotropic. Nonetheless, both the kinetic helicity, which is conserved in non-magnetized ideal barotropic flows, and the cross scalar can be of interest in the evolution of the system and might also play a role, when source terms for cross and magnetic helicity are present.

2.4 Basic magnetic and velocity field measures in GWMHD

In this section, we describe and briefly discuss some basic quantities in GWMHD. These are the kinetic, magnetic and gravitational wave energy and the kinetic, cross and magnetic helicity, and the cross scalar.

2.4.1 Kinetic, magnetic and gravitational wave energy

We define the total comoving kinetic energy

$$E_K = \frac{\tilde{h}}{2} \int \mathrm{d}V \langle v^2(\mathbf{x}) \rangle, \tag{2.67}$$

where V is the comoving volume over which one integrates and $\langle v^2 \rangle$ is the root mean square velocity as defined over an ensemble average. The averaging is not necessary in the volume integration, however typically we are interested in spectral densities and in the context of turbulence only statistical measures provide valuable information, as we do not have information about more specific initial conditions. Moreover, we introduce a dimensionless measure for the comoving kinetic energy

$$e_K = \frac{1}{2V} \int \mathrm{d}V \langle v^2(\mathbf{x}) \rangle, \tag{2.68}$$

where V is the total volume over which one integrates, e.g. $V \sim d_H^3$, where d_H is the size of the horizon. Similarly one can define the magnetic energy density as

$$E_M = \frac{1}{8\pi} \int \mathrm{d}V \langle \tilde{B}^2(\mathbf{x}) \rangle, \tag{2.69}$$

where V is the comoving volume over which one integrates. For convenience, we introduce the Alfven velocity

$$\mathbf{b} = \frac{\mathbf{B}}{\sqrt{4\pi(\tilde{h})}}. \tag{2.70}$$

Moreover, we introduce a dimensionless measure for the comoving magnetic energy

$$e_M = \frac{1}{2V} \int \mathrm{d}V \langle b^2(\mathbf{x}) \rangle, \tag{2.71}$$

We also introduce the total comoving gravitational wave energy (Misner et al. 1973)

$$E_G = \int \mathrm{d}V \rho_G = \frac{a^2}{32\pi G} \int \mathrm{d}V \sum_{ij} \langle \tilde{H}^2_{ij,0}(\mathbf{x}) \rangle, \tag{2.72}$$

where we average the strain over several length-scales and ρ_G is the gravitational wave energy density. We also introduce the GW energy density per $\log(k)$ in Fourier space $e_G(k)$ by

$$\frac{1}{V} \int \mathrm{d}V \rho_G = \int \mathrm{d}\log(k) e_G(k) = \frac{a^2}{32\pi G} \int \mathrm{d}\log(k) \frac{4\pi k^3}{(2\pi)^6} \sum_{ij} \langle |\tilde{H}^2_{ij,0}(\mathbf{k})|^2 \rangle, \tag{2.73}$$

where the factor $\sum_{ij}\langle|\tilde{H}^2_{ij,0}(\mathbf{k})|^2\rangle$ only depends on the length scale k in homogeneous isotropic systems. Additional, the gravitational energy density parameter (today) is

$$\Omega_G = \frac{a^2}{12H_0^2}\sum_{ij}\langle\tilde{H}^2_{ij,0}(\mathbf{x})\rangle = \int \mathrm{d}\log(k)P_G(k), \tag{2.74}$$

where H_0 is the present Hubble parameter and we used $\Omega_i = \rho_i/\rho_c$, where $\rho_c = 3H_0^2/(8\pi G)$. Moreover $P_G(k)$ is the gravitational wave power spectrum. In the following we discuss several topological measures of MHD turbulence.

2.4.2 Kinetic helicity

In hydrodynamic incompressible system, there are two basic non-trivial conserved quantities, one is the kinetic energy and the other is the kinetic helicity. The total kinetic helicity

$$\mathcal{H}_K = \int \mathrm{d}V h_K = \int \mathrm{d}V \mathbf{v}\cdot\boldsymbol{\omega} \tag{2.75}$$

measures the cork-screw like motion in a fluid, i.e. the degree of vortical motion of a fluid particle along its trajectory. Note, that one key assumption that we make here is the isotropy of the system. Strictly speaking however, helicity breaks isotropy as there is a sense of rotation in the system and thus the system is no longer invariant under parity transformations. Nonetheless, we treat the system as effectively "semi"-isotropic in the sense that there is no mean vorticity $\langle\boldsymbol{\omega}\rangle =$, no mean flow $\langle\mathbf{v}\rangle = 0$ and no mean magnetic field $\mathbf{B} = 0$, i.e. there is no preferential direction of motion other than that of rotation. In barotropic and ideal non-magnetized flows kinetic helicity is conserved, as long as there are no flows of helicity in or out of the volume V. Further, a transformation of the type $\mathbf{v} \to \mathbf{v} + \nabla\phi$, where ϕ is some scalar field, which corresponds to the addition of compressible motion, only leads to hydrodynamic changes in the kinetic helicity if $\boldsymbol{\omega}$ lies within the surface of the volume over which one integrates. Hence, in general as long as there is no net out- or inflow of vorticity in the volume V the total kinetic helicity is conserved. As we see later on also for the magnetic helicity, kinetic helicity is conserved under gauge transformation of the vector potential of the vorticity as long as there are no net vorticity in- or out-flows into the system. For convenience, we introduce the parameter

$$\lambda_K = \frac{\langle \boldsymbol{\omega} \cdot \mathbf{v} \rangle}{\sqrt{\langle v_s^2 \rangle \langle \omega^2 \rangle}} \tag{2.76}$$

which measures the amount of kinetic helicity in the system normalized to the kinetic energy with possible values in the range of $[-1, 1]$. Where v_s is the absolute value of the solenoidal component of the velocity field $\mathbf{v}_s = \mathbf{P} \cdot \mathbf{v}$, where P is the projection operator with components P_{ij}. A nonzero baroclinic vector is generally a source of kinetic helicity if the velocity has a component which is parallel to the baroclinic vector. Moreover, other parity violating topological quantities like the magnetic helicity can drive the production of kinetic helicity. Note that technically a hydro-dynamically viscous flow with $H_K = 0$ and $h_K \neq 0$ can develop into a flow with $H_K \neq 0$ simply due to dissipation. In that case, h_K at smaller scales gets damped away, due to the more efficient dissipation, whereas h_K on larger scales is barely affected by dissipation and therefore H_K would attain a non-zero value. Such a process is in general also of interest for the total production of other topological measures like cross helicity, cross current and magnetic helicity, yet a prior spatial imbalance of these topological features is nonetheless required.

2.4.3 Cross helicity

In incompressible MHD, there are two conserved topological measures, one of those is the cross helicity. The cross helicity

$$\mathcal{H}_C = \int \mathrm{d}V h_C = \int \mathrm{d}V \mathbf{v} \cdot \tilde{\mathbf{B}}, \tag{2.77}$$

measures the alignment of magnetic field lines with the velocity field.The change of the cross helicity density follows from (2.64) and (2.54), and is given by

$$\partial_\tau h_C(\mathbf{x}, \tau) = \partial_\tau \left(\mathbf{v} \cdot \tilde{\mathbf{B}} \right) = \nabla \cdot \left[\mathbf{v} \times \left(\mathbf{v} \times \tilde{\mathbf{B}} \right) - \tilde{\mathbf{B}} \frac{v^2}{2} \right] - \tilde{\mathbf{B}} \cdot \frac{\nabla \tilde{p}}{\tilde{h}}. \tag{2.78}$$

Under the assumption that $\tilde{\mathbf{B}} \perp \mathbf{n}$, where $\mathbf{n}$ is a surface normal vector of some enclosing surface of the volume, then the cross helicity is invariant in ideal systems with an barotropic equation of state. Therefore, a production of cross helicity is possible when magnetic fields are present and the system is non-adiabatic. Then, the net rate of production is

$$\partial_\tau H_C \propto -\int \mathrm{d}V \frac{\tilde{\mathbf{B}} \cdot \nabla \tilde{p}}{\tilde{h}} \propto -\int \mathrm{d}V \frac{\tilde{p}}{\tilde{h}_b^2} \tilde{\mathbf{B}} \cdot \nabla \tilde{h} \propto -\int \mathrm{d}V \left[\frac{\delta \tilde{p}_{\mathrm{nad}}}{\tilde{h}_b^2} \tilde{\mathbf{B}} \cdot \nabla \tilde{p}_{\mathrm{ad}} \right], \tag{2.79}$$

where $\delta p_{\mathrm{ad}} \ll p$ is the fluctuating adiabatic component of the pressure and $\delta p_{\mathrm{nad}} \ll p$ is the fluctuating non-adiabatic component. The subscript b denotes a spatially constant background value. In the first proportionality relation we simply dropped the pure divergence terms, while in the second we applied partial integration and neglected higher order terms, as these do not impact the conclusion and we generally neglected terms like $p\mathbf{B} \cdot \nabla p \propto \nabla \cdot (\mathbf{B}p^2)$ as such terms are pure divergence terms. Ultimately, one arrives at the final proportionality by neglecting all contributions to the pressure which can be written as some divergence of some quantity like $p_{\mathrm{ad}} \nabla p_{\mathrm{ad}}$, and by using $\rho \propto p_{\mathrm{ad}}$. Note that cross-helicity production from non-adiabatic effects requires some initial magnetic field and both adiabatic and non-adiabatic fluctuations to be present. Technically, this is possible if the flow is magnetized and the fluid is non-adiabatic, as inhomogeneous magnetic fields source adiabatic fluctuations, even if none were present before. The occurrence of sizable non-adiabatic fluctuations may be a bigger question mark than the production of initial magnetic fields. Moreover, cross helicity is subject to both resistive and viscous damping. In general, cross helicity may be relevant around matter radiation equality, due to the presence of non-adiabatic pressure. Yet it could also appear in the very early universe due to some as of yet undiscovered processes. Lastly, we also introduce a dimensionless parameter for the cross helicity

$$\lambda_C = \frac{\langle \mathbf{B} \cdot \mathbf{v} \rangle}{\sqrt{\langle v^2 \rangle \langle B^2 \rangle}}. \tag{2.80}$$

Next, we will briefly discuss the magnetic helicity.

2.4.4 Magnetic helicity

As mentioned before, there are two basic fundamental topological conserved quantities, the first being the aforementioned cross helicity and the second is the magnetic helicity. The magnetic helicity

$$\mathcal{H}_M = \int \mathrm{d}V h_M = \int \mathrm{d}V \tilde{\mathbf{A}} \cdot \tilde{\mathbf{B}} \tag{2.81}$$

measures the alignment of the magnetic field with its vector potential, similar to the kinetic helicity albeit with respect to the vorticity rather than the velocity field.In Coulomb gauge $\nabla \cdot \mathbf{A} = 0$, one finds

$$\mathbf{A}(\mathbf{r}) = \nabla \times \int \mathrm{d}^3\mathbf{r}' \frac{\mathbf{B}(\mathbf{r}')}{4\pi|\mathbf{r} - \mathbf{r}'|}. \tag{2.82}$$

Magnetic helicity can also be stated as an alignment of $\mathbf{B}$ with $\nabla \times \mathbf{B} \propto \mathbf{J}$, although this alignment integrated over the volume V is not conserved. Further Maxwell's equations (2.44) implies that the production of a non-zero magnetic helicity requires in Coulomb gauge

$$\partial_\tau(\tilde{\mathbf{B}} \cdot \tilde{\mathbf{A}}) = \partial_\tau(\tilde{\mathbf{B}} \cdot (\frac{\nabla}{\nabla^2} \cdot \tilde{\mathbf{B}}) = -\tilde{\mathbf{B}} \cdot \tilde{\mathbf{E}} + \nabla \times \tilde{\mathbf{E}} \cdot \frac{\nabla}{\nabla^2} \times \tilde{\mathbf{B}}. \tag{2.83}$$

This implies that the production of magnetic helicity requires some degree of alignment between the electric and magnetic field. For example charged flows can lead to a production of magnetic helicity and similarly the aforementioned chiral anomaly effect. Given a constant charge density, the production of magnetic helicity due to some net-charge density is

$$\partial_\tau(\tilde{\mathbf{B}} \cdot \tilde{\mathbf{A}}) = \frac{\tilde{\rho}_c}{\tilde{\sigma}} \left[\tilde{\mathbf{B}} \cdot \mathbf{v} - \tilde{\mathbf{B}} \cdot \frac{\nabla}{\nabla^2} \nabla \cdot \mathbf{v} - \boldsymbol{\omega} \cdot (\frac{\nabla}{\nabla^2} \times \tilde{\mathbf{B}})\right]. \tag{2.84}$$

Hence, the production of magnetic helicity due to some net charge requires some degree of correlation between the magnetic and velocity field.

In case that there is no net charge distribution or other variations between the charges, e.g. chiral imbalance or resistive damping, magnetic helicity is conserved if $\mathbf{B} \perp \mathbf{n}$, like the cross helicity in adiabatic flows, where $\mathbf{n}$ is again a surface vector. Besides, the criterion $\mathbf{B} \perp \mathbf{n}$ also ascertains that the defined total magnetic helicity is invariant under gauge transformations $\mathbf{A} \to \mathbf{A} + \nabla\phi$ and hence physical, where ϕ is some scalar field, analogously as for the kinetic helicity. Otherwise, there would be a troubling ambiguity in the defined magnetic helicity. Additionally, we introduce another dimensionless parameter

$$\lambda_B = \frac{\langle \mathbf{B} \cdot \mathbf{A} \rangle}{\sqrt{\langle A^2 \rangle \langle B^2 \rangle}}, \tag{2.85}$$

where $\mathbf{A}$ is given by (2.82). Next, we discuss the cross scalar which is the only parity-invariant quadratic topological measure in isotropic and homogeneous MHD turbulence.

2.4.5 Cross scalar

Lastly, we introduce another quadratic measure of MHD turbulence. We construct it as a combination of $\mathbf{v}$, $\mathbf{B}$ and ∇.For near charge neutral flows, one has

$$\nabla \cdot \tilde{\mathbf{j}} = 0 = \nabla \cdot (\mathbf{v} \times \tilde{\mathbf{B}}) = \boldsymbol{\omega} \cdot \tilde{\mathbf{B}} - \mathbf{v} \cdot \tilde{\mathbf{j}} \tag{2.86}$$

where we have used the MHD approximation (2.47). Thus, there is only one unique way to combine these two vectors and the nabla operator into a scalar (safe for some additionally powers of ∇^2 and arbitrary linear combinations) and we denote it as

$$E_C = \int \mathrm{d}V e_C = \int \mathrm{d}V \mathbf{v} \cdot \left(\nabla \times \tilde{\mathbf{B}}\right) = \int \mathrm{d}V \tilde{\mathbf{B}} \cdot (\nabla \times \mathbf{v}) \,. \tag{2.87}$$

We refer to $\mathbf{B} \cdot \boldsymbol{\omega}$ as the cross vorticity and $\mathbf{j} \cdot \mathbf{v}$ as the cross current. As these two quantities are equal in MHD we will refer to these as the cross scalar. The structure of this quantity is on the surface quite similar to that of the kinetic and magnetic helicity (in Coulomb gauge). However, in parity invariant systems ($\mathbf{v}$ is a vector and $\mathbf{B}$ is a pseudovector), only the magnetic and kinetic energy spectra and the cross scalar can be nonzero, whereas the magnetic, kinetic and cross helicity vanish. Therefore, a nonzero cross scalar even though cannot act as a source term for some helicity density, however it might still impact the evolution of the different helicities. Cross scalars are generally appear when there is a component of the electric field e.g. during the magnetogenesis process, that has a component which is parallel to the fluid flow, like for net charged flows. The rate of change of the cross scalar density, where we neglect dissipative and resistive contributions, is

$$\begin{aligned}\partial_\tau(\boldsymbol{\omega}\cdot\tilde{\mathbf{B}}) =&\tilde{\mathbf{B}}\cdot[\nabla\times(\mathbf{v}\times\boldsymbol{\omega})]+\boldsymbol{\omega}\cdot\left[\nabla\times(\mathbf{v}\times\tilde{\mathbf{B}})\right]-\frac{\tilde{\mathbf{B}}}{\tilde{h}}\cdot(\mathbf{v}\times\nabla\partial_\tau\tilde{p})-\tilde{\mathbf{B}}\cdot\boldsymbol{\omega}\frac{\partial_\tau\tilde{p}}{\tilde{h}}\\ &+\tilde{\mathbf{B}}\cdot\frac{\nabla\tilde{\rho}\times\nabla\tilde{p}}{\tilde{h}^2}+\frac{\tilde{\rho}_c}{\tilde{\sigma}}\boldsymbol{\omega}^2. \end{aligned}\tag{2.88}$$

As mentioned prior, the last term describes the aligning between the magnetic and vorticity field if a net zero charge is present. The second to last term describes a generation of the cross-scalar due to an alignment of the magnetic field with the baroclinic vector. Moreover, the first two terms general show the change of the cross-scalar due to the structure of the MHD flow itself. Lastly, we introduce a dimensionless parameter for the cross scalar

$$\lambda_J=\frac{\langle\mathbf{B}\cdot\boldsymbol{\omega}\rangle}{\sqrt{\langle\omega^2\rangle\langle B^2\rangle}},\tag{2.89}$$

In the next chapter we look at homogeneous isotropic MHD turbulence with gravitational waves. Generally, we focus only on incompressible systems but we will also touch upon compressible MHD. We also discuss MHD turbulence and gravitational waves produced by turbulence.

3 | MHD turbulence and GW

One general information, from here on out we will drop the ˜ from comoving variables and unless specified otherwise all variables discussed here are comoving in the radiation dominated phase. In the previous chapter we described MHD in an expanding universe and some basics about the production of gravitational waves. Here, we focus on a particular class of problems in MHD, which is homogeneous and isotropic MHD turbulence and the generation of gravitational waves by MHD turbulence. Also, we mentioned some particular quantities like topological measures and so forth, where we have already defined stochastic quantities like the dimensional parameters (2.76), (2.80), (2.85), (2.89). Note that the definition of these parameters is valid without averaging, yet such a definition is not of interest to us. First, we discuss spectral correlation quantities in MHD turbulence.

3.1 Spectral correlation functions

As, we discuss in the next section in more detail, turbulent systems are best described by stochastic measures. Here we primarily assume that the system of interest is homogeneous and isotropic in a stochastic sense.

In hydrodynamic turbulence a relevant type of auto-correlation functions are

$$S_p(r) = \langle |\mathbf{v}(\mathbf{x}) - \mathbf{v}(\mathbf{x} + \mathbf{r})|^p \rangle. \tag{3.1}$$

Note that the $\langle\rangle$ denotes a ensemble average e.g. an average over different initial conditions with the same basic stochastic properties e.g. the same initial S_p. Note that because of stochastic homogeneity the function S_p does not depend on $\mathbf{x}$ and because of stochastic isotropy it only depends on the distance r between the two locations. For $p = 1$ one has the one-point function also known as the mean value, for a isotropic system one has $S_1 = 0$. Next, for $p = 2$ one has the two point auto-correlation function and S_2, also known as the standard deviation since $S_1 = 0$, vanishes only if there are no inhomogeneities in the different initialization of the flow $\mathbf{v}$. Furthermore, for $p = 3$ one has three point function, also known as skewness, which in turbulent evolution is always non-zero, as we discuss later on in more detail. There are of course several more stochastic quantities for different p in (3.1) but also for functions involving $\mathbf{b}$ and ρ and mixtures of these different variables. For us the Fourier presentation of these correlation functions is generally the most useful e.g. functions like $\langle \mathbf{v}(\mathbf{k})\mathbf{v}(-\mathbf{k})\rangle$, where $k \sim 1/r$ is the wave number.

In homogeneous isotropic incompressible MHD turbulence there are six fundamental scalar (three) and pseudo-scalar (three) two-point functions (see the following correlation functions and subsection 3.2.2).Whereas, in compressible MHD turbulence there are three additional scalar two point functions but no additional pseudo-scalars. Here, we focus only on those that are sufficient in describing incompressible MHD, while we briefly discuss the additional compressible two point function later on. These correlation functions are the kinetic, magnetic and cross correlation two-point functions. For convenience we split a general bulk flow into a dilatational, solenoidal and background component

$$\mathbf{v} = \mathbf{v}_d + \mathbf{v}_s + \mathbf{v}_0, \tag{3.2}$$

with the properties $\nabla \times \mathbf{v}_d = 0$ and $\nabla \cdot \mathbf{v}_s = 0$, and the subscript d denotes a dilatational field component, while the subscript s denotes the solenoidal field component. Additional, the background component $\mathbf{v}_0 = 0$ in isotropic systems.

Then, in Fourier-space the equal time velocity two-point function for solenoidal velocity fluctuations is

$$\langle v_s^i(\mathbf{k},\tau) v_s^j(\mathbf{q},\tau)\rangle = \frac{(2\pi)^6}{4\pi k^3}\delta(\mathbf{k}-\mathbf{q})\left[\left(\delta_{ij} - \frac{k_i k_j}{k^2}\right) E_s(k,\tau) - i\epsilon_{iju}\frac{k_u}{k} H_K(k,\tau)\right], \tag{3.3}$$

where $E_s(k,\tau)$ is the kinetic energy spectrum for solenoidal motion and $H_K(k,\tau)$ is a measure for the kinetic helicity with $H_K(k,\tau) \leq E_d(k,\tau)$. Next, for dilatational velocity fluctuations we have

$$\langle v_d^i(\mathbf{k},\tau) v_d^j(\mathbf{q},\tau)\rangle = \frac{(2\pi)^6}{2\pi k^3}\delta(\mathbf{k}-\mathbf{q})\frac{k_i k_j}{k^2}E_d(k,\tau), \tag{3.4}$$

where E_d is the kinetic energy spectrum of dilatational motion. Consequently, we define the total kinetic energy spectrum as $E_u = E_d + E_s$. Furthermore, in homogeneous and isotropic turbulence $\langle v_d^i v_s^j\rangle = 0$, as in that case there is no spectral function $F_{ij}(\mathbf{k})$ with $k_j F_{ij} = 0$ and $\epsilon_{imn} k_m F_{nj} = 0$.

Analogously, for magnetic field fluctuations one has

$$\langle b^i(\mathbf{k},\tau) b^j(\mathbf{q},\tau)\rangle = \frac{(2\pi)^6}{4\pi k^3}\delta(\mathbf{k}-\mathbf{q})\left[\left(\delta_{ij} - \frac{k_i k_j}{k^2}\right)E_b(k,\tau) - i\epsilon_{iju}\frac{k_u}{k}H_b(k,\tau)\right], \tag{3.5}$$

where E_b is the energy spectrum of Alfvenic fluctuations and H_b is a measure of magnetic helicity with $H_b(k,\tau) \leq E_b(k,\tau)$.

Moreover we also introduce the two point function for the mixture of Alfvenic and velocity fluctuations

$$\langle v_s^i(\mathbf{k},\tau) b^j(\mathbf{q},\tau)\rangle = \frac{(2\pi)^6}{4\pi k^3}\delta(\mathbf{k}-\mathbf{q})\left[\left(\delta_{ij} - \frac{k_i k_j}{k^2}\right)H_C(k,\tau) - i\epsilon_{iju}\frac{k_u}{k}E_C(k,\tau)\right], \tag{3.6}$$

where H_C is the cross helicity and E_C is the cross scalar. Sine $\mathbf{b}$ is solenoidal, correlations between magnetic and dilatational fluctuations also vanish in homogeneous and isotropic systems $\langle v_d^i b^j\rangle = 0$. Also, the cross helicity density is constrained by $H_C(k,\tau) \leq \sqrt{E_s(k,\tau)E_b(k,\tau)}$ and the cross scalar is constrained by $E_C(k,\tau) \leq \sqrt{E_s(k,\tau)E_b(k,\tau)}$. These are not the only constraints for these different quantities as there are additional dependencies that we discussing in the next subsection.

The above defined kinetic energy density is related to the total kinetic energy by the relation

$$\langle e_K\rangle = \int \mathrm{d}\ln(k) E_u(k) = \int \mathrm{d}\ln(k)\left[E_s(k) + E_d(k)\right], \tag{3.7}$$

where e_K is defined in (2.68). For the magnetic energy one has

$$\langle e_M \rangle = \int \mathrm{d}\ln(k) E_b(k), \tag{3.8}$$

where e_M is defined in (2.71). Moreover for the cross helicity, one has

$$\langle h_C \rangle = \sqrt{4\pi\langle\rho\rangle} \int \mathrm{d}\ln(k) H_C(k), \tag{3.9}$$

where h_C has been defined in (2.77). Further, the kinetic helicity is

$$\langle h_K \rangle = \int \mathrm{d}\ln(k) k H_K(k), \tag{3.10}$$

where h_K has been defined in (2.75). Next, the magnetic helicity density in Coulomb gauge is

$$\langle h_M \rangle = 4\pi\langle\rho\rangle \int \mathrm{d}\ln(k) \frac{H_b(k)}{k}, \tag{3.11}$$

where h_M has been defined in (2.81). Lastly, the cross scalar is

$$\langle e_C \rangle = \sqrt{4\pi\langle\rho\rangle} \int \mathrm{d}\ln(k) k E_C(k), \tag{3.12}$$

where e_C has been defined in (2.87). In the following subsection we discuss how the different topological quantities H_K, H_M, H_C and E_C influence their respective parameter space.

3.1.1 Interdependencies

Now we look at the allowed range of the different alignments, as the above constraints are insufficient, e.g. a system extremal cross and magnetic helicity also requires a maximal cross-scalar and kinetic helicity. First, we introduce several dimensionless parameters that measure the relative amount of cross helicity, magnetic helicity, kinetic helicity and cross scalar. We parameterize the kinetic helicity as

$$\lambda_K(k,\tau) = \frac{H_K(k,\tau)}{E_s(k,\tau)}. \tag{3.13}$$

with $-1 \leq \lambda_K \leq 1$. Similarly, we parameterize the magnetic helicity as

$$\lambda_B(k,\tau) = \frac{H_b(k,\tau)}{E_b(k,\tau)}, \tag{3.14}$$

with $-1 \leq \lambda_B \leq 1$. The cross helicity is parameterized as

$$\lambda_C(k,\tau) = \frac{H_C(k,\tau)}{\sqrt{E_s(k,\tau)E_b(k,\tau)}}, \tag{3.15}$$

with $-1 \leq \lambda_C \leq 1$. Lastly, we parameterize the cross current as

$$\lambda_J(k,\tau) = \frac{E_C(k,\tau)}{\sqrt{E_s(k,\tau)E_b(k,\tau)}}, \tag{3.16}$$

with $-1 \leq \lambda_J \leq 1$.

A effective way to analyze helical systems is the helical decomposition of the kinetic and Alfven velocity (Lesieur 1972). The velocity field can thus be written in terms of polarized states as

$$\mathbf{v}(\mathbf{k}) = v_+(\mathbf{k})\mathbf{h}_+(\mathbf{k}) + v_-(\mathbf{k})\mathbf{h}_-(\mathbf{k}). \tag{3.17}$$

Analogously, we can perform such a split for magnetic fields and find

$$\mathbf{b}(\mathbf{k}) = b_+(\mathbf{k})\mathbf{h}_+(\mathbf{k}) + b_-(\mathbf{k})\mathbf{h}_-(\mathbf{k}) \tag{3.18}$$

where the basis vectors are an orthonormal solution to the eigenvalue equation

$$i\mathbf{k} \times \mathbf{h}_\pm(\mathbf{k}) = k\mathbf{h}_\pm(\mathbf{k}). \tag{3.19}$$

The coefficients $v_\pm$ and $b_\pm$ are complex numbers.

Then, the helical decomposition can be used to easily identify the respective energy and helicity spectrum with the absolute value of the coefficients of the respective decomposition. Thus, the energy density is $E_s(\mathbf{k}) = \langle |v_+|^2 + |v_-|^2 \rangle$ and the normalized kinetic helicity density corresponds to $H_K(\mathbf{k}) = \langle |v_+|^2 - |v_-|^2 \rangle$. Analogously for the magnetic fields one finds for the magnetic energy density is $E_b(\mathbf{k}) = |b_+|^2 + |b_-|^2$ and the normalized magnetic helicity density corresponds to $H_b(\mathbf{k}) = |b_+|^2 - |b_-|^2$. Then one can invert this relation to find the absolute value of the coefficients in terms of the different spectra

$$\langle |v_\pm|^2 \rangle = \frac{E_s \pm H_K}{2} = E_s \frac{1 \pm \lambda_K}{2}, \quad \langle |b_\pm|^2 \rangle = \frac{E_b \pm H_b}{2} = E_b \frac{1 \pm \lambda_B}{2}. \tag{3.20}$$

Moreover, for the cross helicity one finds

$$\lambda_C = \frac{\langle |v_+||b_+| \rangle \cos\alpha_+ + \langle |v_-||b_-| \rangle \cos\alpha_-}{\sqrt{E_s E_b}} \tag{3.21}$$

and for the cross-current one finds

$$\lambda_J = \frac{\langle |v_+||b_+| \rangle \cos\alpha_+ - \langle |v_-||b_-| \rangle \cos\alpha_-}{\sqrt{E_s E_b}}, \tag{3.22}$$

where we did not average over the angles and the angles $\alpha_\pm$ denote the different complex phases between $v_\pm$ and $b_\pm$ and are here free parameters in $[0, \pi)$. Applying (3.20) in (3.21), (3.22), we find

$$\sqrt{1 \pm \lambda_K} \sqrt{1 \pm \lambda_B} \cos\alpha_\pm = \lambda_J \pm \lambda_C. \tag{3.23}$$

The angular dependency can be dropped to find the inequality

$$\sqrt{1 \pm \lambda_K} \sqrt{1 \pm \lambda_B} \geq |\lambda_J \pm \lambda_C|. \tag{3.24}$$

Consequently, when choosing a set of initial conditions for helical MHD turbulence one may need to take the above constraint into account.

In particular a state with $|\lambda_C| + |\lambda_J| > 1$ requires non-zero kinetic and magnetic helicity spectra. On the other hand, for system with a zero cross helicity and cross scalar spectrum, there are no constraints on the magnetic and kinetic helicity spectra. Also, at scales where the magnetic helicity is extremal, i.e. $\lambda_B(k) = \pm 1$, it follows $\lambda_C(k) = \pm\lambda_J(k)$. Hence, one might expect that a nonzero cross current affects a system with magnetic helicity, since an extremal magnetic helicity would require that the cross current has to vanish or a non-trivial cross-helicity would have to be present, which we will investigate here. As we discuss later on, in homogeneous isotropic turbulence, if the cross-helicity and cross current spectra are zero, then the cross current spectrum will remain zero. Consequently, one may wonder if systems with non-zero cross-scalar exhibit interesting behavior, especially in systems with magnetic helicity. Furthermore, if both the magnetic and cross helicity are extremal then also the kinetic helicity and the cross current have to be extremal. In the following we will discuss general basics about MHD turbulence for incompressible and compressible systems.

3.2 MHD turbulence

MHD turbulence is a form of turbulence which appears in a magnetized plasma. Hydrodynamic turbulence is generally describes a solution to the fluid equations which is chaotic, i.e. minor variations in the initial conditions lead to significant deviations in the evolution. These solutions generally require that the dissipative term is much smaller than the self-interaction term. Therefore, turbulence is only possible when

$$\left| \frac{\mathbf{v}\cdot\nabla\left(h\mathbf{v}\right)}{h} + \frac{\mathbf{v}}{h}\partial_\tau p + \frac{\nabla p}{h} - \frac{(\nabla\times\mathbf{B})\times\mathbf{B}}{4\pi h} \right| \gg \left| \nu\left(\nabla^2\mathbf{v} + \frac{1}{3}\nabla\left[\nabla\cdot\mathbf{v}\right]\right)\right| . \qquad (3.25)$$

Note that the overall equation has the dimension L/T^2, where L is a characteristic length scale, while T is a characteristic time scale of the system. The right side has the dimension $\nu/(LT)$. Consequently, multiplying both sides by T^2/L gives the dimensionless fluid equations where on the right side the numerical scaling factor $\nu T/L^2$ appears. The inverse of the scaling factor is also known as Reynolds number Re$= L^2/(T\nu)$. In hydrodynamic systems the Reynolds number can also be written as Re$= v_c L/\nu$, where

$v_c \sim L/T$ is a characteristic velocity scale. Note, that the above argument assumes that the pressure contribution ∇p is not considerably larger than the non-linear velocity contribution $\mathbf{v} \cdot \nabla \mathbf{v}$, otherwise the problem may, at least on first sight, be more complicated. This is in particular of interest in compressible systems. However, in MHD one also has to take into account an inhomogeneous magnetic field and hence a better estimate for the Reynolds number Re=$\max(v_c, b_c)L/\nu$. Again this argument is a slightly more complicated as it also requires a slight adjustment of the relevant scale L: $\max(v_c, b_c) \sim L/T$. A small Reynolds number Re$\ll$Re$_c$, where Re$_c$ is some critical Reynolds number, then implies that the damping is dominant and therefore the nonlinear and chaotic evolution is suppressed. On the other hand Re$\gg$Re$_c$ implies that the chaotic nature of the system is dominant and the system is turbulent.

The picture in MHD is even more complicated when one takes the evolution of the magnetic field itself into account. Magnetic fields themselves can also evolve in a chaotic manner if

$$\left|\frac{1}{4\pi\sigma}\nabla \times (\nabla \times \mathbf{B})\right| \ll |\nabla \times (\mathbf{v} \times \mathbf{B})| \,. \tag{3.26}$$

Analogously, to the hydrodynamic case, one can define a magnetic Reynolds number Re$_m$ $= 4\pi\sigma v_c L$. For the sake of comparison one typically introduces another number, the so called magnetic Prandtl number Pm=Re$_m$/Re= ν/η. If, Pm$\gg 1$ magnetic fields undergo less damping than the fluid motion, whereas for Pm$\ll 1$ it is the other way around. For systems with Pm$\gg 1$, the estimate for the kinetic Reynolds-number should be of the order of the max model, however in the opposite case one expects a more intermediary estimate for the initial kinetic Reynolds-number if $b_c \gg v_c$. Moreover, if the kinetic Reynolds number is sub-critical Re$\ll$Re$_c$ one expects that magnetic turbulence is typically suppressed even if Re$_m$ $\gg$Re$_c$. As we discuss explicitly later on, in the early universe Pm$\gg 1$ and Re$_m$ $\gg 1$ on respective horizon scale with $v \sim c_s$, but that is not generally the case for the kinetic Reynolds number.

As already mentioned with respect to the pressure term, technically the nature of the evolution of the system does not only depend on the Reynolds number but may also depend on the degree of vortical to dilatational motion in the flow and magnetic fields. Hence, there may be different types of turbulent evolution, as we briefly discuss in the following two subsections. As we discuss later on incompressible MHD turbulence maximally cross-helical systems with e.g. $\mathbf{v} = \mathbf{b}$ are highly deterministic as the non-linear evolution is effectively frozen in and the system only undergoes resistive and viscous dissipation, yet viscous dissipation may lead to the onset of non-linear evolution later on. Therefore, Re$\gg$Re$_c$ in general is not a sufficient criteria for the establishment of turbulence, yet in general it is typically a necessary condition for the appearance of turbulence. Ultimately, a deterministic analysis of turbulence is generally not useful, as precise knowledge of the initial conditions of the system of interest is usually not available. Typically, turbulent systems are compared on the basis of certain stochastic variables. In the following, we discuss the incompressible MHD equations and incompressible turbulence, thereafter we discuss compressible MHD. Here we also follow in part the books (Lesieur 2008, Biskamp 1993).

3.2.1 Incompressible MHD equations

Incompressible flows are flows, where the density along a fluid trajectory remains constant. From (2.53) it follows that the total derivative of the energy density is

$$(\partial_\tau + \mathbf{v} \cdot \nabla)\, \rho = -h\nabla \cdot \mathbf{v} - \mathbf{v} \cdot \nabla p. \tag{3.27}$$

Consequently the energy density along the fluid trajectory remains constant if $h\nabla \cdot \mathbf{v} = -\mathbf{v} \cdot \nabla p$. Hence, $\nabla \cdot \mathbf{v}$ is in general a higher order term in the fluctuating velocity, density or magnetic field, if the density along the flow remains unchanged. Therefore, the incompressibility condition in the perturbative limit reads $\nabla \cdot \mathbf{v} \approx 0$ and hence an incompressible flow is purely vortical. Obviously, a barotropic non-magnetized plasma can never develop into an incompressible or near-incompressible flow. Moreover, the incompressibility is generally ill-applied to systems with $v \gtrsim c_s$.

Taking the divergence of the velocity equation (2.65) one finds

$$\nabla \cdot \partial_\tau \mathbf{v} = -\nabla \cdot (\mathbf{v} \cdot \nabla)\, \mathbf{v} - \frac{\nabla^2 p}{h_b} + \frac{1}{h_b^2} \nabla h \cdot \nabla p + \frac{1}{4\pi h_b} \nabla \cdot ([\nabla \times \mathbf{B}] \times \mathbf{B}) \approx 0. \quad (3.28)$$

Note, that the term $\nabla h \cdot \nabla p$ is for barotropic flows a second order term in the pressure fluctuation and can therefore be neglected with respect to the ∇p term. Then, it becomes clear that the pressure fluctuations of a near incompressible flow are of $\mathcal{O}(v^2, b^2)$. The pressure fluctuation for an incompressible flow is

$$\nabla^2 p_t = -h_b \left(\nabla \cdot [\mathbf{v} \cdot \nabla]\right) \mathbf{v} + \frac{1}{4\pi} \left(\nabla \cdot [\mathbf{B} \cdot \nabla]\right) \mathbf{B}, \quad (3.29)$$

where $p_t = p + B^2/(4\pi)$. Hence, the incompressibility condition allows us to neglect variations of the radiation energy density and the specification of an equation of state in studying the evolution of velocity and magnetic field variations. This type of pressure has several interesting properties, first and foremost the "turbulent" pressure depends on the global properties of the flow, rather than just the local flow. Particularly, real space simulations can be numerically more difficult for incompressible flows than for compressible flows. Note that incompressible turbulence is a highly non-local phenomenon, as the change of the flow along a particle trajectory in ideal flows only depends on the pressure gradient, which is non-local. As already mentioned the constraint $\nabla \cdot \mathbf{v} = 0$ is only reasonable at first order in the velocity. For a hydrodynamic ideal flow, energy conservation together (2.53) with (3.29) gives

$$\nabla \cdot \mathbf{v} = -\frac{\partial_\tau \rho}{h} - \mathbf{v} \cdot \nabla \ln(h) = \frac{\partial_\tau}{c_s^2} \left(\frac{\nabla}{\nabla^2} \cdot [\mathbf{v} \cdot \nabla] \right) \mathbf{v} + \frac{1 + c_s^2}{c_s^2} \mathbf{v} \cdot \nabla \left(\frac{\nabla}{\nabla^2} \cdot [\mathbf{v} \cdot \nabla] \right) \mathbf{v}, \quad (3.30)$$

where we assumed a barotropic equation of state $p = c_s^2 \rho$. A dimensional analysis then yields

$$\nabla \cdot \mathbf{v} \sim \left(\frac{v_c}{c_s} \right)^2 \frac{v_c}{L}, \quad (3.31)$$

where L is again a characteristic length scale and v_c is a characteristic velocity and we used $\partial_\tau \sim v_c/L$. Consequently, the incompressibility condition can only be reasonable for subsonic flows $v^2 \ll c_s^2$. Generally $\nabla \cdot \mathbf{v} \neq 0$, yet for sufficiently subsonic flows $\nabla \cdot \mathbf{v} = 0$ may be a reasonable approximation. Note, that incompressibility is typically useful in vortical subsonic flows, yet in magnetically dominant MHD turbulence, it may prove insufficient as magnetic fields seed both solenoidal and dilatational velocity perturbations.

One interesting aspect of turbulence is that it typically develops in a self-similar manner and the energy spectrum generally is approximately described by a $k^{-2/3}$ Kolmogorov spectrum in the so-called inertial range in Fourier space (Kolmogorov 1941). As we mention later on, the energy spectrum of turbulence typically consists of a large scale tail and an injection scale or integral scale k_I, where most of energy scale is located, the inertial range and the dissipation scale, where the inertial range describes the range of scales where energy is transported from the injection to the dissipation scale k_d. The Kolmogorov scaling is found by simple dimensional argument. The kinetic energy density per enthalpy density has the units L^2/T^2. Moreover, the energy dissipation rate ϵ has the units L^2/T^3, the wave number has dimension L^{-1} and the viscosity has the units L^2/T. Then, the smallest relevant scale in the system due to dissipation should be of order

$$l_d \sim \left(\frac{\nu}{\epsilon^{1/3}}\right)^{3/4}. \tag{3.32}$$

Furthermore, assuming that the rate of energy-dissipation is scale independent, the spectral energy density has to be of order

$$E(k) \approx C_K \left(\frac{\epsilon}{k}\right)^{2/3}, \tag{3.33}$$

and we assumed homogeneity and isotropy. The constant C_K appearing in (3.33) is the Kolmogorov constant with a value of $\sim 1.5,\ 1.6$ (Yeung & Zhou 1997) in hydrodynamic 3D turbulence. The Kolmogorov constant in 3D MHD has larger values $C_K \sim 3,\ 4$ (Verma & Bhattacharjee 1995, Beresnyak 2011). Kolmogorov's law can be generalized to higher order correlation function, such that

$$S_p(k) \propto k^{-\zeta(p)}, \tag{3.34}$$

where S_p has been defined in real space in (3.1) and $\zeta(p) = p/3$ in the inertial range. In general, the energy dissipation rate is not scale-independent and one expects a slightly steeper spectrum. A correction to the above scaling is usually based on the assumption of log-normality on the stochastic distribution of the energy dissipation rate (Kolmogorov 1962, Frisch et al. 1978). In particular corrections for ζ_2 are minor and generally become only relevant for $p \gtrsim 4$ (Anselmet et al. 1984). This deviation is related to intermittency, non-Gaussianity, small-scale inhomogeneity and anisotropy of turbulent systems, see e.g. (Frisch 1991). As we discuss below this is an even bigger issue for compressible system than it is for incompressible systems, where the deviation towards Kolmogorov's law is primarily due to the different nature of energy transfer in strongly compressible systems. Intermittency is a well known feature of purely compressible initially Gaussian distributed density fluctuations in the matter dominated phase, where fragmentation due to gravitational instabilities triggers the appearance of structure in the universe and the basis of life as we know it (Peebles 1994). In principle such a deviation can effectively also be understood by the appearance of an additional dimensionless quantity like $(L/l_d)^\beta$. Then, there is a more direct impact of the small scale component on the overall energy transfer. Moreover, the influence of non-Gaussianity becomes increasingly relevant at smaller scales and for higher order correlation function. However, towards fourth order correlation function and at larger scales, the assumption of Gaussianity is overall reasonable and will be used later on as the so-called quasi-normal approximation (Lesieur 2008, ch. 5.8.4, 7.1). Note, that at small scales not only Gaussianity but also stochastic isotropy and inhomogeneity are questionable assumptions, but typically are expected too not impact the large-scale behavior in a significant manner.

Note, that Kolmogorov's law technically can also be applied in flows with a $\langle \mathbf{v} \rangle \neq 0$, by simply performing a Lorentz or Galilean transformation. Yet, for magnetic fields the system there are no similar invariant transformations for a state with non-zero to zero mean field. Consequently, the above argument is not applicable to magnetized systems, especially those with non-zero mean magnetic fields. Kolmogorov's law tells us about the scaling in the inertial range, however for us the scaling of the spectrum at scales much larger than the integral scale is also of particular interest. Furthermore, in the infrared part of the spectrum a k^5 spectrum generally appears in turbulent systems (Lesieur & Schertzer 1978, Caprini & Durrer 2002, Jedamzik & Sigl 2011), if the initial infrared tail has a much steeper slope like k^6. In principle, less steep infrared tails like k^4 do in general at least not on the largest scales develop into a k^5 slope.

For incompressible systems, one can express the MHD equations in a symmetric manner by introducing Elsässer variables $\mathbf{z}^\pm = \mathbf{v} \pm \mathbf{b}$. The MHD equations in terms of the Elsässer variables are

$$\frac{\partial \mathbf{z}^\pm}{\partial t} = -\left(\mathbf{z}^\mp \cdot \nabla\right) \mathbf{z}^\pm - \frac{\nabla p_t}{\rho_b + p_b} + \nu_+ \nabla^2 \mathbf{z}^\pm + \nu_- \nabla^2 \mathbf{z}^\mp \tag{3.35}$$

$$\nabla^2 p_t = -(p_b + \rho_b)\partial_i \partial_j z_i^+ z_j^- , \tag{3.36}$$

where $\nu_\pm = \nu \pm 1/(4\pi\sigma)$. Elsässer variables are particularly useful in studying systems with nontrivial stochastic alignments between velocity and Alfven fields. For example a system with an extremal cross helicity will have either $\mathbf{z}^+ = 0$ or $\mathbf{z}^- = 0$ and consequently one sees that such a system can only undergo viscous and resistive damping. In Fourier space the incompressible MHD equations are

$$\partial_\tau z_i^\pm(\mathbf{k}, \tau) = i P_{ij}(\mathbf{k}) \int \frac{\mathrm{d}^3\mathbf{q}}{(2\pi)^3} \mathbf{z}^\mp(\mathbf{p}) \cdot \mathbf{q} z_j^\pm(\mathbf{q}) - \nu_+ k^2 z_i^\pm(\mathbf{k}) - \nu_- k^2 z_i^\mp(\mathbf{k}). \tag{3.37}$$

Next, we will discuss some aspects of the more general compressible flow.

3.2.2 Compressible MHD

When one does not set $\nabla \cdot \mathbf{v} = 0$, the problem of compressible MHD turbulence arises. Now, on top of the six scalar and pseudoscalar two point functions that appear in incompressible MHD turbulence and are shown in section 3.1 there are three additional two-point scalar functions that appear in compressible MHD turbulence. For once the density autocorrelation two point function $\langle\delta\delta\rangle$ and the dilatational velocity correlation function $\langle v_d v_d\rangle$ appear. Moreover, one can also construct the density and dilatational velocity cross-correlation function $\langle\delta\nabla\cdot\mathbf{v}\rangle = -\langle\mathbf{v}\cdot\nabla\delta\rangle$. The equality is due to the assumption of isotropy since $\nabla\cdot\langle\mathbf{v}\delta\rangle = 0$. For convenience we introduce the density contrast δ defined by $\rho = \rho_b(1+\delta)$. Explicitly, we define the three additional cross correlation functions as

$$\langle v_d^i(\mathbf{k}) v_d^j(-\mathbf{k})\rangle = \frac{(2\pi)^6}{2\pi k^3} D_{ij}(\mathbf{k}) E_d(k), \tag{3.38}$$

$$\langle v_d^i(\mathbf{k})\delta(\mathbf{k})^*\rangle = -i\frac{k_i}{k}\frac{(2\pi)^6}{2\pi k^3}\frac{1+c_s^2}{c_s} E_{\delta v}(k), \tag{3.39}$$

$$\langle\delta(\mathbf{k})\delta(\mathbf{k})^*\rangle = \frac{(2\pi)^6}{2\pi k^3}\frac{(1+c_s^2)^2}{c_s^2} E_\delta(k), \tag{3.40}$$

where we have introduced the factor $(1+c_s^2)/c_s$ for convenience for relativistic fluids. Note, that one cannot construct additional non-reducible non-trivial two point functions for stochastically homogeneous and isotropic MHD turbulence. Moreover, the evolution equation for the density contrast is, following from (2.66),

$$\partial_\tau\delta = -(1+c_s^2)\left[(1+\delta)\nabla\cdot\mathbf{v} + \mathbf{v}\cdot\nabla\delta + \nu\nabla\cdot\left(\nabla\frac{v^2}{2} - \frac{2}{3}\mathbf{v}\nabla\cdot\mathbf{v}\right) + \frac{(\nabla\times\mathbf{b})^2}{4\pi\sigma}\right]. \tag{3.41}$$

Analogously, to the incompressible case one finds for the Elsässer variables

$$\begin{aligned}\partial_\tau\mathbf{z}^\pm =& -\mathbf{z}^\mp\cdot\nabla\mathbf{z}^\pm + c_s^2\nabla\cdot\mathbf{z}^\pm\left(z^\pm \mp \frac{z^+ - z^-}{2c_a}\right) - c_a(1-\delta)\nabla\delta + \nu^+\nabla^2\mathbf{z}^\pm + \nu^-\nabla^2\mathbf{z}^\mp \\ &+ \frac{\nu^+ + \nu^-}{3}\nabla\nabla\cdot\mathbf{z}^\pm,\end{aligned} \tag{3.42}$$

where $c_a = c_s^2/(1+c_s^2) = 1/4$ for $c_s^2 = 1/3$. The dilatational component can be simply isolated by applying the projector D_{ij}. In particular, for the purely dilatational two point Elsässer functions one finds

$$\langle\frac{k_i}{k} z_i^\pm(\mathbf{k}) z_j^\pm(-\mathbf{k})\rangle = \langle\frac{k_i}{k} z_i^\pm(\mathbf{k}) z_j^\mp(-\mathbf{k})\rangle, \tag{3.43}$$

meaning that the magnetic component, but also the solenoidal velocity vanishes in the correlation function of isotropic homogeneous turbulence if one of the components is dilatational. In compressible systems, the nature of turbulence is overall more complicated. Unlike for incompressible systems, first order terms like $\delta\nabla \cdot \mathbf{v}$ appear in the fluid equations. These first order terms are responsible for the acoustic nature of the compressible motion. Hence, on top of the non-linear evolution one also needs to take acoustic oscillations into account. Consequently, constructive or destructive interference of waves with similar wave-numbers plays a role in the non-linearity. Therefore, purely dilatational turbulence should be less chaotic than incompressible turbulence. As we discuss later on in more detail for non-relativistic super-sonic turbulence we expect for the spectrum of dilatational motion a spectrum that is stepper than a Kolmogorov's law with an inertial range scaling of k^{-1}. Moreover, one expects that due to the interference that energy transfer is considerably slower and the system remains longer in coherence.

On scales of the order of the CMB horizon ($\sim$ 200Mpc) the cosmological fluid in the radiation dominated phase is approximately incompressible (density perturbations $\delta \sim 10^{-5}$) (Planck Collaboration et al. 2018). Albeit, on small scales these perturbations are at best only poorly constrained, due to Silk damping (Jeong et al. 2014). Here, we only consider turbulent fluctuations with $v \ll c_s \sim c$, however this does not guarantee that incompressibility is a reasonable approximation, as one also requires appropriate initial conditions e.g. $E_s \gg E_d$. Additionally, incompressibility may not be reasonable in magnetically dominated MHD turbulence. Furthermore, in the matter dominated phase the incompressibility constraint becomes unreasonable due to gravitational instabilities. However, this is not a critical issue as the imprint of the evolution in the matter dominated phase is expected to be negligible. Next, we discuss unequal time correlation functions.

3.3 Unequal Time Correlations

In section 3.1 we discussed several different two-point correlation functions for isotropic homogeneous turbulence. However, in all of these cases we only looked at correlation functions of the type $\langle v_i(\mathbf{k},\tau)v_j(-\mathbf{k},\tau)\rangle$ and not at the more generally type of unequal time correlation functions $\langle v_i(\mathbf{k},\tau)v_j(-\mathbf{k},\tau')\rangle$. Unequal time correlations (UTC) play a important role in the generation of gravitational waves from MHD turbulence. For a recent review on UTCs in hydrodynamical turbulence see (He et al. 2017). In general the nature of UTCs depends on the type of observer. Here, we generally have a Eulerian viewpoint when studying MHD turbulence i.e. we are not studying the MHD turbulence from an observer that is comoving with the flow (Lagrangian viewpoint), but rather from a fixed viewpoint. Note, that for the structure functions of the equal time correlation function one only requires the assumption of isotropy and homogeneity. Yet, decorrelation requires us to solve the fluid equations at different times and compare how much the flow at different times but at the opposite point in Fourier space are related. Due to the chaotic nature of turbulence, one expects that for $\|\tau-\tau'\|\to\infty$ $\langle v_i(\mathbf{k},\tau)v_j(-\mathbf{k},\tau')\rangle\to 0$, even if turbulent energy is constantly injected into the system. A general Ansatz for the UTC in homogeneous isotropic turbulence is

$$\langle v_i(\mathbf{k},\tau)v_j(-\mathbf{k},\tau')\rangle = \langle v_i(\mathbf{k},\tau)v_j(-\mathbf{k},\tau)\rangle f(k,\tau,\tau'). \tag{3.44}$$

Hence, the function $f(k,\tau,\tau')$ describes how the system decorrelates. As mentioned an exact calculation generally requires some solution of the fluid equations, which is quite difficult. In general we discuss and apply a particular method here, in order to solve the fluid equations. This method that we discuss later is known as Eddy-Damped-Quasi-Normal-Markovian approximation (EDQNM). The EDQNM approximation can be used to evaluate equal time correlation functions. Yet, the approximation does not possess any memory, i.e. due to the Markovian Ansatz. Generally, other tools or models are required to gain insight into unequal time correlations, which we will only briefly mention here.

One of the first partially successful models for handling the chaotic nature of turbulence in a semi-analytical manner is Kraichnan's Direct Interaction Approximation (DIA) (Kraichnan 1959) and the Random Coupling Model (RCM) (Kraichnan 1961). The idea of these approaches lies in not directly solving the Navier-Stokes equation, but by introducing a random forcing term $\mathbf{f}$ and to solve the appearing stochastic equations in a perturbative manner for the changes of the velocity $\delta\mathbf{v}$ due to a small random forcing $\delta\mathbf{f}$ contribution. One famous problem of the DIA is that it predicts the scaling of the inertial range spectrum as $k^{-1/2}$, which is in conflict with the observation of a Kolmogorov scaling $k^{-2/3}$ in hydrodynamical turbulence. This problem has been resolved in Kraichnan's Lagrangian History DIA (LHDIA) (Kraichnan 1965*b*), where he studied the problem in terms of flow-comoving variables. Indeed the LHDIA reproduces the Kolmogorov spectrum, which is somewhat remarkable as the stochastic spatial properties of the flow at a given time should be identical in the different frameworks. The problem is generally due to the appearance of infrared divergences ($k \to 0$) in these methods, which in Kraichnan's DIA is partially resolved due to a partial re-summation of the divergence. Furthermore, there is one interesting key difference between the LHDIA and the DIA in that the LHDIA is invariant under so-called random Galilean transformations (RGT) of the velocity field. The RGT is a transformation of the type $\mathbf{v}(\mathbf{k}, \tau) \to \exp(-i\mathbf{k} \cdot \mathbf{u}\tau)\mathbf{v}(\mathbf{k}, \tau)$, where $\mathbf{u}$ is some random velocity with a Gaussian distribution with zero mean and standard deviation U. These transformations are also referred to as sweeping, and in general an invariance under RGT corresponds to an invariance under random sweeping. Note, that similar problems generally also plague different semi-analytical approaches, although progress is being made (Verma 2004, Zhou 2010). Here, and at other points in this thesis, we look at semi-phenomenological models in studying turbulence. In the following we discuss the random sweeping approximation as model for decorrelation.

3.3.1 Random sweeping approximation

One important phenomenological model in understanding turbulent decorrelation is based upon the above mentioned invariance under random sweeping in stochastic incompressible, isotropic and homogeneous turbulence. For an ideal hydrodynamic flow which is being swept by some spatially constant large scale velocity field $\mathbf{u}$, the evolution is described by (Kraichnan 1964)

$$\partial_\tau \mathbf{v}(\mathbf{k},\tau) \approx -i\mathbf{k}\cdot\mathbf{u}\mathbf{v}(\mathbf{k},\tau), \tag{3.45}$$

where we neglected the self-interaction and pressure term, which are negligible as long as $u \gg v$. Then, one has the simple solution

$$\mathbf{v}(\mathbf{k},\tau) = \exp\left[-i\mathbf{k}\cdot\mathbf{u}(\tau-\tau_0)\right]\mathbf{v}(\mathbf{k},\tau_0). \tag{3.46}$$

Therefore, one can now calculate the UTC two point function by plugging the above expression into $\langle v_i(\mathbf{k},\tau)v_j(-\mathbf{k},\tau')\rangle$. Furthermore, due to the randomness of the transformation one also has to average over the normal distributed velocity $\mathbf{u}$ with variance U^2. Consequently, one finds for the general unequal time velocity correlation function

$$\langle v_i(\mathbf{k},\tau)v_j(-\mathbf{k},\tau+\Delta\tau)\rangle = \exp\left(-\frac{1}{2}k^2U^2\Delta\tau^2\right)\langle v_i(\mathbf{k},\tau)v_j(-\mathbf{k},\tau)\rangle. \tag{3.47}$$

We refer to the time scale $\tau_E(k) = (kU)^{-1}$ as the Eulerian eddy turnover, as it measures for how long the turbulent system remains coherent. One obvious issue is the as of yet unspecified velocity scale. The most obvious Ansatz is the rms velocity of the turbulent flow, and generally best fitting to experiments and simulations is the one-dimensional rms-velocity e.g. $\langle v_1^2\rangle$. Hence, we set

$$\langle U^2\rangle = \frac{2}{3}\int_{-\infty}^{\infty} E_K(k)\mathrm{d}\ln(k) = \langle v_1^2\rangle. \tag{3.48}$$

Finally, the Eulerian eddy turnover rate can be approximated as

$$\tau_E(k) = \left[\frac{2}{3}k^2\int_{-\infty}^{\infty} E_K(q)\mathrm{d}\ln(q)\right]^{-1/2}. \tag{3.49}$$

Henceforth, the resulting decorrelation function for turbulent velocity fluctuations in incompressible homogeneous and isotropic turbulence is

$$f_{\mathrm{RSA}}(k,\tau,\tau') = \exp\left[-\frac{1}{2}\left(\frac{\tau-\tau'}{\tau_E}\right)^2\right]. \tag{3.50}$$

The above discussed sweeping effect has already been observed experimentally in the 50s (e.g. Favre 1965) and later also numerically (Rubinstein & He 2003, Dong & Sagaut 2008).

As, mentioned before in the Eulerian and Lagrangian framework decorrelation is different. In the Lagrangian framework the observer is comoving along a given fluid trajectory and hence the observer will not notice the effect of a Galilean transformation. Therefore, the random sweeping approximation is not a useful model for Lagrangian fluctuations. In particular, the overall description of decorrelation is similar, yet the details differ in several aspects. Firstly, decorrelation of the Lagrangian velocity correlation function can be described by simply replacing the Eulerian eddy turnover time by the Lagrangian eddy turnover time $\tau_E \to \tau_L$ in (3.50). One common approximation for the Lagrangian eddy turnover time, also known as local straining time, is (Frisch et al. 1974, Pouquet et al. 1976)

$$\tau_L^{-1}(k) \approx c_1\sqrt{\int_0^k qE(q)\mathrm{d}q}, \tag{3.51}$$

where c_1 is a coefficient of $\mathcal{O}(1)$. Since, the energy spectrum has to be equal in the Lagrangian and Eulerian framework of isotropic and homogeneous turbulence one requires that the time-scale over which energy transport is effective needs to be the same in both formulations. Due to the fact that sweeping is not of relevance for the Lagrangian decorrelation, the local straining time is anticipated to be the relevant time scale for energy transport in turbulence (Pouquet et al. 1976). The Gaussian decorrelation function (3.50) is a reasonable model for the initial description of decorrelation, yet becomes less reliable towards smaller scales $k \gg k_I$ and over longer time scales $\gtrsim \tau_E$. For example, the above model only allows for positive values f, yet negative values of f are also observed in simulations and in particular towards smaller scales the decorrelation function behaves like a damped oscillation (Rubinstein & He 2003). Note, as we discuss further below for the solenoidal component of the flow, negative values and oscillatory behavior may only have a minor relevance, whereas for the dilatational component it is far more important (Li et al. 2013). However, over the timescales for which $f \gtrsim 0.1$, the above approximation is very reasonable and reliable. Nonetheless, of interest are not only potential corrections to f but also to τ_E. The simple model (3.49) is reasonable for small scales but becomes a less reliable estimate of the decorrelation time-scale towards larger scales and also towards longer times scales.

Here we use the following correction, which also accounts for the pressure and non-liner velocity term based on the incompressibility constraint (Kaneda 1993)

$$U^2(k) = \int_{-\infty}^{\infty} h\left(\frac{q}{k}\right) E(q) \mathrm{d}\ln(q), \tag{3.52}$$

with

$$h(x) = \frac{1}{24}\left(13 - 8x^2 + 3x^4\right) + \frac{1}{16x}(1-x^2)^3 \ln\left[\frac{1+x}{|1-x|}\right]. \tag{3.53}$$

Note that the above correction, as mentioned, only takes the non-linear contributions at first order in the energy spectrum into account, factors like kinetic helicity however cannot be simply replaced by a scale independent sweeping velocity and as we see later on when explicitly discussing the EDQNM equations, terms like helicity appear as second order terms, which makes a simple approximation more complicated and therefore we do not discuss these factors here. More advanced approximations e.g. based on Pade-approximation (Kaneda et al. 1999) would significantly increase computation times and hence are not of interest here. However, it has been argued that a non-zero kinetic helicity leads to a reduction of the sweeping velocity and hence an increase in the timescale (Rubinstein & Zhou 1999). Next, we briefly discuss how decorrelation may appear and/or differ from the hydrodynamic description.

3.3.2 UTCs in MHD

So far we have neglected magnetic fields in the discussion, which further complicate the picture in several manners. For once, the MHD equations are not invariant under a Alfvenic Galilean transformation i.e. $\mathbf{b} \to \mathbf{b} + \mathbf{b}_0$, where $\mathbf{b}_0$ is a background field. This break in the invariance led to the assumption that in weak MHD turbulence $b_0^2 \gg \langle b^2 \rangle$, the inertial range scaling will follow the DIA prediction $k^{-1/2}$ in the inertial range, the so called Iroshnikov-Kraichnan spectrum, rather than the Kolmogorov spectrum (Iroshnikov 1964, Kraichnan 1965*a*).In particular the dominant time-scale for energy transfer would be of $\mathcal{O}(kb_0)^{-1}$ i.e. magnetic sweeping would dominate energy transfer. Therefore, one would expect a pile-up of energy at small scales compared to the case of strong Alfvenic ($b_0^2 \sim \langle b^2 \rangle$) incompressible MHD turbulence. However, the Iroshnikov-Kraichnan model is still an isotropic model, which is not the case in Alfvenic MHD turbulence due to the non-zero $\mathbf{b}_0$. Here we are only interested in cases where $\mathbf{b}_0 = 0$ and we are only interested in cases where the Pm$\gg$ 1. In particular, Goldreich and Sridhar (Goldreich & Sridhar 1995) find that even MHD turbulence with ($b_0^2 \sim \langle b^2 \rangle$) should show a Kolmogorov spectrum in the plane perpendicular to the mean flow, rather than the Iroshnikov-Kraichnan spectrum, which has also been observed in simulations (Müller et al. 2003, Müller & Grappin 2005, Brandenburg & Kahniashvili 2017). We will therefore assume, that the above hydrodynamic decorrelation model based on sweeping is also reliable for MHD turbulence, although we will account for magnetic sweeping in the eddy turnover time. Therefore, we also anticipate a Kolmogorov spectrum for isotropic MHD turbulence, as the magnetic sweeping effect is generally corrected by locally anisotropic nature of the energy-transfer. In general the nature of the UTCs in MHD turbulence can be far more variable. For example, the ideal maximally cross helical MHD equations are trivial, i.e. the flow does not change. In that case, one would expect that the decorrelation function is given by $f(k, \tau, 0) = 1$. For non-ideal systems one would still have decorrelation due to viscous and resistive damping for extremal cross helical states. Also, magnetic helicity will likely end up making the problem more complicated, since the conservation of magnetic helicity drives an inverse cascade of magnetic and henceforth kinetic energy, which should heavily modify the nature of decorrelation at large scales. Generally, the previously discussed RSA does not take the

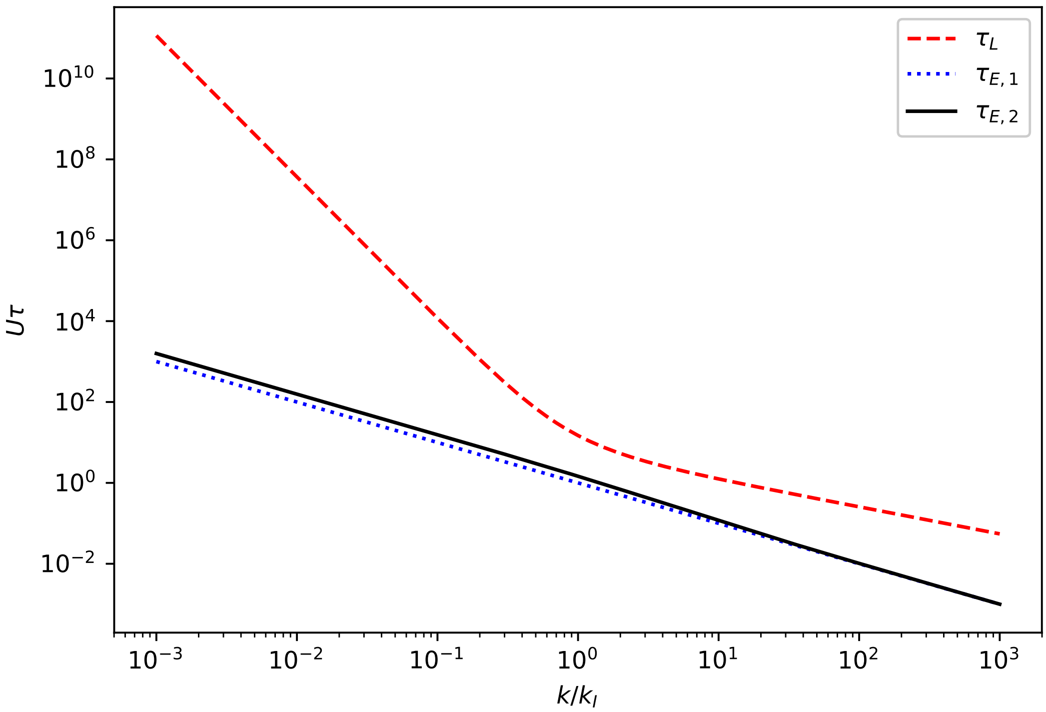

Figure 3.1: The Lagrangian eddy turnover time (3.51) (red, dashed) and the Eulerian eddy turnover time based on (3.52) (black, solid) and based on (3.49) (blue, dotted) normalized to $U = v_1$ as a function of the dimensionless wavenumber k/k_I for a Kolmogorov spectrum with a k^5 large scale tail.

turbulent energy transfer directly into account, yet as mentioned before the Lagrangian eddy turnover time is relevant for energy transfer and $\tau_L \gg \tau_E$ as can be seen in figure (3.1), although as discuss soon energy transfer itself can be effectively incorporated in a simple manner. However, for an inverse cascade energy transfer may occur on much shorter timescales than τ_L at scales $k \lesssim k_I$. Consequently, the impact of magnetic helicity should lead to significant modifications to the decorrelation and time scale, we will generally use a somewhat simplistic extended model for this purpose, yet we have not performed any full numerical simulations or experiments to check the reliability of these simple models in MHD, which is beyond the scope of the present thesis.

3.3.3 Decorrelation due to forcing

When we study the evolution of MHD turbulence, we are generally concerned with the free evolution, however when studying the generation of gravitational waves we also need to account for the generation of MHD turbulence, as we discuss later. Moreover, the above analysis only applies to freely decaying turbulence. Since we also consider the build-up of the turbulent spectrum, we require an estimate for the decorrelation at those times. A simple model is to assume that the turbulence gets produced by a purely randomized forcing (white noise). Then the change of the velocity is

$$\partial_\tau \mathbf{v}(\mathbf{k}, \tau) = \mathbf{w}(\mathbf{k}, \tau), \tag{3.54}$$

where $w(\mathbf{k}, \tau)$ is the random forcing.Since, white noise is uncorrelated we have

$$\langle w_i(\mathbf{k}, t') w_j(\mathbf{k}, t) \rangle \propto P\delta(t - t'), \tag{3.55}$$

where we assume that P, the average amplitude of the force, is constant in time. This gives then the decorrelation function for the forcing

$$f_{\mathrm{forc}}(\mathbf{k}, \tau, \tau') = \frac{\tau' - \tau_0}{\tau - \tau_0}, \tag{3.56}$$

for $\tau' < \tau$ and τ_0 is the time where the forcing is switched on.The above model is only applicable when the forcing dominates the non-linear evolution.

3.3.4 Decorrelation of dilatational fluctuations

So far, we have only focused on the incompressible UTC. For the dilatational flow component and purely compressible flows the problem is slightly more complicated. As discussed before, due to the primarily wave-like nature of dilatational fluctuations the non-linear transfer will be suppressed due to destructive interference. However, in the presence of solenoidal motion and magnetic fields, one generally expects that non-linear evolution will also affect dilatational motion. Due to the wave-like nature the decorrelation function for a purely dilatational flow will be a wave function like $\cos(c_s k\Delta\tau)$. This is also known as the linear wave propagation model (Lee et al. 1992). Nonetheless, solenoidal motion will also lead to sweeping of the dilatational fluctuations and this is described by the swept-wave model (Li et al. 2013). Thus, the resulting decorrelation function is

$$f_{\rm sw}(\mathbf{k},\Delta\tau,0) = \exp\left[-\frac{1}{2}\left(\frac{\Delta\tau}{\tau_E(k)}\right)^2\right]\cos\left[c_s k\Delta\tau\right],, \tag{3.57}$$

where the sweeping time scale τ_E depends only on the solenoidal velocity component and not on the dilatational component of the flow. As we discuss later, even for purely compressible turbulence more substantial rates of decorrelation may be present, i.e. some τ_E based on dilatational fluctuations and further studies are necessary, especially for $v \sim c_s$.

3.3.5 Summary of the different UTC functions

In the present section, we discussed that the decorrelation of velocity and magnetic field two point function is primarily due to the sweeping effect, which acts typically acts on a shorter time-scale than the energy-transport related local straining time, $\tau_E < \tau_L$. Then the unequal time two point correlation function for solenoidal velocity fluctuations is

$$\langle v_i^s(\mathbf{k},\tau')v_j^{s*}(\mathbf{q},\tau)\rangle = \exp\left[-\frac{(\tau'-\tau)^2}{2\tau_E^2(k,\tau)}\right]\frac{(2\pi)^6}{4\pi k^3}\delta(\mathbf{k}+\mathbf{q})\left[P_{ij}(\mathbf{k})E_s(k,\tau) - i\epsilon_{ijl}\frac{k^l}{k}H_K(k,\tau)\right]. \tag{3.58}$$

Similarly, the unequal time two point correlation function for Alfvenic fluctuations is

$$\langle b_i(\mathbf{k},\tau')b_j^*(\mathbf{q},\tau)\rangle = \exp\left[-\frac{(\tau'-\tau)^2}{2\tau_E^2(k,\tau)}\right]\frac{(2\pi)^6}{4\pi k^3}\delta(\mathbf{k}+\mathbf{q})\left[P_{ij}(\mathbf{k})E_b(k,\tau) - i\epsilon_{ijl}\frac{k^l}{k}H_b(k,\tau)\right], \tag{3.59}$$

and for the cross correlation two point function

$$\langle v_i(\mathbf{k},\tau')b_j^*(\mathbf{q},\tau)\rangle = \exp\left[-\frac{(\tau'-\tau)^2}{2\tau_E^2(k,\tau)}\right]\frac{(2\pi)^6}{4\pi k^3}\delta(\mathbf{k}+\mathbf{q})\left[P_{ij}(\mathbf{k})H_C(k,\tau) - i\epsilon_{ijl}\frac{k^l}{k}E_C(k,\tau)\right]. \tag{3.60}$$

Furthermore, the two point unequal time dilatational correlation function is

$$\langle v_d^i(\mathbf{k},\tau')v_d^j(\mathbf{q},\tau)\rangle = \frac{(2\pi)^6}{2\pi k^3}\exp\left[-\frac{(\tau'-\tau)^2}{\tau_E^2(k,\tau)}\right]\cos\left[c_s k(\tau-\tau')\right]\delta(\mathbf{k}-\mathbf{q})\frac{k_i k_j}{k^2}E_d(k,\tau). \tag{3.61}$$

Note, that as mentioned before these models are questionable for scenarios with magnetic helicity due to the inverse cascade as these models do not account for the energy transfer. In that case, we suggest the following simple correction for the UTC, e.g. in (3.58) one should replace $E_s(k,\tau)$ by $\sqrt{E_s(k,\tau)E_s(k,\tau')}$. Also, for a incompressible system with maximal cross helicity, one expects $\tau_E \to \infty$, due to the freeze-out of the flow. Additionally, we choose for the characteristic sweeping time

$$\tau_E^{-1}(k,\tau) = k\sqrt{\int_{-\infty}^{\infty} h\left(\frac{q}{k}\right)\max\left(E_s(q),E_b(q)\right)\mathrm{d}\ln(q)}, \tag{3.62}$$

where $h(x)$ has been defined in (3.53). Moreover, when the turbulence is forced, we consider for example for the velocity correlations the model

$$\begin{aligned}\langle v_i(\mathbf{k},\tau)v_j(-\mathbf{k},\tau')\rangle = &\left[\frac{\tau'-\tau_0}{\tau-\tau_0}\theta(\tau_m-\tau)+\frac{\tau'-\tau_0}{\tau_m-\tau_0}\theta(\tau_m-\tau')\theta(\tau-\tau_m)+\theta(\tau'-\tau_m)\right]\cdot\\ &\exp\left[-\frac{1}{2}\left(\frac{\tau-\tau'}{\tau_E(k,\tau)}\right)^2\right]\langle v_i(\mathbf{k},\tau)v_j(-\mathbf{k},\tau)\rangle,\end{aligned} \tag{3.63}$$

where τ_m is the time where the forcing stops and $\tau > \tau'$. In the following section, we discuss the aforementioned Eddy Damped Quasi Normal Markovian (EDQNM) approximation. Thereafter, we discuss the production of gravitational waves by MHD turbulence.

3.4 EDQNM approximation

So far we have discussed several key aspects of MHD turbulence, now we discuss a key method in studying MHD turbulence. In general, analytical models of turbulence are rather limited due to the chaotic nature of the problem. Similarly, direct numerical simulations are difficult to handle, as turbulence is a phenomenon which is only present for large scales L, since it requires Re= $vL/\nu \gg 1$, and one has to solve the equations over many grid-spacing's l_g e.g. $L \sim 1000 l_g$, yet this leads to a significant limitation in the resolvable scales especially when one is interested in the large scale dynamics these limitations can be quite problematic. Therefore, one also has to look at semi-analytical models to study MHD turbulence. These models come with their own limitations, yet they can be of additional assistance together with other methods to gain a better understanding of MHD turbulence. Of particular usefulness is the Eddy-Damped-Quasi-Normal-Markovian (EDQNM) approximation. First, we lay out the basics of the EDQNM approximation for incompressible systems and discuss later its generalization for compressible systems.

3.4.1 Incompressible spectral two point evolution functions

Due to the incompressibility, one requires at most 6 evolution functions for the different two point scalar and pseudo-scalar functions. We begin by looking at the Quasi-Normal part of the EDQNM approximation, also known as the Quasi-Normal approximation (Chou 1940, Millionshtchikov 1941) and the relevant spectral equations were for hydrodynamic non-helical turbulence were independently first derived by Proudman and Reid, and Tatsumi (Proudman & Reid 1954, Tatsumi 1957). Here, we generally use the Elsässer variables with the evolution equations 3.37. For convenience we then introduce the following spectral functions for the Elsässer variables, which are related to the previously defined two point spectra by

$$E^{\pm} = E_s + E_b \pm 2H_C, \quad E^R = E_s - E_b, \quad H^{\pm} = H_K + H_b \pm 2E_C, \quad H^R = H_K - H_b. \tag{3.64}$$

Then using 3.37 one finds the evolution equations for the different correlation functions

$$\left(\partial_\tau + 2k^2\nu^+\right) E^\pm(k) = 2k^3 P_{ib}(k) k_a \int \frac{\mathrm{d}^3\mathbf{q}}{(2\pi)^8}\ \mathrm{Im}\left[\langle z_i^\pm(-\mathbf{k}) z_a^\mp(\mathbf{p}) z_b^\pm(\mathbf{q})\rangle\right] - 2k^2\nu_- E^{\mathrm{R}}(k), \tag{3.65}$$

$$\left(\partial_\tau + 2k^2\nu^+\right) H^\pm(k) = 2k^2 \epsilon_{bil} k_l k_a \int \frac{\mathrm{d}^3\mathbf{q}}{(2\pi)^8}\ \mathrm{Re}\left[\langle z_i^\pm(-\mathbf{k}) z_a^\mp(\mathbf{p}) z_b^\pm(\mathbf{q})\rangle\right] - 2k^2\nu_- H^R(k), \tag{3.66}$$

$$\begin{aligned}\left(\partial_\tau + 2k^2\nu^+\right) E^{\mathrm{R}}(k) = k^3 k_a P_{ib}(k) \int \frac{\mathrm{d}^3\mathbf{q}}{(2\pi)^8}\ \mathrm{Im}\Big[&\langle z_i^+(\mathbf{k}) z_a^+(-\mathbf{p}) z_b^-(-\mathbf{q})\rangle \\ &- \langle z_i^-(-\mathbf{k}) z_a^-(\mathbf{p}) z_b^+(\mathbf{q})\rangle\Big] - k^2\nu_- \left(E^+(k) + E^-(k)\right),\end{aligned} \tag{3.67}$$

$$\begin{aligned}\left(\partial_\tau + 2k^2\nu^+\right) H^R(k) = k^2 k_a \epsilon_{bil} k_l \int \frac{\mathrm{d}^3\mathbf{q}}{(2\pi)^8}\ \mathrm{Re}\Big[&\langle z_i^-(-\mathbf{k}) z_a^-(\mathbf{p}) z_b^+(\mathbf{q})\rangle \\ &+ \langle z_i^+(\mathbf{k}) z_a^+(-\mathbf{p}) z_b^-(-\mathbf{q})\rangle\Big] - k^2\nu_- \left(H^+(k) + H^-(k)\right),\end{aligned} \tag{3.68}$$

where $\mathbf{p} = \mathbf{k} - \mathbf{q}$ and Im refers to the imaginary part, while Re refers to the real part of the three point functions. Generally, the transport of energy in turbulence occurs in triads where energy is shifted between all sets of the three modes $\mathbf{p}$, $\mathbf{k}$ and $\mathbf{p}$ withc $\mathbf{p} + \mathbf{q} = \mathbf{k}$. One obvious observation is that if the fluctuations are purely random i.e. distributed by a Gaussian function with zero mean, then the above equations reduce to a system of equations which can be easily solved and only describes resistive and viscous damping. Consequently, MHD turbulence is not a Gaussian process, yet nonetheless an initially near Gaussian velocity distribution function remains nearly Gaussian distributed (Anselmet et al. 1984, Lesieur 2008) in isotropic homogeneous turbulence. In total four different types of three point correlation functions appear in these equations. Similarly, one can now derive the evolution equation for the three point functions, which will require four point function and the evolution equation for the four point function in principle will require five point function and so on. Thus, one needs to solve an infinite number of equations, however one typical way of closing such a hierarchy of equations is to invoke a relation between higher and lower order correlation functions. For zero-mean Gaussian distributed velocity fields, any even higher order correlation function can be expressed in terms of two point functions, while any odd correlation function vanishes. Here, we invoke such a closure where we express the four point functions, which appear in the evolution equation of the three point functions, by a product of two point functions. Since the stochastic properties of the velocity fluctuations can in general not be described by a normal distribution, this is also known as Quasi-Normal approximation. The relation between the four-point and two-point function is known as Isserlis theorem (ISSERLIS 1916) and states

$$\langle ABCD\rangle = \langle AB\rangle\langle CD\rangle + \langle AC\rangle\langle BD\rangle + \langle AD\rangle\langle CB\rangle. \tag{3.69}$$

Here, the A, B, C, D are the components of the fields $\mathbf{z}^{\pm}$.

3.4.2 Schematic of the EDQNM approximation

In a schematic manner the three point functions are

$$\langle v_k v_q v_r\rangle(\tau) = \int_{\tau_0}^{\tau} d\tau' e^{-\left[\nu(k^2+q^2+r^2)(\tau-\tau')\right]} \sum_s \langle v_k v_q\rangle(\tau')\langle v_r v_s\rangle(\tau'), \tag{3.70}$$

where τ_0 is the initial time, the subscripts k, q, r and s are the different momenta and one sums or integrates over the different momenta s. Note that the above schematic is quite simplistic and neglects several important factors, which we also explore in further detail. One important thing to note is that in the limit $\nu \to 0$, the contributions of the two point functions at different times τ' are weighted in the same manner. The three point function and hence also the two-point functions have a very long memory, which is incompatible with the above discussed nature of decorrelations. The resulting equations were first solved by Ogura (Ogura 1963) for the kinetic energy and O'Brien and Francis for the evolution of the spectrum of a passive scalar (O'Brien & Francis 1962). In both cases the solutions became unphysical in that in both cases negative values appeared in the inertial range for the respective spectra. Hence, the QN approximation is non-realizable. The problem was first explained and understood by Orszag (Orszag 1970, Orszag 1977), and is due to over-blown three point functions which is due to the long memory times. And the non-Gaussianity in the four point function generally provides a damping for the three point functions, which is lost in the QN approximation. Other semi-analytical theories like the aforementioned DIA and LHDIA (Kraichnan 1959, Kraichnan 1965*b*) which apply the assumption of Gaussianity to the forcing, are realizable theories although the DIA fails in reproducing the Kolmogorov spectrum.

Kraichnan's DIA effectively leads to equations of the type

$$\langle v_k v_q v_r \rangle(\tau) = \int_{\tau_0}^{\tau} d\tau' e^{-\left[\nu(k^2+q^2+r^2)(\tau-\tau')\right]} G(\tau, \tau') \sum_s \langle v_k v_q \rangle(\tau') \langle v_r v_s \rangle(\tau'), \tag{3.71}$$

where $G(\tau, \tau')$ is the relevant Green's function which is calculated with the forcing at linear order in perturbation theory of a small Gaussian distributed forcing and associated change in the velocity. The approach is relatively extensive and numerically quite expensive and technically one would have to work with the LHDIA due to the mentioned problems of the DIA with respect to random sweeping. A key solution to the problem with the QN is to use a DIA inspired Ansatz by incorporating an additional Green's function into the evolution equations to provide the additional damping. Orszag (Orszag 1970) proposed a phenomenological model based on the eddy-turnover time to model the Green's function as $G \sim \exp(-\nu_d(q)(\tau - \tau'))$, where $\nu_d(q) \sim \sqrt{E(q)q^2}$ was taken as the eddy-turnover time. This model is also known as EDQN approximation, due to the additionally introduced eddy damping. However, this model still does not guarantee realizability. Consequently, another modification has been introduced, which is to markovianize the appearing energy spectra (Orszag 1977). Note that the eddy turnover time mentioned here is effectively the Lagrangian eddy turnover time, as it is directly related to the energy transfer. Thus, any significant change in $E(k)$ occurs within one eddy turnover time, yet the above EDQN model primarily takes contributions from within a relevant eddy turnover time into account and the eddy turnover time as defined in (3.51) is a growing function of the wave number. Hence, one can markovianize the appearing spectral functions with respect to the damping and one finds the EDQNM approximation, which is schematically given by

$$\langle v_k v_q v_r \rangle(\tau) = \int_{\tau_0}^{\tau} d\tau' e^{-\left[\left(\nu(k^2+q^2+r^2)+\nu_d(k)+\nu_d(q)+\nu_d(p)\right)(\tau-\tau')\right]} \sum_s \langle v_k v_q \rangle(\tau) \langle v_r v_s \rangle(\tau). \quad (3.72)$$

The EDQNM is a realizable model and it also reproduces the Kolmogorov spectrum in hydrodynamic turbulence and it is compared to models like the QN or the DIA and LHDIA less expensive to compute.

For MHD Pouquet (Pouquet et al. 1976) suggested the following damping factor

$$\nu_d(k) = c_1 \sqrt{\int_0^k \mathrm{d}q\, q\, (E^+(q) + E^-(q))} + c_2 \sqrt{k \int_0^k \mathrm{d}q E^{\mathrm{B}}(q)}, \quad (3.73)$$

where the first term corresponds to the eddy turnover time with coefficient c_1 and the second term corresponds to the Alfven effect c_2, which is related to the Iroshnikov-Kraichnan spectrum. Since recent numerical simulations suggest that incompressible isotropic homogeneous MHD turbulence is in several instances, but maybe not for all degrees of the different topological alignments, best described by a Kolmogorov spectrum (Müller et al. 2003, Brandenburg & Kahniashvili 2017) we will ignore the Alfven effect due to the local anisotropic correction in the energy transfer and set $c_2 = 0$. However, we stress again that a Kolmogorov that these are still not fully resolved issues in MHD modeling. The first term is the already discussed eddy turnover damping rate. For pure hydrodynamics, Kolmogorov's law implies $c_1 \sim 0.3$ based on a Kolmogorov constant of 1.5 (Pouquet et al. 1976). Yet, as mentioned before in MHD turbulence the Kolmogorov constant is larger and at the same time equipartition between magnetic and kinetic energy increases the value of c_1 by a factor $\sqrt{2}$ to around 0.42. Nonetheless, this is still smaller than that potentially expected value of c_1 for a Kolmogorov constant of ~ 3, hence we apply $c_1 = 0.45$ as an approximation for MHD, rather than $c_1 \sim 0.3$ to better accommodate MHD effects.

3.4.3 Incompressible MHD EDQNM equations

Now, we look at the explicit evolution equations for the three point functions

$$\begin{aligned}
&\Big(\partial_\tau + \nu_+(k^2 + k'^2 + q'^2)\Big)\,\langle z_i^{s_1}(\mathbf{k}) z_j^{s_2}(\mathbf{k}') z_l^{s_3}(\mathbf{q}')\rangle = \\
&- ik_a P_{ib}(\mathbf{k}) \int \frac{\mathrm{d}^3\mathbf{q}}{(2\pi)^3} \langle z_j^{s_2}(\mathbf{k}') z_l^{s_3}(\mathbf{q}') z_a^{-s_1}(\mathbf{p}) z_b^{s_1}(\mathbf{q})\rangle - \nu_- k^2 \langle z_i^{-s_1}(\mathbf{k}) z_j^{s_2}(\mathbf{k}') z_l^{s_3}(\mathbf{q}')\rangle \\
&- ik'_a P_{jb}(\mathbf{k}') \int \frac{\mathrm{d}^3\mathbf{q}}{(2\pi)^3} \langle z_i^{s_1}(\mathbf{k}) z_l^{s_3}(\mathbf{q}') z_a^{-s_2}(\mathbf{p}') z_b^{s_2}(\mathbf{q})\rangle - \nu_- k'^2 \langle z_i^{s_1}(\mathbf{k}) z_j^{-s_2}(\mathbf{k}') z_l^{s_3}(\mathbf{q}')\rangle \\
&- iq'_a P_{lb}(\mathbf{q}') \int \frac{\mathrm{d}^3\mathbf{q}}{(2\pi)^3} \langle z_i^{s_1}(\mathbf{k}) z_j^{s_2}(\mathbf{k}') z_a^{-s_3}(\mathbf{p}'') z_b^{s_3}(\mathbf{q})\rangle - \nu_- q'^2 \langle z_i^{s_1}(\mathbf{k}) z_j^{s_2}(\mathbf{k}') z_l^{-s_3}(\mathbf{q}')\rangle,
\end{aligned} \tag{3.74}$$

where $\mathbf{p}' = \mathbf{k}' - \mathbf{q}$ and $\mathbf{p}'' = \mathbf{q}' - \mathbf{q}$, and the signs s_1, s_2, s_3 are either $+$ or $-$ for the different three point functions. Also, all the appearing Elsässer variables are evaluated at time τ, as the time-argument has been neglected for the sake of visibility. For convenience, we neglect the ν_- damping term, as $\nu_- \sim \nu_+$ for the systems of interest and the deviations shall only have a minor effect on the precise details of the suppression of non-linear evolution around the damping scale and all the basic properties like the general suppression of turbulent evolution around the damping scale are still guaranteed, similar magnetic evolution is also dominated by the transfer of magnetic to kinetic energy at those scales. Thus, for simplicity we generally set the rate of viscous and resistive damping for all three point functions as $(\nu_+ + \nu_-)(k^2 + q^2 + p^2)$. This approach is generally not applicable for systems with small Prandtl-numbers, yet we do not look at such systems here. Taking equation (3.74) together with the eddy damping and markoviazation and evaluating the four point functions using Isserlis theorem (3.69) gives the EDQNM equations for the three point functions. Next, these three point function can be employed to evaluate the two point functions. A brief example, on how these terms are calculated is found in appendix A.1. For the rate of change of $E^+(k)$

given by (3.65) one finds

$$\begin{aligned}
\left[\partial_\tau + 2\nu_+ k^2\right] E^{\pm}(k) &= \frac{1}{2}\int_0^\infty \mathrm{d}q \int_{|k-q|}^{k+q} \mathrm{d}p \gamma(k,q,p,\tau) k^2 qp \Big[\Lambda_1(k,q,p)\tilde{E}^{\mp}(p)\tilde{E}^{\pm}(q) \\
&- \Lambda_2(k,q,p)\tilde{E}^R(p)\tilde{E}^R(q) + \Lambda_3(k,q,p)\tilde{E}^R(p)\tilde{E}^R(k) - \Lambda_4(k,q,p)\tilde{E}^{\mp}(p)\tilde{E}^{\pm}(k) \\
&- \Lambda_3(k,q,p)\tilde{E}^R(q)\tilde{E}^{\pm}(k) + \Lambda_2(k,q,p)\tilde{E}^R(k)\tilde{E}^{\pm}(q) - \Lambda_5(k,q,p)\tilde{H}^R(p)\tilde{H}^R(q) \\
&- \Lambda_6(k,q,p)\tilde{H}^R(p)\tilde{H}^R(k) + \Lambda_7(k,q,p)\tilde{H}^R(q)\tilde{H}^{\pm}(k) - \Lambda_8(k,q,p)\tilde{H}^R(k)\tilde{H}^{\pm}(q)\Big] \\
&- 2\nu_- k^2 E^R(k). \qquad (3.75)
\end{aligned}$$

Similarly, the EDQNM equations for the energy difference (3.67) read

$$\begin{aligned}
\left[\partial_\tau + 2\nu_+ k^2\right] E^R(k) &= \frac{1}{4}\int_0^\infty \mathrm{d}q \int_{|k-q|}^{k+q} \mathrm{d}p \gamma(k,q,p,\tau) k^2 qp \Big[2\Lambda_1(k,q,p)\tilde{E}^R(p)\tilde{E}^R(q) \\
&- \Lambda_2(k,q,p)\sum_{\pm}\tilde{E}^{\mp}(p)\tilde{E}^{\pm}(q) + \Lambda_3(k,q,p)\tilde{E}^R(p)\sum_{\pm}\tilde{E}^{\pm}(k) - \Lambda_4(k,q,p)\tilde{E}^R(k)\sum_{\pm}\tilde{E}^{\mp}(p) \\
&- 2\Lambda_3(k,q,p)\tilde{E}^R(q)\tilde{E}^R(k) + \Lambda_2(k,q,p)\sum_{\pm}\tilde{E}^{\mp}(k)\tilde{E}^{\pm}(q) - \Lambda_5(k,q,p)\sum_{\pm}\tilde{H}^{\pm}(p)\tilde{H}^{\mp}(q) \\
&- \Lambda_6(k,q,p)\tilde{H}^R(p)\sum_{\pm}\tilde{H}^{\pm}(k) + 2\Lambda_7(k,q,p)\tilde{H}^R(q)\tilde{H}^R(k) - \Lambda_8(k,q,p)\sum_{\pm}\tilde{H}^{\pm}(k)\tilde{H}^{\mp}(q)\Big] \\
&- \nu_- k^2 \sum_{\pm} E^{\pm}(k). \qquad (3.76)
\end{aligned}$$

Analogously, one finds for (3.66)

$$\begin{aligned}
\left[\partial_\tau + 2\nu_+ k^2\right] H^{\pm}(k) &= \frac{1}{2}\int_0^\infty \mathrm{d}q \int_{|k-q|}^{k+q} \mathrm{d}p \gamma(k,q,p,\tau) k^2 qp \Big[2\Lambda_9(k,q,p)\tilde{E}^{\mp}(p)\tilde{H}^{\pm}(q) \\
&+ \Lambda_{10}(k,q,p)\tilde{H}^R(p)\tilde{E}^R(q) + \Lambda_8(k,q,p)\tilde{E}^R(p)\tilde{H}^R(q) - \Lambda_6(k,q,p)\tilde{H}^R(p)\tilde{E}^R(k) \\
&+ \Lambda_3(k,q,p)\tilde{E}^R(p)\tilde{H}^R(k) - \Lambda_4(k,q,p)\tilde{H}^{\pm}(k)\tilde{E}^{\mp}(p) + \Lambda_7(k,q,p)\tilde{E}^{\pm}(k)\tilde{H}^R(q) \\
&- \Lambda_3(k,q,p)\tilde{E}^R(q)\tilde{H}^{\pm}(k) + \Lambda_2(k,q,p)\tilde{E}^{\pm}(q)\tilde{H}^R(k) - \Lambda_8(k,q,p)\tilde{E}^R(k)\tilde{H}^{\pm}(q)\Big] \\
&- 2\nu_- k^2 H^R(k). \qquad (3.77)
\end{aligned}$$

Lastly, one finds for the helicity difference (3.68)

$$\begin{aligned}
&\left[\partial_\tau + 2\nu_+ k^2\right] H^R(k) = \frac{1}{4}\int_0^\infty \mathrm{d}q \int_{|k-q|}^{k+q} \mathrm{d}p\gamma(k,q,p,\tau)k^2 qp\Big[4\Lambda_9(k,q,p)\tilde{E}^R(p)\tilde{H}^R(q) \\
&+ \Lambda_{10}(k,q,p)\sum_\pm \tilde{H}^\mp(p)\tilde{E}^\pm(q) + \Lambda_8(k,q,p)\sum_\pm \tilde{E}^\pm(p)\tilde{H}^\mp(q) - \Lambda_6(k,q,p)\tilde{H}^R(p)\sum_\pm \tilde{E}^\pm(k) \\
&+ \Lambda_3(k,q,p)\tilde{E}^R(p)\sum_\pm \tilde{H}^\pm(k) - \Lambda_4(k,q,p)\tilde{H}^R(k)\sum_\pm \tilde{E}^\mp(p) + 2\Lambda_7(k,q,p)\tilde{E}^R(k)\tilde{H}^R(q) \\
&- 2\Lambda_3(k,q,p)\tilde{E}^R(q)\tilde{H}^R(k) + \Lambda_2(k,q,p)\sum_\pm \tilde{E}^\pm(q)\tilde{H}^\mp(k) - \Lambda_8(k,q,p)\sum_\pm \tilde{E}^\mp(k)\tilde{H}^\pm(q)\Big] \\
&- \nu_- k^2 \sum_\pm H^\pm(k).
\end{aligned} \tag{3.78}$$

The notation $\sum_\pm g_\pm$ is read as $g_+ + g_-$. Additionally, here the ˜ refers to a spatial rescaling specifically $\tilde{E}(k) = E(k)/k^3$. Furthermore, the different scale dependent coefficients are given by

$$\begin{aligned}
\Lambda_1(k,q,p) &= k^2\left(1-c_{pk}^2\right)\left(1+c_{qk}^2\right), & \Lambda_2(k,q,p) &= k^2 c_{qk}c_{pk}\left(c_{pk}c_{qk}-c_{qp}\right), \\
\Lambda_3(k,q,p) &= q^2 c_{qk}c_{qp}\left(c_{qp}c_{qk}-c_{pk}\right), & \Lambda_4(k,q,p) &= q^2\left(1-c_{qp}^2\right)\left(1+c_{qk}^2\right), \\
\Lambda_5(k,q,p) &= k^2\left(c_{pk}c_{qk}-c_{qp}\right), & \Lambda_6(k,q,p) &= q^2\left(c_{qk}c_{qp}-c_{pk}\right), \\
\Lambda_7(k,q,p) &= q^2 c_{qp}\left(c_{pk}-c_{qk}c_{qp}\right), & \Lambda_8(k,q,p) &= k^2 c_{pk}\left(c_{qp}-c_{pk}c_{qk}\right), \\
\Lambda_9(k,q,p) &= k^2\left(1-c_{pk}^2\right)c_{qk}, & \Lambda_{10}(k,q,p) &= k^2 c_{qk}\left(c_{qp}-c_{qk}c_{pk}\right),
\end{aligned} \tag{3.79}$$

where the functions c_{pk}, c_{qk} and c_{qp} are the cosines of the interior angles opposite the triangle sides q, p and k:

$$c_{pk}(k,q,p) = \frac{p^2+k^2-q^2}{2pk}, \qquad c_{qk}(k,q,p) = \frac{q^2+k^2-p^2}{2qk}, \qquad c_{qp}(k,q,p) = \frac{k^2-p^2-q^2}{2qp}. \tag{3.80}$$

These coefficients result from the product of the different projection operators scale dependent coefficients. This set of equations constitutes the full EDQNM approximation in incompressible MHD and its different solutions are one of the key focuses of this thesis.

Moreover, the function $\gamma(k, q, p, \tau)$ is the integrated damping function

$$\gamma(k, q, p, \tau) = \frac{1 - \exp\left[-\left(\nu_d(k) + \nu_d(p) + \nu_d(q)\right)(\tau - \tau_0)\right]}{\nu_d(k) + \nu_d(p) + \nu_d(q)}, \tag{3.81}$$

where τ_0 is the time at which the free decay of turbulence begins and at time τ_0 the three point functions vanish and the stochastic nature of the velocity fluctuations is perfectly described by a normal distribution.

3.4.4 Large scale behavior of the EDQNM equations

Now, we also investigate the $k \to 0$ behavior for the scaling of the large scale tail of the spectrum. In the limit $k \to 0$, $p \to q \sim k_I \gg k$ provide the largest contributions. Consequently, one can neglect all terms where one of the spectral functions depends on k and this gives

$$\partial_\tau E^\pm(k) \approx \frac{k^3}{2} \int_0^\infty \mathrm{d}q \int_{|k-q|}^{k+q} \frac{\mathrm{d}p}{k} \gamma(0, q, p, \tau) qp \Big[\Lambda_1(k, q, p) \tilde{E}^\mp(p) \tilde{E}^\pm(q)$$
$$- \Lambda_2(k, q, p) \tilde{E}^R(p) \tilde{E}^R(q) - \Lambda_5(k, q, p) \tilde{H}^R(p) \tilde{H}^R(q)\Big]. \tag{3.82}$$

Note that the large-scale tail of the energy spectra is not affected by the cross scalar and $E^+(q)E^-(p) \sim E^+(q)E^-(q) \sim E_s^2 + E_b^2 + 2E_sE_b - 4H_C^2(q)$. Therefore, maximal cross helicity in a system with equipartition $E^R = 0$ and $H^R = 0$ implies that on large scales there is no change in the large scale tail. Next, we introduce the transformation $p = q + \epsilon k$ and use that in the limit $k \to 0$ $c_{qp} \approx -1$, $c_{qk} \approx -c_{pk} \approx \epsilon$ and find

$$\partial_\tau E^\pm(k) \approx \frac{k^5}{2} \int_0^\infty \mathrm{d}q \int_{-1}^{1} \mathrm{d}\epsilon \gamma(0, q, q, \tau) q^2 \Big[(1 - \epsilon^4) \tilde{E}^\mp(q) \tilde{E}^\pm(q)$$
$$+ (1 - \epsilon^2)\epsilon^2 \tilde{E}^R(q) \tilde{E}^R(q) + (1 - \epsilon^2) \tilde{H}^R(q) \tilde{H}^R(q)\Big]. \tag{3.83}$$

Performing the ϵ integration finally yields

$$\partial_\tau E^\pm(k) \approx k^5 \int_0^\infty \mathrm{d}q \gamma(0, q, q, \tau) q^2 \Big[\frac{4}{5}\left(\tilde{E}^+(q)\tilde{E}^-(q)\right) + \frac{2}{15}[\tilde{E}^R(q)]^2 + \frac{2}{3}[\tilde{H}^R(q)]^2\Big]. \tag{3.84}$$

One clear observation is that the large scale spectrum always develops a k^5 spectrum and that it only has a nonlinear growing mode, and in the limit $k \to 0$ it can never decay, as viscous or resistive decay becomes increasingly negligible towards large scales. Secondly, the large scale cross helicity has an even steeper spectrum than a k^5 large scale tail, since $\partial_\tau E^+(k) = \partial_\tau E^-(k)$ at large scales at $\mathcal{O}(k^5)$. This also implies that on the largest scales, totally maximal cross helical turbulence never appears by turbulent evolution itself. A similar analysis can be performed for the other spectra. For the energy difference at large scales one finds

$$\partial_\tau E^R(k) \approx k^5 \int_0^\infty \mathrm{d}q\gamma(0,q,q,\tau)q^2\Big[\frac{4}{5}[\tilde{E}^R(q)]^2 + \frac{2}{15}\left(\tilde{E}^+(q)\tilde{E}^-(q)\right) + \frac{2}{3}\left(\tilde{H}^+(q)\tilde{H}^-(q)\right)\Big]. \tag{3.85}$$

The rate of change of the energy difference is overall comparable to that of the $E^\pm$ spectra. Here we neglected all the terms that involve a spectral function at k, which is in general naive as one may have terms which scale in k as $E(k)$, however the cosine at zeroth order in k lead to vanishing coefficients for all the terms involving a spectrum at scale k and thus the above discussion does not change, when taking such terms into account. For the spectra $H^\pm$ and H^R this discussion is insufficient as all the ϵ integration at $\mathcal{O}(k^5)$ vanishes and one needs to take terms up to $\mathcal{O}(k)$ in the different cosine into account. At $\mathcal{O}(k)$ the cosines are $c_{qp} \approx -1$, $c_{qk} \approx \epsilon + (k/q)\epsilon^2/2$ and $c_{pk} \approx -\epsilon + (k/q)\epsilon^2/2$ in the limit $k \to 0$. Secondly, one can no longer neglect all terms which involve a spectral function at scale k and one requires to lowest order in k at least the terms with the coefficient Λ_6 and Λ_7. Thirdly, the term with spectral functions at p and q also give additional contribution due to Taylor series approximation of the spectral function at wave number p. Henceforth, we find for (3.77) in the limit $k \to 0$

$$\begin{aligned}\partial_\tau H^\pm(k) =& \frac{2}{15}k^6 \int_0^\infty \mathrm{d}q\gamma(0,q,q,\tau)q\Big[6\tilde{E}^\mp(q)\tilde{H}^\pm(q) - 2\tilde{H}^R(q)\tilde{E}^R(q) \\ &+ q\left(2\partial_q\tilde{E}^\mp(q)\tilde{H}^\pm(q) + \partial_q\tilde{H}^R(q)\tilde{E}^R(q) - \partial_q\tilde{E}^R(q)\tilde{H}^R(q)\right)\Big] \\ &+ \frac{1}{3}k\left[E^R(k) - E^\pm(k)\right]\int_0^\infty \mathrm{d}q\gamma(0,q,q,\tau)q^3\tilde{H}^R(q).\end{aligned} \tag{3.86}$$

One general thing to note is that the spectra $H^{\pm}$ and H^R (as we see below) develop a k^6 large scale spectrum, since the energies develop at most a k^5 and no shallower large scale tail as long as the initial spectra do not possess shallower large scale tails, which we assume here. Also, $\partial_\tau H^+ \neq \partial_\tau H^-$ implies that the large scale tail of the cross scalar also has a k^6 scaling. In particular, the appearance of a scaling term which is directly proportional to the energy spectra at wave-number k is noteworthy, since a trailing solution of the helicity with respect to the energies implies an exponential growth or decay. Now, for (3.78) we explicitly find

$$\begin{aligned}\partial_\tau H^R(k) =& \frac{1}{15}k^6 \int_0^\infty \mathrm{d}q \gamma(0,q,q,\tau) q \Big[12\tilde{E}^R(q)\tilde{H}^R(q) - 2\sum_{\pm} \tilde{H}^{\pm}(q)\tilde{E}^{\mp}(q) \\ &+ q\left(4\partial_q \tilde{E}^R(q)\tilde{H}^R(q) + \sum_{\pm}\partial_q \tilde{H}^{\pm}(q)\tilde{E}^{\mp}(q) - \sum_{\pm}\partial_q\tilde{E}^{\pm}(q)\tilde{H}^{\mp}(q)\right)\Big] \\ &+ \frac{2}{3}E_b(k)k\int_0^\infty \mathrm{d}q\gamma(0,q,q,\tau)q^3\tilde{H}^R(q). \end{aligned} \tag{3.87}$$

The large scale estimate of the cross helicity spectrum also requires higher order corrections, yet a calculation with the above first order corrections indicates that the large scale tail of the cross helicity has a steeper scaling than k^6. However, we anticipate e.g. simply due to the appearance of second derivatives that the symmetry between $\partial_\tau E^+$ and $\partial_\tau E^-$ for $k \to 0$ is broken at the k^7 level. Hence, cross helicity without an initially shallower spectrum may develop a k^7 large scale tail, while the cross scalar, magnetic and kinetic helicity may develop a k^6 large scale tail and the kinetic and magnetic energy may develop a k^5 large scale tail. Consequently all the pseudo-scalar functions appearing in MHD have a steeper large scale spectrum by a factor k than their associated scalar. Similarly, the cross scalar and the cross helicity have a steeper scaling by a factor k compared to respectively the other scalar and pseudo-scalar functions. Furthermore, the change of the magnetic helicity directly proportional to $E(k)$ corresponds to

$$\partial_\tau H_b(k) \propto -\frac{1}{3}E_b(k)k\int_0^\infty \mathrm{d}q\gamma(0,q,q,\tau)\left(H_K(q) - H_b(q)\right). \tag{3.88}$$

Also, on large scale ($k \to 0$) one has $E_b(k,\tau)k = \zeta(\tau)|H_b(k,\tau)|$. Of particular interest is the case $\zeta(\tau_0) \sim 1$, which effectively corresponds to near maximal magnetic helicity. Due to the maximal helicity and helicity conservation constraint one anticipates $\zeta(\tau) \sim 1$ at later times. Consequently, one anticipates in the case of near maximal helicity

$$\partial_\tau H_b(k) \propto \frac{1}{3}|H_b(k)| \int_0^\infty \mathrm{d}q\gamma(0,q,q,\tau)\left(H_b(q) - H_K(q)\right), \tag{3.89}$$

such that

$$H_b(k,\tau) \propto \exp\left[\mathrm{sgn}[H_b(k,\tau)] \int_{\tau_0}^{\tau} \frac{\mathrm{d}\tau'}{3} \int_0^\infty \mathrm{d}q\gamma(0,q,q,\tau')\left(H_b(q,\tau') - H_K(q,\tau')\right)\right]. \tag{3.90}$$

Note, that for $H_K(k) = H_b(k)$ there is no change in the large scale magnetic helicity. Since the timescale for energy transfer scales as $v(k_I)k_I \propto \tau^{-1}$ and all the factors in the integral primarily depend on the quantities at k_I, one expects that the integral scales with $\int \mathrm{d}\tau/\tau$ and the large scale magnetic helicity follows a power law $H_b(k,\tau) \propto \tau^\beta$. For an inverse cascade one explicitly requires

$$\mathrm{sgn}[H_b(k,\tau)] \int_0^\infty \mathrm{d}qH_b(q,\tau') \gtrsim \mathrm{sgn}[H_b(k,\tau)] \int_0^\infty \mathrm{d}qH_K(q,\tau'). \tag{3.91}$$

Therefore, if both the kinetic helicity and magnetic helicity have the same sign, than at first the kinetic helicity would have to either change sign or decay substantially, in case of a prior dominance, in order for an inverse cascade to be established Next, we briefly discuss one important aspect of the spectral evolution in turbulence, which is self-similarity in the evolution, i.e. in high Reynolds number systems, the spectrum at a given point can be related to the spectrum at a later time by scaling relations.

3.4.5 Self-similar Evolution

As discussed before, due to viscous dissipation and turbulent energy transport the different turbulence spectra evolve and the overall energy decays, as long as there is no injection of energy. In particular, this evolution can become self-similar (de Karman

& Howarth 1938, Lesieur & Schertzer 1978). Thus, the early and late evolution of the spectra are related by scaling laws and the energy spectrum at a given time, as soon as the evolution is self-similar, may be written as

$$E(k,\tau) = E_A \left(\frac{\tau}{\tau_D}\right)^a F\left(\frac{k}{k_I(\tau)}\right) \tag{3.92}$$

where $k_I(\tau)$ is the evolving integral scale, E_A is the initial amplitude of the energy spectrum, F is a spectral function that describes the shape of the spectrum, a is a power law index, τ_D is the effective evolution time scale, i.e. the initial local straining time. Additionally, the rate of change of the energy for incompressible systems corresponds to terms of the type

$$\partial_\tau v^2 \sim \mathbf{v}\cdot\mathbf{k}v^2 \sim kv^3. \tag{3.93}$$

Furthermore $v^2 \sim \int \mathrm{d}\log(k)E(k)$ and one finds roughly

$$k_I(\tau) \sim k_I(\tau_0)\left(\frac{\tau}{\tau_D}\right)^{-(1+a/2)}. \tag{3.94}$$

Now, we look at (3.84) and define

$$\begin{aligned}\partial_\tau C_{LS}(\tau) &= k^{-5}\partial_\tau E^{\pm}(k)\\ &\approx \int_0^\infty \mathrm{d}q\gamma(0,q,q,\tau)q^2\Big[\frac{4}{5}\left(\tilde{E}^+(q)\tilde{E}^-(q)\right) + \frac{2}{15}[\tilde{E}^R(q)]^2 + \frac{2}{3}[\tilde{H}^R(q)]^2\Big],\end{aligned} \tag{3.95}$$

which is scale independent for large scales and only depends on time. Therefore, we expect the following relation to hold for self-similar evolution

$$C_{LS}(\tau) = C_{LS}(\tau_0)\left(\frac{\tau}{\tau_D}\right)^\gamma, \tag{3.96}$$

with

$$\gamma = \frac{\partial\log(C_{LS})}{\partial\log(\tau)}. \tag{3.97}$$

Then we have

$$\left(\frac{k_I(\tau)}{k}\right)^s E(k,\tau) \propto \left(\frac{k_I(\tau)}{k}\right)^s \tau^a F^{\pm}(k/k_I) \propto \tau^{-s(1+a/2)+a} \propto \tau^{\gamma}, \tag{3.98}$$

where $s = 5$ and $k \ll k_I$. Thus we find the scaling relations

$$k_I(\tau) \propto \tau^{-b} = \tau^{-(2+\gamma)/(s+2)} \tag{3.99}$$

$$E(k,\tau) \propto \tau^a = \tau^{2(\gamma-s)/(s+2)} F(k/k_I(\tau)), \tag{3.100}$$

where we used $b = 1 + a/2$ In the case that the initial large scale tail follows a shallower power law k^c than k^5, we have $\gamma = 0$ and $s = c < 5$. As mentioned before, one has $\gamma > 0$ in cases where the large scale tail appears due to the turbulent evolution. For the normal cascade, one usually finds $\gamma \sim 0$, as we see later, is a reasonable approximation, yet for an inverse cascade this is not the case. In particular, for $\gamma = 0$, corresponding to the conservation of the Loitsiansky constant (Batchelor & Proudman 1956), and $s = 5$, we find $b = 2/7$ and $a = -10/7$. The conservation of magnetic helicity implies $b^2/k_I \propto$const and leads to $a = -2/3$ and $b = 2/3$. Therefore, for a system with extremal magnetic helicity and $s = 5$ we expect $\gamma \approx 8/3$. One particular case where the above considerations are likely not applicable is that of extremal cross helicity, since there is no evolution and one expects $a \sim b = 0$ and the evolution is practically only due to direct decay, although as noted before the natural occurring large scale tail of the cross helicity spectra is expected to follow a k^7 rather than a k^5 slope and thus there is the potential for a deviation, as such a system is not expected to evolve in a purely extremal manner over all large scales. Often, $\gamma = 0$ is chosen and one varies s to accommodate the different scenarios (Brandenburg & Kahniashvili 2017, e.g.). For example, the scaling behavior of extremal magnetic helicity corresponds also to $s = 1$ and $\gamma = 0$. Next, we use some of the tools discussed here and apply them in part to a discussion about compressible systems.

3.4.6 Compressible contributions

In the previous sections, we primarily looked at the case $\nabla \cdot \mathbf{v} \approx 0$, although we also discussed some basics about compressible systems in subsection 3.2.2. As mentioned before in the context of the fluids and flows discussed here, the incompressibility constraint may be substantially violated even if $v \ll c_s$ particularly for a radiation dominated magnetized fluid. Note, that here we primarily focus on incompressible flows, but it is nonetheless important to have a better grasp on potential flaws of this approximation and their impact. Again one important difference between compressible and incompressible systems are additional linear terms in the evolution equations other than the dissipative terms. These terms are responsible for the wave-like nature of dilatational modes and generally the implied comparably short interference times of $\mathcal{O}(1/(c_s k))$, which for subsonic systems are always much smaller than the relevant eddy turnover time. Hence, in subsonic purely compressible systems energy transfer is dominated by acoustic oscillations and interference generally suppresses the non-linear transfer.

In incompressible hydrodynamical turbulence and also in several instances in MHD turbulence, one expects that the inertial range of the energy spectra has a $k^{-2/3}$ Kolmogorov spectrum. Yet, for compressible hydrodynamic energy spectra, this may not be the case. The rate of the non-linear energy transfer is effectively of the order $kv(k)$ at scale k and the frequency of a sound wave is $c_s q$ at scale q. A substantial non-linear energy transfer requires at least $kv(k) \gtrsim c_s q$. For supersonic flows this can be easily satisfied for a large range of modes k for a given q. Yet, for subsonic flows $k \gg q$ is a criteria for the modes involved in a comparably substantial transfer of energy. Note that the largest possible value of q of relevance for energy transfer is that of the dissipation scale k_d. This implies for purely compressible turbulence that any somewhat substantial non-linear energy transfer requires a inertial range with a length of about $k_d/k_I \sim c_s/v(k_d)$. Furthermore, one expects a scale dependent suppression of the energy transfer rate of $\mathcal{O}(v(k)/c_s)$. This implies that the energy transfer rate of strongly compressible systems behaves as $\epsilon \to \epsilon(k) \propto \epsilon_0 v(k)/c_s$, where ϵ_0 is some scale independent energy transfer rate. Plugging this re-scaling of the energy transfer rate into (3.33) gives

$v^2 \propto k^{-1}$ for strongly compressible systems. Note, that by this argument the value of ϵ_0 may also directly depend on the Reynolds number and the ratio $c_s/v(k_I)$.

Now, we take a more detailed look on the overall dynamics. The solutions for the linearized ideal compressible MHD equations (3.41) and (3.42) for $v, b \ll c_s$ are

$$\mathbf{v}_d(\mathbf{k}, \tau) = \mathbf{v}_{d,0}(\mathbf{k}) \cos\left(c_s k\tau + \phi_0\right), \tag{3.101}$$

$$\delta(\mathbf{k}, \tau) = \delta_0(\mathbf{k}) \sin\left(c_s k\tau + \phi_0\right), \tag{3.102}$$

where δ_0, $\mathbf{v}_{d,0}$ and ϕ_0 are dependent initial conditions for the amplitudes and phase. Note that the dynamically relevant timescale for nonlinear transfer is $kv(k) \gg c_s k$ and so any substantial subsonic purely dilatational flow is at most only mildly affected by deviations to the above solution. The only effective type of transfer is that of resonant interactions of the compressible modes and as we discuss these may play an important role in partially vortical or magnetized flows. If we neglect non-linearity in the evolution, the solutions for the three compressible two point functions (3.38), (3.39) and (3.40) are

$$E_d(k, \tau) = \bar{E}_d(k, \tau) \cos^2\left(c_s k\tau + \zeta(k, \tau)\right), \tag{3.103}$$

$$E_{\delta v}(k, \tau) = \frac{1}{2}\bar{E}_d(k, \tau) \sin\left(2c_s k\tau + 2\zeta(k, \tau)\right), \tag{3.104}$$

$$E_\delta(k.\tau) = \bar{E}_d(k, \tau) \sin^2\left(c_s k\tau + \zeta(k, \tau)\right), \tag{3.105}$$

where $\bar{E}_d(k)$ is the envelope spectrum for the dilatational energy spectrum. We expect that these relations hold for substantially subsonic flows with $v, b \ll c_s$, and that the above relation holds even in the presence of vorticity, as non-linear effects act on much larger time-scales. Note that we have introduced two time dependent parameters, since not only the envelope spectrum may develop due to non-linear evolution but also an overall phase-shift $\zeta(k, \tau)$ due to the non-linear terms may appear. Here, we assume that the above relations hold and the problem of compressible MHD reduces from $9 \to 8$ partially independent two point functions. If we further neglect the phase shift we have another reduction down to effectively seven relevant evolution equations. We also introduce $\phi(k,\tau) = c_s k\tau + \zeta(k,\tau)$. The relevant evolution equation for the envelope spectrum is then given by

$$\partial_\tau \bar{E}_d = \partial_\tau (E_d + E_\delta). \tag{3.106}$$

For the envelope spectrum the relevant Green's function is effectively the same as for the solenoidal spectra, i.e. it only represents damping. Although, as we see below the problem for the appearing and relevant three-point functions is more complicated and involves many more equations, although mostly due to only minor variations. Analogously, for the phase shift one finds

$$\partial_\tau \zeta = \frac{\sin(4\phi)}{4}\partial_\tau \bar{E}_d + \cos(2\phi)\partial_\tau E_{\delta v} + \sin(2\phi)\partial_\tau (E_\delta - E_d). \tag{3.107}$$

In the discussion here, we will neglect the phase shift $\zeta(k,\tau)$ for now and assume that it will not have any relevant impact on the dynamics. The different equations, that involve purely compressible components, are of the type

$$\partial_\tau o_i = i\Omega_{ij} o_j + g_i(\tau), \tag{3.108}$$

where Ω_{ij} can be a symmetric or anti-symmetric matrix depending on the choice of the o_i which is a vector e.g. of the different three point functions and g_i is some source vector of the different four point functions in the case that the o_i are three point functions. The matrix Ω_{ij} simply describes the linear coupling between the different types of compressible n-point functions, as we discuss below. For an initially Gaussian system, e.g. for the case that the o_i represent three point function which initially vanish at time τ_0, one finds

$$o_i(\tau) = S^{-1}_{ij} \exp\left(-i\omega_j(\tau - \tau_0)\right) \int_{\tau_0}^{\tau} \mathrm{d}\tau' \exp\left(i\omega_j(\tau' - \tau_0)\right) S_{jm} g_m(\tau'). \tag{3.109}$$

For the case that the o_i only consist of three point functions which only involve the compressible components δ and v_d the unique eigenvalues up to a sign are

$$\omega_1 = c_s(k+q+p), \quad \omega_2 = c_s(k-q+p), \quad \omega_3 = c_s(k+q-p), \quad \omega_4 = c_s(k-q-p) \quad (3.110)$$

and the number of the independent purely compressible three-point equations is 8 ($= 2 \cdot 3 + 2$). The other four eigenvalues correspond to the negative frequencies of the already shown, e.g. $\omega_5 = -\omega_1$ and so on. Explicitly, the components of the o_i are three point functions of the type $\langle v_d(\mathbf{k})v_d(\mathbf{q})v_d(\mathbf{p})\rangle$, $\langle \delta(\mathbf{k})\delta(\mathbf{q})\delta(\mathbf{p})\rangle$, $\langle v_d(\mathbf{k})v_d(\mathbf{q})\delta(\mathbf{p})\rangle$ and $\langle v_d(\mathbf{k})\delta(\mathbf{q})\delta(\mathbf{p})\rangle$, where the last two appear effectively threefold due to the three distinguishable permutations of the wave-vector arguments. Another class of solutions are three point functions where one component is solenoidal, like $\langle v_s(\mathbf{k})v_d(\mathbf{q})v_d(\mathbf{p})\rangle$, $\langle v_s(\mathbf{k})\delta(\mathbf{q})v_d(\mathbf{p})\rangle$ and $\langle v_s(\mathbf{k})\delta(\mathbf{q})\delta(\mathbf{p})\rangle$. Note that there are several different three point functions of this type e.g. also $\langle b(\mathbf{k})\delta(\mathbf{q})\delta(\mathbf{p})\rangle$ and with permutations of the different wave-vectors. However, each of the different cases of this type can be expressed as a four dimensional system with eigenvalues $\pm c_s(q-p)$ and $\pm c_s(q+p)$. Lastly, one also has the case that only one of the appearing components in the three point functions is dilatational e.g. the o_i are of the type $\langle v_s(\mathbf{k})v_s(\mathbf{q})v_d(\mathbf{p})\rangle$ and $\langle v_s(\mathbf{k})v_s(\mathbf{q})\delta(\mathbf{p})\rangle$. Then, the frequency is $\pm c_s p$ and the dimension of this system is 2. As before there are several different o_i like $\langle b(\mathbf{k})v_s(\mathbf{q})\delta(\mathbf{p})\rangle$ and with permutations of the wave-vectors. Similarly, for o_i that contain different compressible two point functions $E_d(k)$, $E_\delta(k)$ and $E_{\delta v}(k)$, the eigenvalues of the system are $\pm c_s k$ and the dimension of the system is 3, and one may need to add $o_i(\tau_0)$ to the right hand side of (3.109) as the two point functions may have a non-trivial initial condition. Moreover, purely solenoidal three point functions are treated as for the incompressible and only the related four point functions differ. In order to markovize and deal with non-physical features, as for the incompressible case, one also needs to introduce an additional damping term. Thus, the above Green's function has to be modified to

$$\exp\left[-(\nu(k,q,p) + i\omega_j)(\tau - \tau_0)\right] \int_{\tau_0}^{\tau} \mathrm{d}\tau' \exp\left[(\nu(k,q,p) + i\omega_j)(\tau' - \tau_0)\right], \qquad (3.111)$$

where $\nu(k,q,p)^{-1}$ measures the effective turbulent correlation time at the wave numbers k,q,p. The markovization should only be applied to the function $\bar{E}_d$ and not to the cos and sin functions. We assume that $\nu(k,q,p) \sim \nu_d(k,q,p)$ as for the incompressible case, yet it now also needs to include a factor based on the dilatational velocity (with potentially different coefficients).

No.	**Triple Correlation**	**related four point functions**
T0	$\langle[\mathbf{v}_s,\mathbf{b}][\mathbf{v}_s,\mathbf{b}][\mathbf{v}_s,\mathbf{b}]\rangle$	$\langle[\mathbf{v}_s,\mathbf{b}][\mathbf{v}_s,\mathbf{b}]\rangle\langle[\mathbf{v}_s,\mathbf{b}][\mathbf{v}_s,\mathbf{b}]\rangle$
T1	$\langle[\mathbf{v}_d,\delta][\mathbf{v}_s,\mathbf{b}][\mathbf{v}_s,\mathbf{b}]\rangle$	$\langle[\mathbf{v}_s,\mathbf{b}][\mathbf{v}_s,\mathbf{b}]\rangle\langle[\mathbf{v}_s,\mathbf{b}][\mathbf{v}_s,\mathbf{b}]\rangle$,$\langle[\mathbf{v}_d,\delta][\mathbf{v}_d,\delta]\rangle\langle[\mathbf{v}_s,\mathbf{b}][\mathbf{v}_s,\mathbf{b}]\rangle$
T2	$\langle[\mathbf{v}_d,\delta][\mathbf{v}_d,\delta][\mathbf{v}_s,\mathbf{b}]\rangle$	$\langle[\mathbf{v}_d,\delta][\mathbf{v}_d,\delta]\rangle\langle[\mathbf{v}_d,\delta][\mathbf{v}_d,\delta]\rangle$,$\langle[\mathbf{v}_d,\delta][\mathbf{v}_d,\delta]\rangle\langle[\mathbf{v}_s,\mathbf{b}][\mathbf{v}_s,\mathbf{b}]\rangle$
T3	$\langle[\mathbf{v}_d,\delta][\mathbf{v}_d,\delta][\mathbf{v}_d,\delta]\rangle$	$\langle[\mathbf{v}_d,\delta][\mathbf{v}_d,\delta]\rangle\langle[\mathbf{v}_d,\delta][\mathbf{v}_d,\delta]\rangle$

Table 3.1: Types of three point functions (second row) and their assoicated Gaussian four point functions (thrid row) in compressible isotropic, homogeneous and barotropic MHD turbulence. The bracket e.g. $[\mathbf{v}_d,\delta]$ is a place-holder for either δ or $\mathbf{v}_d$.

For the rest of this subsection, we discuss qualitatively the different types of three point functions that appear in compressible MHD turbulence as listed in table 3.1 and focus on the types T1, T2 and T3. First, the type T3 only appears in the evolution of compressible two point functions and a significant energy transfer may be possible for triads with e.g. $\omega_i - c_s(k \pm q) \approx 0$ or if the oscillatory behavior after temporal integration of the three point function is e.g. of the type $\cos^2(c_s k\tau)$ and without an effectively canceling complement like $-\sin^2(c_s k\tau)$, such that on average the contribution does not vanish. The former criteria can only be fulfilled if one of the wave-numbers involved is sufficiently small and the other two are sufficiently large or in certain cases where $p \sim k \sim q$. In the first case, one expects relevant contributions for wave-numbers $k \sim \mathcal{O}(k_I c_s/v(k_I))$ for a range of wave-numbers $c_s|q-p| \sim qv(q)$ (or permutations of k,q,p). While in the latter case one may have conditions of the type $|2k-2q+p| \sim kv(k)$ for $k \sim q \sim p$. One thing to note is that the range of relevant wave numbers that involve significant non-linear contributions in purely compressible systems is much smaller than in the incompressible case for $v \ll c_s$. Furthermore, terms of the type T3 should not lead to an effective transport of energy in substantially subsonic systems. Note that due to the reduced range of modes that contribute, the rate of energy transfer in compressible turbulence is roughly smaller by a factor $v(k)/c_s$ compared to the rate in incompressible turbulence.

When the system is initially purely incompressible, the generation of dilatational motion is due to three point functions of the type T1 i.e. a compressible component at scale k and two solenoidal components appear in the relevant three-point function. As mentioned before, in that case one has $\omega_i = c_s k$. Consequently, the initial generation of dilatational motion can only be effective at large scales $k \lesssim k_I c_s/v(k_I)$ in substantially subsonic systems. Thereafter, a significant amplification is possible, as terms involving e.g. $\langle \mathbf{v}_d \mathbf{v}_d \rangle(\mathbf{k}) \langle \mathbf{v}_s \mathbf{v}_s \rangle(\mathbf{q})$ can lead to resonant contributions e.g. oscillatory functions of the type $\sin^2(c_s k(\tau - \tau_0))$ which do not trivially vanish on average and contribute as an important channel for a transfer of solenoidal to dilatational energy. These types of three point functions also contribute to the other direction, i.e. a transfer of dilatational to solenoidal energy in an efficient manner. Such transfer terms imply that the incompressibility condition $\nabla \cdot \mathbf{v} \lesssim (v/c_s)^2 k_I v(k_I)$ may not be realistic, and one has to expect considerably larger fractions of dilatational to solenoidal energy even for $v \ll c_s$ with respect to the incompressibility constraint. Lastly, one also has to consider the other mixed three point function T2. As for T1, T2 can appear in all two-point evolution equations, however four point functions that are quadratic in the purely compressible two point functions e.g. $E_d E_\delta$ that appear in the evolution of T2 cannot contribute to the rate of change of the two point functions. This is due to the fact that an irrotational and non-magnetized barotropic MHD system cannot generate any vorticity or magnetic fields. The appearance of such terms would otherwise imply that there is a back-reaction contribution from dilatational on solenoidal motion which leads to either a generation of magnetic or vortical energy or to a dilatational energy transfer, which is forbidden. Hence, three point functions of the type T2 do not impact the evolution of the different two point functions by four point functions of the type $\bar{E}_d^2$. However, three point functions of the type T2 can still impact the evolution of the two point functions by four point functions of the type $\bar{E}_d E_s$. Note, these functions suffer from similar structural constraints as those of type T3, meaning they may at most be relevant for only a relatively small range of wave-numbers q or p or on very large scales. Therefore, only the type T1 may have a substantial impact on compressible turbulence in addition to the purely solenoidal three point functions T0. Note that the impact of functions of type T1 on the evolution of $\bar{E}_d$ is of the type $\partial_\tau \bar{E}_d(k) \propto \bar{E}_d(k)c(k,\tau)$, where $c(k,\tau)$ depends on the solenoidal spectra. Consequently, these terms do not directly provide any non-linear coupling between the dilatational spectra at different scales and these terms cannot act as an initial source of dilatational motion, which is due to less-efficient three-point functions like T2 and T3 and the other class of contributions from T1, i.e. the purely solenoidal four point functions. Overall, this indicates that it may suffice to only take three point functions of the type T0 and T1 and some sufficiently small generic source term for $\bar{E}_d(k)$, e.g. based on a k^{-1} spectrum, into account, as well as a sink term for the solenoidal energies, in order to ascertain energy conservation, into account.

In conclusion, even in substantially subsonic turbulence compressible factors can play a role in the evolution, due to an effective transfer of energy between dilatational and solenoidal modes, and they may even play an important role at large scales. However, in this thesis we will mostly neglect these compressible effects and focus primarily on the incompressible system, yet we note that compressible effects may play a nontrivial and important role even in substantially subsonic homogeneous and isotropic MHD. In the following we briefly discuss the large scale behavior of purely compressible turbulence as an example.

3.4.7 Compressible Large Scale Behavior

The case of a purely compressible turbulent system can be studied self-consistently for MHD turbulence, as no magnetic fields and vorticity are generated if none is previously present. For convenience we introduce

$$\bar{\delta} = \frac{c_s}{1+c_s^2}\delta, \quad \mathbf{v}_d(\mathbf{k}) = \frac{\mathbf{k}}{k} v_d(\mathbf{k}) \tag{3.112}$$

with $v_d^*(\mathbf{k}) = -v_d(-\mathbf{k})$. Explicitly for this case the vector o_i for the relevant three point functions can be constructed as

$$\begin{aligned}\mathbf{o} = \Big(& v_d(\mathbf{p})v_d(\mathbf{q})v_d^*(\mathbf{k}),\ \bar{\delta}(\mathbf{p})v_d(\mathbf{q})v_d^*(\mathbf{k}),\ v_d(\mathbf{p})\bar{\delta}(\mathbf{q})v_d^*(\mathbf{k}),\ \bar{\delta}(\mathbf{p})\bar{\delta}(\mathbf{q})v_d^*(\mathbf{k}) \\ & v_d(\mathbf{p})v_d(\mathbf{q})\bar{\delta}^*(\mathbf{k}),\ \bar{\delta}(\mathbf{p})v_d(\mathbf{q})\bar{\delta}^*(\mathbf{k}),\ v_d(\mathbf{p})\bar{\delta}(\mathbf{q})\bar{\delta}^*(\mathbf{k}),\ \bar{\delta}(\mathbf{p})\bar{\delta}(\mathbf{q})\bar{\delta}^*(\mathbf{k})\Big)\end{aligned} \tag{3.113}$$

and the matrix Ω_{ij} is symmetric and given by

$$\Omega = c_s \begin{bmatrix} \mathbf{A} & k\mathbb{1}_4 \\ k\mathbb{1}_4 & \mathbf{A} \end{bmatrix}, \quad \mathbf{A} = -\begin{bmatrix} 0 & p & q & 0 \\ p & 0 & 0 & q \\ q & 0 & 0 & p \\ 0 & q & p & 0 \end{bmatrix},$$

where $\mathbb{1}_4$ is the 4×4 identity matrix. The rate of change of the dilatational energy corresponds to (see (3.106))

$$\begin{aligned}\partial_\tau \langle v_d(\mathbf{k})v_d^*(\mathbf{k}) + \bar{\delta}(\mathbf{k})\bar{\delta}^*(\mathbf{k})\rangle = \int \frac{\mathrm{d}^3\mathbf{q}}{(2\pi)^3} c_{qk} \Big[&(c_{qp}q - c_s^2 p)\mathrm{Im}\langle o_1\rangle \\ &+ (1+c_s^2)\left(k\mathrm{Im}\langle o_7\rangle - q\mathrm{Im}\langle o_4\rangle\right)\Big],\end{aligned} \tag{3.114}$$

where the different o_i are given in (3.113). Note that unlike for the incompressible equations, the compressible equations have an explicit dependence on c_s^2 and thus a relativistic plasma may behave differently than a non-relativistic gas or plasma $c_s \ll 1$. In the limit $k \ll k_I$ we find (also see subsection 3.4.4)

$$\begin{aligned}\partial_\tau \bar{E}_d(k) \propto & k^3 \int_0^\infty \mathrm{d}q \int_{-1}^1 \mathrm{d}\epsilon\, qp\epsilon \Big[-(q + c_s^2 p)\mathrm{Im}\langle o_1\rangle \\ &+ (1+c_s^2)\left(k\mathrm{Im}\langle o_7\rangle - q\mathrm{Im}\langle o_4\rangle\right)\Big].\end{aligned} \tag{3.115}$$

In order to estimate the large scale behavior we have to look at the functions g_i in detail, as is done in appendix A.2. The key takeaway there is that one expects $\bar{E}_d(k) \propto k^5$ at large scales ($k \ll k_I$). One potential and important difference in particular for supersonic systems should be the appearance of an effective evolution equation of the type $\partial_\tau \bar{E}_d(k) \propto \bar{E}_d(k)$. Otherwise, as argued before, in appendix A.2 we do not find other terms that could suggest important non-linear energy transfer in substantially subsonic purely compressible turbulence. Thus as discussed in subsection 3.3.4, we also expect that the discussed decorrelation model for compressible correlations should be reliable in substantially subsonic turbulence, but not necessarily for $v \gtrsim c_s$.

3.5 Quasi-normal GW equation

In the following we focus on the generation of a stochastic background of gravitational waves by MHD turbulence. First, we briefly look at the rate of change of gravitational wave energy density.

3.5.1 Gravitational wave energy density

The strain of the gravitational wave is as discussed before described by (2.31)

$$\partial_\tau^2 \tilde{H}_{ij}(\mathbf{k},\tau) + 2\mathcal{H}\partial_\tau \tilde{H}_{ij}(\mathbf{k},\tau) + k^2 \tilde{H}_{ij}(\mathbf{k},\tau) = 16\pi G a^{-2}\left(\rho^b + p^b\right) P_{ijlm}\left[\pi_{lm}(\mathbf{k}) + \pi_{lm}^{\text{em}}(\mathbf{k})\right], \tag{3.116}$$

where π_{lm} and π_{lm}^{em} are given by (2.30) and (2.32) respectively. We fix the initial conditions, such that the initial strain vanishes $H_{ij}(\mathbf{k},\tau_0) = 0$ and there are no initial source terms present $\partial_\tau H_{ij}(\mathbf{k},\tau_0) = 0$. This equation has the following solution

$$H_{ij}(\mathbf{k},\tau) = 16\pi G\left[A_{ij}(\mathbf{k},\tau)\frac{\sin(k\tau)}{k\tau} - B_{ij}(\mathbf{k},\tau)\frac{\cos(k,\tau)}{k\tau}\right], \tag{3.117}$$

where

$$A_{ij}(\mathbf{k},\tau) = \int_{\tau_0}^{\tau} a^{-2}(\tau')\cos(k\tau')\tau'\pi_{ij}^T(\mathbf{k},\tau')\mathrm{d}\tau' \tag{3.118}$$

and

$$B_{ij}(\mathbf{k},\tau) = \int_{\tau_0}^{\tau} a^{-2}(\tau')\sin(k\tau')\tau'\mathrm{d}\pi_{ij}^T(\mathbf{k},\tau')\tau' \tag{3.119}$$

with

$$\pi_{ij}^T(\mathbf{k},\tau) = P_{ijlm}(\mathbf{k})(\rho_b + p_b)\int \frac{\mathrm{d}^3\mathbf{q}}{(2\pi)^3}\left[v_l(\mathbf{q},\tau)v_m(\mathbf{p},\tau) + b_l(\mathbf{q},\tau)b_m(\mathbf{p},\tau)\right], \qquad (3.120)$$

where

$$P_{ijlm}(\mathbf{k}) = P_{il}(\mathbf{k})P_{jm}(\mathbf{k}) - \frac{1}{2}P_{ij}(\mathbf{k})P_{lm}(\mathbf{k}) \qquad (3.121)$$

is the Fourier transform of the quadratic projector (2.22). Then the change of the strain is

$$\partial_\tau H_{ij}(\mathbf{k},\tau) = \frac{16\pi G}{k\tau^2}\left[A_{ij}(\mathbf{k},\tau)\left(k\tau\cos(k\tau) - \sin(k\tau)\right) + B_{ij}(\mathbf{k},\tau)\left(k\tau\sin(k\tau) + \cos(k\tau)\right)\right]. \qquad (3.122)$$

Consequently, one finds for the two point correlation function of the temporal rate of change of the strain tensor

$$\begin{aligned}\langle|\partial_\tau H_{ij}(\mathbf{k},\tau)|^2\rangle = \left(\frac{16\pi G}{k\tau^2}\right)^2 \Big[&\langle|A_{ij}(\mathbf{k},\tau)|^2\rangle\left(k\tau\cos(k\tau) - \sin(k\tau)\right)^2 \\ &+ \langle|B_{ij}(\mathbf{k},\tau)|^2\rangle\left(k\tau\sin(k\tau) + \cos(k\tau)\right)^2 \\ &+ \left(\langle B_{ij}(\mathbf{k},\tau)A_{ij}(-\mathbf{k},\tau)\rangle + \langle A_{ij}(\mathbf{k},\tau)B_{ij}(-\mathbf{k},\tau)\rangle\right)\cdot \\ &\left(k\tau\cos(k\tau) - \sin(k\tau)\right)\left(k\tau\sin(k\tau) + \cos(k\tau)\right)\Big], \end{aligned} \qquad (3.123)$$

where the averaging only affects the A_{ij} and B_{ij} and specifically only the π_{ij}^T element there. Hence, this can be restated more clearly as

$$\langle|\partial_\tau H_{ij}(\mathbf{k},\tau)|^2\rangle = \left(\frac{16\pi G}{\tau}\right)^2 \int_{\tau_0}^{\tau}\frac{\mathrm{d}\tau'\ \tau'}{a^2(\tau')}\int_{\tau_0}^{\tau}\frac{\mathrm{d}\tau''\ \tau''}{a^2(\tau'')}F_O(k,\tau,\tau',\tau'')\langle\pi_{ij}^T(\mathbf{k},\tau')\pi_{ij}^T(-\mathbf{k},\tau'')\rangle, \qquad (3.124)$$

where

$$\begin{aligned}F_O(k,\tau,\tau',\tau'') =& \cos(k[\tau-\tau'])\cos(k[\tau-\tau'']) + \frac{1}{k^2\tau^2}\sin(k[\tau-\tau'])\sin(k[\tau-\tau'']) \\ &- \frac{1}{k\tau}\left[\cos(k[\tau-\tau'])\sin(k[\tau-\tau'']) + \cos(k[\tau-\tau''])\sin(k[\tau-\tau''])\right]. \end{aligned} \qquad (3.125)$$

Here, we are only interested in modes which are well within the horizon such that the averaging procedure in the definition of the energy is applicable. Consequently, we focus on the case $k\tau \gg 1$ and thus the oscillatory function can be approximated as

$$F_O(k, \tau, \tau', \tau'') \approx \cos(k[\tau - \tau']) \cos(k[\tau - \tau'']) \approx \frac{1}{2} \cos(k[\tau' - \tau'']), \tag{3.126}$$

where we averaged over a few $k\tau$ in the last step. Note, that the correlation function $\langle \pi^T_{ij}(\mathbf{k}, \tau')\pi^T_{ij}(-\mathbf{k}, \tau'')\rangle$ is a four point function in the velocity and magnetic fluctuations, yet unlike the four point functions appearing in the quasi-normal MHD approximation, this one involves unequal time velocity and magnetic correlation functions. In the QN MHD approximation magnetic and velocity variations are described by a multivariate Gaussian distribution at fourth order, which allows us to apply Isserlis theorem (3.69) . As discussed before, the fluctuations are not Gaussian and this may play an even bigger role for the unequal four point functions. Here, we assume that the assumption of Gaussianity is also a reasonable approximation for higher order unequal time correlation functions, which as discussed before is reasonable for the two point function, and that Isserlis theorem is also to the unequal time correlation function, even though the prerequisites are not fully met. We suspect that deviations due to non-Gaussianity in the unequal time four point correlation functions will be minor or at most relevant at small scales $k \ll k_I$, that are usually of less interest to us. The appearing four point correlation function corresponds to

$$\begin{aligned}&\langle \pi^T_{ij}(\mathbf{k}, \tau')\pi^T_{ij}(-\mathbf{k}, \tau'')\rangle = (\rho_b + p_b)^2 P_{mngh}(\mathbf{k}) \int \frac{\mathrm{d}^3\mathbf{q}}{(2\pi)^3} \int \frac{\mathrm{d}^3\mathbf{q}'}{(2\pi)^3} \cdot \\ &\langle [v_m(\mathbf{q}, \tau')v_n(\mathbf{p}, \tau') + b_m(\mathbf{q}, \tau')b_n(\mathbf{p}, \tau')] \, [v_g(\mathbf{q}', \tau'')v_h(\mathbf{p}', \tau'') + b_g(\mathbf{q}', \tau'')b_h(\mathbf{p}', \tau'')]\rangle,\end{aligned} \tag{3.127}$$

where $\mathbf{p} = \mathbf{k} - \mathbf{q}$ and $\mathbf{p}' = \mathbf{k} - \mathbf{q}'$. Next, we apply Isserlis theorem together with (3.58), (3.59), (3.60) and (3.61) to find

$$\langle \pi_{ij}^T(\mathbf{k},\tau')\pi_{ij}^T(-\mathbf{k},\tau'')\rangle = (\rho_b + p_b)^2 \frac{(2\pi)^4}{4} \int \frac{\mathrm{d}^3\mathbf{q}}{(qp)^3} \Big[E_t^2(q,p,\tau')S^+(k,q,p)$$
$$+ 4H_t^2(q,p,\tau')c_{qk}c_{pk} + S^-(k,q,p)\Big(4E_d(q,\tau')E_d(p,\tau')\cos\left[c_s q(\tau'-\tau'')\right]\cos\left[c_s p(\tau'-\tau'')\right]\Big)$$
$$+ 2\Big(D(k,q,p)E_s(q,\tau')E_d(p,\tau')\cos\left[c_s p(\tau'-\tau'')\right]$$
$$+ D(k,p,q)E_s(p,\tau')E_d(q,\tau')\cos\left[c_s q(\tau'-\tau'')\right]\Big)\Big], \tag{3.128}$$

where c_{pk} and c_{qk} are the cosine of the interior angles as defined in (3.80) and

$$E_t^2(q,p,\tau) = E_s(q,\tau)E_s(p,\tau) + E_b(q,\tau)E_b(p,\tau) + 2H_C(q,\tau)H_C(p,\tau) \tag{3.129}$$
$$H_t^2(q,p,\tau) = H_b(q,\tau)H_b(p,\tau) + H_k(q,\tau)H_K(p,\tau) + 2E_C(q,\tau)E_C(p,\tau) \tag{3.130}$$
$$S^{\pm}(k,q,p) = \left(1 \pm c_{qk}^2\right)\left(1 \pm c_{pk}^2\right) \tag{3.131}$$
$$D(k,q,p) = (1 + c_{qk}^2)(1 - c_{qp}^2). \tag{3.132}$$

The gravitational wave density power spectrum then becomes

$$P_G(k,\tau) = \frac{2H_0^2\bar{\Omega}_r^{\,2}}{3\pi}\frac{a^2k^3}{\tau^2}\int \frac{\mathrm{d}^3\mathbf{q}}{(qp)^3}\int_{\tau_0}^{\tau}\frac{\mathrm{d}\tau'\ \tau'}{a^2(\tau')}\int_{\tau_0}^{\tau}\frac{\mathrm{d}\tau''\ \tau''}{a^2(\tau'')}\cos\left(k[\tau'-\tau'']\right)\cdot$$
$$f_{\mathrm{RSA}}(q,\tau',\tau'')f_{\mathrm{RSA}}(p,\tau',\tau'')\Big[E_t^2(q,p,\tau')S^+(k,q,p) + 4H_t^2(q,p,\tau')c_{qk}c_{pk}$$
$$+ 2\Big(D(k,q,p)E_s(q,\tau')E_d(p,\tau')\cos\left[c_s p(\tau'-\tau'')\right]$$
$$+ D(k,p,q)E_s(p,\tau')E_d(q,\tau')\cos\left[c_s q(\tau'-\tau'')\right]\Big) + 4S^-(k,q,p)\Big(E_d(q,\tau')E_d(p,\tau')\cdot$$
$$\cos\left[c_s q(\tau'-\tau'')\right]\cos\left[c_s p(\tau'-\tau'')\right]\Big)\Big], \tag{3.133}$$

where we used $\rho_b + p_b = (4/3)\rho_c\bar{\Omega}_r$ in the radiation dominated phase and $\bar{\Omega}_r$ is the modified radiation energy density parameter, and the function f_{RSA} is the decorrelation function as defined in (3.50). The modified radiation energy is $\bar{\Omega}_r = \Omega_r(g_0/g(T_0))^{1/3}$, where $g(\tau_0)$ represents the initial relativistic degrees of freedom at time τ_0 and $g_0 = 3.36$ represents the present day relativistic degrees of freedom. Above, one has to perform two time integrations from τ_0 to τ and the appearing times τ' and τ'' are not ordered e.g. one has the two cases $\tau' > \tau''$ and $\tau' \leq \tau''$ for the unequal time correlation function. For us it is more convenient to bring the above equation into a time ordered form, by differentiating and reintegrating, as the integrand does not explicitly depend on time τ and $a(\tau)/\tau$ ∼const. Therefore we take the temporal derivative of (3.133)

$$\partial_\tau P_G(k,\tau) = \frac{4H_0^2\Omega_r^2}{3\pi}\frac{k^3}{\tau}\int \frac{\mathrm{d}^3\mathbf{q}}{(qp)^3}\int_{\tau_0}^{\tau}\frac{\mathrm{d}\tau'\ \tau'}{a^2(\tau')}\cos\left(k[\tau-\tau']\right) f_{\mathrm{RSA}}(q,\tau,\tau') f_{\mathrm{RSA}}(p,\tau,\tau')\cdot$$
$$\Big[E_t^2(q,p,\tau)S^+(k,q,p) + 4H_t^2(q,p,\tau)c_{qk}c_{pk} + 2\Big(D(k,q,p)E_s(q,\tau)E_d(p,\tau)\cos\left[c_s p(\tau-\tau')\right]$$
$$+ D(k,p,q)E_s(p,\tau)E_d(q,\tau)\cos\left[c_s q(\tau-\tau')\right]\Big) + 4S^-(k,q,p)\Big(E_d(q,\tau)E_d(p,\tau)\cdot$$
$$\cos\left[c_s q(\tau-\tau')\right]\cos\left[c_s p(\tau-\tau')\right]\Big)\Big], \tag{3.134}$$

and reintegration gives the time-ordered equation, where we also apply $a(\tau) = H_0\tau\sqrt{\bar{\Omega}_r}$.

$$P_G(k,\tau) = \frac{4\bar{\Omega}_r k^3}{3\pi}\int\frac{\mathrm{d}^3\mathbf{q}}{(qp)^3}\int_{\tau_0}^{\tau}\frac{\mathrm{d}\tau'}{\tau'}\int_{\tau_0}^{\tau'}\frac{\mathrm{d}\tau''}{\tau''}\cos\left(k[\tau'-\tau'']\right) f_{\mathrm{RSA}}(q,\tau',\tau'') f_{\mathrm{RSA}}(p,\tau',\tau'')\cdot$$
$$\Big[E_t^2(q,p,\tau')S^+(k,q,p) + 4H_t^2(q,p,\tau')c_{qk}c_{pk} + 2\Big(D(k,q,p)E_s(q,\tau')E_d(p,\tau')\cdot$$
$$\cos\left[c_s p(\tau'-\tau'')\right] + D(k,p,q)E_s(p,\tau')E_d(q,\tau')\cos\left[c_s q(\tau'-\tau'')\right]\Big)$$
$$+ 4S^-(k,q,p)\Big(E_d(q,\tau')E_d(p,\tau')\cos\left[c_s q(\tau'-\tau'')\right]\cos\left[c_s p(\tau'-\tau'')\right]\Big)\Big]. \tag{3.135}$$

Note, that we generally neglect the evolution $\bar{\Omega}_r$ as it is typically quite sudden, such that an overall scaling factor suffices. This equation describes the generation of energy in the form of gravitational waves at a given wave number k from stochastic velocity and magnetic field spectra, that are described by a normal distribution. Next, we discuss some of the basic properties of this solution for typical causal turbulence spectra.

3.5.2 Scaling behavior of the MHD-GW-equation

Here, we look at the basic behavior of the MHD-GW-equation at large and intermediary scales. Similar to the discussion in the subsections 3.4.4 and 3.4.5 we apply the same type of approximation for the large scales, i.e. we neglect contributions from scales $k \ll k_I$

and look at the overall scaling behavior. As before we look at the angular factors e.g. c_{qk} at lowest non-trivial level in k and we resolve the p-Integration in the same manner. We also neglect helicities and the cross scalar and assume that the solenoidal component dominates. Thus we have $q \sim p = q + \epsilon k \gg k$, $c_{qk} = -c_{pk} = \epsilon$ and $c_{qp} = -1$, where ϵ takes values in the range $[-1, 1]$. Consequently, in the limit $k \to 0$ we find the following shape for the large scale GW spectrum

$$P_G(k,\tau) \approx \frac{8\bar{\Omega}_r k^3}{3} \int_0^\infty \frac{\mathrm{d}q}{q^4} \int_{\tau_0}^{\tau} \frac{\mathrm{d}\tau'}{\tau'} \int_{\tau_0}^{\tau'} \frac{\mathrm{d}\tau''}{\tau''} f_{\mathrm{RSA}}(q,\tau',\tau'')^2 \cdot \\ \left[\frac{56}{15} E_t^2(q,q,\tau') - \frac{8}{3} H_t^2(q,q,\tau') + \frac{64}{15} E_d(q,\tau')^2 \cos^2\left[c_s q(\tau' - \tau'')\right]\right]. \tag{3.136}$$

Thus, at large scales the spectrum scales with k^3 and therefore less steeply than the large scale tails of the different MHD turbulence spectra. Furthermore, the mixture term involving dilatational and solenoidal fluctuations $E_d E_s$ does not affect the evolution of the large scale tail in the limit $k \to 0$. Now, we look at how the spectrum scales with basic properties of the turbulence flow, like the initial amplitude of the inertial scale e.g. $\max[v^2(k_I), b^2(k_I)] \sim E_A$, see (3.92), and the value of the integral scale k_I itself. Here, we assume that the turbulence is dominated by solenoidal motion. Note that the initial Eddy turnover rate is approximated as $\tau_E^{-1}(q) \sim \mathcal{O}(q\sqrt{E_A}) \ll \tau_0^{-1}$ for $q \gtrsim k_I$. Then, the τ'' integration can be approximated as

$$\int_{\tau_0}^{\tau'} \frac{\mathrm{d}\tau''}{\tau''} \exp\left[-\frac{\tau}{\tau_E(q,\tau')}\right] \approx \frac{\tau_E(q,\tau')}{\tau'} \tag{3.137}$$

and this leads to

$$P_G(k,\tau) \approx \frac{8\bar{\Omega}_r k^3}{3} \int_0^\infty \frac{\mathrm{d}q}{q^4} \int_{\tau_0}^{\tau} \frac{\mathrm{d}\tau'}{\tau'^2} \tau_E(q,\tau') \left[\frac{56}{15} E_t^2(q,q,\tau') - \frac{8}{3} H_t^2(q,q,\tau') + \frac{64}{15} E_d(q,\tau')^2\right]. \tag{3.138}$$

Moreover, the final integration over time will effectively only be required over a timescale $[\tau_0, \tau_0 + \alpha\tau_E(q,\tau_0)]$, where α is some constant of $\mathcal{O}(1)$. We also introduce $K = k/k_I$ and $Q = q/k_I$ and $\tau_E(k) \sim k_I K \bar{v}(k)$. If we ignore the details of the temporal evolution of the different spectra like E_s and the time τ_E, one finds for $k \ll k_I$

$$P_G(k,\tau) \approx \frac{16\bar{\Omega}_r K^3}{3k_I^2(\tau_0)} \int_{-\infty}^{\infty} \frac{\mathrm{d}\log(Q)}{Q^5} \frac{56\alpha}{15 E_A(\tau_0)\tau_0^2} E_A^2(\tau_0) F^2(Q), \tag{3.139}$$

where we assumed equipartition between magnetic and kinetic energy. Therefore, one has approximately for $k \ll k_I$

$$P_G \propto k^3 E_A(\tau_0)/k_I^2(\tau_0). \tag{3.140}$$

Note that this Ansatz neglects the build-up of the turbulent spectrum. As, we discuss later the scaling with regards to E_A is more steeper and i.e. $\propto E_A^{3/2}$, which implies that the estimate in the second temporal integration is off. In particular the build-up of the turbulent spectrum has been neglected which introduces another time-scale into the system τ_b over which the turbulence is initially forced and it is not directly related to the energy scale E_A. The GW spectrum generated due to the build up can be estimated as follows, first we have $E(k,\tau) \propto (\tau - \tau_0)(\tau_b)$ for $\tau_0 + \tau_b \geq \tau \geq \tau_0$. The unequal time correlation function, as previously discussed, can be accordingly estimated as $f_{RSA}(q,\tau',\tau'') = (\tau'' - \tau_0)/(\tau' - \tau_0)$, and take $\tau = \tau_0 + \tau_b$ we find

$$P_G(k,\tau_0+\tau_b) \approx \frac{16\bar{\Omega}_r K^3}{3} \int_{-\infty}^{\infty} \frac{\mathrm{d}\log(Q)}{Q^3} \frac{56}{15} \left[\frac{1}{2}\frac{\tau_0}{\tau_b} + \mathcal{O}\left(\frac{\tau_b^0}{\tau_0^0}\right)\right] E_A^2(\tau_0) F^2(q/k_I(\tau_0)), \tag{3.141}$$

where we restrict ourselves to the case $\tau_b \ll \tau_0$, note that the used forcing does not depend on the scale and hence a factor k_I^{-2} does not explicitly appear and interestingly for small build up times $\tau_b \ll \tau_0$ the efficiency of the generation of a GW background increases. Note, that this also implies that for $\tau_b \to 0$ there is a singularity, hence a correct treatment of the buildup and the decorrelation around the buildup as shown in (3.63) is necessary in order to ascertain that no non-realizable features appear. However, this expression also now depends on E_A^2 rather than E_A. Both of these features, i.e. the buildup and the decay will have an impact on the shape of the spectrum and we will specifically analyze these cases numerically.

Now, we also look at the scaling behavior in the respective inertial range i.e. at scales $k_d \gg k \gg k_I$, where k_d is the dissipative scale. The energy spectra generally decrease towards smaller scale e.g. they may follow Kolmogorov's $k^{-2/3}$ law in the inertial range. Moreover, contributions from scale q and p are effectively suppressed by a factor q^{-2} and p^{-2} respectively. Similarly, the spectra scale as k^5 on large scale $k \ll k_I$ and hence they are again strongly suppressed. Therefore, the dominant contributions appear from around the integral scale. Hence, terms involving $q \sim k \gg p \sim k_I$ and $p \sim k \gg q \sim k_I$ contribute significantly. We simply use the symmetry in $p \leftrightarrow q$ to introduce a factor of 2 and fix $p = k + \epsilon q \gg q$. The angular functions up to and including are

$$c_{pk} \approx 1 - \left(\frac{q}{k}\right)^2 (1 - \epsilon^2), \quad c_{qp} = c_{qk} \approx -\epsilon, \tag{3.142}$$

where we neglect other higher order corrections in q/k in the latter two function, as these are not of relevance. Consequently, one finds by performing the p-Integration

$$\begin{aligned}
&P_G(k,\tau) = \frac{16\bar{\Omega}_r}{3} \int \frac{\mathrm{d}q}{q} \int_{\tau_0}^{\tau} \frac{\mathrm{d}\tau'}{\tau'} \int_{\tau_0}^{\tau'} \frac{\mathrm{d}\tau''}{\tau''} \cos\left(k[\tau' - \tau'']\right) f_{\mathrm{RSA}}(k,\tau',\tau'') \cdot \\
&\Big[\frac{16}{3} E_t^2(q,k,\tau') + 8\frac{q}{k} H_t^2(q,k,\tau') - \frac{8q}{3}\partial_k H_t^2(q,k,\tau') + \frac{16}{5}\Big(E_s(q,\tau') E_d(k,\tau') \cdot \\
&\cos\left[c_s k(\tau' - \tau'')\right] + E_s(k,\tau') E_d(q,\tau') \cos\left[c_s q(\tau' - \tau'')\right]\Big) + \frac{32}{5}\frac{q^2}{k^2}\Big(E_d(q,\tau') E_d(k,\tau') \cdot \\
&\cos\left[c_s q(\tau' - \tau'')\right] \cos\left[c_s k(\tau' - \tau'')\right]\Big)\Big].
\end{aligned} \tag{3.143}$$

As long as $\tau_E \ll \tau$ in solenoidal dominated turbulence, we can approximate the cosine as $\cos[k(\tau' - \tau'')] \sim 1$ in the integration range and as before the integration range is effectively one Eddy turnover time in the τ'' integration at scale k. For a system with dominating solenoidal energy, we have to account for the damping term damping and hence as before the second integration is occurs over a time $\tau_E(k, \tau_0) \ll \tau_0$, while the second time integration is over a time scale that is dominated by the flow at the integral scale and hence does not introduce another k-dependence, consequently one expects in the inertial range $k_d \gg k \gg k_I$that

$$P_G(k,\tau) \propto \frac{1}{k}\max(E_s(k,\tau_0+\tau_b), E_s(k,\tau_0+\tau_b)). \tag{3.144}$$

However, when dilatational motion is dominant, the above argument cannot be directly applied as the contributions are suppressed by a factor q^2/k^2 and hence one has to account for contributions with $k \sim q \sim p$ for which the coefficient $S^- \sim 1$ is possible in contrast to $S^- \sim q^2/k^2$ for $q \ll k$. Since, one expects $E_d \propto k^{-1}$ in the inertial range and the τ'' integration also gives another factor $1/k$ due to the cosine, we anticipate a scaling of $E_d(k,\tau)/k^2$ in dilatational dominated turbulence in the inertial range. Summarizing, for a Kolmogorov spectrum, that is typical for solenoidal dominated turbulence, we expect a $k^{-5/3}$, potentially also a $k^{-8/3}$ spectrum, while in "dilatational turbulence" with a k^{-1} spectrum we expect a k^{-3} scaling in the inertial range. This concludes our discussion on magneto-hydrodynamics and associated gravitational waves in the radiation dominated phase. In the next chapter, we briefly discuss magnetogenesis scenarios in the early universe, the viscous and resistive evolution and aspects of the matter dominated phase.

4 | Magnetogenesis and Dissipation in the Early Universe

In this chapter, we discuss mechanisms which may occur in the early universe, that can produce a sizable stochastic background of magnetic fields on large scales in the early universe. We refer to the early universe as the radiation dominated epoch and other preceding phases like inflation or even intermittently varying phases like runaway-phase transitions, i.e. a radiation dominated phase preceding an inflationary phase which precedes a radiation dominated phase (potentially several such phases may have occurred). We focus primarily on scenarios where turbulent evolution is of importance in the overall prediction of the large scale tail of the MHD turbulent spectra. Scenarios which can drive the production of large scale tails with $k^{5-\alpha}$, where $\alpha > 0$ are steeper than what can occur due to free evolution of the MHD turbulence, will not be discussed here. Shallower tails are possible at least for some substantial subrange e.g. $[k_{\min}, k_I]$ with $k_{min} \ll k_I$ if a substantial long-lasting forcing of the initial turbulence is present or if the coherent magnetic fluctuations are quickly expanded over large scales during a conformal symmetry breaking inflationary phase (Turner & Widrow 1988), comparably to the appearance of the near scale-invariant large scale power spectrum of density fluctuations

$$\langle |\delta|^2(k) \rangle \approx A_s \left(\frac{k}{k_s} \right)^{n_s - 1} , \tag{4.1}$$

with $n_s \approx 0.96$ and $A_s \approx 2 \cdot 10^{-9}$ (Planck Collaboration et al. 2018) that is thought to occur as a result of inflation (Bardeen et al. 1983). Here, we generally neglect the impact of primordial density perturbations on the evolution of the magnetic field, since, as we discuss later, for the scenarios of interest primordial density fluctuations at most affect the fluctuations in a negligible manner (Wagstaff et al. 2014). Therefore, we primarily look only at thermally sourced MHD turbulence or at the very least at MHD turbulence that has undergone thermalization within the radiation dominated phase. In particular we focus on thermal first order phase transitions, especially the electroweak phase transition, although the discussion for the evolution of the initial MHD turbulence applies for any causal scenarios. Note, that as the temperature decreases, due to the expansion, the effective particle degrees of freedom g contributing to the radiation energy density $\rho_r \propto gT^4$ shrinks, as the pair production of pairs / the pairs annihilate with $m_i \gtrsim T$ ceases. Furthermore, the conservation of the entropy density during adiabatic expansion implies $g(aT)^3$ =const. and thus $\rho_r \propto g^{-1/3}$ during adiabatic expansion. At present $g_0 = 3.38$, while in the SM $g(T) \to 106.75$ for $T \gg m_t$ (Planck Collaboration et al. 2018), where $m_t \approx 175$ GeV is the top mass (Tanabashi et al. 2018). Furthermore, we look at the dissipative properties of the early universe, e.g. resistive damping of magnetic fluctuations and viscous damping of MHD fluctuations due to photons and left-handed neutrinos. Lastly, we briefly discuss how the evolution in the matter dominated phase may impact present day traces of primordial magnetic fields, as we otherwise primarily focus on the radiation dominated phase.

4.1 Magnetogenesis

In the context of the MHD approximation, any initial state without magnetic fields, will remain non-magnetized at later stages. Consequently, magnetic fields cannot be produced under the assumptions of the neutral MHD approximation. Technically, the production of magnetic fields requires vortical electric fields. This may occur in the context of charged flows with a non-zero solenoidal component i.e. vortical currents. Of particular interest as a source of magnetic fluctuations are substantially coherent charge fluctuations on or near the horizon scale of the respective epoch paired with baroclinity, which enables the generation of vorticity. As noted before, baroclinity requires that the pressure has a non-adiabatic component. One important non-adiabatic component is the pressure fluctuation due to entropy fluctuations and and the related baroclinity follows from (2.58)

$$\nabla\rho \times \nabla p_{\mathrm{rel}} = \frac{1}{2\partial_\tau \rho} \sum_{i,j,k} \left[\left(c_i^2 - c_j^2 \right) \left(\partial_\tau \rho_j \nabla \rho_k \times \nabla \rho_i - \partial_\tau \rho_i \nabla \rho_k \times \nabla \rho_j \right) \right]. \tag{4.2}$$

Note, that in any multi-component fluid with $c_i \neq c_j$and $\nabla\rho_i \nparallel \nabla\rho_j$ the pressure is partly non-adiabatic , even if every component by itself is described by a barotropic equation of state $p_i = c_i^2 \rho_i$. For different massive components i and j or for a massive component i and an effectively massless component j one has $c_i \neq c_j$ or if the different components have differing and significant chemical potentials $\mu_i \lesssim m_i/T$. Consequently, as long as Re$\gg$ 1 there is generally some minor amount of vorticity present. As discussed in subsection 3.4.6, compressible motion generally leads to a growth of vorticity if some vorticity is initially present. For example, primordial density fluctuations can cause an amplification of the initial vorticity on scales where $k\delta(k) \gtrsim \mathcal{H}(\tau)$ with a potential amplitude of $\omega(k) \sim k\delta(k)$. In a similar manner, any initially present magnetic field can be amplified by either solenoidal or dilatational velocity fluctuations, if Re$\gg$ 1 and $\mathrm{Re}_m \gg 1$. Thus, primordial density fluctuations should lead to the appearance of magnetic fields with potential amplitudes of $b(k) \sim \delta(k)$, if some non-zero magnetic field is initially present. This is possible if there are charge fluctuations on sufficiently large scales k with $\mathrm{Re}(k) \gg 1$. However, viscous damping is an important factor that reduces the range of scales where this mechanism can be important. Furthermore, subsequent turbulent decay, in the case that Re$\gg$ 1, should lead to a reduction of $b(k)$, $\delta(k)$ and $\omega(k)$ on smaller scales.

Initially magnetic fields can be produced by a battery mechanism. The Euler equation with a net charge in a relativistic plasma is

$$\partial_\tau \mathbf{v} + \mathbf{v} \cdot \nabla \mathbf{v} = -\frac{\mathbf{v}}{h} \partial_\tau p - \frac{\nabla p}{h} + \frac{\mathbf{j} \times \mathbf{B}}{h} - \frac{\rho_c}{h} \left(\mathbf{E} + \mathbf{v} \times \mathbf{B} \right). \tag{4.3}$$

At first order in p, v and B, we assume that the flow is balanced due to the net neutrality assumption and find

$$\mathbf{E} = -\frac{\nabla p}{\rho_c}. \tag{4.4}$$

Thus, (2.44) with (4.4) gives

$$\partial_\tau \mathbf{B} = -\frac{\nabla \rho_c \times \nabla p}{\rho_c^2}. \tag{4.5}$$

This mechanism, in the context of an electron-ion plasma, is known as the Biermann battery (Biermann 1950) . The above equation cannot be applied for a charged single component fluid, as the assumption of $\partial_\tau \mathbf{v} \approx 0$ at first order would not be justifiable due to the global net charge. Obviously, this quantity is strongly related to the aforementioned baroclinity, with ρ being replaced by ρ_c. Terms like $\nabla \rho_{c,i} \times \nabla p_i$ vanish for barotropic components. However mixture terms involving different species with different sound speeds do not vanish. In the early universe, two particular important charged species are quarks and charged leptons, which then act as a generic source of seed magnetic fields. Therefore, one indeed expects that independently of the precise detail that as long as Re$\gg$ 1 primordial density fluctuations source magnetic fields and vorticity of a comparable order of magnitude $\delta \sim v_s \sim b$ on scales $\delta k \gtrsim \mathcal{H}(\tau)$. Note, that magnetic fields from the scale-invariant primordial density fluctuations are not of interest to us, as these are generally quite small and are mostly seeded on small scales. The general existence of some initial source term for vorticity and magnetic fields, which can undergo further amplification, is nonetheless important and simplifies the following arguments significantly as no detailed discussion on the precise source terms of vorticity and magnetic fields is required if there is already a significant source term for strong dilatational motion present. The problem is then just if sufficient e-folds can be realized. In the following we look at cosmological first order phase transitions as a source of kinetic and magnetic fluctuations.

4.1.1 Cosmological Phase Transitions

The universe evolves in different phases, e.g. the dark energy dominated phase which began a few billion years ago and was preceded by a matter dominated phase and piror to that by a radiation dominated phase. These particular cosmological phases are phases in an asymptotic sense and the transition between these phases is smooth. Other types of smooth transitions are recombination and reionization, as even after recombination and prior to reionization some minor degree of ionization is present.Moreover, there is another type of cosmological phase transition which may not be smooth and these appear when the fundamental interaction of the quantum fields undergo a symmetry breaking. Particular examples are the chiral and deconfinement transition at the QCD scale ∼200 MeV (Polyakov 1978, Susskind 1979) and the electroweak symmetry breaking at ∼100 GeV (Kirzhnits & Linde 1976). In the standard model, these transitions are smooth or at most of second order (Buchmuller et al. 1994, Chatrchyan et al. 2012, Stephanov 2004). A classical example of an effective potential in which symmetry breaking can appear is that of a real scalar field

$$V(\phi) = A\phi^4 + B|\phi|^3 + C\phi^2 \tag{4.6}$$

with real valued A, B and C.

The potential is shown for two different classes of coefficients A, B and C in figure 4.1. On the left panel a first order phase transition is illustrated for a single scalar field that drives the transition and on the second the same case is illustrated for a second order phase transition. In general, the picture can be far more complex due to additional higher order couplings e.g. $D\phi^5$ and there may be additional fields appearing in the potential, e.g. in the context of the electroweak transition, some theories predict additional scalar fields other than just the one Higgs-field and the additional fields could even be vector fields. Cosmological first order phase transitions are of particular interest as these can provide the necessary condition for the appearance of baryon asymmetry (Kuzmin et al. 1985) or may appear due to dark sector physics e.g. dark matter cou-

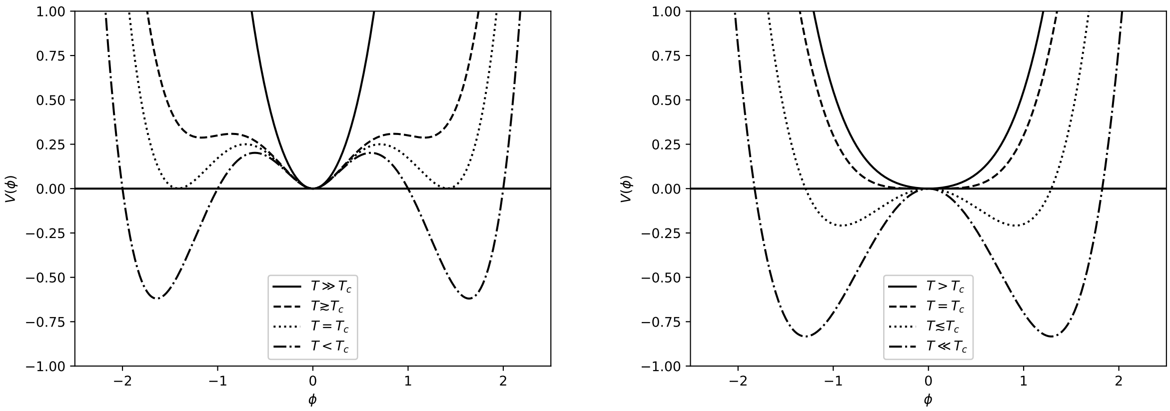

Figure 4.1: Examples of real scalar field phase transition. On the left panel, one sees a typical example of a first order phase transition mediated either exactly or effectively by a real scalar field. At temperatures bigger than some critical temperature $T \gg T_c$ (solid) the potential only has a minimum at the present vacuum expectation value, while at lower temperatures but with $T \gtrsim T_0$ (dashed), a slight extremum or saddle point can appear. Then, at the critical temperature $T = T_c$ (dotted) the system has now two minima with the same energy level that are separated by a potential barrier. Lastly, at even lower temperatures $T < T_c$ (dash-dotted) the system has a new energetic minimum with a potential barrier that separates the old vacuum expectation value from the new vacuum expectation value. The original ground state is symmetric in $\phi \to -\phi$, while the scalar field now settles in one of the two new ground states and thus breaks this symmetry. Additional, there is no direct transition from the old state to the new state and the scalar field tunnels between the two states, where the tunneling probability depends on the energy difference between the two ground states and the height of the barrier. On the right panel, the case of a smooth phase transition is shown. Note, that for $T \gg T_c$ (solid) and $T = T_c$ (dashed), there is only one minimum present, while for $T < T_c$ (dotted and dash-dotted) a new minimum appears to which the scalar field will settle. In contrast to the case on the left panel there is no potential barrier and hence the scalar field immediately settles into the new ground state and as in the other case symmetry is broken. A first order phase transition generally requires in (4.6) $A > 0$, $C > 0$ and $B < \sqrt{32C/9}$, while a second order phase transition is possible when $C < 0$ and/or $B < 0$ and $A > 0$.

plings (Schwaller 2015). For every photon there are roughly $\eta_B \approx 6.1 \cdot 10^{-10}$ baryons around (Cyburt et al. 2016). Note, that the number density of charged leptons is comparable to the baryon asymmetry as the universe is practically charge-free (Caprini & Ferreira 2005), but the lepton asymmetry may be much larger than the baryon asymmetry due to neutrinos (Serpico & Raffelt 2005, e.g). Hence, one anticipates that initially there has been nearly an equivalent amount of baryons and antibaryons around which annihilate and leave a trace amount of baryons. Any process that can lead to a baryon-number asymmetry needs to fulfill the Sakharov conditions (Sakharov 1967), that require baryon-number violation, C (particle-antiparticle- or charge-symmetry)and CP (P: left-right-symmetry) violation, and the process needs to be out of thermal equilibrium, which is in principal guaranteed to a small degree due to the cosmological expansion. First order phase transitions are not in thermal equilibrium and thermal FOPTs are out of equilibrium over shorter timescales and in a more severe manner than the cosmological expansion. Moreover, first order phase transition source fluid motion which can drive the evolution of magnetic fields and vorticity, but also generate magnetic fields and vorticity on its own (Vachaspati 1991, Cutting et al. 2019). During a first order phase transition, a new vacuum state appears to which a probabilistic transition is possible, as described before. Then, regions of the fluid transform into the new phase and begin to expand outward with a velocity v_w, also known as bubble wall velocity. These bubbles form and collide until the entire fluid is in the new energetically favorable state. The rate at which the bubbles appear is effectively of the type $\Gamma \propto exp\left[-\beta\tau\right]$ and the duration of the transition is roughly β^{-1} (Turner et al. 1992). Thus, the typical size of a bubble is $D = 2v_w\beta^{-1}$. Another important quantitative measure of the transition is the latent heat normalized to the radiation energy density α, which parameterizes the strength of the transition. For a thermal phase transition $\alpha \lesssim \rho(\tau_{\rm pt})$ and $\beta \gtrsim \mathcal{H}(\tau_{\rm pt})$, where $\tau_{\rm pt}$ is the time at the onset of the phase transition. Note that a part of the latent heat is converted into kinetic and magnetic energy i.e. the expansion of the bubbles, while the other part is simply transformed into thermal energy of the cosmological plasma. Then, due to non-linear evolution the kinetic energy is gradually transformed into heat in the radiation dominated phase. We parameterize the total kinetic energy that can be produced in a thermal phase transition by $\kappa_v \alpha$, similarly one can define κ_b for the initially seeded magnetic energy. Such a split is in generally difficult to define, as kinetic and magnetic energy is constantly transformed into kinetic and magnetic energy. Here, we assume that $\kappa_b = 0$ and assume that the magnetic energy is provided primarily by the kinetic energy due to MHD turbulence.

Furthermore, the different types of first order phase transitions can be distinguished by v_w. If $v_w \ll c_s$ the transition is a deflagration and solenoidal motion can quickly appear (Cutting et al. 2019). For $v_w \sim c_s$, compressible effects become important and this type of phase transition is known as a hybrid. Lastly, for $v_w \gg c_s$ one has detonations and solenoidal motion is initially barely produced (Cutting et al. 2019). The efficiency parameter κ_v strongly depends on the bubble wall velocity and on the phase transition strength α. This is illustrated in figure 4.2, which is based on solving the Clausius-Clapeyron equations for a relativistic gas (Espinosa et al. 2010) without electromagnetic fields and background expansion. If background expansion is neglected, the value of β does not impact the efficiency, however when the background expansion becomes relevant e.g. $\beta \lesssim H(\tau_{\mathrm{pt}})$, κ_v becomes even smaller (Cai & Wang 2018). As can clearly be seen, κ_v peaks in the hybrid phase. The peak is roughly given by the intermediary velocity in the hybrid case

$$v_w^{\max} \sim \frac{2c_s + \sqrt{\alpha^2 + \frac{2}{3}\alpha}}{2(1+\alpha)}. \tag{4.7}$$

Furthermore, for deflagrations and detonations $\kappa_v \propto \alpha$ and for hybrid PTs $\kappa_v \propto \sqrt{\alpha}$, for $\alpha \ll 1$. In table 4.1, we show some possible phase transition parameters for some potential first order thermal phase transition scenarios. The bubble wall velocity is not shown, as for some scenarios it may vary significantly depending on the exact parameters. For models, that involve strong phase transitions e.g. $\alpha \gtrsim 0.1$ it will typically be large $0.1 \lesssim v_w \lesssim 0.9$ (Mégevand & Sánchez 2010). Baryogenesis FOPT models generally require small velocities $v_w \lesssim 0.01 - 0.1$ due to temporal constraints,

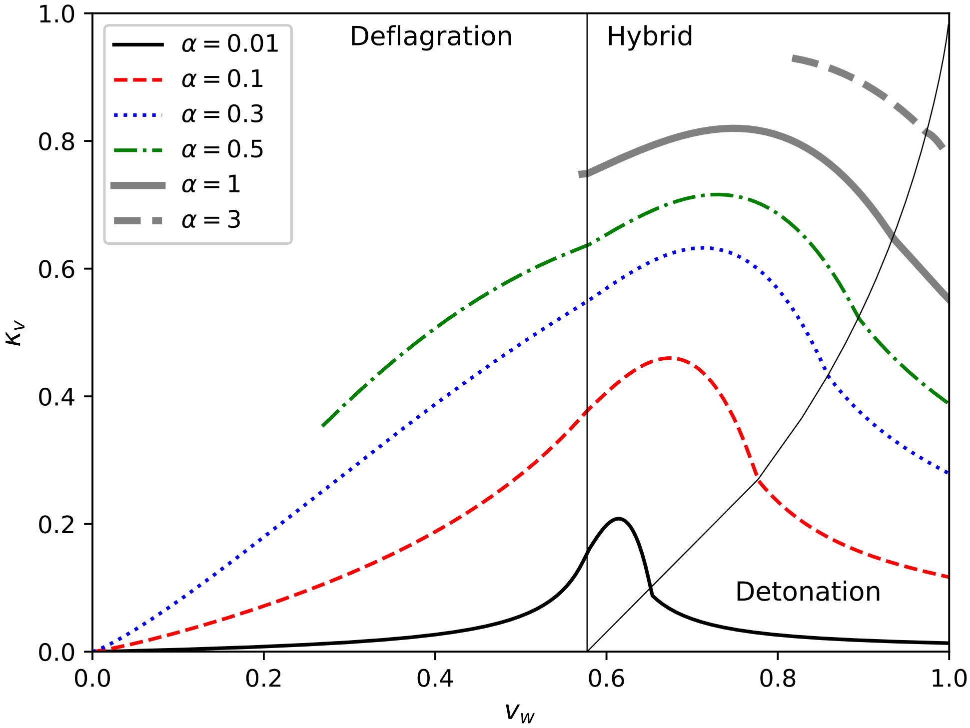

Figure 4.2: Here we show the efficiency parameter for the generation of kinetic energy κ_v as a function of v_w (bubble wall velocity) for different α (latent heat) in a first order phase transition based on calculations by (Espinosa et al. 2010). The two thin solid black lines separate the different regimes, where the bubble evolves as a deflagration, hybrid or as a detonation and correspond to the lower and upper Chapman-Jouguet points. Note that for $\alpha > 1/3$ there are only solutions for some $v_w \gtrsim 1 - (3\alpha)^{-10/13}$.

Model	$\beta/\mathcal{H}(\tau_{\rm pt})$	α	$T_{\rm pt}$ **[GeV]**	**Refs**
Higgs-Portal	6.4	0.2	56	(Espinosa et al. 2008)
MSSM singlet extension	6	0.14	76	(Huber et al. 2016)
Higgs doublet	660	0.11	52	(Huber et al. 2016)
SM plus Dim 6	160	0.13	63	(Huber et al. 2016)

Table 4.1: Examples of parameter sets for BSM thermal first order phase transitions scenarios with different duration β^{-1}, strength α, and $T_{\rm pt}$. Note, that for the different models also vastly different parameters are possible and also the precise v_w are often not known, as it may also vary quite strongly with the coupling strength and temperature (Mégevand & Sánchez 2010). This list is not exhaustive and only focuses on potentially thermal FOPTS at GeV scales, serving as an illustration.

although values with $0.2 \lesssim v_w \lesssim c_s$ may also be sufficient for baryogenesis (Kozaczuk 2015). Note, that vacuum phase transition typically have $\alpha \gg 1$ and the duration is much longer than the then-age of the universe i.e. $\beta \ll \mathcal{H}(\tau_{\rm pt})$. Additionally, the bubble wall velocity is not necessarily constant and it is possible that $v_w \to 1$ (Bödeker & Moore 2009, Caprini et al. 2016), i.e. the bubbles may run away. Here, we assume that the bubbles do not run away, and that the bubble wall velocity is near constant.

4.1.2 MHD topology from a FOPT

So far we have discussed that cosmological first order phase transitions can act as a source of significant magnetic fields and vortical fluid motion. Now, we focus on specific quadratic quantities, like the cross- and magnetic helicity. As we discuss later on, a system with a non-trivial cross- and magnetic helicity spectrum also acts as a source for kinetic helicity and cross scalar spectra. In ideal MHD, the total magnetic helicity is conserved and in barotropic or incompressible ideal MHD the cross helicity is conserved. One quantity that may easily and readily appear in such magnetogenesis scenarios is a non-trivial cross-scalar, as it requires that

$$\nabla\rho \times \nabla p \propto \nabla\rho_c \times \nabla p, \tag{4.8}$$

which is usually satisfied to some degree. The appearance of parity violating correlations like the magnetic helicity is less trivial. Of particular interest are phase transitions that also lead to baryogenesis and/or leptogenesis as these require CP violation and should lead to the appearance of some magnetic helicity (Cornwall 1997, Vachaspati 2001, Wagstaff & Banerjee 2016). The appearance of magnetic helicity is strongly tied to a non-trivial kinetic helicity spectrum and similarly the appearance of cross helicity is strongly tied to magnetic or kinetic helicity and the cross scalar. In baryogenesis scenario only a small fractional magnetic helicity may be sourced (Vachaspati 2001). Another process, that is of interest in the generation of the magnetic helicity is the chiral anomaly (Boyarsky et al. 2012, Pavlović et al. 2016, Pavlović et al. 2017, Brandenburg et al. 2017). Right handed and left handed particles are affected slightly differently in a magnetic field and this leads to an additional effective contribution in Ohm's law known as the chiral magnetic effect. Similarly, magnetic helicity also directly impact the number density of left- and right-handed particles. Furthermore, at finite temperature another effect is of interest, the chiral vortical effect, where a non-trivial kinetic helicity can source a substantial chiral anomaly due to the so-called gravitational anomaly in the thermal field theory (Kharzeev et al. 2016, e.g.). This is important, since a substantial chiral anomaly is required to generate a substantial total net magnetic helcitiy. Here we will not study the impact of the chiral anomaly on the MHD turbulence. Note that in contrast to the previous discussion, the precise initially generated total magnetic and or cross helicity during the magnetogenesis phase e.g. the phase transition is of importance, as e.g. compressible turbulent energy cannot drive a significant generation of total magnetic and cross helicity after the phase transition as for the magnetic energy itself. In the next section we discuss the resistive and viscous properties of the early universe.

4.2 Viscous and Resistive Damping in Radiation Dominated Universe

One major factor in the evolution of MHD turbulence is viscous and resistive decay (Biskamp 1993). Direct decay of magnetic fluctuations occurs only by resistive dissipation, but also indirect decay in systems with Re$\gtrsim$ 1 is possible. The indirect decay channel dominates magnetic dissipation in systems with Pm$\gg$ 1. Kinetic fluctuations undergo direct decay due to viscous damping, yet indirect decay of kinetic fluctuations in systems with Pm$\ll$ 1, Re$\gg$ 1 Re$_m$ $\gg 1$ is also important. In the early universe, in the context of the standard model, viscous decay dominates i.e. Pm$\gg$ 1 (Wagstaff et al. 2014, Jedamzik et al. 1998). Here we discuss the key factors that drive viscous dissipation in the radiation dominated phase i.e. neutrinos and photons, and those that govern resistive decay i.e. leptons and quarks (Baym & Heiselberg 1997). In the standard model, at sufficiently high temperatures $T \gg 1$ MeV, all standard model particles are tightly coupled by the electroweak interaction, with the exception of the gluons which are coupled to the quarks by the strong interaction and thus couple only indirectly to the other SM particles by the electroweak force. Due to the small baryon asymmetry and charge neutrality, the electromagnetic cross section decreases as soon as the thermal bath can no longer support the production of e^+e^--pairs and later when the atoms recombine. Additionally, due to the large mass of the $W^{\pm}$ and Z^0 bosons the weak interaction becomes too weak to sufficiently couple the neutrinos to the other particles. However, as temperature decreases, as the universe expands, the cross-section decreases, due to a suppression of pair-production and later on due to gradual recombination. In general the evolution of MHD turbulence in the radiation dominated universe can be split into 4 different phases, that we discuss in detail in the following subsections. For $T \gg 10$ MeV the fluid may be turbulent, while for temperatures 40 MeV$\gtrsim T \gtrsim 2$ MeV neutrino decoupling suppresses turbulent transport and leads to a significant direct decay of the kinetic flow. Thereafter, at temperatures 1 MeV$\gtrsim T \gtrsim 10$ keV, the system may again freely evolve. Then, towards last scattering at $T \sim 0.3$ eV, the system undergoes significant viscous damping due to the free-streaming of photons. First we look at viscous damping by neutrinos.

4.2.1 Viscous damping by neutrinos

For temperatures $T \gtrsim 2$ MeV, the thermal movement of coupled neutrinos damp fluctuations on length scales $L \gtrsim \lambda_{\mathrm{mfp},\nu}$, where $\lambda_{\mathrm{mfp},\nu}$ is the mean free path of neutrinos. At smaller temperatures neutrinos do no longer couple, at least not significantly, to the cosmological fluid and thus no longer impact the evolution of fluctuations in the radiation dominated phase. The physical mean free path of neutrinos for $T \lesssim 100$ GeV is approximately (Jedamzik et al. 1998)

$$\lambda_{mfp,\nu} = \frac{1}{G_F^2 T^2 (n_l + n_q)}, \tag{4.9}$$

where G_F is the Fermi constant, and n_l and n_q are the physical lepton and quark number densities given by $n_{l,q} = 6 g_{l,q} \zeta(3) T^3/(7\pi^2)$ and $g_{l,q}$ count the lepton and quark degrees of freedom. Consequently the neutrino viscosity

$$\nu(T) \propto \frac{g_\nu}{g(T)} \frac{\lambda_{\mathrm{mfp},\nu}(T)}{5a(T)} \tag{4.10}$$

grows quickly with a^4, where g_ν represents the degrees of freedom of the neutrinos. The neutrinos decouple from the cosmic fluid when $\lambda_{\mathrm{mfp},\nu}(T) \sim H^{-1}(T)$, which corresponds to $T \approx 2$ MeV, prior to $\mathrm{e}^+\mathrm{e}^-$ annihilation at $T \lesssim m_e$. Consequently, at $T \lesssim 2$ MeV previously present kinetic fluctuations in the plasma have been dissipated and the Reynolds number on the horizon scale for a flow with $v \sim 1$ is Re~ 1. Note, that on smaller scales a different Reynolds number would apply i.e. related to the free streaming of neutrinos and the diffusing photons. Therefore, after neutrino diffusion damping the only traces of subhorizon MHD fluctuations is the magnetic energy and magnetic helicity spectrum with $k_I b(k_I, 2\ \mathrm{MeV}) \sim \mathcal{H}(2\ \mathrm{MeV})$. On scales $k^{-1} \lesssim \lambda_{\mathrm{mfp},\nu}$, the above treatment cannot be applied anymore, as the neutrinos do not substantially couple with the other relevant particles, e.g. photons and electrons, and the fluid approximation breaks down. This is can be effectively resolved in the context of the fluid approximation by introducing a drag term α, such that $\nu k^2 \to \alpha \sim \lambda^{-1}_{\mathrm{mfp},\nu}$ for $k \gtrsim \lambda^{-1}_{\mathrm{mfp},\nu}$ (Banerjee & Jedamzik 2004).

4.2.2 Viscous damping by photons

After the neutrino decoupling and electron-positron annihilation, the mean free path of photons is dominated by Compton scattering with the electrons and positrons. Thus, the physical mean free path of photons is approximately (Jedamzik et al. 1998)

$$\lambda_{mfp,\gamma} \approx \frac{1}{\sigma_{KN}\sqrt{n_{\mathrm{pair}}^2 + n_e^2}}, \tag{4.11}$$

where σ_{KN} is the Klein-Nishima cross section and n_{pair} is the physical density e^+e^- pairs in the plasma (Wagstaff et al. 2014), which is of relevance prior to electron-positron annihilation. For $T \gg 1$ MeV $n_{\mathrm{pair}} \gg n_e$ and for $T \ll 1$ MeV $n_{\mathrm{pair}} \ll n_e$. The number density of pairs is approximately (Jedamzik & Fuller 1994)

$$n_{\mathrm{pair}} \approx \left(\frac{2m_e T}{\pi}\right)^{3/2} \exp\left[-\frac{m_e}{T}\right]\left(1 + \frac{15}{8}\frac{T}{m_e}\right), \tag{4.12}$$

for $T \lesssim 140$ MeV. While the number density of free electrons is

$$n_e = X_e \frac{\Omega_b \rho_c}{m_p}\left(\frac{T}{T_0}\right)^3, \tag{4.13}$$

where $X_e \approx 1$ in most of the radiation dominated phase and $\Omega_b \rho_c$ is the density of baryons today, while $T_0 \approx 2.35 \cdot 10^{-4}$ eV is the present CMB temperature. However, as soon as the electrons together with the protons form hydrogen atoms, as other atoms recombine earlier, X_e drastically shrinks and is approximately given by the Saha equation

$$\frac{X_e^2}{1 - X_e} = 2.38 \cdot 10^{16}\left(\frac{\mathrm{eV}}{T}\right)^{3/2} \exp\left[-\frac{13.6\ \mathrm{eV}}{T}\right] \tag{4.14}$$

for $T \gtrsim 0.3$ eV. For $T \lesssim 0.3$ eV and roughly till reionization the processes that drive recombination are slower than the overall expansion and a residual ionization $X_e \sim$

10^{-4} remains (Peebles 1968), which the above approximation does not account for. Ultimately, in the temperature range 0.3 eV$\lesssim T \lesssim$ 1 MeV recombination is the major driver in the increase of the viscosity. The photon viscosity is

$$\nu(T) \propto \frac{g_\gamma}{g(T)} \frac{\lambda_{\mathrm{mfp},\gamma}(T)}{5a(T)}, \tag{4.15}$$

which grows with a^2 significantly slower than the neutrino viscosity, where g_γ represents the degrees of freedom of the photons. Analogously to the neutrino case, photons decouple at $T \sim 0.3$ eV and practically the only causally produced fluctuations that are not dissipated by then are magnetic fluctuations with or without magnetic helicity with $k_I b(k_I, 0.3 \text{ eV}) \sim \mathcal{H}(0.3 \text{ eV})$. As for the neutrino case, we also introduce a drag term for the photons based on the mean free path. For the total dissipative factor we use a simple composite model to interpolate between the free-streaming and scale independent viscosity regime

$$\nu k^2 \to \frac{\nu_\gamma k_\gamma^2 + \alpha_\gamma \frac{k^2}{k_\gamma^2}}{\left(\frac{k_\gamma}{k}\right)^2 + \left(\frac{k}{k_\gamma}\right)^2} \theta(T - 0.3 \text{ eV}) + \frac{\nu_\nu k_\nu^2 + \alpha_\nu \frac{k^2}{k_\nu^2}}{\left(\frac{k_\nu}{k}\right)^2 + \left(\frac{k}{k_\nu}\right)^2} \theta(T - 2 \text{ MeV}), \tag{4.16}$$

where $k_\gamma = 2\pi/\lambda_{\mathrm{mfp},\gamma}$ and $k_\nu = 2\pi/\lambda_{\mathrm{mfp},\nu}$.

4.2.3 Viscous damping above the electroweak scale

For temperatures $T \gtrsim m_W$, the electromagnetic and weak interactions are comparable and the neutrinos cannot decouple. Therefore, at temperatures above the electroweak scale $T \gtrsim 100$ GeV, free streaming does not dominate viscous dissipation in the standard model. Thus, the viscosity is dominated by collisions due to the electroweak interaction in the symmetric phase. The comoving viscosity is (Arnold et al. 2000)

$$\nu = \frac{5^3 3^5}{2a(T)\pi^4} \frac{1}{9\pi^2 + 224(5 + \frac{1}{2})} \frac{1}{g'^4 \log\left(\frac{1}{g'}\right)}, \tag{4.17}$$

where g' is the electroweak coupling constant and ${g'}^2 \sim \alpha$ around the electroweak scale. In general the viscosity is of the order g^{-4}. Further, the above viscosity is comparable to the neutrino free streaming viscosity at $T \sim 50$ GeV.

4.2.4 Resistive damping

In contrast to the viscosity in the early universe, the resistivity does not vary as substantially as the viscosity and remains only relevant on small scales $k \gg \mathcal{H}(T)$ and/or for small field strengths. Prior to the QCD transition but after the electroweak transition at 100 GeV$\gtrsim T \gtrsim 100$ MeV quarks and leptons contribute to the conductivity, while at smaller temperatures $T \gtrsim 1$ MeV electron-positron pairs and protons (negligibly) contribute. However, due to the strong interaction the impact of quarks on the conductivity is less relevant compared to the leptons even above the QCD scale. For $T \lesssim 1$ MeV, the residual electrons provide the conduction. At even higher higher temperatures $T \gtrsim m_{\mathrm{W}} \approx 80$ GeV, the $\mathrm{W}^{\pm}$ bosons contribute to the conductivity and above the electroweak symmetry breaking temperature, the conductivity depends on the electroweak interaction. Since the viscosity significantly dominates, the precise details of the resistive damping are less important and hence we focus on a simplified approximation for the conductivity. The physical conductivity can be estimated as

$$\sigma \sim \frac{ne^2\tau_c}{T}, \tag{4.18}$$

where τ_c is the physical collision time, q is the charge and n is the physical number density of particles involved in the collisions (Banerjee & Jedamzik 2004, Baym & Heiselberg 1997). The collision time can be estimated as $\tau_c \sim 1/(n\sigma_t)$, where the cross section is approximately given by

$$\sigma_t \sim \left(\frac{e^2}{T}\right)^2 \log \Lambda_C, \tag{4.19}$$

where Λ_C is the Coulomb logarithm. Thus, the physical conductivity can be approximated as

$$\sigma \sim \frac{T}{e^2 \log \Lambda_C} \tag{4.20}$$

and it is independent of the density. Then, the comoving resistivity is

$$\eta \sim \frac{\alpha \log \Lambda_C}{4\pi a T} \tag{4.21}$$

for $T \gtrsim m_e$ and $\alpha = e^2$ is the fine-structure constant and the Coulomb logarithm can be estimated as $\Lambda_C \sim \alpha^{-1}$. Therefore, the comoving resistivity is nearly constant for $m_W \gtrsim T \gtrsim m_e$ except for variations of Λ_C and variations in $g(T)$. For non-relativistic charged particles $T < m_i$ the above estimate is not applicable and the conductivity is given by the Drude model. In particular, in (4.18) T is replaced by m_e, similarly σ_t is adjusted. Therefore, for $T \lesssim m_e$ one finds (Banerjee & Jedamzik 2004)

$$\eta \approx \frac{n_e}{X_e \eta_B \sqrt{n_e^2 + n_{\text{pair}}^2}} \frac{\alpha \log \Lambda_C}{4\pi a m_e} \left(\frac{\pi m_e}{2T}\right)^{3/2} \tag{4.22}$$

where the prefactor $\propto n_e$ appears due to the reduction in the ionization degree with

$$\Lambda_C \sim \frac{1}{6\sqrt{\alpha\pi}} \sqrt{\frac{m_e^3}{n_e} \frac{T}{m_e}}, \tag{4.23}$$

where n_e is given in (4.13) for $T \ll m_e$. In the next subsection we look at the respective Reynolds numbers e.g. at the comoving horizon scale for $v = 1$, as these represent the maximally relevant Reynolds numbers.

4.2.5 Cosmological Reynolds numbers

In the previous subsections we discussed the relevant viscosities and the resistivity in the very early universe, now we look at the Reynolds numbers in the early universe, some particularly relevant scales are $v = 1$ and the cosmological horizon. We also partly summarize the previous subsections. The physical cosmological horizon at a given temperature can be estimated as

$$d_{H,\mathrm{ph}} \approx \left(\frac{\mathrm{MeV}}{T}\right)^2 \left(\frac{g_0}{g}\right)^{1/2} 10^{21}\mathrm{MeV}^{-1} \approx \left(\frac{\mathrm{MeV}}{T}\right)^2 \left(\frac{g_0}{g}\right)^{1/2} 2\cdot 10^5 \text{ km}, \quad T \gg 1 \text{ eV}. \tag{4.24}$$

This scale is considerably larger than the inverse temperature and thus implicates generally quite large Reynolds-numbers, as long as decoupling is negligible. Furthermore the comoving (today) horizon scale is

$$d_H \approx \frac{\mathrm{MeV}}{T}\left(\frac{g_0}{g}\right)^{1/6} 5\cdot 10^{30}\mathrm{MeV}^{-1} \approx \frac{\mathrm{MeV}}{T}\left(\frac{g_0}{g}\right)^{1/6} 30 \text{ pc} = \frac{1\text{ MeV}}{T}\left(\frac{g_0}{g}\right)^{1/6} 3\cdot 10^9 \text{ Hz}^{-1}, \tag{4.25}$$

for $T \gg 1$ eV. Then, we can calculate the cosmological relevant Reynolds-number and these are shown in figure 4.3. In principle, in a turbulent system the relevant Reynolds number will always be smaller, even if the initial state is a turbulent flow with $v = 1$ and $k_I \sim \mathcal{H}$, due to turbulent energy transport. Technically, as a consequence of free streaming the relevant Reynolds number can be more complicated on scales smaller than the largest relevant mean free path of some coupled particle species. In such a case a larger Reynolds-number corresponding to the next largest mean free path in the fluid is relevant or a Reynolds number related to the free streaming coefficient α. However, we expect that processes on scales smaller than the largest relevant mean free path are irrelevant for the evolution of the large scale magnetic fields and phase transition remnants. As one can clearly see, resistive damping is mostly negligible compared to viscous dissipation and at high temperatures $T \gtrsim 10^{11}$ GeV both Reynolds numbers increase with temperature and the Prandtl number is near constant. In fact, the conductivity scales as $\sigma \propto g^{-2}T^{-1}$ and the viscosity as $g^{-4}T$. Therefore, Pm$\propto g^{-6}$ (Durrer & Neronov 2013) at high temperatures and it primarily depends on variations in the coupling strength and variations in the relevant species, e.g. quarks do not contribute significantly due to the strong interaction, yet become more relevant at higher temperatures e.g. at a potential GUT scale. Below the electroweak scale, the viscosity increases considerably as the neutrinos begin to decouple from the rest of the fluid,

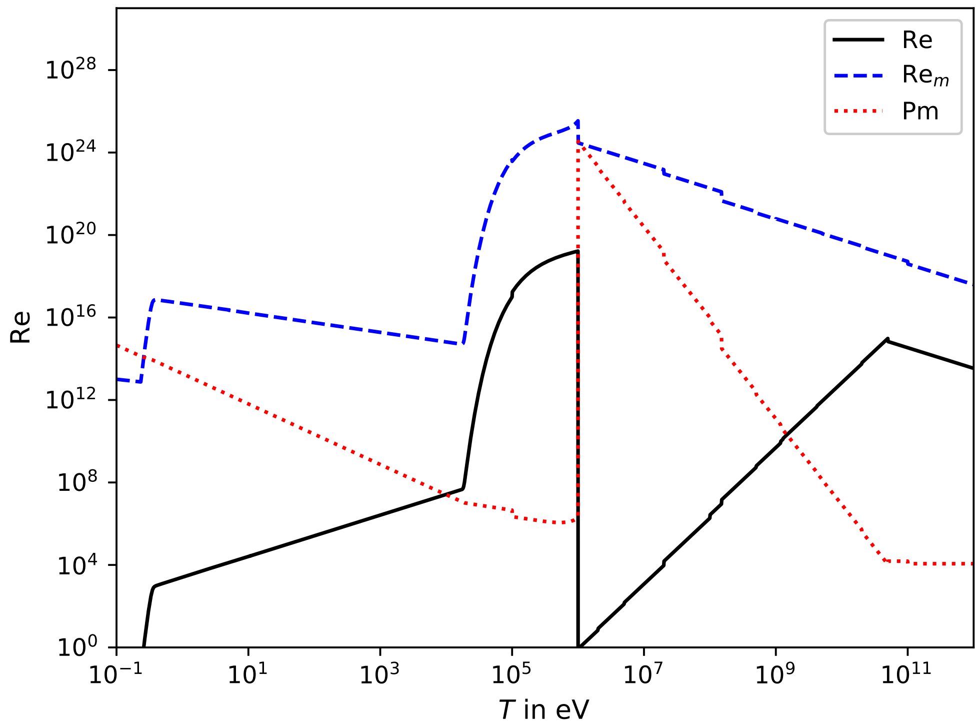

Figure 4.3: Magnetic (solid black) and kinetic (blue dashed) Reynolds-numbers and Prandtl number (red dotted) for $v = 1$ and $L = d_H$ (see (4.25) plus deviation in matter dominated phase), i.e. the maximally possible Reynolds numbers. The viscosity is given by (4.15), (4.10) and (4.17) and the resistivity is given by (4.22) with additional coefficients ($\mathcal{O}(1)$) given in (Baym & Heiselberg 1997). For $T \gtrsim 50$ GeV, $\mathrm{Re}_m \propto \mathrm{Re}$ and for 1 MeV$\lesssim T \lesssim 50$ GeV neutrino free streaming dominates. In the temperature range 20 keV$\lesssim T \lesssim 1$ MeV electron positron pairs are annihilated and photon decoupling dominates the viscosity and at around $T \sim 0.3$ eV the plasma recombines with a residual ionization $X_e \sim 10^{-4}$. Note, that for all temperatures in the radiation dominated phase Pm$\gg 1$. Also, the transition at $T \sim 1$ MeV is in reality not a step function and the variations in $g(T)$ are also not instantaneous. Similarly, the bump in conductivity at $T \sim 1$ MeV is an artifact of the modeling, which in by itself is not critical for the following calculations since Pm$\gg 1$. Additionally, we did not include ambipolar and hydrogen diffusion which becomes important after photon decoupling (Banerjee & Jedamzik 2004).

yet the neutrinos do not contribute to the conductivity and hence it is not affected by the decoupling. At around $T \sim 1$ MeV electrons and positrons annihilate leading to a decrease in the density of charged particles and thus a reduction in the conductivity. Similarly, the viscosity, which is now dominated by free streaming photons after the neutrinos have fully decoupled, increases as the photons can diffuse over longer distances due to a decrease in the number of Compton scattering events. After the pairs are annihilated, the conductivity grows again and only falls slightly after recombination, while the viscosity increases until the photons have decoupled at $T \sim 0.3$ eV. Around this time, at $T \sim 1$ eV, the universe transitions into the matter dominated phase, which we briefly discuss later on. The charged particles that sustain the magnetic field do not fully recombine and a residual ionization remains until reionization, due to star formation, where the universe becomes strongly ionized again, which is roughly indicated by the still large magnetic Reynolds number at $T \lesssim 0.3$ eV (Peebles 1994). Similarly, after recombination and prior to reionization viscous and resistive damping are dominated by ambipolar and hydrogen diffusion of free electrons and protons, and the Reynolds number increases again potentially allowing turbulent transport on certain scales (Banerjee & Jedamzik 2004) (not sketched in figure 4.3). In principle, in a turbulent system the relevant Reynolds number will always be smaller than those shown in figure 4.3, even if the initial state is a turbulent flow with $v = 1$ with $k_I \sim \mathcal{H}$ due to turbulent energy transport. Technically, due to free streaming this can be even more complicated, as on scales smaller than the largest relevant mean free path, free streaming and/or the next largest mean free path of some particle species determines the Reynolds number. However, we expect that processes on scales smaller than the largest relevant mean free path are irrelevant for the evolution of the large scale magnetic fields and phase transition remnants (neglecting topological defects). In the next section, we discuss how the matter dominated phase will impact the evolution of large scale MHD turbulence.

4.3 Impacts of matter dominated phase on the Evolution of primordial magnetic fields

MHD turbulence evolves differently in the matter dominated phase than in the radiation dominated phase. For example $\tau \propto a$ in the radiation dominated phase, while $\tau \propto a^{1/2}$ in the matter dominated phase. Additionally, the equations describing the evolution of a cosmological fluid differ in the matter dominated phase from those in the radiation dominated phase and an additional Hubble drag term appears in the velocity equation $H\mathbf{v}$ that damps fluctuations on large scales. Therefore, the velocity for which no drag term appears now corresponds to $\tilde{\mathbf{v}} \propto a\mathbf{v}$ and is no longer constant with respect to the background evolution. Due to this, turbulent transport is less efficient in the matter dominated phase compared to the radiation dominated phase. Moreover, density fluctuations lead to gravitational potential fluctuations and clustering, since the pressure is significantly smaller, which is responsible for structure formation: stars, galaxies, galaxy clusters (Peebles 1994). The resulting formation of stars leads to a reionization of the universe and can help sustain relatively strong magnetic fields potentially even on large scales. Also, a causal magnetic field spectrum will have an effective eddy turnover rate of $k_I b(k_I) \sim H$ after recombination, due to viscous decay and energy transfer, and thus the non-linear evolution will be strongly affected by the Hubble drag term, as the rates are of the same order. As before $k_I \tilde{v}(k_I) \propto \tau^{-1}$, but with $\tilde{v}$ rather than v and specifically $k_I v(k_I) \propto (a\tau)^{-1}$ which grows faster than the corresponding Hubble rate. Thus, the turbulent transport on these large scales for causally produced primordial magnetic fields appears negligible. Consequently in the matter dominated phase, primordial MHD turbulence is expected to barely evolve. Nonetheless, viscous and resistive effects can play an important role. After recombination ambipolar diffusion, i.e. the diffusion of electrons through the slightly ionized medium, and hydrogen diffusion dominate resistive and viscous damping respectively prior to reionization (Banerjee & Jedamzik 2004). In particular for weak magnetic fields ambipolar diffusion may be an important source of magnetic dissipation. Here we do not focus on these cases and hence neglect ambipolar diffusion and and for the previously discussed reasons only focus on the radiation dominated phase. Since the magnetic energy scales like radiation, we also have $b \propto a^{-1/2}$ in the matter dominated regime, i.e. the Alfven velocity of the magnetic fields that evolved till the matter radiation equality are further reduced by a factor $a_{\rm eq}^{1/2} \sim 1.7 \cdot 10^{-2}$. In principal one may also express the Alfven velocity of primordial magnetic fields simply in terms of the radiation energy density. To summarize, the evolution of MHD turbulence on the largest scales in the matter dominated phase should be rather simple and mostly corresponds to near frozen-in turbulence for sufficiently strong magnetic fields. The evolution of MHD turbulence on small CMB scales will be more complicated as a result of structure formation. Since b^2 nearly constant (energy conservation) due to gravitational collapse, the magnetic field strength grows as $B \propto \sqrt{1+\delta}$, where δ is the the collapsing density perturbation $\delta \gg 1$. These initial primordial seed fields or battery post-recombination batteries (Takahashi et al. 2005) can thus be responsible for providing the seed fields of galaxies, that are further amplified by a dynamo (Kulsrud 1999*a*). Particularly around and after reionization these structures can act as a source of magnetic fields and may dominate the magnetic field spectrum at smaller scales. Also, strong magnetic outflows from active galactic nuclei may also be present (Hoyle 1969, Daly & Loeb 1990). Furthermore, cosmic ray currents may source and sustain even substantial intergalactic magnetic fields (Miniati & Bell 2011). In the next section we discuss on established constraints on large scale magnetic fields in the present universe.

4.4 Constraints

As we have mentioned before, some correlated magnetic fields should be present on all causally possible scales or even beyond on seemingly acausally correlated scales for inflationary magnetogenesis. However, thus far there is, to our present knowledge, no confirmed detection of cosmological large-scale inter-galactic magnetic fields (IGMF), yet their strength can be constrained (Durrer & Neronov 2013, Subramanian 2016). For a good overview on present constraints see also (Subramanian 2016, Table 1). Direct detections or estimates of IGMF so far are not possible as there are many effects that can mimic the effects of IGMF and a sufficient distinction is as of yet not possible. Secondly, even a direct detection of an IGMF would not directly allow, at least at the present, to distinguish its origin. On very small scales IGMF are dissipated due to resistive damping, while above the horizon an observation of super horizon correlations is not possible and any superhorizon magnetic field would appear as a nearly homogeneous background field that introduces a preferred direction and would be a clear indication of an inflationary sourced magnetic field. In between these scales, experiments to constrain IGMF are required to assess the potential strengths of primordial magnetic fields, if possible.

Some of the most important processes for constraints on these magnetic fields are Zeeman splitting, Faraday rotation and synchrotron radiation. Moreover, several cosmological key observables like the CMB are also affected by primordial magnetic fields and their presence would produce signatures in the CMB. Additionally, charged particles, in particular cosmic rays, are directly affected by cosmological magnetic fields. Typically, magnetic field strengths are not expressed in natural units and not in terms of the present day Alfven velocity, which we generally use here, but rather in terms of the often for magnetic fields used unit Gauss

$$B(k) \approx b(k)\sqrt{4\pi\rho_b} = b(k)10^{-4}\ \mathrm{G}, \tag{4.26}$$

where we used $h^2\Omega_b = 0.0224$ (Planck Collaboration et al. 2018). Note that with respect to the Alfven velocity at mater radiation equality one effectively finds

$$B(k) \approx b_{\mathrm{eq}}(k)\sqrt{4\pi\rho_r} \approx b_{\mathrm{eq}}(k)1.72 \cdot 10^{-6}\ \mathrm{G}. \tag{4.27}$$

First we look at the impact of magnetic fields on atomic emissions in particular the Zeeman effect.

4.4.1 Zeeman Effect

The Zeeman effect describes the split of an atomic transition into distinguishable sub-states depending on the magnetic field strength and magnetic moment of the atom. Then, the energy levels change, depending on the spin and angular momentum of the electron in the atom, linearly dependent on $\Delta E \propto B$, where the proportionality factor is known and it depends on the angular momenta and spins. The most common element in the universe is atomic hydrogen. Due to the primordial density perturbations, the atomic hydrogen collected into clouds. If the cloud of atomic gas can substantially contract, hydrogen molecules can form (Peebles 1994, Loeb & Furlanetto 2013). This is possible if the gas does not have a too large angular momentum and the gravitational attraction can overcome the pressure of the gas. The formation of stars, produces ionizing radiation that can ionize these atomic clouds. However, dust can shield the outer regions of large atomic clouds and can suppress a substantial ionization of these clouds. One generally finds that the intergalactic medium was not fully reionized till around $z \sim 6$ (Becker et al. 2001). Additionally, as mentioned, in higher density regions hydrogen is primarily present as molecular hydrogen H_2. Yet, stars do not only produce ionizing but also molecular dissociating radiation which can keep the clouds atomic. Furthermore, H_2 molecule dissociating radiation has an energy level $\sim$4.5 eV that is below the Gunn-Peterson trough $\gtrsim 10.2$ eV and hence can only be shielded against in high density H_2 clouds (Stecher & Williams 1967). Stars with a hot spectrum, i.e. blue stars (massive stars or white dwarfs) produce more ionizing radiation 13.6 eV$\sim 10^5$K than red stars (low mass to average or old stars), that produce considerable dissociating radiation (Kaufmann 1991). These atomic low density clouds are particular of interest as the atoms can remain substantially long in the ground state, assuming the gas had enough time to cool, or the gas has a temperature $T \lesssim 8000$K upon formation. Such clouds can exist in the ISM at present (Cox 2005), the IGM at high redshift and still also in the present IGM in high density regions where sufficient shielding is possible. In that case, a transition between the spin up and down state of the bound electron becomes likely in cold atomic hydrogen clouds, which produces radiation with a narrow line at

21 cm, the so called 21 cm line. However, a red-shift due to cosmic expansion leads to a decrease of the energy and thus making the assessment non-trivial. The Zeeman effect specifically splits the degeneracy of the different hyperfine-structure transition, which can be analyzed in the frequency difference of right and left handed polarized photons (Wolfe et al. 2008) . Due to the additional information from shifts in the polarization, the redshift can be distinguished from the Zeeman effect. This method led to an observation of fields strengths of about 10^{-4} G in atomic clouds, which are also present in the inter-galactic medium (IGM) (Wolfe et al. 2008) and hence stronger large scale fields in the IGM are excluded, due to non-observation. Note that the Zeeman effect can only tell us something about the field-strength in the respective gas cloud but it cannot provide information about the integral scale of magnetic field and its origin, yet we can at least infer that large scale coherent IGMF have at most a field strength of 10^{-4} G.

4.4.2 Faraday-Rotation

Another important signature of magnetic fields is Faraday rotation. Photons that pass an ionized medium that is imbued by a magnetic field will undergo a change in their polarization. Note, that this is only relevant if the light has a non-vanishing average polarization. One very important source of polarized light in the universe are blazars (Angel & Stockman 1980), i.e. active galactic nuclei that emit a jet of highly energetic particles in our line of sight. These accelerated particles emit polarized photons due to synchrotron radiation in the magnetic field of the AGN/jet. Faraday rotation differs from Zeeman splitting in the way it can be used to constrain magnetic fields, since the degree of Faraday rotation depends on the distance the photon travels through the coherently magnetized medium. The degree of rotation of the polarization corresponds to the rotation measure (Durrer & Neronov 2013)

$$\mathrm{RM} = \frac{e^3}{2\pi m_e^2} \int_0^L n_e(l) B_{\parallel}(l) \mathrm{d}l, \tag{4.28}$$

where $B_{\parallel}$ is the comoving line of sight magnetic field strength and the angle of the rotation is λ^2RM, where λ is the wavelength of the rotated photon (Durrer & Neronov 2013). Then, one needs to look at several wave-lengths to extract the initial polarization of the light. An estimate of the magnetic field strength is in generally not straightforward possible, as the free electron density in the region of interest is unknown and may vary strongly over the line of sight. A first order estimate for the electron density is the average free electron density in the universe and this leads to present constraints of

$$B \lesssim 2 \cdot 10^{-9} \left(\frac{l}{d_{H,\mathrm{ph}}} \right)^{-1/2} \mathrm{G}, \tag{4.29}$$

where $l = 2\pi/k$ is the correlation length (Blasi et al. 1999, Durrer & Neronov 2013). Then, one may also look at other signatures that can be used to estimate the charged density variations in the IGM. Of particular interest is the Lyman alpha forest. As discussed before in the universe there are many hydrogen clouds are present. Cold atomic hydrogen gas clouds emit the 21 cm line, yet in warm or hot atomic hydrogen gas louds other quantized transitions dominate, particularly the Lyman alpha transition. The Lyman alpha transition is a sign of a warm hydrogen gas cloud, where the variation of the line position allows an estimate of the distance towards a given gas cloud and the intensity of the line allows an estimate of the density and hence a more precise estimate of the free electron density (Blasi et al. 1999), that imply slightly tighter constraints at small scales. These estimates have been further improved with more modern simulations and the constraints became tightened to around 0.65 nG at the horizon and 1.7 nG at a Mpc scale (Pshirkov et al. 2016). Additionally, the magnetic field in more dense structures like gas clouds and/or galaxies may be significantly stronger than the IGMF in low density regions, which also would have to be effectively accounted for. Another important problem is that the galactic magnetic fields leads to a significant rotation measure itself that can overshadow IGMF, due to the much larger electron densities even though the relevant distances may be considerably smaller. In theory a subtraction of the rotation measure by the galactic magnetic field may suffice to get an improved estimate of the extragalactic component to the rotation measure, yet the models of the cosmological magnetic field still require considerable improvement (Jansson & Farrar 2012*a*, Jansson & Farrar 2012*b*). In principle Faraday rotation measurements from discrete sources like a blazar can be cross-correlated with the observation of synchrotron emission, that scale with B^2 from diffuse sources, e.g. cosmic rays that propagate through a magnetized medium, to estimate the strength of intergalactic magnetic fields (Lazarian & Pogosyan 2016, e.g.).

4.4.3 CMB

The CMB is still the best testing bed for pristine signatures of the very early universe. And as such, CMB observations allow constraints on primordial magnetic fields (Durrer 2007, Shaw & Lewis 2012). Magnetic fields impact the CMB in several different ways, first magnetic fields source velocity (especially vorticity) and density fluctuations in the CMB at smaller scales and the turbulent evolution also sources thermal energy due to viscous dissipation. Also, primordial density fluctuations are nearly Gaussian distributed, yet magnetic fluctuations source non-Gaussianity in the density correlation functions. Moreover, magnetic fields also change the polarization of the CMB due to the aforementioned Faraday rotation. Furthermore, spectral distortions i.e. deviations of the CMB from a black body are driven by primordial magnetic fields and a shift of the acoustic peaks in the CMB, corresponding to a change of the effective speed of sound due to the Alfven velocity $c_s^2 \to c_s^2 + b^2$, are a consequence of primordial IGMF. One of the most well studied CMB observables are anisotropies in the temperature auto-correlation function. The maximal size of the temperature anisotropies $\Delta T \sim 10^{-5} T$ can then be used to constrain magnetic fields, as these also produce anisotropies in the CMB and corresponds to 4.27

$$\frac{\Delta T}{T} \gtrsim 10^{-5} \left(\frac{B}{10^{-7}\mathrm{G}} \right)^2 , \tag{4.30}$$

since $b \gtrsim 1$ corresponds to $\rho_B \gtrsim \rho_\gamma$. Note that this estimate is only of relevance on scales above the Silk damping scale ~ 1 Mpc. Therefore, the CMB allows to easily set constraints on large scale intergalactic magnetic field at a level of $10^{-8} - 10^{-9}$ G. Another type of constraint comes from correlations that involve polarization of the CMB. Due to temperature anisotropies and Thomson scattering, the CMB develops so-called E-modes (linear polarization) at the 10% level of temperature anisotropies (Rees 1968). Of particular interest for magnetic fields are the so-called B-modes (circular polarization) e.g. as produced by Faraday rotation. There are many other astrophysical sources of CMB B-modes e.g. dust re-emission, gravitational lensing and gravitational waves, that also need to be taken into account. Temperature and Polarization data together provide at present constraints for magnetic fields $B(1\text{ Mpc}) \lesssim 2 \cdot 10^{-9}$ G on Mpc scales (Planck Collaboration et al. 2016, Sutton et al. 2017) based on data provided by the Planck satellite and BICEP2 / Keck Array. Present continuing and near-future CMB polarization observations are expected to provide tighter constraints by factors of $2-10$ (Sutton et al. 2017). Those analysis are generally based on two point functions, yet one can also look at the theoretical imprint of primordial magnetic fields in higher order CMB correlation functions. In particular, a study of three point functions provides slightly stronger constraints of $B \lesssim 0.6$ G (Trivedi et al. 2014). For specific models i.e. specific power laws of the magnetic auto correlation function, the above constraints become even tighter.

4.4.4 Gamma Rays

Gamma-ray astronomy may be able to already detect the presence of IGMF and thus provide lower limits on the strength of IGMF (Neronov & Vovk 2010, Durrer & Neronov 2013). Again, one of the objects of major interest are blazars. The high energy photons produced by the blazar will interact with the lower energy photons that constitute the extragalactic background light and can produce a charged secondary emission of highly energetic e^+e^- pairs (Gerasimova et al. 1962). These electron and positrons will predominantly move in the same direction as the incident high energy photon, if no magnetic fields are present. In a magnetic field, electrons and positrons are deflected and the beam essentially broadens. Furthermore, these charged particles also up-scatter photons via inverse Compton scattering to higher energies, which should produce a significant flux of GeV photons. Hence the non-observation of a correlated beam of GeV photons from a blazar that emits TeV photons indicates that either due to some mechanism the up-scattering of GeV photons is suppressed or that a sufficiently strong magnetic field is present which deflects the electrons and positrons sufficiently such that the photons are up-scattered in a more broader region, such that the Fermi space telescope can no longer detect the respective flux. Then, the angle over which no sufficient strong flux was detected (i.e. the telescope aperture and sensitivity) gives an lower limit on the strength of large scale magnetic field $B \gtrsim 10^{-16}$ G (Taylor et al. 2011) or even lower corresponding to more conservative assumptions $B \gtrsim 10^{-19}$ G (Finke et al. 2015) on Mpc scales. The key assumption is that the electron positrons pairs primarily cool by upscattering CMB photons, however instabilities in the plasma may provide a more effective energy loss mechanism (Broderick et al. 2012, Schlickeiser et al. 2012). These instabilities however may not become substantially important for cooling and depends strongly on the angular momentum and energy distribution in the e^+e^- beam (Miniati & Elyiv 2013, Durrer & Neronov 2013, Kempf et al. 2016). Thus the lower constraints are thus far still contested. There are other observations that are related to those gamma ray observations that also indicate the presence of helical primordial magnetic fields (Tashiro et al. 2014, Chen et al. 2015) with $B \gtrsim 10^{-14}$ G at 10 Mpc scales based on three-point functions of γ-ray arrival directions. At smaller scales, these constraints become even tighter roughly scaling with k_I^{-1}.

4.4.5 Potential future constraints

In the near or not-so-distant future, gravitational waves and an extragalactic cosmic ray source and composition identification may open up new avenues to constrain causally generated primordial magnetic fields. At present gravitational waves can already constrain inflationary magnetogenesis (Barrow et al. 1997, Caprini & Durrer 2002) based on nucleosynthesis constraints on the energy density parameter of gravitational waves (Kernan et al. 1996). There are currently two classes of detectors or surveys that either already detected or are expected to detect gravitational waves. Earth based detectors have gained particular attention as these led to the first detection of gravitational waves in a frequency window of $10 - 10^4$ Hz and the observation of a black hole merger event (Abbott et al. 2016). In the future an array of pulsars that is monitored by present and future earth based radio telescope, which observe correlations in the variations of arrival times of the pulsed light from pulsars (Verbiest et al. 2016, e.g.), is expected to detect gravitational waves at nHz frequencies (Bonetti et al. 2018), which may also provide constraints on first order QCD phase transitions and related magnetic fields (Caprini et al. 2010). However in the future another class of gravitational wave observatories, space based detectors, may become available. Of particular interest is the planned detector LISA that could observe gravitational waves in the frequency range $10^{-4} - 10^{-1}$ Hz, as these may constrain gravitational waves from first order phase transition at $T \sim 10$ GeV to $T \sim 10$ TeV (see (4.25)), which also include electroweak phase transitions (Caprini et al. 2016, Amaro-Seoane et al. 2017). In the far future μHz gravitational waves may also become observable (Sesana et al. 2019) and provide a window in between the QCD and electroweak transition and may also be of interest for strong helical magnetic fields from an electroweak transition as we discuss in subsection 5.2.2. Another interesting prospect for constraints on IGMF are cosmic rays. The deviation of the arrival direction of cosmic rays from their source may be used to constrain intergalactic magnetic fields, yet a substantially certain source identification is not yet possible. However, cosmic rays may already provide constraints which are comparable to the CMB constraints (Bray & Scaife 2018) based on potential source identification due to correlations between the anisotropy in the arrival directions of cosmic rays and extragalactic objects (Aab et al. 2018).

5 | Evolution of primordial magnetic fields and associated gravitational waves

So far, we have discussed and derived the basic equations that describe MHD turbulence (primarily incompressible) in the early universe and the generation of gravitational waves by MHD turbulence. Now, we will present and discuss solutions to those equations. First we take a look at the EDQNM equation and thereafter we look at the simulated gravitational wave spectra.

5.1 Solutions to the EDQNM equations

Here we discuss solutions of the previously discussed EDQNM equations for different initial conditions. We solve the equations on a logarithmic grid and in a manner that ascertains near numerically total energy, cross and magnetic helicity conservation in the nonlinear component of the evolution equations. Nonetheless, numerical problems led us to introduce a routine which in general does violate said evolution at some occasions (see section B.3). For details on the numerical treatment, we refer to the appendix B. One general thing to note is that we introduce an additional viscous damping term to speed up the computation and it fixes the inertial maximal length of the inertial to around three orders in magnitude, for details have a look at the section B.3. Otherwise, we will only briefly discuss aspects of the numerical approach here. First we look at the special case of a mirror-symmetric system i.e. all helicities vanish.

5.1.1 Reflectional-Symmetric MHD

For non-helical MHD, the EDQNM equations (3.75),(3.76), (3.77) and (3.78) greatly simplify and one finds for (3.75)

$$\begin{aligned}\left[\partial_\tau + 2\nu_+ k^2\right] E(k) = \frac{1}{2}\int_0^\infty \mathrm{d}q \int_{|k-q|}^{k+q} \mathrm{d}p \gamma(k,q,p,\tau) k^2 qp \Big[\Lambda_1(k,q,p)\tilde{E}(p)\tilde{E}(q) \\ - \Lambda_2(k,q,p)\tilde{E}^R(p)\tilde{E}^R(q) + \Lambda_3(k,q,p)\tilde{E}^R(p)\tilde{E}^R(k) - \Lambda_4(k,q,p)\tilde{E}(p)\tilde{E}(k) \\ - \Lambda_3(k,q,p)\tilde{E}^R(q)\tilde{E}(k) + \Lambda_2(k,q,p)\tilde{E}^R(k)\tilde{E}(q)\Big] - 2\nu_- k^2 E^R(k).\end{aligned} \tag{5.1}$$

For 3.76 one finds for non-helical systems

$$\begin{aligned}\left[\partial_\tau + 2\nu_+ k^2\right] E^R(k) = \frac{1}{4}\int_0^\infty \mathrm{d}q \int_{|k-q|}^{k+q} \mathrm{d}p \gamma(k,q,p,\tau) k^2 qp \Big[2\Lambda_1(k,q,p)\tilde{E}^R(p)\tilde{E}^R(q) \\ - 2\Lambda_2(k,q,p)\tilde{E}(p)\tilde{E}(q) + 2\Lambda_3(k,q,p)\tilde{E}^R(p)\tilde{E}(k) - 2\Lambda_4(k,q,p)\tilde{E}^R(k)\tilde{E}(p) \\ - 2\Lambda_3(k,q,p)\tilde{E}^R(q)\tilde{E}^R(k) + 2\Lambda_2(k,q,p)\tilde{E}(k)\tilde{E}(q) + 2\Lambda_5(k,q,p)\tilde{H}(p)\tilde{H}(q) \\ + 2\Lambda_8(k,q,p)\sum_{\pm}\tilde{H}(k)\tilde{H}(q)\Big] - 2\nu_- k^2 E(k).\end{aligned} \tag{5.2}$$

Lastly, for 3.77 one finds for parity invariant MHD turbulence

$$\begin{aligned}\left[\partial_\tau + 2\nu_+ k^2\right] H(k) = \frac{1}{2}\int_0^\infty \mathrm{d}q \int_{|k-q|}^{k+q} \mathrm{d}p \gamma(k,q,p,\tau) k^2 qp \Big[2\Lambda_9(k,q,p)\tilde{E}(p)\tilde{H}(q) \\ - \Lambda_4(k,q,p)\tilde{H}(k)\tilde{E}(p) - \Lambda_3(k,q,p)\tilde{E}^R(q)\tilde{H}(k) - \Lambda_8(k,q,p)\tilde{E}^R(k)\tilde{H}(q)\Big],\end{aligned} \tag{5.3}$$

where we have fixed $E = E^+ = E^-$, $H^R = 0$ and $H = H^+ = -H^-$ and the Λ_i are given in (3.79). Note that these choices are self-consistent e.g. $\partial_\tau H^R = 0$. The rate of change of the total cross scalar in the ideal case is

$$\begin{aligned}\int_0^\infty \frac{\mathrm{d}k}{k}\frac{\partial H}{\partial\tau} =& \frac{1}{2}\int_0^\infty \frac{\mathrm{d}k}{k}\int_0^\infty \mathrm{d}q \int_{|k-q|}^{k+q} \mathrm{d}p \gamma(\tau,k,q,p) k^2 qp \Big[\Big(2\Lambda_9(p,k,q) \\ &- \Lambda_4(k,p,q)\Big)\tilde{E}(q)\tilde{H}(k) - \left(\Lambda_3(k,q,p) + \Lambda_8(q,k,p)\right)\tilde{E}^R(q)\tilde{H}(k)\Big].\end{aligned} \tag{5.4}$$

Furthermore,

$$\int_{|k-q|}^{k+q} \mathrm{d}pp\,(\Lambda_3(k,q,p)+\Lambda_8(q,k,p)) \leq \int_{|k-q|}^{k+q} \mathrm{d}pp\,(2\Lambda_9(p,k,q)-\Lambda_4(k,p,q)) \leq 0, \quad (5.5)$$

for all k, q, which indicates that for $E^R \leq 0$ (magnetic domination), the cross scalar only decays. Note, that a significant absolute cross scalar is only possible for near equipartition $|E^R| \ll E$. Generally, one also has $|E^R(q)| \leq E(q)$ meaning the cross color, with the same sign on all scales, is also likely to undergo decay in many cases, although a generation of the cross scalar is possible. Therefore, at least within the context of the EDQNM approximation any stochastic alignment between the current and velocity field decays and hence in non-helical incompressible MHD there is no growing mode for the total cross-scalar. Hence, one expects that non-helical turbulence with and without some initial cross-scalar in particular in system with Pm$\gg$ 1 should evolve without any considerable difference, as the cross scalar is expected to decay. Furthermore, the cross scalar only directly impacts the energy difference but not the total energy as it does not explicitly appear in (5.1). However, it should be noted that the above argument is not directly applicable when the cross-scalar spectrum is more complicated e.g. when it has multiple roots. For the simulation we generally use an initial spectrum of the type

$$f(k) = C\frac{k^n}{a+k^{n_b}}e^{-k/k_d}, \quad (5.6)$$

where we choose $a = (n_b - n)/n$, while the value of C depends on the initial total energy chosen and we generally set $k_d = 10k_I$ as the integral scale. For the kinetic and magnetic energy we generally choose $n_b/2 = n = 5$ and for the cross scalar we set $n = 6$ and $n_b = 11$. The choice of the already initially chosen large scale tail is based on the discussion in subsection 3.4.4. For example a initial choice of $n = 5$ for the cross scalar is not justifiable based on turbulent non-linear evolution alone. Table 5.1 shows the different mirror symmetric scenarios that we discuss here, where an energy of 0.1 corresponds to a velocity of ~ 0.4. These parameters are chosen to represent some

ID	$v^2/2$	$b^2/2$	λ_J
S1	0.1	0.1	0
S2	0	0.1	0
S3	0.1	0.1	0.9

Table 5.1: Reflection-Symmetric Scenarios: The value λ_J denotes the amount of cross-scalar by a constant ratio as defined in (3.16), and $v^2/2$ and $b^2/2$ are the total kinetic and magnetic energy that is initialized. We use as initial condition (5.6) with $n = n_b/2 = 5$ for the cross scalar $n = 6$ an $n_b = 11$ and hyperviscous damping as described in appendix B.3.

rather extreme scenarios. The simulations are initialized at $T = 150$ GeV, which reflects, up to a factor of $\mathcal{O}(1)$, typical electroweak phase transition scales. Furthermore, we assume here an initial integral scale of $L_I = 0.3 d_H(150 \text{ GeV})$. Therefore, these scenarios correspond to a phase transition with $v_w \sim c_s$, $\alpha \sim 0.2 - 0.3$ and $\beta^{-1} \sim L_I$. We integrate the system up to around a temperature of $T \sim 1$ eV corresponding to matter-radiation equality. Additional, all energy densities and topological quantities plotted are dimensionless comoving quantities ($c^2 = 1$), as defined in section 3.1. First, in figure 5.1 we show the evolution of the system S1 (see table 5.1). Initially the turbulent energy spectra develop a near-Kolmogorov spectrum with a spectral index of -0.63 to then undergoes more significant decay at $T \lesssim 100$ MeV until turbulent transfer of magnetic to kinetic energy is suppressed due to the expansion. Here, the maximal length of the inertial range is limited by the introduction of an additional damping term, that allows reduces the range of scales we would otherwise have to take into account and also reduces the integration time significantly. The kinetic energy at $T = 3$ MeV shows the transition between the free-streaming and dissipative regime, where at larger scales kinetic energy is still dissipated while at smaller scales kinetic energy is re-excited by the magnetic field in the free-streaming regime, which leads to the reemergence of an inertial range. For $T \lesssim 10$ keV, photon decoupling sets in and at around $T \lesssim 10$ eV, prior to matter-radiation equality and last scattering, turbulence may restart again. Note that the MHD spectra will undergo further evolution. As can be seen in figure 4.3 $\mathrm{Re}_m \sim 10^{13}$ with $v = 1$ and $L = d_H$. Here we have $b \sim 10^{-6}$ and $L_I/d_H \sim 10^{-7}$, which means that $\mathrm{Re}_m(b, k_I) \sim 1$ at recombination. Taking (4.27) into account, the range

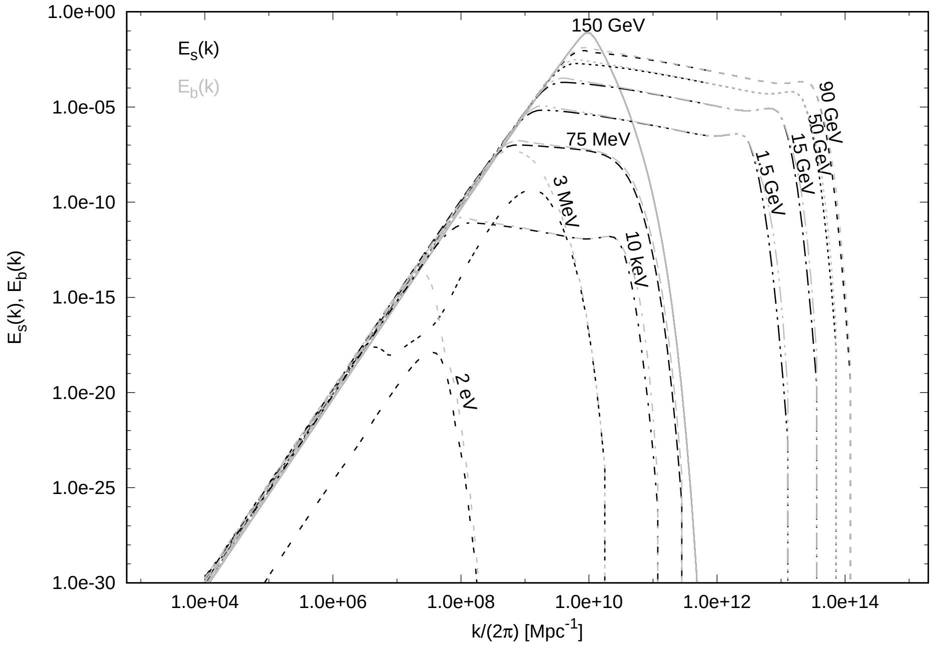

Figure 5.1: Evolution of a magnetic field spectrum sourced at $T = 150$ GeV with an equipartition between kinetic and magnetic energy (solid lines) corresponding to S1 in table 5.1, where the color black represents the kinetic spectrum, while the color grey represents the magnetic energy spectrum. The spectra are shown for $T = 90$ GeV (short dashed), $T = 50$ GeV (dotted), $T = 15$ GeV (long dashed dotted), $T = 1.5$ GeV (long dashed double dotted), $T = 75$ MeV (long dashed), $T = 3$ MeV (triple dotted), $T = 10$ keV (short dashed dotted) and $T = 2$ eV (short double dashed). The x-axis denotes the comoving wave-number (today) and the y-axis the energy spectra in units 1/2. Hyperviscous damping B.3 limits the inertial range in the high temperature regime to around three orders of magnitude in k. The inertial range scaling differs slightly from Kolmogorov's $-2/3$ law and has an effective power law index of -0.63. At around $T \sim 100$ MeV to $T \sim 1$ MeV neutrino decoupling impacts the evolution, while at temperatures $T \lesssim 10$ keV photon decoupling becomes relevant and at a $T \sim 1$ eV turbulence may reemerge on smaller scales. In this particular case, magnetic dissipation will become important after recombination and the peak of the spectrum will be dissipated by resistive damping, yet this is not of importance for the large scale tail at Mpc or even kpc scales.

where magnetic dissipation may be important, prior to reionization, for electroweak seeded magnetogenesis is roughly $B(k_I) \lesssim 10^{-13}$G. This means that the last spectrum shown at $T \sim 2$ eV does not correspond to the present day spectrum, however the large scale component of the spectrum, should remain nearly constant, while other factors like galactic magnetic outflows and cosmic rays may be of bigger importance at small scales regardless. Next, in figure 5.2 we show in the left panel the evolution of an initially purely magnetic system S2 and find no significant deviation from the scenario S1 other than a slightly smaller amplitude, as there is overall less turbulent energy sourced initially. On the right panel, we look at incompressible MHD turbulence with a non-zero cross-scalar

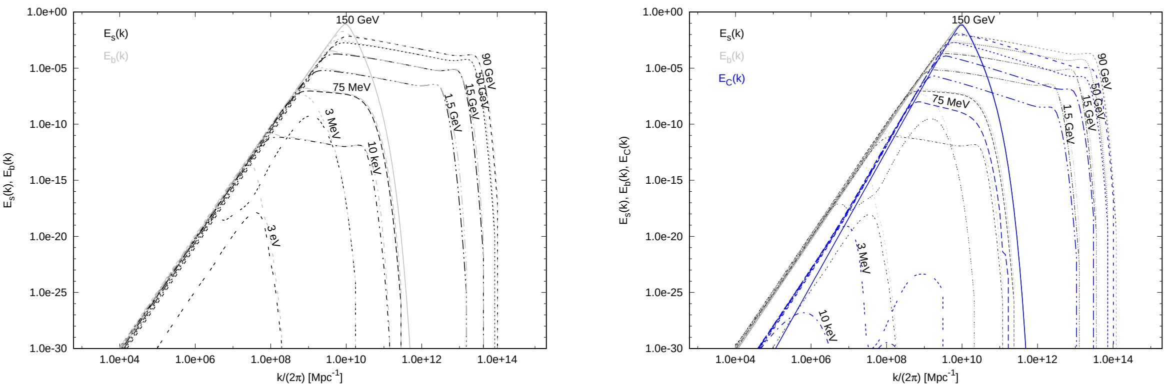

Figure 5.2: Evolution of a magnetic field spectrum sourced at $T = 150$ GeV with only magnetic energy according to S2 (left panel) and with an equipartition between kinetic and magnetic energy and a near maximal purely positive cross scalar according to S3 (right panel) in table 5.1. On the left panel, the color black represents the kinetic spectrum, while the color grey represents the magnetic energy spectrum. On the right panel the color blue represents the absolute value of the cross scalar spectrum and the other lines (thinner) are again the magnetic (grey) and kinetic energy (black) spectrum. The spectra are shown at $T = 90$ GeV (short dashed), $T = 50$ GeV (dotted), $T = 15$ GeV (long dashed dotted), $T = 1.5$ GeV (long dashed double dotted), $T = 75$ MeV (long dashed), $T = 3$ MeV (triple dotted), $T = 10$ keV (short dashed dotted), $T = 3$ eV (short double dashed). Note, that the x-axis denotes the comoving wave-number (today) and the y-axis the different spectra. Also, the inertial range scaling of the cross scalar is k^{-1}, which differs from the near Kolmogorov spectrum which is still present for energy spectra. Moreover, the large scale tail of the cross scalar follows a k^6 slope as discussed in sub-subsection 3.4.4.

S3. In the incompressible parity-invariant QN MHD equations, the cross scalar remains always 0 if the cross scalar spectrum vanishes at some point, thus the scenario with non-zero cross scalar may lead to distinct properties in the evolution. Yet, there are no relevant deviations and as discussed before, one generally expects that the cross-scalar is simply dissipated. Due to neutrino decoupling most of the cross scalar spectrum is dissipated at around $T \gtrsim 1$ MeV, however the large scale component of the cross-scalar drives the evolution of a small scale cross scalar in the free-streaming regime and hence neutrino decoupling does not completely damp any initially present cross scalar (see the cross scalar spectrum at $T = 3$ MeV), nonetheless it still undergoes significant decay and is nearly completely dissipated prior to photon decoupling. Additionally, the cross scalar spectrum shows a steeper inertial range spectrum with spectral index ~ -1. Furthermore, there appears to be a very important deviation in the spectral index of the large scale tail of the cross scalar spectrum. As discussed in subsection 3.4.4, the cross-scalar should develop a k^6 large scale tail which appears to be the case for around three orders of magnitude in k, but at even larger scales a k^5 spectrum develops. This is a numerical artifact and has to do with an averaging procedure that we employ to ascertain energy and helicity conservation in the numerical calculation of the nonlinear component of the EDQNM equations. In particular, the difference in scaling between the cross scalar and energy spectra at large scales is due to the fact that the coefficients Λ_i, that appear in the cross scalar evolution equation, vanish at the $\mathcal{O}(k^2)$ level for terms like $E(q)H(p)$ or $\mathcal{O}(k^0)$ level for terms like $E(k)H(q)$ only in the p-integration. Whereas, for the energy integration this is not the case. Here, we average over an allowed grid ($\mathbf{k}+\mathbf{q}+\mathbf{p}=0$) for different k, q, p prior to integration over p with a logarithmic distribution of sampling points, as is discussed in detail in appendix B. Then, it turns out that the averaged Λ_i do not exactly vanish at lowest possible order in k, but a residual contribution due to the non-linear grid average leads to the appearance of a k^5 large scale tail for the cross scalar at large scales. Luckily this does not appear to impact the overall evolution, so we do not devote any time on resolving this issue. Also, at small scales for an inertial range with less than three orders of magnitude in k, we do not expect this to be a problem for the turbulent small scale evolution. Lastly, in figure 5.3 we look at the overall temporal scaling behavior of the total turbulent energy (right panel) and the integral scale (left panel). Initially, the integral scale increases rather quickly as the system settles into the self-similar phase. Next, towards neutrino decoupling the integral scale freezes in. After the free-streaming affects the turbulent spectra, i.e. $L_I \ll \lambda_{\mathrm{mfp},\nu}$ another self-similar phase of turbulent evolution begins. Thereafter at $T \sim 10$ keV photon decoupling affects the turbulent evolution. Photon decoupling leads to a significant deviation from the typical temporal power law scaling, due to the fact that the relative growth of the free mean path of photons is slower than that of the neutrinos. The turbulent spectra may still undergo decay in photon freestreaming regime until the effective Lagrangian eddy turnover time is compatible to the Hubble time. However, for the specific field strengths and integral scale magnetic dissipation becomes of relevance around recombination for these cases, as previously discussed. Regardless, the large scale tail of the spectrum will remain

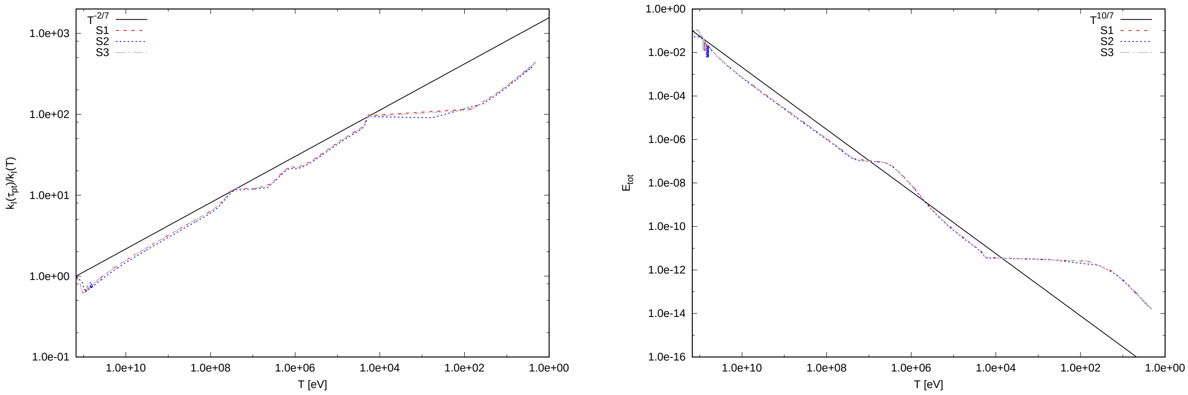

Figure 5.3: Evolution of total turbulent energy and integral scale, relative to the initial integral scale e.g. at the phase transition, for the different scenarios S1 (red, dashed), S2 (blue, dotted) and S3 (dot-dashed, grey) as represented in table 5.1 as a function of the temperature T. Note that the different scenarios barely differ from each other. The power laws correspond to the scaling laws for the total energy and integral scale as discussed in subsection 3.4.5 with $\gamma = 0$. The two plateau like phases at $T \sim 10$ GeV and 10 eV$\lesssim T \lesssim 10^4$ eV correspond to neutrino and photon decoupling respectively, note that the respective phases remain slightly longer and primarily affect the turbulence due to free streaming e.g. at $T \sim 10$ eV. The overall evolution of the spectra is best described by $\gamma \sim 0.085 - 0.1$ i.e. a slight growth of the large scale tail. This corresponds to ($\gamma = 0.1$) $E \propto \tau^{-1.4}$ and $k_I \propto \tau^{-0.3}$ rather than power law indices of -1.429 and -0.286 ($\gamma = 0$) respectively. After last scattering turbulence may be quickly reestablished and then frozen in due to ambipolar diffusion.

frozen and only the overall expansion is of interest. Overall, the energy loss rate $\tau^{-7/5}$ is slightly smaller than the often-discussed $\tau^{-10/7}$ scaling (see subsection 3.4.5). While for the integral scale the scaling corresponds to $\tau^{3/10}$ and is slightly faster than the $\tau^{2/7}$ scaling. This corresponds to $\gamma \sim 0.1$ in subsection 3.4.5. In summary, incompressible MHD turbulence evolves effectively in only one very simple manner and other factors like cross scalar or initial magnetic dominance do not impact the evolution in any relevant way, except for minor initial variations. In the following subsection we discuss our findings regarding helical MHD.

5.1.2 Helical MHD

In incompressible helical MHD, the overall system is more complex, not only due to the fact that three more spectral functions are of interest, but specifically due to the appearance of two more ideal invariants. These other topological measures may impact how the cross scalar and the different energies evolve. In general, due to the conservation of magnetic and cross helicity, one at least expects that there are also growing modes for the cross scalar present. Moreover, in ideal or Pm= 1 MHD one expects that the conservation of cross helicity dominates that of magnetic helicity and the system should hence at some time become trivial, i.e. the rates of change of the different spectra should become negligible as soon as cross helicity attains its maximal value. As is well known, the presence of magnetic helicity leads to a drastic change in the large scale tail of the energy spectra, where turbulent energy is shifted to larger scales (see 3.4.5). Another interesting quantity is the kinetic helicity, which is conserved in ideal hydrodynamic turbulence. Kinetic helicity is one of the key components in the generation and the sustaining of galactic magnetic fields by the so-called α-dynamo (Parker 1970, Kulsrud 1999*b*). Consequently, it is also of interest to wonder and study in what manner kinetic helicity may impact isotropic and homogeneous MHD turbulence. Typical, kinetic helicity is expected to undergo a simple and direct cascade in hydrodynamic turbulence, yet even there the properties of the specific spectrum may lead to different behavior (Waleffe 1992). As already seen, in the previous section neutrino decoupling damps cross scalar and hence it will also damp kinetic and cross helicity, however turbulent processes can lead to a small cross and kinetic helicity being present on smaller scales. Moreover, magnetic helicity can source kinetic helicity, if none is present prior, while kinetic helicity also sources a non-trivial magnetic helicity spectrum. Table 5.2 shows the key parameters for the different helical scenarios that we will discuss here. As before, the simulations are initialized at $T = 150$ GeV with an initial integral scale of $L_I = 0.3 d_H$ (150 GeV). We integrate the system up to around a temperature of $T \sim 1$ eV corresponding to matter-radiation equality. Here, we will only look at some of these cases in detail and look at the other in terms of their temporal scaling properties. In figure 5.4, we show an MHD system with magnetic helicity according to H2 in table 5.2. On the left panel, one sees the evolution of the kinetic and magnetic energy spectra. One key difference to the non-helical scenarios is a significant shift of the large scale tail of the spectrum towards smaller k. This is an inverse cascade and as discussed in subsection 3.4.5 occurs due to the conservation of magnetic helicity. Thus, the large scale tail is effectively parallel shifted by four orders of magnitude in k

ID	$v^2/2$	$b^2/2$	λ_J	λ_K	λ_B	λ_C
H1	0.1	0.1	0	0.9	0.9	0
H2	0.1	0.1	0	0	0.1	0
H3	0.1	0.1	0	0	0.01	0
H4	0.1	0.1	0.4	0	0.4	0
H5	0.1	0.1	0.1	0.1	0.1	10^{-3}
H6	0.1	0.1	0	0	10^{-4}	0
H7	0.1	0.1	0	0.9	0	0
H8	0.1	0.1	0.4	0.4	0	0
H9	0.1	0.1	0	0	10^{-8}	0

Table 5.2: Helical Scenarios: The value λ_J denotes the amount of cross-scalar in the system given by a constant ratio as defined in (3.16). The value λ_K denotes the amount of normalized kinetic helicity by a constant ratio as defined in (3.13). The value λ_B denotes the amount of cross-scalar by a constant ratio as defined in (3.14). The value λ_C denotes the amount of cross-scalar by a constant ratio as defined in (3.15). We generally use as initial condition (5.6) with $n = n_b/2 = 5$ for the energy spectra. For the helicities, except the cross helicity, and the cross scalar spectra we use $n = 6$ and $n_b = 11$, while for the cross helicity we apply $n = 7$ and $n_b = 12$ as discussed in subsection 3.4.4.

up to around matter-radiation equality. As we discuss soon, the integral scale grows as $L_I \propto \tau^{2/3}$ up to around $T \sim 100$ eV. After last scattering, unlike for the specific non-helical cases discussed here, turbulence can recommence in the photon free-streaming regime and magnetic dissipation remains negligible. The inverse cascade can then effectively proceed until $k_I b(k_I) \sim \mathcal{H}(\tau)$, as the eddy turnover rate grows slower than the Hubble rate. Next, in figure 5.5 we showcase an MHD system with kinetic helicity according to H7 in table 5.2. On the right panel one sees the development of the magnetic and kinetic helicity. Immediately after initialization a non-trivial magnetic helicity spectrum is generated with $\int \mathrm{d}k H_b(k)/k^2 \approx 0$. The magnetic helicity spectrum traces the kinetic helicity spectrum. However, here the magnetic helicity does not drive an inverse cascade, at least not initially. And the system behaves in the same manner as parity invariant turbulence. Also, at temperatures $\lesssim 100$ MeV, a net total magnetic helicity seems to appear. In principal, kinetic helicity produces a magnetic helicity spectrum and the magnetic helicity then decays at the small scales due to resistive damping. Thus, net magnetic helicity can be produced by resistive damping. Moreover, this is only an effective method if Re$\gg 1$ and Re$_m \gtrsim 1$. Therefore, the net magnetic helicity found here is primarily the result of a smoothing and cut-off procedure to ascertain numerical

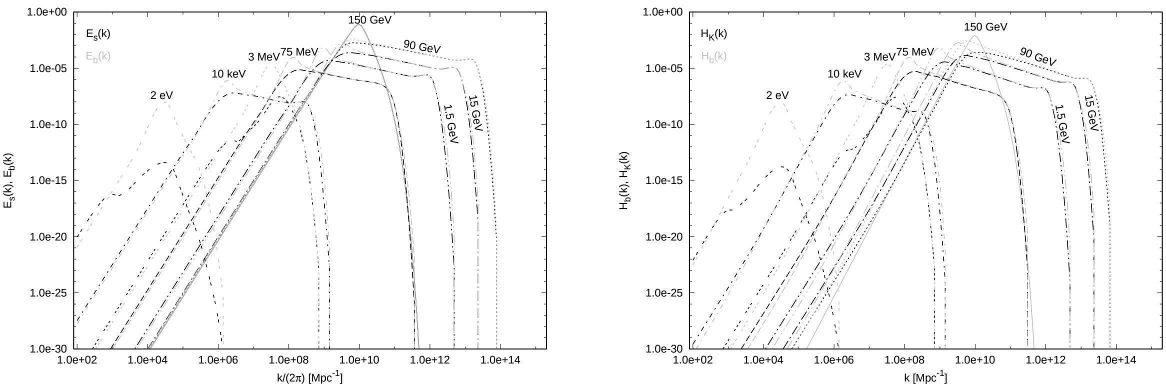

Figure 5.4: Evolution of a magnetic field spectrum sourced at $T = 150$ GeV with an equipartition between kinetic and magnetic energy and near maximal magnetic helicity according to H2 in table 5.2 (solid lines). On the left panel we show the evolution of the magnetic (grey) and kinetic (black) energy spectra and on the right panel we show the absolute magnetic (grey) and absolute kinetic (black) helicity spectrum. Note that here the cross scalar and helicity always remain zero, however the kinetic helicity, even though it is initially zero, attains a non-trivial spectrum. The spectra are shown for $T = 90$ GeV (dotted), $T = 15$ GeV (dashed dotted), $T = 1.5$ GeV (dashed double dotted), $T = 75$ MeV (dashed), $T = 3$ MeV (triple dashed), $T = 10$ keV (short dashed dotted), $T = 2$ eV (double dashed). Note, that the x-axis denotes the comoving wave-number (today) and the y-axis denotes the relevant spectra. One clearly finds a significantly different evolution of the MHD turbulence for magnetic helicity dominated turbulence compared to parity invariant MHD. In particular, the large scale tail does not remain nearly constant but is shifted to larger scales (smaller k), by around four orders of magnitude in k. Secondly, since the total magnetic helicity is conserved only a slight amount of magnetic energy is dissipated due to neutrino decoupling. Prior to last scattering, the MHD turbulence is effectively frozen in at $T \sim 10^2$ eV. Note that the kinetic helicity that is excited by the magnetic helicity has the same sign as the magnetic helicity, and traces the magnetic helicity spectrum at most scales except around the integral scale. The energy spectra follow a near Kolmogorov spectrum, while the two helicities have a k^{-1} scaling in the inertial range. The large scale tail of the energy spectra has the k^5, while the helicities show the k^6 behavior. Also, the magnetic helicity leads to a more distinctive peak of the magnetic energy spectrum due to the k^6 scaling of the magnetic helicity. This spectrum at $T \sim 2$ eV does not represent the present day spectrum and in this particular case turbulence can restart in the photon freestreaming regime and shift the peak of the spectrum until $k_I b(k_I) \sim \mathcal{H}(\tau)$.

stability of the solver, and in principle this can be further improved (see appendix B.3 for details). Nonetheless, this method of magnetic helicity production is quite intriguing and could even be an important source of magnetic helicity in the very early or present day universe. Furthermore, this indicates that a magnetic field spectrum with roots will at most lead to a delayed inverse cascade due to the smaller total net magnetic helicity. Now, in figure 5.6 we show the impact that a relatively small cross helicity (similar for larger cross helicities) has on the MHD turbulence evolution according to H5 in table 5.2. Initially, the energy spectra and also the cross helicity undergo an inverse cascade due to the also initialized magnetic helicity. However, the cross helicity remains nearly

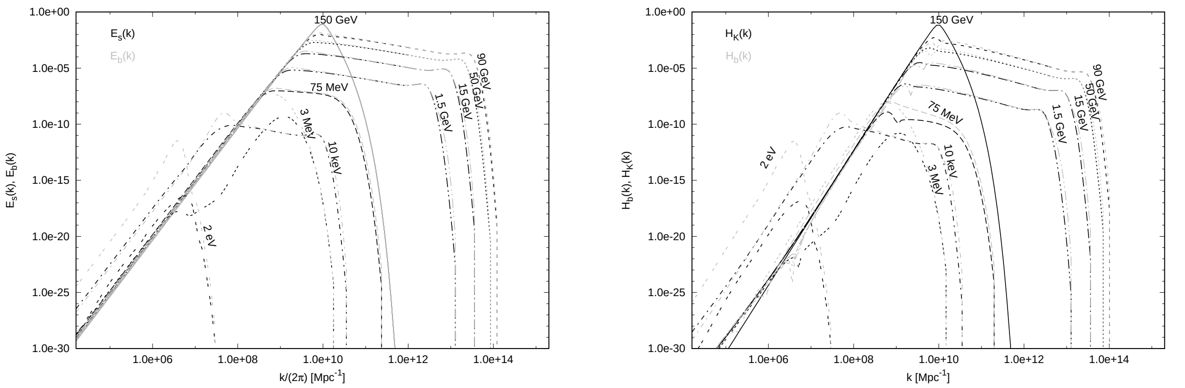

Figure 5.5: Evolution of a magnetic field spectrum sourced at $T = 150$ GeV with an equipartition between kinetic and magnetic energy and near maximal kinetic helicity according to H7 in table 5.2 (solid lines). On the left panel we show the evolution of the magnetic (grey) and kinetic (black) energy spectra and on the right panel we show the absolute magnetic (grey) and absolute kinetic (black) helicity spectra. Note that here the cross scalar and helicity always remain zero, however the magnetic helicity, even though it is initially zero, attains a non-trivial spectrum. The spectra are shown at $T = 90$ GeV (short dashed), $T = 50$ GeV (dotted), $T = 15$ GeV (long dashed dotted), $T = 1.5$ GeV (long dashed double dotted), $T = 75$ MeV (long dashed), $T = 3$ MeV (triple dotted), $T = 10$ keV (short dashed dotted), $T = 2$ eV (short double dashed). Note, that the x-axis denotes the comoving wave-number (today) and the y-axis the different spectra. Initially, the system evolves similarly to the non-helical case i.e. the kinetic helicity does not affect the evolution. However, after neutrino decoupling an inverse cascade seems to appear, resulting from the appearance of some minor total non-zero magnetic helicity $\int \mathrm{d}k H_b(k)/k^2 \neq 0$. In fact kinetic helicity sources a magnetic helicity spectrum with $\int \mathrm{d}k H_b(k)/k^2 = 0$ and due to resistive decay and numerical artifacts, e.g. due to smoothing, some non-zero total magnetic helicity appears that drives an inverse cascade. Another interesting observation is that the sourced magnetic helicity seeds significant kinetic helicity after neutrino decoupling i.e. kinetic helicity has an effect on the turbulence even after neutrino decoupling. The magnetic helicity sourced by a purely positive kinetic helicity spectrum, gains positive values around k_I and negative values for $k \ll k_I$ and $k \gg k_I$.

conserved like the magnetic helicity even during the inverse cascade and as soon as it becomes maximal the turbulence freezes in, i.e. the system is dominated by the direct dissipative terms in the evolution equation even though $\mathrm{Re}_m \gg \mathrm{Re} \gg 1$. The decoupling of the neutrinos leads to a complete decay of the cross helicity and in contrast to the non-helical case (see right panel in figure 5.2) the cross scalar is also completely dissipated as the cross helicity suppresses a quick reappearance of turbulence on small scales in the free-streaming regime. Therefore, any causally produced cross helicity, that appears at temperatures $T \gtrsim 100$ GeV and becomes maximal, is dissipated and is unlikely to even produce an imprint in the cosmological neutrino background. Smaller cross helicities could become relevant due to generation of a cross scalar, when magnetic helicity is present, that may survive neutrino decoupling, as shown in the right panel of

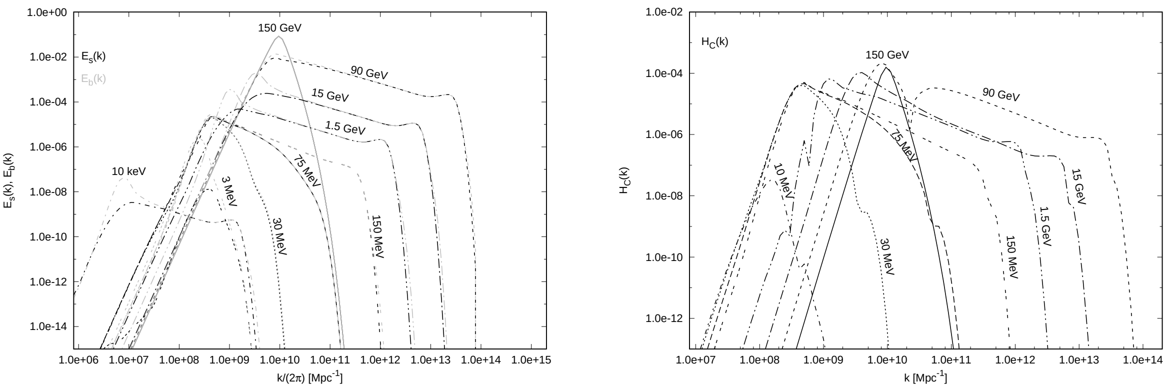

Figure 5.6: Partial evolution of a magnetic field spectrum sourced at $T = 150$ GeV with an equipartition between kinetic and magnetic energy and with magnetic, kinetic and cross helicity and cross scalar according to H5 in table 5.2 (solid lines). Here we focus on the impact of the cross helicity on a system with magnetic and kinetic helicity and a non-trivial cross-scalar. We only look at a part of the evolution where the relatively small cross helicity becomes of interest. On the left panel we show the evolution of the magnetic (grey) and kinetic (black) energy spectra. On the right panel we showcase the evolution of the cross helicity (black). The spectra are shown at $T = 90$ GeV (dashed), $T = 15$ GeV (long dashed dotted), $T = 1.5$ GeV (long dashed double dotted), $T = 150$ MeV (double dashed), $T = 75$ MeV (long dashed), $T = 30$ MeV (dotted), $T = 3$ MeV (short triple dashed) and $T = 10$ keV (left) or $T = 10$ MeV (right) (dashed-dotted). Note, that the x-axis denotes the comoving wave-number (today). The magnetic helicity leads to the appearance of an inverse cascade. At around $T \sim 200$ MeV cross helicity becomes dominant and the turbulent evolution halts. Then, energy losses are only due to direct dissipation. Afterwards, the cross helicity is being completely dissipated by the decoupling of the neutrinos and the inverse cascade can restart again. Similarly, the cross scalar is also completely dissipated, unlike for systems without cross helicity, after neutrino decoupling. The cross helicity also develops a k^7 large scale tail as discussed in subsection 3.4.4. Also, when the cross helicity is maximal the energy spectrum develops a k^{-1} inertial range. Moreover, initially the total positive cross helicity develops a negative valued inertial range and gains more power at the integral scale. Note, that the small bump for the cross helicity in the dissipative range shows another sign-change in the spectrum.

figure 5.2. The stalling effect of cross helicity could however have an impact on gravitational waves from MHD turbulence that is dominated by a non-trivial cross-helicity. Note, that similar to magnetic helicity only the total value of the cross helicity is of relevance. Additionally, as discussed in subsection 3.4.4, we observe a k^7 large scale tail for the cross helicity spectrum.

Lastly, we look at the evolution of the integral and energy scale in the radiation dominated phase. In figure 5.7, we show the temporal scaling for the different helical scenarios as given in table 5.2. As discussed in subsection 3.4.5 the integral scale in magnetic helicity driven MHD turbulence grows as $\tau^{2/3}$ and the energy scale decays with $\tau^{-2/3}$. In all scenarios, except for H7 and H8, a total net magnetic helicity is initially present. The scenario H1 represents MHD turbulence with initially near maximal

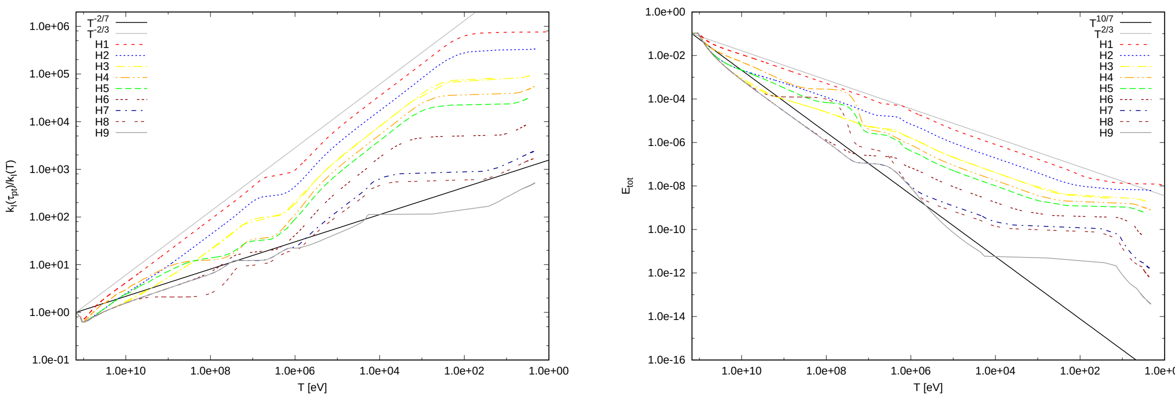

Figure 5.7: Evolution of total turbulent energy and integral scale, relative to the initial integral scale e.g. at the phase transition, for the different scenarios H1 (red, dashed), H2 (blue, dotted), H3 (yellow, dot-dashed), H4 (orange, double dot-dashed), H5 (green, long dashed), H6 (dark-red, triple dashed), H7 (dark-blue, short dashed-dotted), H8 (brown, double dashed) and H9 (dark-grey, solid) as represented in table 5.2 as a function of the temperature T. The black and grey solid lines indicate the normal MHD cascade and the magnetic helicity driven inverse cascade (see subsection 3.4.5 with $\gamma = 0$). There are several interesting processes to note, but also numerical difficulties and modeling problems e.g. due to hyper-viscous damping that come to the forefront, as we discuss in the sub-subsection here.

magnetic and kinetic helicity. With the exception of the neutrino and photon decoupling phase the magnetic energy follows an inverse cascade. Scenario H5 includes all topological measures from the beginning with a small total cross helicity. As soon as the cross helicity attains a maximal state, turbulence also stalls. This behavior is also observed in the case with magnetic (H4) or kinetic helicity (H8) and a non-trivial cross scalar. However, in these cases there is no initial net cross helicity present. Immediately after the start of the turbulent evolution, a net cross scalar is produced due to dissipation of the cross helicity spectrum at small scales and the total cross helicity is of the order $k_I/k_d E_{\rm tot}$, where k_d is the dissipative wave number. Here, the precise effect is probably too large due to the hyperviscous damping and in realistic scenarios we would anticipate a much smaller cross helicity production, yet as for the magnetic helicity production it is generally an interesting process when the Reynolds number is somewhat small i.e. Re$\sim$ 100 for a brief time during the magnetogenesis phase. Furthermore, in these scenarios also magnetic helicity is dissipated. This is a problem of the solver that we apply, as we also cutoff small spectral values for stability reasons, however cross helicity does suppress the evolution of turbulence quite strongly even during the phase where the cross helicity is nearly fully dissipated and so the magnetic helicity transfer is strongly suppressed and it gets now easily dissipated by these cutoff effects (see appendix B.3). This numerical effect also affects scenarios with some initial magnetic helicity and without cross correlations. We illustrate the problem in the left panel of figure 5.8, where we show the change of the total magnetic helicity $\mathcal{H}_b$ and the change of the total cross helicity H_C. Moreover, here the numerical loss of the total magnetic helicity in particular is not continuous but step wise. As discussed before, the magnetic helicity remains preserved for most of the evolution if it is initially sufficiently large, i.e. very small initial magnetic helicities cannot drive a sufficient inverse cascade prior to the resistive dissipation becoming important e.g. $k_I H_b(k_I) \lesssim 10^{-13}$ at the electroweak horizon. Afterwards, in the matter dominated phase, turbulent evolution with Pm$\gg 1$ and Re$\gg 1$ can proceed again and as discussed before the large scale tail is further shifted to larger scales. Generally, in none of the scenarios discussed here cross helicity will have an impact on the strength or the spectrum of magnetic fields today.

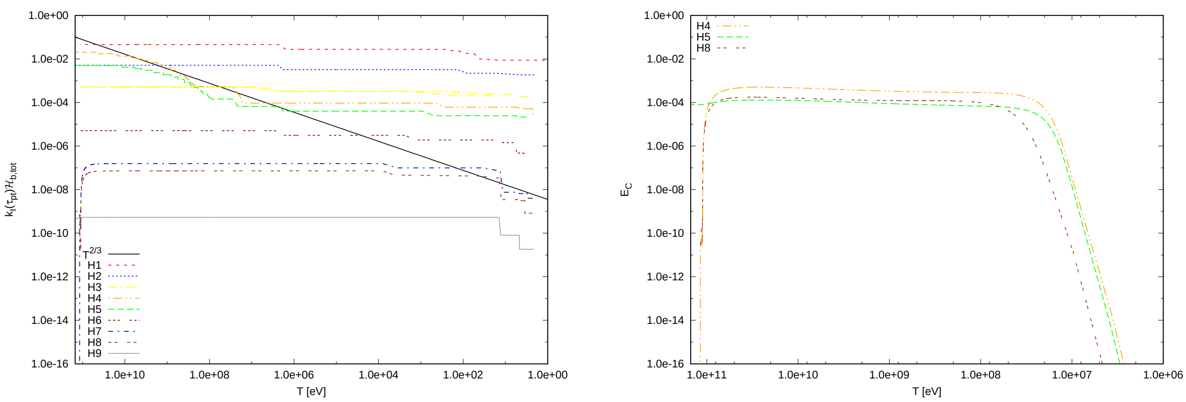

Figure 5.8: Here we show the total magnetic (left panel) and cross helicity (right panel) evolution. On the left panel, one finds for the scenarios H4 and H5 a decay of magnetic helicity during the maximally cross helical phase. The decay occurs in a step-wise manner following the $\tau^{-2/3}$ scaling and indicates that it is primarily due to numerical artifacts.. In the other scenarios, this problem is, to a lesser extent, also observed and becomes more problematic for small magnetic helicities. The problem is due to an introduced cut-off procedure that keeps the solution stable, and is explained in appendix B.3. On the right panel, we show the evolution of the total cross helicity H_C that initially appears in the scenarios H4 and H8, that contain no initial cross helicity. In contrast to the magnetic helicity, the cross helicity varies slightly over time and is then gradually dissipated during neutrino decoupling. The cutoff issue that impacts the magnetic helicity does not appear to impact the cross helicity evolution in a significant manner. For further details see the caption of figure 5.7.

5.2 Solutions to the GW equation

Here we focus on the solutions of (3.135), which gives the gravitational wave energy density parameter spectrum originating from MHD turbulence. We do not solve the EDQNM equations in order to calculate the GW spectrum, rather we use the temporal and spatial scaling laws to solve for the GW spectrum, which is significantly less expensive to calculate than solving the coupled system of equations, for details see appendix C. Also, we express the spectra as a function of the frequency rather than the wave number. The peak frequency of the gravitational wave spectrum is given by (Caprini & Figueroa 2018)

$$f_{GW} = 2.6 \cdot 10^{-8} x_k \left[\frac{g_{pt}}{100}\right]^{\frac{1}{6}} \left(\frac{T_{pt}}{\mathrm{GeV}}\right) \mathrm{Hz}, \tag{5.7}$$

where $x_k = 2\pi k_I / H_{pt}$ with k_I / H_{pt} representing the normalized integral scale of the gravitational wave spectrum at the phase transition characterized by a_{pt} and temperature T_{pt}. Moreover, we focus on somewhat extreme scenarios. As is shown in figure 4.2, in first order phase transitions most fluid motion can be produced in a hybrid scenario i.e. v_w between the Chapman-Jouguet points. Here, we will look predominantly at cases with $v_w = c_s$ for which (Espinosa et al. 2010).

$$\kappa_v(c_s, \alpha) \approx \frac{\alpha^{2/5}}{0.017 + (1+\alpha)^{2/5}}. \tag{5.8}$$

For most of the time, we assume that the turbulence is linearly produced within the duration of the phase transition and we integrate the system typically over a timespan of $20\tau_{pt}$. This timespan is generally sufficient, since due to the turbulent cascade and the overall expansion the rate of gravitational wave production quickly becomes negligible, an exception that we also discuss is the low-frequency tail for MHD turbulence that undergoes a maximal magnetic helical inverse cascade.

5.2.1 Different Unequal Time Correlations

In the literature, there have been several different approaches applied to treating the decorrelation function in the GW equation, as discussed in (Caprini et al. 2009) that are based on the Lagrangian eddy turnover time and on an simple top-hat-Ansatz, that only takes modes into account with $|\tau - \tau'| \lesssim k^{-1}$ and the previously discussed Eulerian eddy turnover time (Niksa et al. 2018). In figure 5.9 we compare different approaches for the

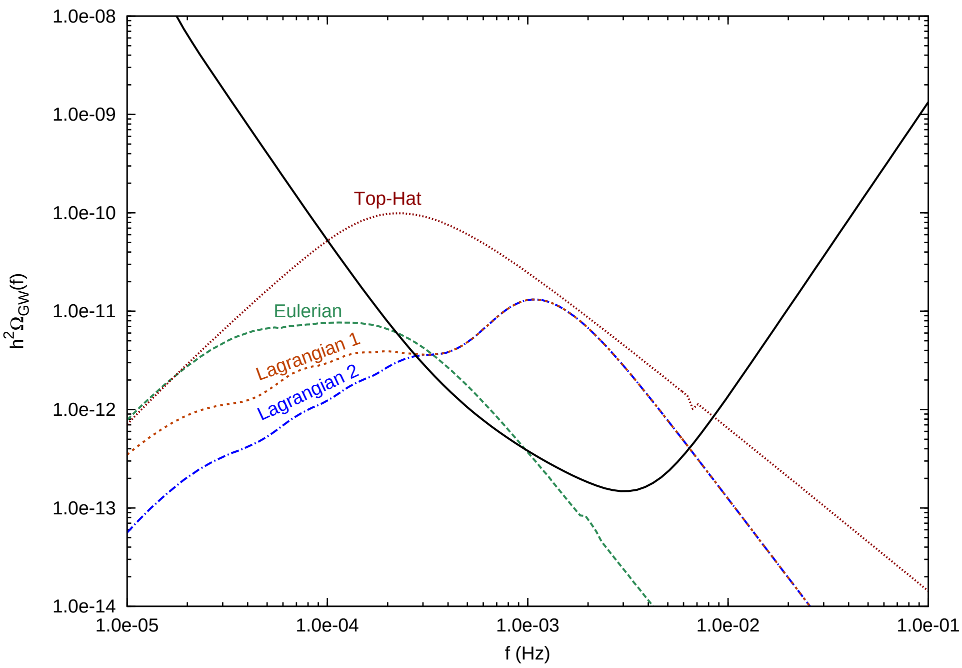

Figure 5.9: The gravitational wave spectrum for the Higgs portal scenario with $\alpha = 0.17$, $\beta/H_{pt} = 12.5$, $T_{pt} \approx 60$ GeV (Espinosa et al. 2008, Caprini et al. 2016). The lines denote the LISA sensitivity curve (black, solid), the top hat UTC model (dark-red, dotted), the Lagrangian UTC (Lagrangian 1, red, dotted), the Lagrangian UTC with a temporal cutoff (Lagrangian 2, blue dash-dotted) i.e. only contributions with $\tau_L(k) \leq \tau$ are counted, and the Eulerian UTC model (green, dashed). At observable frequencies our calculations based on the sweeping model lead to an amplitude that is a factor of 10 smaller compared to the top hat model at the peak. This is primarily due to the shorter correlation time at small scales. Furthermore, we have assumed that the turbulence is linearly sourced during the phase transition with the duration β^{-1}. At small frequencies, the spectra scale with f^3, while at high frequencies the top-hat model leads to a $f^{-5/3}$ tail and for the Eulerian and Lagrangian UTC model to a $f^{-8/3}$ high frequency tail.

choice of the UTC and look at a particular scenario for a Higgs portal with $\alpha = 0.17$, $\beta/H_{pt} = 12.5$, $T_{pt} \approx 60$ GeV (Espinosa et al. 2008, Caprini et al. 2016). One interesting finding here is that for the Lagrangian eddy turnover time, at least for these specific parameter sets, we do not observe negative energies, as have been reported in (Caprini et al. 2009). The reason as to why we do not find partially negative gravitational wave energy spectra is the introduction of the decorrelation function scaled to the forcing, see sub-subsection 3.3.3. In fact, without this correction we would indeed reproduce negative values for the Lagrangian decorrelation rate, although this is less of an issue for the Eulerian UTC Ansatz. One clear observation is, that the Eulerian UTC Ansatz, which is the appropriate Ansatz here, leads to an overall much smaller total gravitational wave energy and the peak of the spectrum is shifted towards smaller frequencies in contrast to the other two models. On smaller frequencies the Eulerian UTC leads to an overall larger amplitude than the Lagrangian Ansatz, albeit still mostly smaller than the amplitude for the top-hat Ansatz. Another important observation is that the top-hat model and the Eulerian UTC model nearly agree at high frequencies. Moreover, the high frequency tail differs significantly between the Eulerian (same for Lagrangian) $f^{-8/3}$ and the Top-Hat model $f^{-5/3}$. For the Lagrangian model, we have also looked at a cutoff from contributions in the integral of $\tau_L(q) \leq \tau$ noted as Lagrangian 2, which leads to an overall smaller spectrum at low frequencies. Nonetheless, a similar cutoff however has no effect on the Eulerian model results. The solid black line indicates the optimal LISA sensitivity curve as used in Caprini & Figueroa (2018) and based on (Thrane & Romano 2013, Moore et al. 2015, Amaro-Seoane et al. 2017).

5.2.2 Parametric Dependence of GW spectrum

Now, we look at the overall dependence of the spectrum on the total initially seeded turbulent energy density, which we parameterize as

$$\Omega_{\rm turb} = \alpha \kappa_v / \Omega_r = 2/3(v^2 + b^2)/\Omega_r, \tag{5.9}$$

and the initial integral scale $L_I = 2v_w H_{pt}/\beta$. Additionally, we generally assume equipartition $v = b$. At first we focus only on incompressible turbulence. The left panel in figure 5.10 shows an L_I^2 scaling of the overall energy spectrum and an associated shift of the peak frequency towards higher frequencies for smaller L_I. The shape of the spectrum itself is effectively invariant under variations of L_I. There is a clear deviation towards

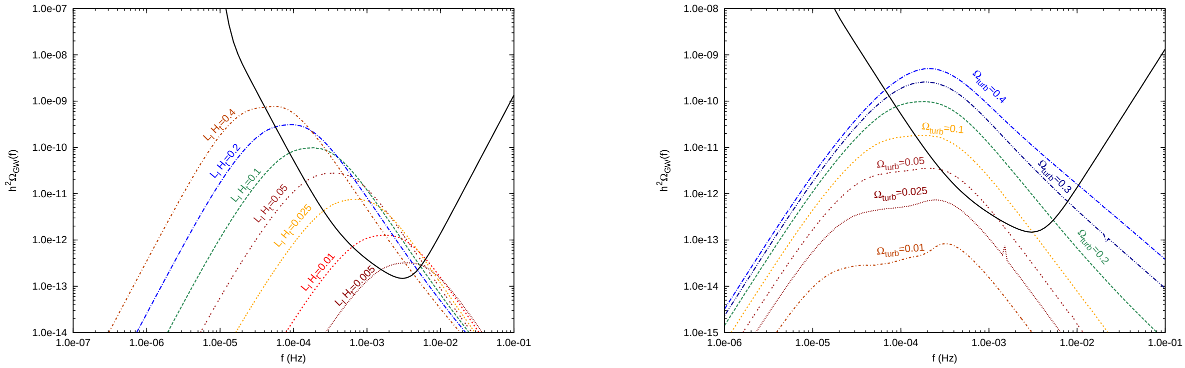

Figure 5.10: On the left panel, we show the dependence of the GW spectrum, produced by incompressible MHD turbulence, on the initial integral scale L_I, where $\Omega_{\rm turb} = 0.2$ ($\alpha \sim 0.3$) is the initial energy density parameter and $T_{pt} = 100$ GeV has been chosen. From top to bottom the lines correspond to $L_I H_{pt} = 0.4, 0.2, 0.1, 0.05, 0.025, 0.01, 0.005$ (dark-orange, blue, green, brown, orange, red, dark-red), which we denote as $L_I H_t$ for a bit more brevity in the panel. On the right panel, we show the dependence on the initial total turbulence density parameter Ω_{turb} for $L_I H_{pt} = 0.1$ ($\beta/H_{pt} \sim 10$), where the lines from top to bottom correspond to $\Omega_{\rm turb} = 0.4, 0.3, 0.2, 0.1, 0.05, 0.025, 0.01$ (blue, dark-blue, green, orange-yellow, brown, dark-red, dark-orange). One noteworthy observation is that the amplitude of the GW spectrum scales with L_I^2. The dependence on $\Omega_{\rm turb}$ is more complicated, the peak of the spectrum roughly scales as with $\Omega_{\rm turb}^2.4$. The small frequency tail has a scaling which scales between $\Omega_{\rm turb}$ and $\Omega_{\rm turb}^{1.5}$ for high to low $\Omega_{\rm turb}$. Additional, the large frequency tail itself has for large $\Omega_{\rm turb}$ a $f^{-5/3}$ dependence and for $\Omega_{\rm turb} \lesssim 0.1$ one finds a $f^{-8/3}$ law, as for the top-hat filter UTC function.

large values of $L_{pt}H_{pt}$ in the shape of the spectrum. Interestingly, the small frequency tail is barely shifted, when L_I is shifted. On the right panel, the dependence on $\Omega_{\rm turb}$ is shown and here the impact is far more complicated. In particular, there appears to be no simple power law scaling of $\Omega_{\rm GW}(f)$ with $\Omega_{\rm turb}$. For large $\Omega_{\rm turb} \gtrsim 0.2$ (corresponding to $\Omega_{\rm kinetic} \gtrsim 0.1$) the high frequency tail scales as $f^{-5/3}$, while for $\Omega_{\rm turb} \lesssim 0.1$ it scales as $f^{-8/3}$. Furthermore, the small frequency tail and also the peak of the spectrum scale differently with $\Omega_{\rm turb}$ in particular the peak grows with $\Omega_{\rm turb}^{2.4}$ while at small frequencies the spectrum scales $\Omega_{\rm turb}$ to $\Omega_{\rm turb}^{1.5}$ for high to low $\Omega_{\rm turb}$. For intermediary frequencies a plateau develops in the spectrum, that compensates for the difference in scaling.

Next, we study the impact that a turbulent spectrum with maximal magnetic helicity will have on the gravitational waves spectrum. Of particular relevance is the inverse cascade, due to the strong dependence on L_I. On the left and right panel in figure 5.11 one sees that the helical magnetic inverse cascade induces a severe deviation in the scaling at small frequencies, where one finds a f^2 spectral tail, rather than an f^3 tail. For typical electroweak scenarios, this difference will likely not be relevant, yet for higher

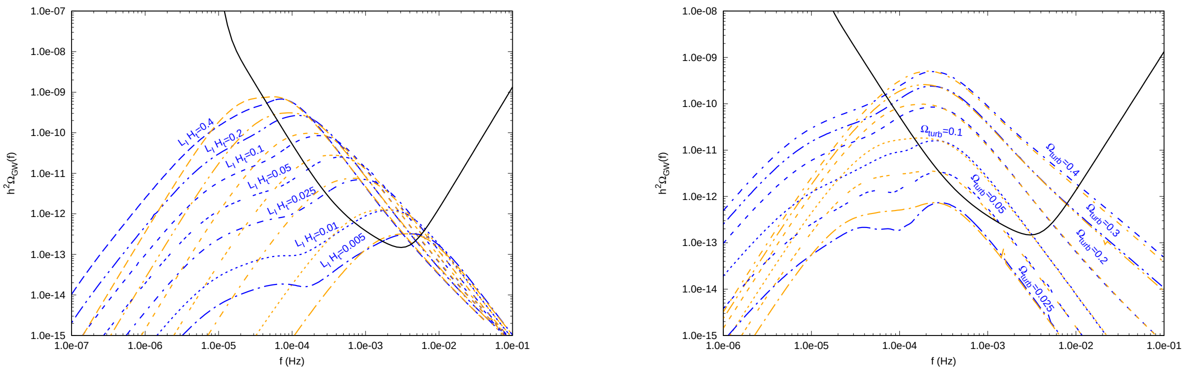

Figure 5.11: On the left panel, we show the dependence of the spectrum on the initial value L_I for maximally magnetic helical MHD systems, where $\Omega_{\text{turb}} = 0.2$ ($\alpha \sim 0.3$) and $T_{pt} = 100$ GeV have been chosen. From top to bottom the lines correspond to $L_I H_{pt} = 0.4, 0.2, 0.1, 0.05, 0.025, 0.01, 0.005$, which we denote as $L_I H_t$ for a bit more brevity in the panel, where blue lines denote the helical case, while orange lines denote the non-helical case. On the right panel, we show the dependence on Ω_{turb} for $L_I H_{pt} = 0.1$ ($\beta/H_{pt} \sim 10$). As for the left panel we also show both the helical (blue) and nonhelical (orange) scenario. From top to bottom the lines correspond to $\Omega_{\text{turb}} = 0.4, 0.3, 0.2, 0.1, 0.05, 0.025$. The high frequency tail is nearly identical in the helical and non-helical cases. However, the small frequency spectra differ i.e. for the magnetic helical inverse cascade a f^2, rather than a f^3 tail appears. Note, that we integrated the system over $100\tau_{pt}$ in order to properly count the contribution from the inverse cascade.

temperature phase transitions e.g. $T_{pt} \sim 1 - 10$ TeV could provide detectable signatures in the low frequency tail that may otherwise not be detectable. Note, that since helicity breaks parity it also induces a net polarization in the graviational waves (Kahniashvili, Campanelli, Gogoberidze, Maravin & Ratra 2008*b*), which would be another clear signature of helicity. Note that unlike for non-helical systems the spectrum appears to scale also non-trivially with L_I. For small L_I a more pronounced secondary peak seems to appear, however we suspect that this is primarily an artifact of the transition from the generation of gravitational waves during the build up of the initial turbulence and the subsequent inverse cascade, which appears more pronounced at small times as the for small L_I the time-scale for the turbulent cascade is much shorter than that of the build up. The precise details of the build up and the exact spectra of magnetic and kinetic helicity and magnetic and kinetic energy may be of critical importance here and as discussed in subsection 3.3.2 one expects variations in the decorrelation function for helical systems that we do not account here. Overall the spectra scale in the same way with L_I. On the other hand the Ω_{turb} dependence in the small frequency tail differs significantly from the behavior for non-helical systems. Here, the spectra now effectively scale with $\Omega_{\rm turb}^{8/3}$ at small frequencies, which is nearly the same as around the peak frequency.

5.2.3 GWs from compressible MHD turbulence

So far we have only focused on gravitational waves from incompressible MHD turbulence. However, compressible MHD turbulence can have a substantial impact on the shape of GW energy spectrum, as we will discuss in the following. Here we generally assume that there is some type of transfer of solenoidal to dilatational turbulent energy and we look at the impact of different transfer models on the appearing gravitational wave spectrum for different initial fractions of dilatational to solenoidal energy densities. Here we generally denote the amount of dilatational energy by a fraction f_d and the solenoidal kinetic energy by a fraction f_s of the total energy density, such that $f_s + f_d = 1$. For convenience, we neglect magnetic fields as one would have to take into account another parameter, yet the precise behavior should not differ significantly. Now, we consider several different models for the temporal evolution of the dilatational mode fraction f_d. First, we assume that the dilatational fluid motion immediately decays into acoustic modes over a time τ_D given in (C.8) even during the phase transition

$$f_d(\tau) = f_{d,i} \begin{cases} 1 - \frac{\tau-\tau_0}{\tau_D}, & \tau < \tau_0 + \tau_D \\ 0, & \tau > \tau_0 + \tau_D, \end{cases} \tag{5.10}$$

where $f_{d,i}$ is the initial dilatational energy fraction and we refer to this as model A. Next, in model B we assume that f_s and f_d are constant.

$$f_d(\tau) = f_{d,i}. \tag{5.11}$$

Another simple model is constructed by assuming that during the phase transition the dilatational fraction is constant and then soon afterwards decays over some time $s\tau_D$.

We refer to this as model C_s and it is given by

$$f_d(\tau) = f_{d,i} \begin{cases} 1, & \tau < \tau_b + \tau_0 \\ 1 - \frac{\tau - \tau_0 - \tau_b}{s\tau_D}, & \tau_0 + \tau_b < \tau < \tau_0 + s\tau_D + \tau_b \\ 0, & \tau > \tau_0 + s\tau_D + \tau_b. \end{cases} \tag{5.12}$$

In particular, we will look at this model with $s = 1$ (C_1) and $s = 2$ (C_2). These scenarios take into account many reasonable cases. We generally integrate the system over a time $\tau_{\rm pt}$, as the acoustic contribution is not sufficiently decorrelated over longer times and this induces difficulties in the calculation e.g. nonphysical energy spectra for a purely dilatational system. For the phase transition parameters studied here, the differences will be minor.

Here we look at two different cases $\Omega_{\rm turb} = 0.2$ and $\Omega_{\rm turb} = 0.1$ (for fluid motion only), as the right panel in figure 5.10 indicates a strongly different behavior in the high frequency tail (the factor of 2 is due to the lack of magnetic energy here) for the purely solenoidal scenario. First we look at the extreme case with very high turbulent energy densities which corresponds to the appearance of an $f^{-5/3}$ high frequency tail. In figure 5.12 we show the gravitational waves from compressible turbulence for different dilatational energy fractions $f_{d,i} = 0.1$ (top left panel), $f_{d,i} = 0.5$ (top right panel) and $f_{d,i} = 0.9$ (bottom left panel) and for the different scenarios A, B, C_1 and C_2. For $f_{d,i} = 0.1$ the impact of dilatational motion on the GW spectrum is rather subtle and only affects the spectrum between 10^{-4} Hz and 10^{-2} Hz. A larger dilatational energy fraction $f_{d,i} = 0.5$ shows an a significantly bigger, yet still relatively not very large, difference. For $f_{d,i} = 0.9$ the difference between the different models become substantial and in particular for the case that the dilatational energy fraction f_d remains constant, the high frequency tail develops an f^{-3} tail. One general observation is that in any of the compressible scenarios the power at the peak of the spectrum is larger than for the purely incompressible case. In the lower right panel, we compare different scenarios, and in particular for $f_{d,i} = 0.5$ and $f_{d,i} = 0.9$ with the model C_1 one only finds a

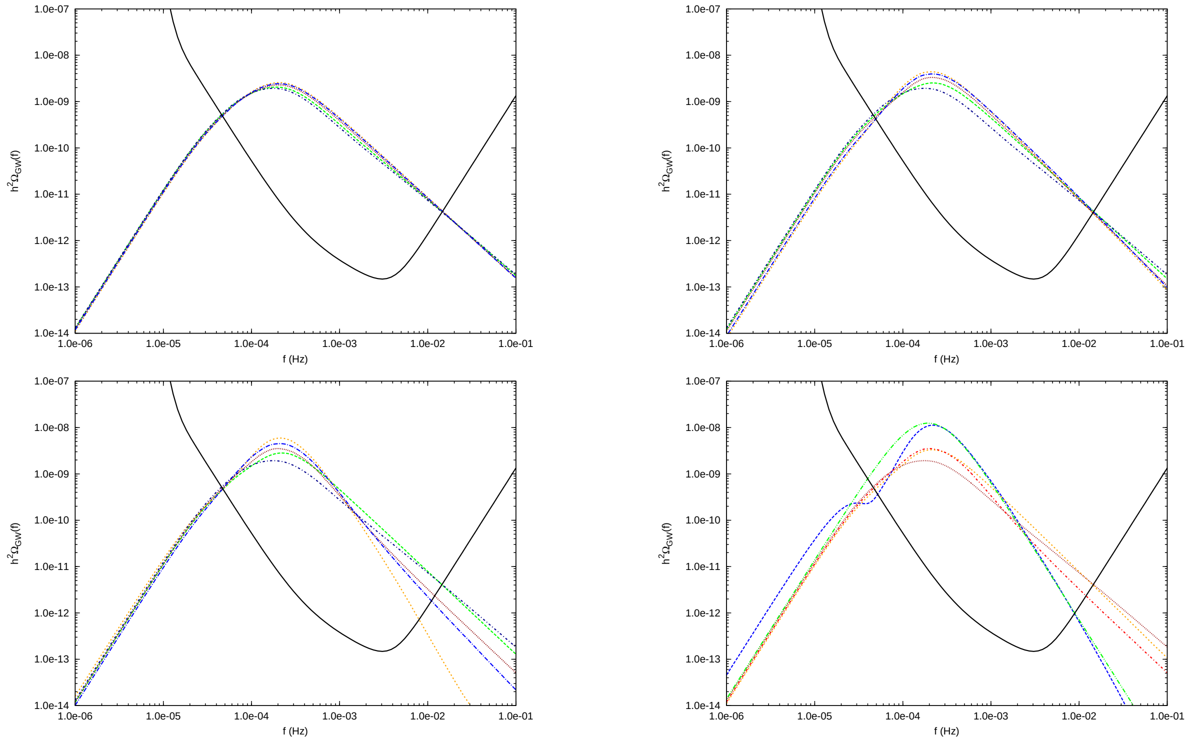

Figure 5.12: The gravitational wave power spectrum for different values of the initial fraction of dilatational modes $f_{d,i} = 0.1$ in the top left, $f_{d,i} = 0.5$ in the top right and $f_{d,i} = 0.9$ in the bottom left panel. Here we assume a kinetic energy density parameter of $\Omega_{\rm tot} = 0.2$. The different lines correspond to the different scenarios: model A (5.10) (green, dashed), model B (5.11) (orange, thick-dotted), model C$_1$ (5.12) (dark-red, thin-dotted) and model C$_2$ (blue, dot-dashed) for the temporal evolution of f_d. Each model is also compared with the case $f_d = 0$ (dark-blue, dot-dashed). In the bottom right panel, we show the cases $f_d = 0$ (brown, thin-dotted), $f_{d,i} = 0.5$ with model C$_1$ (orange, dashed), $f_{d,i} = 0.9$ (red, dot-dashed) with model C$_2$ and $\tau_b = \beta^{-1}$, $f_{d,i} = 0.999$ (blue, long dashed) with model B and extrapolated fitted DNS results (green, double dot-dashed) from Caprini & Figueroa (2018) via (Hindmarsh et al. 2015).

difference in the high frequency tail. The blue dashed line indicates a scenario in which the turbulent spectrum with $f_d = 0.999$ does not undergo any turbulent energy transfer and one finds a deviation of the low-frequency tail in contrast to the other cases. We also show an extrapolated fitted DNS results (green, double dot-dashed) from Caprini & Figueroa (2018) via (Hindmarsh et al. 2015) for purely dilatational systems. This is accurately overlapping with the $f_d = 0.999$ line at most frequencies, however in the small frequency tail there is a considerable deviation. We assume, that this is primarily due to taking contributions into account that impact the system over times longer than the Hubble time at the phase transition. Note, that for the compressible non-constant scenarios for $f_{d,i} = 0.9$ a f^{-2} high frequency tail appears, rather than the $f^{-5/3}$ tail for incompressible turbulence with $\Omega_{\rm turb} \gtrsim 0.2$, which corresponds to strongly compressible turbulence since $v \sim c_s$. Next, we look at the similar figure 5.13. Here, for $f_{d,i} = 0.1$ the difference between the different models is more significant than the case $f_d = 0.5$ with $\Omega_{\rm turb} = 0.2$. Interestingly for $f_d = 0.5$ the different compressible models differ only slightly. For $f_d = 0.9$ also variations of the large scale tail become relevant, although less significantly than for incompressible turbulence. The bottom right panel in figure 5.13 is quite similar to the bottom right panel in figure 5.12. The key difference are the steeper high frequency slopes of the mixed compressible and the incompressible scenarios. In general for smaller $\Omega_{\rm turb}$ the difference between compressible turbulence and incompressible turbulence becomes more significant at the peak, although still less relevant in the small frequency tail. Note that the high frequency tail for $f_{d,i} = 0.9$ for $\Omega_{\rm turb} = 0.1$ is still f^{-2}, yet for $\Omega_{\rm turb} \ll 0.1$ we expect an f^{-3} tail. Nonetheless even a small solenoidal energy density fraction leads to a significant reduction of the peak power by a factor $\sim 3-4$. All these scenarios for the dilatational energy fraction assume a near time-independent dilatational spectrum. In general even for purely dilatational turbulence one anticipates a more involved decorrelation rate, due to the nonlinear evolution, and some energy transfer, which we do not consider here. This concludes our discussion on different turbulent initial conditions and the associated gravitational waves spectra.

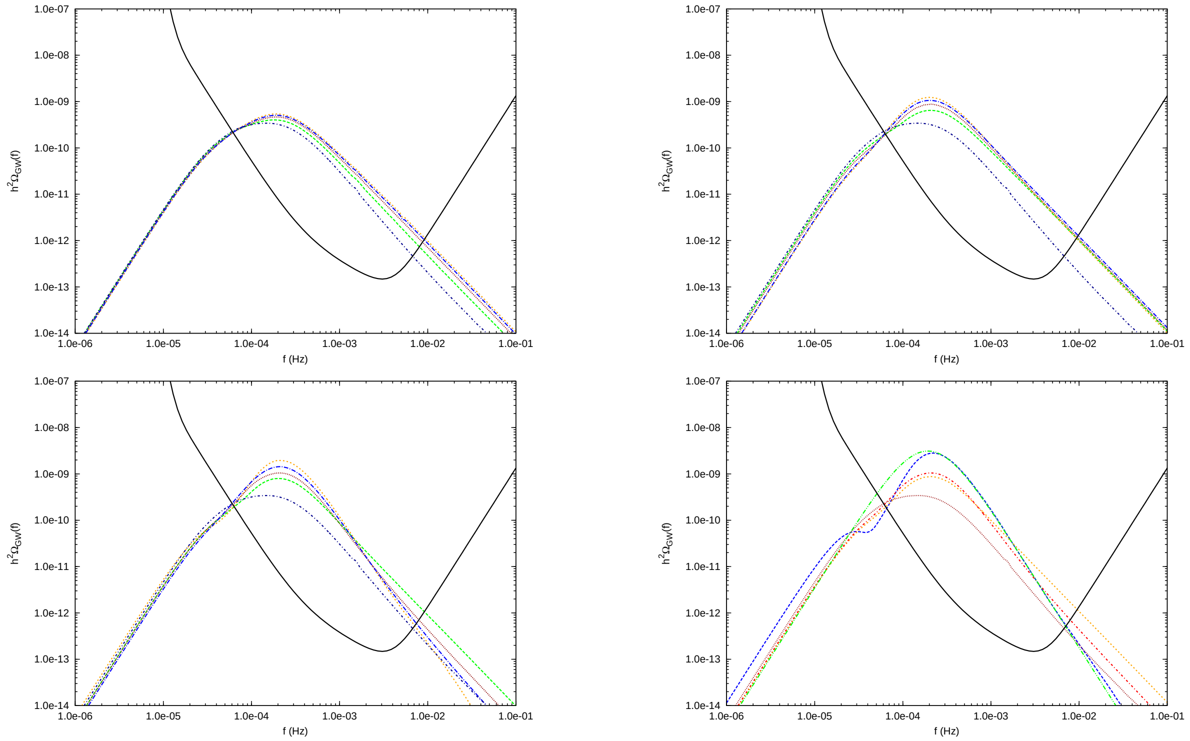

Figure 5.13: The gravitational wave power spectrum for different values of the initial fraction of dilatational modes $f_{d,i} = 0.1$ in the top left, $f_{d,i} = 0.5$ in the top right and $f_{d,i} = 0.9$ in the bottom left panel. Here we assume a kinetic energy density parameter of $\Omega_{\rm tot} = 0.1$. The different lines correspond to the different scenarios: model A (5.10) (green, dashed), model B (5.11) (orange, thick-dotted), model C$_1$ (5.12) (dark-red, thin-dotted) and model C$_2$ (blue, dot-dashed) for the temporal evolution of f_d. Each model is also compared with the case $f_d = 0$ (dark-blue, dot-dashed). In the bottom right panel, we show the cases $f_d = 0$ (brown, thin-dotted), $f_{d,i} = 0.5$ with model C$_1$ (orange, dashed), $f_{d,i} = 0.9$ (red, dot-dashed) with model C$_2$ and $\tau_b = \beta^{-1}$, $f_{d,i} = 0.999$ (blue, long dashed) with model B and extrapolated fitted DNS results (green, double dot-dashed) from Caprini & Figueroa (2018) via (Hindmarsh et al. 2015).

6 | Summary, Conclusions and Outlook

6.1 Summary

Here we have studied the evolution of magnetic fields in the early universe that may originate from a first order electroweak phase transition and the generation of associated gravitational waves. In chapter 2 we discussed the basic equations that govern the evolution of magnetohydrodynamic (MHD) turbulence and the generation of gravitational waves and key quantities like the magnetic and cross helicity. Then, in chapter 3 we looked at the corresponding spectral correlation functions of these quantities in the context of isotropic homogeneous MHD turbulence and described the interdependencies between the different topological measures. Next, we discussed turbulent unequal time correlations (see section 3.3) that are of key importance in the evaluation of gravitational wave spectra from MHD turbulence and we discussed the difference between the Eulerian and Lagrangian eddy turnover time and the impact of vorticity and magnetic fields on the decorrelation rate of acoustic modes in weakly compressible MHD turbulence ($v \lesssim c_s$). Thereafter, we presented the eddy damped quasi normal Markovian (EDQNM) approximation (see section 3.4) self-consistently for the incompressible case, which are spectral evolution equations and are computationally of great interest, as the spatially 3D problem is reduced to a 1D problem, under the assumption of stochastic homogeneity and isotropy.

Moreover, we have discussed the basic large scale behavior of the EDQNM equations, in particular we have shown that the dimensionless (unit $c^2 = 1$) kinetic and magnetic helicity and the cross scalar develop a k^6 large scale tail, rather than the k^5 large scale tail that the energy spectra develop, that means even if MHD turbulence develops into a maximal magnetic helical state, the coherent large scale magnetic field in the large scale tail only have at most a fractional magnetic helicity of the order k/k_I for $k \ll k_I$. For MHD turbulence with a maximal cross helicity, the large scale tail is even steeper and develops a k^7 slope. One also finds that unlike for the energy spectra the large scale tail of the magnetic helicity will undergo an exponential growth for $k \ll k_I$, which represents the inverse cascade. For incompressible non-helical turbulence such terms are only present at $\mathcal{O}(k^6)$ corresponding to a weak growth on small scales. Afterwards, we discussed the well-known nature of self-similar evolution in incompressible MHD turbulence focusing on the non-helical case and on the case of extremal magnetic helicity. Next, we looked at some key properties of subsonic compressible turbulence $v \ll c_s$. We note that in substantially subsonic purely compressible turbulence nonlinear evolution is suppressed. However, as has been particularly discussed in subsection 3.4.7 and appendix A.2 growth modes like $\partial_\tau \bar{E}_d(k) \propto \bar{E}_d(k)$ may become important on large scales. There, we have derived the EDQNM equations for purely compressible subsonic turbulence for radiation dominated gases or plasmas. Furthermore, we note that a nonlinear transfer of dilatational energy is suppressed even when vorticity and magnetic fields are present, yet vorticity and magnetic fields may lead to a substantial decay or growth of an already established dilatational energy spectrum. Here we did not further discuss these problems.

Following we discussed the equations that describe the generation of gravitational waves by homogeneous isotropic compressible MHD turbulence. We noted that turbulence leads to an f^3 low frequency tail in the GW energy spectrum and that the power in the gravitational wave spectrum scales with L_I^2 (the integral scale squared), but the dependence on the energy density is more complicated. Similarly, we also discussed the "inertial range" of the GW energy spectrum and anticipate for purely compressible systems a f^{-3} high frequency tail and in incompressible turbulence a $f^{-5/3}$ to $f^{-8/3}$ high frequency tail. In the following chapter 4, we first discuss basic properties of thermal first order phase transitions, that may have occurred in the early universe and look briefly and conceptually at related magnetogenesis. Next, we presented the viscous and resistive history in the radiation dominated universe in the context of the standard model and in particularly we discussed the impact of the different viscosity-dominated phase on the evolution of primordial MHD and argued that in principle a non-trivial cross scalar and cross helicity as well as kinetic helicity sourced at a phase transition should no longer be present in the system after neutrino decoupling (see in particular figure 4.3). Since one key focus of the discussion here is the radiation dominated phase, we also discussed how the matter dominated phase may have affected the evolution of primordial magnetic fields, and briefly the well-known freeze-out of turbulence with correlation times that have grown to be of the order of the Hubble time at some point in the matter dominated phase, due to turbulent decay. Then, we have briefly discussed our present-day knowledge about correlated magnetic fields on Mpc scales, noting the non-detection, but also the apparent somewhat strong lower limits related to the non-observation of a possibly present and significant GeV photon flux. Also, we mentioned future developments on ways to constrain primordial magnetic fields, noting in particular the potential of future and present gravitational wave detectors, in particular LISA (Amaro-Seoane et al. 2017) as it may allow the observation of a gravitational wave background from a first order phase transitions at GeV and TeV scales.

Finally, in chapter 5, we have shown explicit numerical simulations on the evolution of MHD turbulence in the radiation dominated phase, based on the incompressible EDQNM equations. First, we have looked at mirror-symmetric incompressible MHD turbulence and noted that the large-scale tail remains nearly unchanged, i.e. the comoving magnetic field strength produced by a non-helical magnetogenesis on Mpc scales is constant through the entire evolution, as long as we ignore more complicated feed back in the matter dominated phase as related to structure formation. These simulations illustrated the entire evolution of primordial MHD turbulence in the radiation dominated phase, showcasing the impact of the viscous phases on the evolution in detail (see figure 5.1, 5.2 and 5.3). We find that a nontrivial cross scalar does not substantially affect the evolution of non-helical incompressible MHD turbulence. Secondly, we studied several different scenarios of helical primordial MHD turbulence. For once, we have discussed the well known inverse cascade driven by near extremal magnetic helicity (see figure 5.4). Figure (5.5) showcased a scenario with magnetic and kinetic energy with near maximal kinetic helicity and we do not observe, except for purely numerical artifacts that lead to the appearance of a net total magnetic helicity, any substantial difference in the evolution compared to the nonhelical evolution. Interestingly, the kinetic helicity leads to lasting signatures in the helical MHD turbulence spectrum even after neutrino decoupling. Moreover, we have also studied a scenario with some minor degree of cross helicity (see figure 5.6). The cross helicity can have a substantial impact on the evolution of the primordial magnetic field prior to neutrino decoupling, since it leads to a stall of the turbulent cascade and inverse cascade, in case extremal magnetic helicity is present or develops prior to the appearance of a near-maximally cross helical state. Thus in incompressible MHD turbulence, maximally cross helical MHD turbulence is not affected by nonlinear evolution and only direct viscous and resistive decay impacts the energy spectra. After neutrino decoupling led to a dissipation of the cross scalar, the system evolves according to its magnetic helicity and energy density. Consequently, cross helicity may be only of interest for more direct and pristine probes of the early universe prior to neutrino decoupling. In figure 5.7 and 5.8 we discuss the overall evolution of the different scenarios and note some numerical problems in particular related to magnetic helicity conservation during the final neutrino and photon decoupling stages, for which we have not yet developed a satisfying solution. This problem is particularly apparent in the presence of the cross scalar and cross helicity.

Ultimately, we present numerical studies on the expected primordial gravitational wave background by compressible MHD turbulence in the early universe. First we discussed and showed in figure 5.9, how different assumptions of the unequal time correlation for incompressible MHD turbulence can lead to vastly different gravitational wave energy spectrum, noting in particular that for the Eulerian decorrelation rate, that most accurately describes the relevant decorrelation, the power at higher frequencies will be the smallest compared to the other models by at least 2 orders in magnitude. Thereafter, we showed a parametric dependence on the gravitational wave energy spectrum for different initial integral scales and turbulent energy densities for MHD turbulence without, see figure 5.10 and with helicity, see figure 5.11. We note a simple dependence of the gravitational wave energy density on the initial integral scale of turbulence $\propto L_I^2$ (related to the duration of the phase transition) and a more complex and rich dependence on the turbulent energy density. The inverse cascade generally leads to significantly more power on very small frequencies as a f^2 small frequency tail appears. Lastly, we looked at possible and probable gravitational wave spectra from compressible turbulence assuming different scenarios for the transfer of dilatational to solenoidal energy, noting that generally a higher degree of dilatational motion in fluid leads to more power at the peak of the GW spectrum.

6.2 Conclusions and Outlook

To conclude this thesis, we contemplate what our findings tell us, what we may still miss or overlook and what we deem necessary and vital to understand, or as aptly put by John F. Kennedy "The greater our knowledge increases the greater our ignorance unfolds". Regarding the evolution of MHD turbulence, we find that cross correlations do not affect pristine present traces of present-day primordial magnetic fields in the, so far, visible universe. However one key shortcoming of the numerical study performed here, to trace the evolution of primordial magnetic fields, is the assumption of incompressibility. In particular, in the simulations performed here, even in cases where magnetic energy is dominant, we do not observe a significant inverse transfer in nonhelical turbulence, except for scenarios where a maximally magnetic helicity state develops, as observed and discussed in (Kahniashvili et al. 2013, Brandenburg et al. 2015, Brandenburg & Kahniashvili 2017) for MHD turbulence with $b \gg v$. In these studies it has been found that the comoving integral scale grows with $L_I \propto \tau^{1/2}$ and the energy correspondingly decays with τ^{-1} in MHD turbulence, which is clearly not present in the incompressible MHD turbulence studied here. Thus, we expect that this type of transfer is related to compressible contributions, particular related to potential exponential growth of dilatational fluctuations at large scales (see subsection 3.4.7 and appendix A.2). Therefore, we believe that a concise semi-analytical study as performed here in the case of incompressible MHD turbulence is of considerable interest also for the full set of equations in compressible MHD turbulence. Nonetheless, such an inverse transfer process may still not be sufficient in producing substantial magnetic fields compatible with the gamma-ray constraints (Kahniashvili et al. 2013) for an electroweak FOPT, unlike a substantial inverse cascade by the magnetic helicity (Saveliev et al. 2013, Ellis et al. 2019, e.g.).

Additionally, cross helicity conservation combined with compressible inverse transfer may lead to an even more significant inverse cascade, since the dilatational energy spectra should scale shallower at large scales and maximal cross helicity suppresses any small scale transfer and potentially even the conversion of dilatational to solenoidal energy, while still enabling the inverse transfer. On the other hand, it may suppress the inverse transfer at least partially prior to neutrino decoupling. Of similar interest are also the usual suspects, kinetic and magnetic helicity in compressible MHD turbulence. Also, we did not take the chiral magnetic effect and the chiral vortical effect (Kharzeev et al. 2016, e.g.), in particular the gravitational anomaly contribution to the chiral vortical effect, into account, which can drive a substantial generation of magnetic helicity (Boyarsky et al. 2012, Pavlović et al. 2016, Pavlović et al. 2017). In the presently presented numerical simulations, substantial numerical artifacts are present, particularly related to magnetic helicity non-conservation and due to a slight issue the evolution was primarily driven to the matter-radiation equality, rather than recombination, thus the full impact of the photon decoupling is not shown here. Hence, we deem it important to fully and substantially control these numerical issues in the future.

Regarding the generation of GWs from MHD turbulence, there are several key issues that warrant further investigation. Here we have assumed a linear build up of MHD turbulence, however the bubble wall velocity and also the bubble nucleation rate is typically not constant leading to relevant variations in the build up of the turbulent spectra (Hindmarsh & Hijazi 2019, e.g.). In slight contrast to (Niksa et al. 2018), we assumed that turbulence is generally generated within the duration of phase transition and that the turbulence evolves as in the purely incompressible case, whereas in (Niksa et al. 2018) the inverse transfer of e.g. (Brandenburg & Kahniashvili 2017) was assumed. Thus, these details are specifically of interest in particular for the more general compressible cases. Additionally, we neglect other sources of gravitational waves e.g. as related to scalar field dynamics which are typically sub-dominant in thermal phase transitions (Caprini et al. 2016, e.g.). Furthermore, as discussed in subsection 3.3.2 generation of gravitational wave energy spectra for helical MHD likely requires a modified model for the unequal time correlation function and the precise GW spectra especially around the peak may in reality differ from the presently presented result, potentially even in a substantial manner. Nonetheless, we believe that the appearance of an f^2 low frequency tail and the overall shape to give a rough estimate of the anticipated gravitational wave spectra from helical MHD turbulence.

When studying purely compressible turbulence, we only integrate the system over one Hubble time, and as previously noted by (Caprini et al. 2009, e.g.), for highly coherent turbulence highly oscillatory GW spectra appear in the high frequency tail, even leading to an additional suppression of power in the high frequency tail. This may not only be of importance for the GW signal from purely compressible turbulence but also for the signal of maximally cross-helical MHD turbulence. As noted before, it is thus also crucial to better understand the evolution of compressible cross-correlated MHD turbulence. Solenoidal motion is of most importance in deflagration phase transitions (subsonic bubbles $v_w \lesssim c_s$) and recent simulations indicate that the overall efficiency parameter κ_v in these scenarios may be substantially smaller than assumed here (Cutting et al. 2019), which would further reduce the overall power of the GW energy spectrum, but also the initial integral scale strength of primordial magnetic fields. Furthermore, as discussed here solenoidal motion and magnetic fields lead to a smaller efficiency in the generation of gravitational waves in the high frequency tail. Recent studies indicate that the vorticity is initially produced during the phase transition and afterwards the vortical energy density remains constant, while the dilatational energy is dissipated (Cutting et al. 2019), which appears best represented by the discussed model C_1,see

(5.12). Still, the details regarding the transfer require substantially more attention.

Concluding, there are still many interesting open question that need to be resolved in order to better understand the signatures of primordial gravitational waves and large scale magnetic fields from a cosmological first order phase transition.

A Supplement to EDQNM derivation

A.1 Example on Calculation of the EDQNM equations

Here we briefly discuss as an explicit example a partial derivation of the evolution equation for $E^{\pm}(k)$ (see (3.75))

$$\left(\partial_\tau + 2k^2\nu^+\right) E^{\pm}(k) = 2k^3 P_{ib}(\mathbf{k}) k_a \int \frac{\mathrm{d}^3\mathbf{q}}{(2\pi)^8} \, \mathrm{Im}\left[\langle z_i^{\pm}(-\mathbf{k}) z_a^{\mp}(\mathbf{p}) z_b^{\pm}(\mathbf{q})\rangle\right] - 2k^2\nu_- E^{\mathrm{R}}(k). \tag{A.1}$$

For convenience we neglect the ν_- damping term and the above three point function is explicitly given as

$$\begin{aligned}
&\left(\partial_\tau + \nu_+(k^2+q^2+p^2)\right) \langle z_i^{\pm}(-\mathbf{k}) z_a^{\mp}(\mathbf{p}) z_l^{\pm}(\mathbf{q})\rangle = \\
&ik_c P_{id}(\mathbf{k}) \int \frac{\mathrm{d}^3\mathbf{q}'}{(2\pi)^3} \langle z_a^{\mp}(\mathbf{p}) z_b^{\pm}(\mathbf{q}) z_c^{\mp}(-\mathbf{p}') z_d^{\pm}(-\mathbf{q}')\rangle \\
&- ip_c P_{ad}(\mathbf{p}) \int \frac{\mathrm{d}^3\mathbf{q}'}{(2\pi)^3} \langle z_i^{\pm}(-\mathbf{k}) z_b^{\pm}(\mathbf{q}) z_c^{\pm}(\mathbf{p}'') z_d^{\mp}(\mathbf{q}')\rangle \\
&- iq_c P_{bd}(\mathbf{q}) \int \frac{\mathrm{d}^3\mathbf{q}'}{(2\pi)^3} \langle z_i^{\pm}(-\mathbf{k}) z_a^{\mp}(\mathbf{p}) z_c^{\mp}(\mathbf{p}''') z_d^{\pm}(\mathbf{q}')\rangle,
\end{aligned} \tag{A.2}$$

where $\mathbf{p}' = \mathbf{k} - \mathbf{q}'$, $\mathbf{p}'' = \mathbf{p} - \mathbf{q}'$ and $\mathbf{p}''' = \mathbf{q} - \mathbf{q}'$. This can be directly integrated by markovizing the four point functions

$$\begin{aligned}
&\langle z_i^{\pm}(-\mathbf{k}) z_a^{\mp}(\mathbf{p}) z_l^{\pm}(\mathbf{q})\rangle(\tau) = \gamma(k,q,p,\tau) \\
&ik_c P_{id}(\mathbf{k}) \int \frac{\mathrm{d}^3\mathbf{q}'}{(2\pi)^3} \langle z_a^{\mp}(\mathbf{p}) z_b^{\pm}(\mathbf{q}) z_c^{\mp}(-\mathbf{p}') z_d^{\pm}(-\mathbf{q}')\rangle(\tau) \\
&- ip_c P_{ad}(\mathbf{p}) \int \frac{\mathrm{d}^3\mathbf{q}'}{(2\pi)^3} \langle z_i^{\pm}(-\mathbf{k}) z_b^{\pm}(\mathbf{q}) z_c^{\pm}(\mathbf{p}'') z_d^{\pm}(\mathbf{q}')\rangle(\tau) \\
&- iq_c P_{bd}(\mathbf{q}) \int \frac{\mathrm{d}^3\mathbf{q}'}{(2\pi)^3} \langle z_i^{\pm}(-\mathbf{k}) z_a^{\mp}(\mathbf{p}) z_c^{\mp}(\mathbf{p}''') z_d^{\pm}(\mathbf{q}')\rangle(\tau),
\end{aligned} \tag{A.3}$$

where

$$\gamma(k,q,p,\tau) = \frac{1 - \exp\left[-\nu_+(k^2+q^2+p^2)(\tau-\tau_0)\right]}{\nu_+(k^2+q^2+p^2)}. \tag{A.4}$$

Furthermore, one introduces an additional eddy damping rate by adjusting the viscosity $\nu_+ k^2 \to \nu_d(k) + \nu_+ k^2$ (see 3.73).

As an example, we look only at the line $\propto k_c P_{id}$ in (A.3) and evaluate the four point correlations via Isserlis theorem (3.69). This leads to

$$i\gamma(k,q,p,\tau) k_c P_{id}(\mathbf{k}) \int \frac{\mathrm{d}^3\mathbf{q}'}{(2\pi)^3} \left[\langle z_a^{\mp}(\mathbf{p}) z_c^{\mp}(\mathbf{p}')\rangle\langle z_b^{\pm}(\mathbf{q}) z_d^{\pm}(\mathbf{q}')\rangle + \langle z_a^{\mp}(\mathbf{p}) z_d^{\pm}(\mathbf{q}')\rangle\langle z_b^{\pm}(\mathbf{q}) z_c^{\mp}(\mathbf{p}')\rangle\right]. \tag{A.5}$$

Then, we can apply the correlation functions (3.5) and (3.5) gives, while we neglect the helicities and the cross scalar,

$$\frac{(2\pi)^7}{4p^3q^3} ik_c P_{id}(\mathbf{k}) \left[E^{\mp}(p) P_{ac}(\mathbf{p}) E^{\pm}(q) P_{bd}(\mathbf{q}) + E^R(p) P_{ad}(\mathbf{p}) E^R(q) P_{bc}(\mathbf{q})\right]. \tag{A.6}$$

Then the first two coefficients are given by

$$\Lambda_1 = k_a P_{ib}(\mathbf{k}) k_c P_{id}(\mathbf{k}) P_{ac}(\mathbf{p}) P_{bd}(\mathbf{q}) = k^2(1-c_{pk}^2)(1+c_{qk}^2) \tag{A.7}$$

and

$$\Lambda_2 = -k_a P_{ib}(\mathbf{k}) k_c P_{id}(\mathbf{k}) P_{ad}(\mathbf{p}) P_{bc}(\mathbf{q}) = -k^2 c_{qk} c_{pk}(c_{qp} - c_{qk}c_{pk}), \tag{A.8}$$

and note that we have absorbed a $-$ sign into Λ_2. Therefore the contribution of these terms on the right hand side of (A.1) is

$$\frac{1}{2}k^3 \int \frac{\mathrm{d}^3\mathbf{q}}{(2\pi)p^3q^3} \left[\Lambda_1 E^{\mp}(p)E^{\pm}(q) - \Lambda_2 E^R(p)E^R(q)\right]. \tag{A.9}$$

This procedure needs to be applied for all other terms as well, including helical contributions and the cross scalar, to fully reproduce (3.75).

A.2 Nonlinear compressible functions

Here we explicitly give the functions g_i as described in (3.108) in subsection 3.4.6 and 3.4.7 for purely compressible three point functions given by (3.112) and 3.113. For convenience we introduce the notation $e^v = \langle vv^*\rangle$, $e^d = \langle \delta\delta^*\rangle$ and $e^m = \langle v\delta^*\rangle$. Additionally, we introduce the functions

$$\begin{aligned}
&\Lambda_{11} = c_{qp}\Lambda_{14} - c_s^2(pc_{qk} + qc_{pk}), \quad \Lambda_{12} = c_{qk}\Lambda_{15} - c_s^2(qc_{pk} + kc_{qp}), \quad \Lambda_{14} = c_{qk}q + c_{pk}p \\
&\Lambda_{13} = c_{pk}\Lambda_{16} - c_s^2(pc_{qk} + kc_{qp}), \quad \Lambda_{15} = c_{pk}k + c_{qp}q, \qquad \Lambda_{16} = c_{qk}k + c_{qp}p.
\end{aligned} \tag{A.10}$$

Note, that the terms $\propto c_s^2$ appearing in Λ_{11}, Λ_{12} and Λ_{13} are only of importance in relativistic gases, fluids or plasmas, otherwise these terms are negligible for $c_s \ll 1$. Thus one finds

$$\begin{aligned}
g_1 =& \frac{i}{(2\pi)^3}\Big[e^v(p)e^v(q)\Lambda_{11} + e^v(k)e^v(q)\Lambda_{12} + e^v(p)e^v(k)\Lambda_{13} \\
&+ \left(1 + c_s^2\right)\left(e^m(q)e^m(k)\Lambda_{15} + e^m(p)e^m(k)\Lambda_{16} - e^m(q)e^m(p)\Lambda_{14}\right)\Big],
\end{aligned} \tag{A.11}$$

$$\begin{aligned}
g_2 =& \frac{i}{(2\pi)^3}\Big[e^m(p)e^v(q)\Lambda_{11} - e^v(k)e^m(p)\Lambda_{13} + \left(1 + c_s^2\right)\Big(e^d(p)e^m(k)\Lambda_{16} \\
&- e^d(p)e^m(q)\Lambda_{14} - e^m(q)e^v(k)c_{pk}p + e^m(k)e^v(q)c_{qp}p\Big)\Big],
\end{aligned} \tag{A.12}$$

$$
\begin{aligned}
g_3 =& \frac{i}{(2\pi)^3}\Big[e^m(q)e^v(p)\Lambda_{11} - e^v(k)e^m(q)\Lambda_{12} + \left(1+c_s^2\right)\Big(e^d(q)e^m(k)\Lambda_{15} \\
&- e^d(q)e^m(p)\Lambda_{14} - e^m(p)e^v(k)c_{qk}q + e^m(k)e^v(p)c_{qp}q\Big)\Big],
\end{aligned} \tag{A.13}
$$

$$
\begin{aligned}
g_4 =& \frac{i}{(2\pi)^3}\Big[e^m(q)e^m(p)\Lambda_{11} - \left(1+c_s^2\right)\Big(e^d(q)e^d(p)\Lambda_{14} + e^d(q)e^v(k)pc_{pk} \\
&- e^v(k)e^d(p)qc_{qk} + e^m(q)e^m(k)c_{qp}p + e^m(k)e^m(p)c_{qp}q\Big)\Big],
\end{aligned} \tag{A.14}
$$

$$
\begin{aligned}
g_5 =& \frac{i}{(2\pi)^3}\Big[e^m(k)e^v(p)\Lambda_{13} + e^m(k)e^v(q)\Lambda_{12} + \left(1+c_s^2\right)\Big(e^v(q)e^m(p)kc_{qk} \\
&+ e^v(p)e^m(q)kc_{pk} + e^m(q)e^d(k)\Lambda_{15} + e^d(k)e^m(p)\Lambda_{16}\Big)\Big],
\end{aligned} \tag{A.15}
$$

$$
\begin{aligned}
g_6 =& \frac{i}{(2\pi)^3}\Big[-e^m(k)e^m(p)\Lambda_{13} + \left(1+c_s^2\right)\Big(e^m(q)e^m(p)kc_{pk} + e^v(p)e^d(q)kc_{qk} \\
&+ e^d(p)e^v(k)\Lambda_{16} - e^m(q)e^m(k)pc_{pk} + e^d(k)e^v(q)c_{qp}p\Big)\Big],
\end{aligned} \tag{A.16}
$$

$$
\begin{aligned}
g_7 =& \frac{i}{(2\pi)^3}\Big[-e^m(k)e^m(q)\Lambda_{12} + \left(1+c_s^2\right)\Big(e^m(q)e^m(p)kc_{qk} + e^v(q)e^d(p)kc_{pk} \\
&+ e^d(q)e^v(k)\Lambda_{15} - e^m(p)e^m(k)qc_{qk} + e^d(k)e^v(p)c_{qp}q\Big)\Big],
\end{aligned} \tag{A.17}
$$

$$
\begin{aligned}
g_8 =& \frac{1+c_s^2}{(2\pi)^3}i\Big[e^d(p)e^m(q)kc_{qk} + e^d(q)e^m(p)kc_{pk} - e^m(p)e^d(k)qc_{qp} \\
&- e^d(p)e^m(k)c_{qk}q - e^m(q)e^d(k)pc_{qp} - e^m(k)e^d(q)c_{pk}p\Big].
\end{aligned} \tag{A.18}
$$

Here, the functions g_1, g_4, g_6 and g_7 are purely complex, while the other functions are real valued, since the e^m as defined here are purely complex. Note that the Greens function (3.109) has a real and imaginary part and in the end only the imaginary part of the three point functions affects the evolution of the purely compressible energy spectrum. That means, the complex g_i only appear with the real part of the Greens function, while the real valued g_i appear only with the imaginary component of the Greens function. This has the consequence that there should be no oscillation free contributions to the purely compressible three point functions. In these complex valued functions terms like $\propto e^m e^m$ likely dominate in substantially subsonic strongly compressible turbulence, as these introduce wave function of the type $\sin(2c_s k(\tau'))$ which may provide more significant contributions, when synchronized with terms like $\sin(\omega_i(\tau'))$ on certain scales. In order to grasp the solutions, one technically needs to perform the full diagonalization to ascertain that no substantial sufficiently long-lasting positive interference becomes relevant, which we have not yet done due to temporal constraints. At large scales $k \ll q$ and $p = q + \epsilon k \geq 0$, the above coefficients become

$$\begin{aligned} &\Lambda_{11} \approx \epsilon^2(1-c_s^2)k, \quad \Lambda_{12} \approx -\epsilon q - \epsilon^2 k + c_s^2(q\epsilon + k), \quad \Lambda_{14} \approx -\epsilon^2 k \\ &\Lambda_{13} \approx \epsilon q - c_s^2(p\epsilon - k), \quad \Lambda_{15} \approx -\epsilon k - q, \qquad \Lambda_{16} \approx -q. \end{aligned} \tag{A.19}$$

Again the large scale tail of the compressible spectra evolves according to

$$\begin{aligned} \partial_\tau \bar{E}_d(k) \propto & k^3 \int_0^\infty \mathrm{d}q \int_{-1}^{1} \mathrm{d}\epsilon\, qp\epsilon \Big[-(q + c_s^2 p)\mathrm{Im}\langle o_1 \rangle \\ & + (1 + c_s^2)\left(k\mathrm{Im}\langle o_7\rangle - q\mathrm{Im}\langle o_4\rangle\right)\Big]. \end{aligned} \tag{A.20}$$

In g_1 and g_4 the coefficients $\propto e(q)e(p)$ scale at least as $\propto \epsilon^2 k$, and for g_6 and g_7 these scale with ϵk, and analogously for e.g g_2. We assume, that at large scales the three point function o_i is primarily driven by g_i. Thus, one expects $E_d(k) \propto k^5$ for $k \ll k_I$ as for the solenoidal case. One interesting observation is that unlike for the solenoidal case terms $\propto \bar{E}_d(k)$ can appear, whereas for solenoidal modes there are no linear growth terms at large scales at $\mathcal{O}(E_s(k))$. Nonetheless, in purely substantially subsonic compressible turbulence we do not expect that these terms are of significant important.

B Numerical Treatment of EDQNM equations

Here we briefly describe the numerical scheme used to solve the quasinormal equations. First we start by discussing the discretization and the symmetrization and lastly we discuss the time integration. The scheme is based on a scheme first developed by Kraichnan and Leith (Kraichnan 1967, Leith 1971, Leith & Kraichnan 1972) and further improved by Bowman (Bowman 1996). Here we apply this method and show how total energy, cross helicity and magnetic helicity can be conserved at the same time. Nontheless, for stability reasons we implement readjust the spectra by introducing a cutoff which leads to a slight violation of energy and cross and magnetic helicity conservation.

B.1 Discretization and Symmetrization scheme

We discretize the spectrum on an exponentially distributed grid $k_i = k_{\min} 2^{i/F}$, where F controls the density of points in logarithmic intervals. Also we define $k_{\max} = k_{\min} 2^{N/F}$, where $N+1$ is the total number of points that are being sampled. We apply a 2D mid-point rule for the numerical integration of the two dimensional integral (see e.g. (EDQNM1)). Then, the integration measure for a mode k_l becomes

$$\int_0^\infty \mathrm{d}q \int_{|k-q|}^{k+q} \mathrm{d}p \to \sum_{n=0}^{N} \sum_{m=0}^{N} \theta\left(p_m - |q_n - k_l|\right) \theta\left(|q_n + k_l| - p_m\right) p_m q_n \Delta^2 v_{lnm}, \tag{B.1}$$

where

$$v_{lnm} = \int_{k_{l,-}}^{k_{l,+}} \mathrm{d}k \int_{q_{n,-}}^{q_{n,+}} \mathrm{d}q \int_{p_{m,-}}^{p_{m,+}} \mathrm{d}p \theta\left(p - |q-k|\right) \theta\left(|q+k| - p\right), \tag{B.2}$$

and $\Delta = 2^{1/(2F)} - 2^{-1/(2F)}$, $k_{n,-} = 2^{-1/(2F)}k$ and $k_{n,+} = 2^{1/(2F)}k$. The above volume element with the additional integration in k assures that the integration remains symmetric in the modes k, q and p. Otherwise the triads will not be conserved. We include a factor $\theta\left(p_m - |q_n - k_l|\right) \theta\left(|q_n + k_l| - p_m\right)$ to assure that only triads with center values e.g. q_n that are in the triad itself are taken into account. This is necessary, since the inclusion of modes with non-zero v_{lnm}, yet without e.g. p_m in the triad itself, drive instabilities in the evolution of the equation. We did not find a softer method to deal with these problems, e.g. Kraichnan and Leith (cite here) introduced an symmetric reduction factor for these modes $\propto \min(k_l, q_n, p_m)/\max(k_l, q_n, p_m)$, yet this does not suffice for large Reynolds numbers and non-Kolmogorov like initial conditions, hence we neglect those terms altogether. Note that the volume element v_{lnm} is symmetric under permutations in all three indices. Therefore it is sufficient to only compute $\bar{v}(a-b, a-c) = v_{abc}$ for $a \geq b$ and $a \geq c$. Moreover the coefficients Λ_i and Λ_i^h strongly vary in the p, q-plane, hence these need to be averaged over the volume element. The average of these coefficients reads

$$\begin{aligned}\Lambda_i(k_l, q_n, p_m) \rightarrow f_i(l,n)\tilde{\Lambda}_i(l,n,m) =& \frac{1}{v_{lnm}} \int_{k_{l,-}}^{k_{l,+}} \mathrm{d}k \int_{q_{n,-}}^{q_{n,+}} \mathrm{d}q \int_{p_{m,-}}^{p_{m,+}} \mathrm{d}p \\ & \theta\left(p - |q-k|\right) \theta\left(|q+k| - p\right) \Lambda_i^{ln}\left(k, q, p\right).\end{aligned}$$

The coefficients $\Lambda_i^{ln}(k,q,p)$ are defined as

$$
\begin{aligned}
\Lambda_1^{ln}(k,q,p) &= \frac{k^2}{k_l^2}\left(1-c_{pk}^2\right)\left(1+c_{qk}^2\right), & \Lambda_2^{ln}(k,q,p) &= \frac{k^2}{k_l^2}c_{qk}c_{pk}\left(c_{pk}c_{qk}-c_{qp}\right),\\
\Lambda_3^{ln}(k,q,p) &= \frac{q^2}{q_n^2}c_{qk}c_{qp}\left(c_{qp}c_{qk}-c_{pk}\right), & \Lambda_4^{ln}(k,q,p) &= \frac{q^2}{q_n^2}\left(1-c_{qp}^2\right)\left(1+c_{qk}^2\right),\\
\Lambda_5^{ln}(k,q,p) &= \frac{k^2}{k_l^2}\left(c_{pk}c_{qk}-c_{qp}\right), & \Lambda_6^{ln}(k,q,p) &= \frac{q^2}{q_n^2}\left(c_{qk}c_{qp}-c_{pk}\right),\\
\Lambda_7^{ln}(k,q,p) &= \frac{q^2}{q_n^2}c_{qp}\left(c_{pk}-c_{qk}c_{qp}\right), & \Lambda_8^{ln}(k,q,p) &= \frac{k^2}{k_l^2}c_{qk}\left(c_{qp}-c_{pk}c_{qk}\right),\\
\Lambda_9^{ln}(k,q,p) &= \frac{k^2}{k_l^2}\left(1-c_{pk}^2\right)c_{qk}, & \Lambda_{10}^{ln}(k,q,p) &= \frac{k^2}{k_l^2}c_{pk}\left(c_{qp}-c_{qk}c_{pk}\right).
\end{aligned}
$$

Moreover, the coefficients $f_i(l,n)$ are given as

$$
f_i(l,n) = \begin{cases} k_l^2, & i = 1,2,5,8,9,10 \\ q_n^2, & i = 3,4,6,7 \end{cases} .
$$

As before one only needs to compute $\tilde{\Lambda}_i(a,b,c) = \tilde{\bar{\Lambda}}_i(a-b,a-c)$. In general one one needs to compute the differences from 0 to $2N-1$ and also $\tilde{\bar{\Lambda}}_i(a-b,a-c) \neq \tilde{\bar{\Lambda}}_i(a-c,a-b)$. The damping factors $\gamma(k,q,p)$ are symmetric by construction and there is no need to further alter these. The simplistic integration scheme based on the midpoint rule generally implies errors of the order 10% for $F=4$. This is sufficient since the Gaussian closure scheme, that is applied here, limits the overall precision regardless to a similar level. Note that for the equations involving the evolution of $H^{\pm}(k)$ and $H^R(k)$ we apply a slightly adjusted average

$$
\begin{aligned}
\Lambda_{i,H}(k_l,q_n,p_m) \rightarrow f_i(l,n)\tilde{\Lambda}_{i,H}(l,n,m) =& \frac{1}{v_{lnm}}\int_{k_{l,-}}^{k_{l,+}} \mathrm{d}k \int_{q_{n,-}}^{q_{n,+}} \mathrm{d}q \int_{p_{m,-}}^{p_{m,+}} \mathrm{d}p \\
& \theta\left(p-|q-k|\right)\theta\left(|q+k|-p\right)\Lambda_i^{ln}(k,q,p)\,\frac{k_l}{k}.
\end{aligned}
$$

We find this to be necessary in order to ascertain that magnetic helicity remains conserved up to errors on the level of the machine precision.

The choice of the additional scaling comes from the fact that $H_b(k)/k$ is the conserved quantity. Note one particular downside is that for helical hydrodynamical turbulence, conservation of the dimensional kinetic helicity $H_K(k)k$ is not covered by this scaling, and in fact a factor k/k_l rather than k_l/k would have to be introduced to ascertain the numerical conservation of the hydrodynamical conserved kinetic helicity. Hence the present approach is ill suited in handling helical MHD systems with small magnetic Reynolds numbers $\mathrm{Re}_m \lesssim 1$ and large kinetic Reynold's numbers $\mathrm{Re} \gg 1$, although we note that kinetic helicity is suspected to generally undergo a cascade and hence viscous decay might sufficiently hide any inadequacies in properly handling the purely numerical turbulent decay of kinetic helicity in hydrodynamic or quasi-hydrodynamic systems. Anyway in the present study we do not expect that these inadequacies will have any relevant impact on the system, yet again we cannot fully exclude the possibility that the evolution of non-conserved quantities may be contaminated by larger numerical errors or even by instabilities.

Furthermore, the code does not conserve quantities like

$$\int_0^\infty \frac{\mathrm{d}k}{k} E^\pm(k), \tag{B.3}$$

but rather it conserves these quantities as defined by the trapezoidal rule

$$\frac{1}{2}\sum_{i=1}^{N}(k_i - k_{i-1})\left(\frac{E^\pm(k_i)}{k_i} + \frac{E^\pm(k_{i-1})}{k_{i-1}}\right). \tag{B.4}$$

for the cross helicity and total energy. Besides, the code conserves for the magnetic heliciy the following quantity

$$\frac{1}{8}\sum_{i=1}^{N}(k_i - k_{i-1})\left(\frac{\sum_\pm H^\pm(k_i) - 2H^R(k_i)}{k_i^2} + \frac{\sum_\pm E^\pm(k_{i-1}) - 2H^R(k_{i-1})}{k_{i-1}^2}\right). \tag{B.5}$$

As discussed by the example of a zero net dimensional magnetic helicity, the approach is fully self-sufficient in that a system with a zero magnetic helicity as defined above behaves differently than a system with some net non-zero magnetic helicity as defined above.

B.2 Time integration

In order to solve for the integration in time we use a backwards differentiation formula. We use a modified time step that in case of a trapezoidal rule has the following shape for hydrodynamic turbulence

$$y_l^{n+1} = \exp\left[-2\nu k_l^2 \Delta_{n+1}\right] y_l^n + \frac{1-\exp\left[-2\nu k_l^2 \Delta_{n+1}\right]}{2\nu k_l^2}\left[F_l^{n+1}(\mathbf{y}^{n+1}) + F_l^n(\mathbf{y}^n)\right], \quad \text{(B.6)}$$

where $F(\mathbf{y}, t_n) = \mathbf{y}'_{\nu\to 0}(t_n)$ and the t_n has been dropped for an upper index n. Such schemes have the advantage, that the diffusion equation is solved exactly with arbitrary large timesteps and the size of a timestep only depends on the nonlinear part of the equation. In the case of the MHD equations in terms of the Elsaesser variables, we need to rotate the equations in order to perform a step according to (B.6). For MHD $y_l^{n+1} \to \mathbf{y}_l$ is a six dimensional vector

$$\mathbf{y}_l = \left\{E_l^+, E_l^-, E_l^R, H_l^+, H_l^-, H_l^R\right\}. \quad \text{(B.7)}$$

The transformation of these is then given by

$$\mathbf{M} = \begin{bmatrix} 0 & -1 & 0 & -1 & 0 & 1 \\ 0 & 1 & 0 & -1 & 0 & 1 \\ 0 & 0 & 0 & 1 & 0 & 1 \\ -1 & 0 & -1 & 0 & 1 & 0 \\ 1 & 0 & -1 & 0 & 1 & 0 \\ 0 & 0 & 1 & 0 & 1 & 0 \end{bmatrix}$$

and the back-transform is given by

$$\mathbf{M}^{-1} = \begin{bmatrix} 0 & 0 & 0 & -1/2 & 1/2 & 0 \\ -1/2 & 1/2 & 0 & 0 & 0 & 0 \\ 0 & 0 & 0 & -1/4 & -1/4 & 1/2 \\ -1/4 & -1/4 & 1/2 & 0 & 0 & 0 \\ 0 & 0 & 0 & 1/4 & 1/4 & 1/2 \\ 1/4 & 1/4 & 1/2 & 0 & 0 & 0 \end{bmatrix}$$

The eigenvalues of the transformation corresponding to the viscosity in (B.6) are

$$\boldsymbol{\nu} = \{\nu_+, \nu_+, \nu_+ - \nu_-, \nu_+ - \nu_-, \nu_+ + \nu_-, \nu_+ + \nu_-\}^T . \tag{B.8}$$

Then the analogue of (B.6) for MHD is

$$\mathbf{y}_l^{n+1} = \mathbf{M}^{-1} \exp\left[-2\boldsymbol{\nu} k_l^2 \Delta_{n+1}\right] \mathbf{M}\mathbf{y}_l^n + \mathbf{M}^{-1} \frac{1 - \exp\left[-2\boldsymbol{\nu} k_l^2 \Delta_{n+1}\right]}{2\boldsymbol{\nu} k_l^2} \mathbf{M} \left[\mathbf{F}_l^{n+1}(\mathbf{y}^{n+1}) + \mathbf{F}_l^n(\mathbf{y}^n)\right] . \tag{B.9}$$

This can be generalized towards higher order schemes in an analogues manner. Technically ν depends on the scale factor, hence we take $\nu(t_n)$ for a predictor step and $\nu(t_{n+1})$ for the corrector step.

B.3 Cleaning, hyper-viscosity and hyper-resistivity

In order to stabilize the numerical evaluation and to decrease computation times, we deploy several adjustments and tricks. One important factor is the implementation of an additional viscosity term, the so called hyper-viscosity in order to decrease the inertial range and to increase the length of time-steps which scale with $k_d^{-\alpha}$, where $\alpha > 0$ depends on the scaling of the inertial range i.e. a large k_d implies shorter time-steps. Another important numerical aspect of this is the reduction of points that needs to be sampled. The viscosity is then redefined accordingly

$$\nu k^2 \to \nu k^2 + \nu_{\rm h} k^6, \tag{B.10}$$

where $\nu_{\rm h}$ is the hyper-viscosity coefficient which we choose adaptively to correspond to $Re \lesssim 10^4$ based on the integral scale variables and a Kolmogorov inertial range scaling with the key assumption that at the hyper-viscosity damping scale we have $\mathrm{Re}(k_{d,h}) = 1$. Explicitly, we choose $\nu_h = v_I \mathrm{Re}^{-17/5} k_I^{-21/5}$, where $v_I = v(k_I)$. While for a k^{-1} scaling in the inertial range one should set $\nu_h = v_I \mathrm{Re}^{-3} k_I^{-5}$. Note that these choices are only a rough approximation and the system does not behave like a fully turbulent state with $Re = 10^4$ as the hyper-viscosity does not affect the inertial range in the same manner due to the steeper scaling. This approach is only reasonable whenever Pm$\gg 1$, however if hyper-resistive damping is relevant, one also needs to add a resistive damping coefficient. In general we choose for the hyper resistivity $\eta_h \sim \nu_h/\mathrm{Pm}^{1/3}$, where $Pm = \nu/\eta$ is still based on microphysical rather than hyper-damping terms. Here we do not apply a hyper-resistive damping term in order to ascertain magnetic helicity conservation.

Furthermore, the hyper-viscosity term not only helps in increasing timesteps but it also helps in somewhat suppressing the growth of small scale instabilities. Nonetheless, this itself is not sufficient, to ascertain stability of the system at small scales without excruciatingly small time steps. In order to increase stability we cut the tail of the energy and other spectra at the small scales, where the value of the spectrum has dropped to roughly $10^{-10}\,(E^+(k_I) + E^-(k_I))$. Around this point we generally apply a mixture a of strict cut-off i.e. setting all spectral values at smaller scales to 0 and averaged power-law exponential extrapolation in order to control the system, where the hard-cut off is used when the values of the energy spectrum are not monotonously decreasing towards smaller scales. In general this procedure is reiterated until a monotonous small scale behavior with the aforementioned cut-off persists. We emphasize that the aforementioned problems are not physical but purely numerical, e.g. negative energies appear, which is not a feature of the EDQNM approximation.

Lastly, in order to further improve of the efficiency energy and cross- and magnetic helicity conservation, we evaluate the numerical error in the derivatives and readjust either the maximal or minimal value of the derivative of either the energies, cross- or magnetic helicity, such that the numerical error gets further reduced, which generally improves conservation of the total energy spectral distribution or the two helicities above machine precision, where the width of a spectral interval is otherwise another limiting factor in precision. We repeat this procedure 4 times, which leads to a further reduction of the error. Note that the aforementioned cutoff and extrapolation violates magnetic helicity conservation in cross helicity dominated MHD turbulence and is in general a significant source for a violation in magnetic and cross helicity and energy conservation. An improvement of the cut-off and extrapolation to account for magnetic helicity conservation in these instances is still work in progress.

C | Assumptions in Solving the GWMHD equations

Here we model the spectra of solenoidal MHD turbulence using the von Karman model (von Kármán 1948)

$$E(k) = C_E \frac{K^5}{(c + K^2)^{17/6}} \theta(L_I/\lambda - K), \tag{C.1}$$

where $K = kL_I/(2\pi)$, $k_d = \lambda/(2\pi)$ and $c = 5/12$ corresponds to $E(k)/k$ having a maximum at $K = 1$. The factor C_E is fixed by the following normalization conditions

$$\frac{3}{2}\Omega_{\text{turb}} = \int_{-\infty}^{\infty} \mathrm{d}\ln(K) E(K), \tag{C.2}$$

where Ω_{turb} is the density parameter of either the solenoidal kinetic or magnetic component or the sum of both relative to the radiation energy density parameter Ω_r. Therefore, we arrive at

$$C_E = -\frac{3}{2\pi^{3/2}} \left(\frac{10}{3}\right)^{1/3} \frac{\Gamma(17/6)}{\Gamma(-2/3)} \approx 0.172\, \Omega_{\text{turb}}, \tag{C.3}$$

where we assume $L_I \gg \lambda$ and hence neglected the cutoff scale in the normalization. We assume that the fields evolve in equipartition, thus $E_s = E_b$. For compressible MHD turbulence we use slightly different spectra. We assume a k^{-2} inertial range, if the turbulence is driven by dilatational (purely compressible) modes (e.g. Sun 2017),

$$E_D(k) = C_D \frac{K^5}{(c_D + K^2)^3} \theta(L_I/\lambda - K), \tag{C.4}$$

where $c_D = 1/2$ and

$$C_D = \frac{9}{32\sqrt{2}}\Omega_{\text{turb}} \approx 0.2\Omega_{\text{turb}}. \tag{C.5}$$

Note, that technically a factor $\cos^2(c_s k\tau)$ appears in the dilatational spectrum, however here we average and normalize this factor, in the limit $k\tau \gg 1$, away. For the velocity spectrum we then have

$$E_V(k) = f_d C_D \frac{K^5}{(c_D + K^2)^3}\theta(L_I/\lambda - K) + f_s C_E \frac{K^5}{(c + K^2)^{17/6}}\theta(L_I/\lambda - K), \tag{C.6}$$

where f_d and f_s denote the fraction of dilatational and solenoidal modes, respectively with $f_d + f_s = 1$.

We assume a purely self-similar evolution according to sub-subsection 3.4.5 and section 5.1

$$L_I(\tau) = L_{pt} \begin{cases} 1, \quad \tau \leq \tau_0 + \tau_{\text{b}} \\ \left(\frac{\tau - \tau_0 - \tau_b + \tau_D}{\tau_D}\right)^b, \tau > \tau_0 + \tau_{\text{b}} \end{cases} \tag{C.7}$$

where τ_D is a decay time constant and we set

$$\tau_D = \frac{L_{pt}}{2\sqrt{\langle v_1^2 \rangle}} = \frac{L_{pt}}{\sqrt{2\Omega_{\text{turb},t}}}, \tag{C.8}$$

where v_1 is given by (3.48). Also τ_{b} is the build-up timescale e.g. $\tau_b = \beta^{-1}$ is the duration of the phase transition. Subsequently, we assume for the energy the following temporal evolution

$$\Omega_{\text{turb}}(\tau) = \Omega_{\text{turb},pt} \begin{cases} 1 - \left(\frac{\tau_{\text{b}} - (\tau - \tau_0)}{\tau_{\text{b}}}\right), \quad \tau_0 \leq \tau \leq \tau_0 + \tau_{\text{b}} \\ \left(\frac{\tau_D}{\tau - \tau_b + \tau_D}\right)^a, \quad \tau \geq \tau_{\text{b}} + \tau_0. \end{cases} \tag{C.9}$$

where $a = 1.4$ and $b = 0.3$ for a normal cascade and $a = b = 2/3$ for a magnetic helicity driven inverse cascade. Here L_{pt} is the initial turbulent integral scale and $\Omega_{turb,pt}$ is the peak turbulent density parameter after the turbulence has been excited. We use these spectra and scaling relations to calculate the gravitational wave spectra.

Bibliography

Aab A, Abreu P, Aglietta M, Albuquerque I F M, Allekotte I, Almela A, Alvarez Castillo J, Alvarez-Muñiz J, Anastasi G A, Anchordoqui L, Andrada B, Andringa S, Aramo C, Arsene N, Asorey H, Assis P, Avila G, Badescu A M, Balaceanu A, Barbato F, Barreira Luz R J, Beatty J J, Becker K H, Bellido J A, Berat C, Bertaina M E, Bertou X, Biermann P L, Biteau J, Blaess S G, Blanco A, Blazek J, Bleve C, Boháčová M, Bonifazi C, Borodai N, Botti A M, Brack J, Brancus I, Bretz T, Bridgeman A, Briechle F L, Buchholz P, Bueno A, Buitink S, Buscemi M, Caballero-Mora K S, Caccianiga L, Cancio A, Canfora F, Caruso R, Castellina A, Catalani F, Cataldi G, Cazon L, Chavez A G, Chinellato J A, Chudoba J, Clay R W, Cobos Cerutti A C, Colalillo R, Coleman A, Collica L, Coluccia M R, Conceição R, Consolati G, Contreras F, Cooper M J, Coutu S, Covault C E, Cronin J, D'Amico S, Daniel B, Dasso S, Daumiller K, Dawson B R, de Almeida R M, de Jong S J, De Mauro G, de Mello Neto J R T, De Mitri I, de Oliveira J, de Souza V, Debatin J, Deligny O, Díaz Castro M L, Diogo F, Dobrigkeit C, D'Olivo J C, Dorosti Q, dos Anjos R C, Dova M T, Dundovic A, Ebr J, Engel R, Erdmann M, Erfani M, Escobar C O, Espadanal J, Etchegoyen A, Falcke H, Farmer J, Farrar G, Fauth A C, Fazzini N, Fenu F, Fick B, Figueira J M, Filipčič A, Freire M M, Fujii T, Fuster A, Gaïor R, García B, Gaté F, Gemmeke H, Gherghel-Lascu A, Ghia P L, Giaccari U, Giammarchi M, Giller M, Głas D, Glaser C, Golup G, Gómez Berisso M, Gómez Vitale P F, González N, Gorgi A, Grillo A F, Grubb T D, Guarino F, Guedes G P, Halliday R, Hampel M R, Hansen P, Harari D, Harrison T A, Haungs A, Hebbeker T, Heck D, Heimann P, Herve A E, Hill G C,

Hojvat C, Holt E, Homola P, Hörandel J R, Horvath P, Hrabovský M, Huege T, Hulsman J, Insolia A, Isar P G, Jandt I, Johnsen J A, Josebachuili M, Jurysek J, Kääpä A, Kambeitz O, Kampert K H, Keilhauer B, Kemmerich N, Kemp E, Kemp J, Kieckhafer R M, Klages H O, Kleifges M, Kleinfeller J, Krause R, Krohm N, Kuempel D, Kukec Mezek G, Kunka N, Kuotb Awad A, Lago B L, LaHurd D, Lang R G, Lauscher M, Legumina R, Leigui de Oliveira M A, Letessier-Selvon A, Lhenry-Yvon I, Link K, Lo Presti D, Lopes L, López R, López Casado A, Lorek R, Luce Q, Lucero A, Malacari M, Mallamaci M, Mandat D, Mantsch P, Mariazzi A G, Mariș I C, Marsella G, Martello D, Martinez H, Martínez Bravo O, Masías Meza J J, Mathes H J, Mathys S, Matthews J, Matthiae G, Mayotte E, Mazur P O, Medina C, Medina-Tanco G, Melo D, Menshikov A, Merenda K D, Michal S, Micheletti M I, Middendorf L, Miramonti L, Mitrica B, Mockler D, Mollerach S, Montanet F, Morello C, Morlino G, Mostafá M, Müller A L, Müller G, Muller M A, Müller S, Mussa R, Naranjo I, Nellen L, Nguyen P H, Niculescu-Oglinzanu M, Niechciol M, Niemietz L, Niggemann T, Nitz D, Nosek D, Novotny V, Nožka L, Núñez L A, Oikonomou F, Olinto A, Palatka M, Pallotta J, Papenbreer P, Parente G, Parra A, Paul T, Pech M, Pedreira F, Pękala J, Pelayo R, Peña-Rodriguez J, Pereira L A S, Perlin M, Perrone L, Peters C, Petrera S, Phuntsok J, Pierog T, Pimenta M, Pirronello V, Platino M, Plum M, Poh J, Porowski C, Prado R R, Privitera P, Prouza M, Quel E J, Querchfeld S, Quinn S, Ramos-Pollan R, Rautenberg J, Ravignani D, Ridky J, Riehn F, Risse M, Ristori P, Rizi V, Rodrigues de Carvalho W, Rodriguez Fernandez G, Rodriguez Rojo J, Roncoroni M J, Roth M, Roulet E, Rovero A C, Ruehl P, Saffi S J, Saftoiu A, Salamida F, Salazar H, Saleh A, Salina G, Sánchez F, Sanchez-Lucas P, Santos E M, Santos E, Sarazin F, Sarmento R, Sarmiento-Cano C, Sato R, Schauer M, Scherini V, Schieler H, Schimp M, Schmidt D, Scholten O, Schovánek P, Schröder F G, Schröder S, Schulz A, Schumacher J, Sciutto S J, Segreto A, Shadkam A, Shellard R C, Sigl G, Silli G, Šmída R, Snow G R, Sommers P, Sonntag S, Soriano J F, Squartini R, Stanca D, Stanič S, Stasielak J, Stassi P, Stolpovskiy M, Strafella F, Streich A, Suarez F, Suarez Durán

M, Sudholz T, Suomijärvi T, Supanitsky A D, Šupík J, Swain J, Szadkowski Z, Taboada A, Taborda O A, Theodoro V M, Timmermans C, Todero Peixoto C J, Tomankova L, Tomé B, Torralba Elipe G, Travnicek P, Trini M, Ulrich R, Unger M, Urban M, Valdés Galicia J F, Valiño I, Valore L, van Aar G, van Bodegom P, van den Berg A M, van Vliet A, Varela E, Vargas Cárdenas B, Vázquez R A, Veberič D, Ventura C, Vergara Quispe I D, Verzi V, Vicha J, Villaseñor L, Vorobiov S, Wahlberg H, Wainberg O, Walz D, Watson A A, Weber M, Weindl A, Wiedeński M, Wiencke L, Wilczyński H, Wirtz M, Wittkowski D, Wundheiler B, Yang L, Yushkov A, Zas E, Zavrtanik D, Zavrtanik M, Zepeda A, Zimmermann B, Ziolkowski M, Zong Z, Zuccarello F & Pierre Auger Collaboration 2018 *ApJL* **853**(2), L29.

Abbott B P, Abbott R, Abbott T D, Abernathy M R, Acernese F, Ackley K, Adams C, Adams T, Addesso P, Adhikari R X & et al. 2016 *Physical Review Letters* **116**(6), 061102.

Amaro-Seoane P, Audley H, Babak S, Baker J, Barausse E, Bender P, Berti E, Binetruy P, Born M, Bortoluzzi D, Camp J, Caprini C, Cardoso V, Colpi M, Conklin J, Cornish N, Cutler C, Danzmann K, Dolesi R, Ferraioli L, Ferroni V, Fitzsimons E, Gair J, Gesa Bote L, Giardini D, Gibert F, Grimani C, Halloin H, Heinzel G, Hertog T, Hewitson M, Holley-Bockelmann K, Hollington D, Hueller M, Inchauspe H, Jetzer P, Karnesis N, Killow C, Klein A, Klipstein B, Korsakova N, Larson S L, Livas J, Lloro I, Man N, Mance D, Martino J, Mateos I, McKenzie K, McWilliams S T, Miller C, Mueller G, Nardini G, Nelemans G, Nofrarias M, Petiteau A, Pivato P, Plagnol E, Porter E, Reiche J, Robertson D, Robertson N, Rossi E, Russano G, Schutz B, Sesana A, Shoemaker D, Slutsky J, Sopuerta C F, Sumner T, Tamanini N, Thorpe I, Troebs M, Vallisneri M, Vecchio A, Vetrugno D, Vitale S, Volonteri M, Wanner G, Ward H, Wass P, Weber W, Ziemer J & Zweifel P 2017 *ArXiv e-prints* .

Angel J R P & Stockman H S 1980 *ARA&A* **18**, 321–361.

Anselmet F, Gagne Y, Hopfinger E J & Antonia R A 1984 *Journal of Fluid Mechanics* **140**, 63–89.

Arcadi G, Djouadi A & Raidal M 2019 'Dark matter through the higgs portal'.

Arnold P, Moore G D & Yaffe L G 2000 *Journal of High Energy Physics* **2000**(11), 001.

Banerjee R & Jedamzik K 2004 *PRD* **70**(12), 123003.

Bardeen J M, Steinhardt P J & Turner M S 1983 *Phys. Rev. D* **28**, 679–693.
URL: `https://link.aps.org/doi/10.1103/PhysRevD.28.679`

Barrow J D, Ferreira P G & Silk J 1997 *Phys. Rev. Lett.* **78**(19), 3610–3613.

Batchelor G K & Proudman I 1956 *Philosophical Transactions of the Royal Society of London Series A* **248**, 369–405.

Baym G & Heiselberg H 1997 *Physical Review D* **56**(8), 5254–5259.

Becker R H, Fan X, White R L, Strauss M A, Narayanan V K, Lupton R H, Gunn J E, Annis J, Bahcall N A, Brinkmann J, Connolly A J, Csabai I, Czarapata P C, Doi M, Heckman T M, Hennessy G S, Ivezić Ž, Knapp G R, Lamb D Q, McKay T A, Munn J A, Nash T, Nichol R, Pier J R, Richards G T, Schneider D P, Stoughton C, Szalay A e S, Thakar A R & York D G 2001 *Astronomical Journal* **122**(6), 2850–2857.

Beresnyak A 2011 *Phys. Rev. Lett.* **106**, 075001.

Biermann L 1950 *Zeitschrift Naturforschung Teil A* **5**, 65.

Biskamp D 1993 *Nonlinear magnetohydrodynamics*.

Blasi P, Burles S & Olinto A V 1999 *ApJL* **514**, L79–L82.

Bödeker D & Moore G D 2009 *JCAP* **2009**(5), 009.

Bonetti M, Sesana A, Barausse E & Haardt F 2018 *MNRAS* **477**, 2599–2612.

Bowman J C 1996 *Journal of Scientific Computing* **11**(4), 343–372.
URL: `https://doi.org/10.1007/BF02088952`

Boyarsky A, Fröhlich J & Ruchayskiy O 2012 *Phys. Rev. Lett.* **108**(3), 031301.

Brandenburg A, Enqvist K & Olesen P 1996 *PRD* **54**, 1291–1300.

Brandenburg A & Kahniashvili T 2017 *Physical Review Letters* **118**(5), 055102.

Brandenburg A, Kahniashvili T & Tevzadze A G 2015 *Physical Review Letters* **114**(7), 075001.

Brandenburg A, Schober J, Rogachevskii I, Kahniashvili T, Boyarsky A, Fröhlich J, Ruchayskiy O & Kleeorin N 2017 *ApJL* **845**(2), L21.

Brandenburg A & Subramanian K 2005 *Phys. Rep.* **417**, 1–209.

Bray J D & Scaife A M M 2018 *ApJ* **861**(1), 3.

Broderick A E, Chang P & Pfrommer C 2012 *ApJ* **752**(1), 22.

Brown I A, Christopherson A J & Malik K A 2012 *MNRAS* **423**, 1411–1415.

Buchmuller W, Fodor Z, Helbig T & Walliser D 1994 *Annals of Physics* **234**, 260–299.

Burigana C, Danese L & de Zotti G 1991 *A&A* **246**, 49–58.

Cai R G & Wang S J 2018 *Science China Physics, Mechanics, and Astronomy* **61**(8).

Caprini C & Durrer R 2002 *PRD* **65**(2), 023517.

Caprini C & Durrer R 2006 *PRD* **74**(6), 063521.

Caprini C, Durrer R & Servant G 2009 *JCAP* **12**, 024.

Caprini C, Durrer R & Siemens X 2010 *PRD* **82**(6), 063511.

Caprini C & Ferreira P G 2005 *JCAP* **2005**(2), 006.

Caprini C & Figueroa D G 2018 *Classical and Quantum Gravity* **35**(16), 163001.

Caprini C, Hindmarsh M, Huber S, Konstandin T, Kozaczuk J, Nardini G, No J M, Petiteau A, Schwaller P, Servant G & Weir D J 2016 *JCAP* **4**, 001.

Chatrchyan S, Khachatryan V, Sirunyan A, Tumasyan A, Adam W, Aguilo E, Bergauer T, Dragicevic M, Erö J, Fabjan C & et al. 2012 *Physics Letters B* **716**(1), 30–61.
URL: `http://dx.doi.org/10.1016/j.physletb.2012.08.021`

Chen W, Chowdhury B D, Ferrer F, Tashiro H & Vachaspati T 2015 *MNRAS* **450**(4), 3371–3380.

Chluba J & Sunyaev R A 2012 *MNRAS* **419**, 1294–1314.

Chou P Y 1940 *Chin. J. Phys.* pp. 1–53.

Cornwall J M 1997 *PRD* **56**, 6146–6154.

Cox D P 2005 *ARA&A* **43**(1), 337–385.

Cutting D, Hindmarsh M & Weir D J 2019 *arXiv e-prints* p. arXiv:1906.00480.

Cyburt R H, Fields B D, Olive K A & Yeh T H 2016 *Reviews of Modern Physics* **88**(1), 015004.

Daly R A & Loeb A 1990 *ApJ* **364**, 451.

de Karman T & Howarth L 1938 *Proceedings of the Royal Society of London. Series A - Mathematical and Physical Sciences* **164**(917), 192–215.
URL: `https://royalsocietypublishing.org/doi/abs/10.1098/rspa.1938.0013`

Dong Y H & Sagaut P 2008 *Physics of Fluids* **20**(3), 035105–035105.

Durrer R 2007 *New Astron. Rev.* **51**(3-4), 275–280.

Durrer R & Neronov A 2013 *AAPR* **21**, 62.

Ellis G F R 1973 *in* E Schatzman, ed., ‘Cargese Lectures in Physics’ Vol. 6 of *Cargese Lectures in Physics* p. 1.

Ellis J, Fairbairn M, Lewicki M, Vaskonen V & Wickens A 2019 *JCAP* **2019**(9), 019.

Espinosa J R, Konstandin T, No J M & Quirós M 2008 *PRD* **78**(12), 123528.

Espinosa J R, Konstandin T, No J M & Servant G 2010 *JCAP* **6**, 028.

Espinosa J R, Konstandin T & Riva F 2012 *Nuclear Physics B* **854**, 592–630.

Favre A J 1965 *Journal of Applied Mechanics* **32**, 241.

Finke J D, Reyes L C, Georganopoulos M, Reynolds K, Ajello M, Fegan S J & McCann K 2015 *ApJ* **814**, 20.

Frisch U 1991 *Proceedings of the Royal Society of London Series A* **434**, 89–99.

Frisch U, Lesieur M & Brissaud A 1974 *Journal of Fluid Mechanics* **65**, 145–152.

Frisch U, Pouquet A, Leorat J & Mazure A 1975 *Journal of Fluid Mechanics* **68**, 769–778.

Frisch U, Sulem P L & Nelkin M 1978 *Journal of Fluid Mechanics* **87**, 719–736.

Furlanetto S R & Loeb A 2001 *ApJ* **556**, 619–634.

Gerasimova N M, Nikishov A I & Rosenthal I L 1962 *Journal of the Physical Society of Japan Supplement* **17**, 175.

Goldreich P & Sridhar S 1995 *ApJ* **438**, 763–775.

He G, Jin G & Yang Y 2017 *Annual Review of Fluid Mechanics* **49**, 51–70.

Hindmarsh M & Hijazi M 2019 *arXiv e-prints* p. arXiv:1909.10040.

Hindmarsh M, Huber S J, Rummukainen K & Weir D J 2014 *Phys. Rev. Lett.* **112**(4), 041301.

Hindmarsh M, Huber S J, Rummukainen K & Weir D J 2015 *PRD* **92**(12), 123009.

Hogan C J 1986 *MNRAS* **218**, 629–636.

Hoyle F 1969 *Nature* **223**(5209), 936.

Huber S J & Konstandin T 2008 *JCAP* **9**, 022.

Huber S J, Konstandin T, Nardini G & Rues I 2016 *JCAP* **3**, 036.

Iroshnikov P S 1964 *Soviet Astronomy* **7**, 566.

ISSERLIS L 1916 *Biometrika* **11**(3), 185–190.
URL: `https://doi.org/10.1093/biomet/11.3.185`

Jansson R & Farrar G R 2012*a* *ApJ* **757**, 14.

Jansson R & Farrar G R 2012*b* *ApJL* **761**, L11.

Jedamzik K & Fuller G M 1994 *ApJ* **423**(1), 33–49.

Jedamzik K, Katalinić V & Olinto A V 1998 *PRD* **57**, 3264–3284.

Jedamzik K & Sigl G 2011 *PRD* **83**(10), 103005.

Jeong D, Pradler J, Chluba J & Kamionkowski M 2014 *Physical Review Letters* **113**(6), 061301.

Kahniashvili T, Campanelli L, Gogoberidze G, Maravin Y & Ratra B 2008*a* *PRD* **78**(12), 123006.

Kahniashvili T, Campanelli L, Gogoberidze G, Maravin Y & Ratra B 2008*b* *PRD* **78**(12), 123006.

Kahniashvili T, Gogoberidze G & Ratra B 2008 *Physical Review Letters* **100**(23), 231301.

Kahniashvili T, Tevzadze A G, Brand enburg A & Neronov A 2013 *PRD* **87**(8), 083007.

Kamionkowski M, Kosowsky A & Turner M S 1994 *PRD* **49**, 2837–2851.

Kaneda Y 1993 *Physics of Fluids A* **5**, 2835–2845.

Kaneda Y, Ishihara T & Gotoh K 1999 *Physics of Fluids* **11**, 2154–2166.

Kaspi V M & Beloborodov A M 2017 *Annual Review of Astronomy and Astrophysics* **55**(1), 261–301.
URL: `http://dx.doi.org/10.1146/annurev-astro-081915-023329`

Kaufmann W J 1991 *Universe*.

Kempf A, Kilian P & Spanier F 2016 *A&A* **585**, A132.

Kernan P J, Starkman G D & Vachaspati T 1996 *Phys. Rev. D* **54**, 7207–7214.
URL: `https://link.aps.org/doi/10.1103/PhysRevD.54.7207`

Kharzeev D E, Liao J, Voloshin S A & Wang G 2016 *Progress in Particle and Nuclear Physics* **88**, 1–28.

Kirzhnits D & Linde A 1976 *Annals of Physics* **101**(1), 195 – 238.
URL: `http://www.sciencedirect.com/science/article/pii/0003491676902797`

Kodama H & Sasaki M 1984 *Progress of Theoretical Physics Supplement* **78**, 1.

Kolmogorov A 1941 *Akademiia Nauk SSSR Doklady* **30**, 301–305.

Kolmogorov A N 1962 *Journal of Fluid Mechanics* **13**, 82–85.

Kosowsky A, Mack A & Kahniashvili T 2002 *PRD* **66**(2), 024030.

Kozaczuk J 2015 *Journal of High Energy Physics* **2015**, 135.

Kraichnan R H 1959 *Journal of Fluid Mechanics* **5**, 497–543.

Kraichnan R H 1961 *Journal of Mathematical Physics* **2**, 124–148.

Kraichnan R H 1964 *Physics of Fluids* **7**, 1163–1168.

Kraichnan R H 1965*a* *Physics of Fluids* **8**, 1385–1387.

Kraichnan R H 1965*b* *Physics of Fluids* **8**, 575–598.

Kraichnan R H 1967 *Physics of Fluids* **10**, 1417–1423.

Kulsrud R M 1999*a* *ARA&A* **37**, 37–64.

Kulsrud R M 1999*b* *Annual Review of Astronomy and Astrophysics* **37**(1), 37–64.
URL: `https://doi.org/10.1146/annurev.astro.37.1.37`

Kuzmin V A, Rubakov V A & Shaposhnikov M E 1985 *Physics Letters B* **155**, 36–42.

Lazarian A & Pogosyan D 2016 *ApJ* **818**(2), 178.

Lee S, Lele S K & Moin P 1992 *Physics of Fluids A* **4**, 1521–1530.

Leith C E 1971 *Journal of Atmospheric Sciences* **28**, 145–161.

Leith C E & Kraichnan R H 1972 *Journal of Atmospheric Sciences* **29**, 1041–1058.

Lesieur M 1972 Décomposition dâ€™un champ de vitesse non divergent en ondes d'hélicité Technical report Observatoire de Nice.

Lesieur M 2008 *Turbulence in Fluids* Fluid Mechanics and Its Applications Springer Netherlands.

Lesieur M & Schertzer D 1978 *Journal de Mecanique* **17**, 609–646.

Li D, Zhang X & He G 2013 *PRE* **88**(2), 021001.

Loeb A & Furlanetto S R 2013 *The First Galaxies in the Universe* stu - student edition edn Princeton University Press.
URL: `http://www.jstor.org/stable/j.ctt24hrpv`

Mégevand A & Sánchez A D 2010 *Nuclear Physics B* **825**(1-2), 151–176.

Meneguzzi M, Frisch U & Pouquet A 1981 *Physical Review Letters* **47**, 1060–1064.

Millionshtchikov M 1941 *Dokl. Akad. Nauk SSSR* **32**, 615.

Miniati F & Bell A R 2011 *ApJ* **729**(1), 73.

Miniati F & Elyiv A 2013 *ApJ* **770**, 54.

Misner C, Thorne K & Wheeler J 1973 *Gravitation* number pt. 3 *in* 'Gravitation' W. H. Freeman.

Moore C J, Cole R H & Berry C P L 2015 *Classical and Quantum Gravity* **32**(1), 015014.

Morrissey D E & Ramsey-Musolf M J 2012 *New Journal of Physics* **14**(12), 125003.
URL: `http://dx.doi.org/10.1088/1367-2630/14/12/125003`

Müller W C, Biskamp D & Grappin R 2003 *PRE* **67**(6), 066302.

Müller W C & Grappin R 2005 *Physical Review Letters* **95**(11), 114502.

Neronov A & Vovk I 2010 *Science* **328**, 73.

Niksa P, Schlederer M & Sigl G 2018 *Classical and Quantum Gravity* **35**(14), 144001.
URL: `https://doi.org/10.1088%2F1361-6382%2Faac89c`

O'Brien E E & Francis G C 1962 *Journal of Fluid Mechanics* **13**, 369–382.

Ogura Y 1963 *Journal of Fluid Mechanics* **16**, 33–40.

Orszag S 1977.

Orszag S A 1970 *Journal of Fluid Mechanics* **41**, 363–386.

Parker E N 1970 *ApJ* **160**, 383.

Pavlović P, Leite N & Sigl G 2016 *JCAP* **2016**(6), 044.

Pavlović P, Leite N & Sigl G 2017 *PRD* **96**(2), 023504.

Peebles P J E 1968 *ApJ* **153**, 1.

Peebles P J E 1994 *Principles of physical cosmology*.

Pietroni M 1993 *Nuclear Physics B* **402**, 27–45.

Planck Collaboration, Ade P A R, Aghanim N, Arnaud M, Arroja F, Ashdown M, Aumont J, Baccigalupi C, Ballardini M, Banday A J & et al. 2016 *A&A* **594**, A19.

Planck Collaboration, Aghanim N, Akrami Y, Ashdown M, Aumont J, Baccigalupi C, Ballardini M, Banday A J, Barreiro R B, Bartolo N, Basak S, Battye R, Benabed K, Bernard J P, Bersanelli M, Bielewicz P, Bock J J, Bond J R, Borrill J, Bouchet F R, Boulanger F, Bucher M, Burigana C, Butler R C, Calabrese E, Cardoso J F, Carron J, Challinor A, Chiang H C, Chluba J, Colombo L P L, Combet C, Contreras D, Crill B P, Cuttaia F, de Bernardis P, de Zotti G, Delabrouille J, Delouis J M, Di Valentino E, Diego J M, Doré O, Douspis M, Ducout A, Dupac X, Dusini S, Efstathiou G, Elsner F, Enßlin T A, Eriksen H K, Fantaye Y, Farhang M, Fergusson J, Fernandez-Cobos R, Finelli F, Forastieri F, Frailis M, Franceschi E, Frolov A, Galeotta S, Galli S, Ganga K, Génova-Santos R T, Gerbino M, Ghosh T, González-Nuevo J, Górski K M, Gratton S, Gruppuso A, Gudmundsson J E, Hamann J, Hand ley W, Herranz D, Hivon E, Huang Z, Jaffe A H, Jones W C, Karakci A, Keihänen E, Keskitalo R, Kiiveri K, Kim J, Kisner T S, Knox L, Krachmalnicoff N, Kunz M, Kurki-Suonio H, Lagache G, Lamarre J M, Lasenby A, Lattanzi M, Lawrence C R, Le Jeune M, Lemos P, Lesgourgues J, Levrier F, Lewis A, Liguori M, Lilje P B, Lilley M, Lindholm V, López-Caniego M, Lubin P M, Ma Y Z, Macías-Pérez J F, Maggio G, Maino D, Mandolesi N, Mangilli A, Marcos-Caballero A, Maris M, Martin P G, Martinelli M, Martínez-González E, Matarrese S, Mauri N, McEwen J D, Meinhold P R, Melchiorri A, Mennella A, Migliaccio M, Millea M, Mitra S, Miville-Deschênes M A, Molinari D, Montier L, Morgante G, Moss A, Natoli P, Nørgaard-Nielsen H U, Pagano L, Paoletti D, Partridge B, Patanchon G, Peiris H V, Perrotta F, Pettorino V, Piacentini F, Polastri L, Polenta G, Puget J L, Rachen J P, Reinecke M, Remazeilles M, Renzi A, Rocha G, Rosset C, Roudier G, Rubiño-Martín J A, Ruiz-Granados B, Salvati L, Sandri M, Savelainen M, Scott D, Shellard E P S, Sirignano C, Sirri G, Spencer L D, Sunyaev R, Suur-Uski A S, Tauber J A, Tavagnacco D, Tenti M, Toffolatti L, Tomasi M, Trombetti T, Valenziano L, Valiviita J, Van Tent B, Vibert L, Vielva

P, Villa F, Vittorio N, Wand elt B D, Wehus I K, White M, White S D M, Zacchei A & Zonca A 2018 *arXiv e-prints* p. arXiv:1807.06209.

Polyakov A 1978 *Physics Letters B* **72**(4), 477 – 480.
URL: `http://www.sciencedirect.com/science/article/pii/0370269378907372`

Pouquet A, Frisch U & Leorat J 1976 *Journal of Fluid Mechanics* **77**, 321–354.

Proudman I & Reid W H 1954 *Philosophical Transactions of the Royal Society of London Series A* **247**, 163–189.

Pshirkov M S, Tinyakov P G & Urban F R 2016 *Physical Review Letters* **116**(19), 191302.

Rees M J 1968 *ApJL* **153**, L1.

Rubinstein R & He G W 2003 Springer Japan Tokyo pp. 229–238.

Rubinstein R & Zhou Y 1999 *Physics of Fluids* **11**, 2288–2290.

Sakharov A D 1967 *Soviet Journal of Experimental and Theoretical Physics Letters* **5**, 24.

Saveliev A 2014 Time evolution of primordial magnetic fields and present day extragalactic magnetism Technical report.

Saveliev A, Jedamzik K & Sigl G 2012 *PRD* **86**(10), 103010.

Saveliev A, Jedamzik K & Sigl G 2013 *PRD* **87**(12), 123001.

Schlickeiser R, Ibscher D & Supsar M 2012 *ApJ* **758**(2), 102.

Schober J, Brandenburg A, Rogachevskii I & Kleeorin N 2019 *Geophysical and Astrophysical Fluid Dynamics* **113**(1-2), 107–130.

Schwaller P 2015 *Phys. Rev. Lett.* **115**, 181101.
URL: `https://link.aps.org/doi/10.1103/PhysRevLett.115.181101`

Schwarz D J & Stuke M 2009 *JCAP* **11**, 025.

Serpico P D & Raffelt G G 2005 *PRD* **71**(12), 127301.

Sesana A 2013 *MNRAS* **433**, L1–L5.

Sesana A, Korsakova N, Arca Sedda M, Baibhav V, Barausse E, Barke S, Berti E, Bonetti M, Capelo P R, Caprini C, Garcia-Bellido J, Haiman Z, Jani K, Jennrich O, Johansson P, Khan F M, Korol V, Lamberts A, Lupi A, Mangiagli A, Mayer L, Nardini G, Pacucci F, Petiteau A, Raccanelli A, Rajendran S, Regan J, Shao L, Spallicci A, Tamanini N, Volonteri M, Warburton N, Wong K & Zumalacarregui M 2019 *arXiv e-prints* p. arXiv:1908.11391.

Shaw J R & Lewis A 2012 *PRD* **86**(4), 043510.

Sigl G, Olinto A V & Jedamzik K 1997 *PRD* **55**, 4582–4590.

Starobinskiĭ A A 1979 *Soviet Journal of Experimental and Theoretical Physics Letters* **30**, 682.

Stecher T P & Williams D A 1967 *ApJL* **149**, L29.

Stephanov M 2004 *Progress of Theoretical Physics Supplement* **153**, 139–156.

Subramanian K 2010 *Astronomische Nachrichten* **331**, 110.

Subramanian K 2016 *Reports on Progress in Physics* **79**(7), 076901.

Sun B 2017 *Applied Mathematics and Mechanics* **38**(6), 765–778.

Susskind L 1979 *Phys. Rev. D* **20**, 2610–2618.
URL: `https://link.aps.org/doi/10.1103/PhysRevD.20.2610`

Sutton D R, Feng C & Reichardt C L 2017 *The Astrophysical Journal* **846**(2), 164.

Takahashi K, Ichiki K, Ohno H & Hanayama H 2005 *Phys. Rev. Lett.* **95**(12), 121301.

Tanabashi M, Hagiwara K, Hikasa K, Nakamura K, Sumino Y, Takahashi F, Tanaka J, Agashe K, Aielli G, Amsler C, Antonelli M, Asner D M, Baer H, Banerjee S, Barnett R M, Basaglia T, Bauer C W, Beatty J J, Belousov V I, Beringer J, Bethke S, Bettini A, Bichsel H, Biebel O, Black K M, Blucher E, Buchmuller O, Burkert V, Bychkov M A, Cahn R N, Carena M, Ceccucci A, Cerri A, Chakraborty D, Chen M C, Chivukula R S, Cowan G, Dahl O, D'Ambrosio G, Damour T, de Florian D, de Gouvêa A, DeGrand T, de Jong P, Dissertori G, Dobrescu B A, D'Onofrio M, Doser M, Drees M, Dreiner H K, Dwyer D A, Eerola P, Eidelman S, Ellis J, Erler J, Ezhela V V, Fetscher W, Fields B D, Firestone R, Foster B, Freitas A, Gallagher H, Garren L, Gerber H J, Gerbier G, Gershon T, Gershtein Y, Gherghetta T, Godizov A A, Goodman M, Grab C, Gritsan A V, Grojean C, Groom D E, Grünewald M, Gurtu A, Gutsche T, Haber H E, Hanhart C, Hashimoto S, Hayato Y, Hayes K G, Hebecker A, Heinemeyer S, Heltsley B, Hernández-Rey J J, Hisano J, Höcker A, Holder J, Holtkamp A, Hyodo T, Irwin K D, Johnson K F, Kado M, Karliner M, Katz U F, Klein S R, Klempt E, Kowalewski R V, Krauss F, Kreps M, Krusche B, Kuyanov Y V, Kwon Y, Lahav O, Laiho J, Lesgourgues J, Liddle A, Ligeti Z, Lin C J, Lippmann C, Liss T M, Littenberg L, Lugovsky K S, Lugovsky S B, Lusiani A, Makida Y, Maltoni F, Mannel T, Manohar A V, Marciano W J, Martin A D, Masoni A, Matthews J, Meißner U G, Milstead D, Mitchell R E, Mönig K, Molaro P, Moortgat F, Moskovic M, Murayama H, Narain M, Nason P, Navas S, Neubert M, Nevski P, Nir Y, Olive K A, Pagan Griso S, Parsons J, Patrignani C, Peacock J A, Pennington M, Petcov S T, Petrov V A, Pianori E, Piepke A, Pomarol A, Quadt A, Rademacker J, Raffelt G, Ratcliff B N, Richardson P, Ringwald A, Roesler S, Rolli S, Romaniouk A, Rosenberg L J, Rosner J L, Rybka G, Ryutin R A, Sachrajda C T, Sakai Y, Salam G P, Sarkar S, Sauli F, Schneider O, Scholberg K, Schwartz A J, Scott D, Sharma V, Sharpe S R, Shutt T, Silari M, Sjöstrand T, Skands P, Skwarnicki T, Smith J G, Smoot G F, Spanier S, Spieler H, Spiering C, Stahl A, Stone S L, Sumiyoshi T, Syphers M J, Terashi K, Terning J, Thoma U, Thorne R S, Tiator L, Titov M, Tkachenko N P, Törnqvist N A, Tovey D R,

Valencia G, Van de Water R, Varelas N, Venanzoni G, Verde L, Vincter M G, Vogel P, Vogt A, Wakely S P, Walkowiak W, Walter C W, Wands D, Ward D R, Wascko M O, Weiglein G, Weinberg D H, Weinberg E J, White M, Wiencke L R, Willocq S, Wohl C G, Womersley J, Woody C L, Workman R L, Yao W M, Zeller G P, Zenin O V, Zhu R Y, Zhu S L, Zimmermann F, Zyla P A, Anderson J, Fuller L, Lugovsky V S & Schaffner P 2018 *Phys. Rev. D* **98**, 030001.
URL: `https://link.aps.org/doi/10.1103/PhysRevD.98.030001`

Tashiro H, Chen W, Ferrer F & Vachaspati T 2014 *MNRAS* **445**, L41–L45.

Tatsumi T 1957 *Proceedings of the Royal Society of London Series A* **239**, 16–45.

Taylor A M, Vovk I & Neronov A 2011 *A&A* **529**, A144.

Thrane E & Romano J D 2013 *PRD* **88**(12), 124032.

Trivedi P, Subramanian K & Seshadri T R 2014 *PRD* **89**(4), 043523.

Turner M S, Weinberg E J & Widrow L M 1992 *PRD* **46**, 2384–2403.

Turner M S & Widrow L M 1988 *PRD* **37**, 2743–2754.

Vachaspati T 1991 *Physics Letters B* **265**, 258–261.

Vachaspati T 2001 *Physical Review Letters* **87**(25), 251302.

Verbiest J P W, Lentati L, Hobbs G, van Haasteren R, Demorest P B, Janssen G H, Wang J B, Desvignes G, Caballero R N, Keith M J, Champion D J, Arzoumanian Z, Babak S, Bassa C G, Bhat N D R, Brazier A, Brem P, Burgay M, Burke-Spolaor S, Chamberlin S J, Chatterjee S, Christy B, Cognard I, Cordes J M, Dai S, Dolch T, Ellis J A, Ferdman R D, Fonseca E, Gair J R, Garver-Daniels N E, Gentile P, Gonzalez M E, Graikou E, Guillemot L, Hessels J W T, Jones G, Karuppusamy R, Kerr M, Kramer M, Lam M T, Lasky P D, Lassus A, Lazarus P, Lazio T J W, Lee K J, Levin L, Liu K, Lynch R S, Lyne A G, Mckee J, McLaughlin M A, McWilliams S T, Madison D R, Manchester R N, Mingarelli C M F, Nice D J, Osłowski S, Palliyaguru N T, Pennucci T T, Perera B B P, Perrodin D, Possenti A, Petiteau A, Ransom S M, Reardon D, Rosado P A, Sanidas S A, Sesana A, Shaifullah G, Shannon R M, Siemens X, Simon J, Smits R, Spiewak R, Stairs I H, Stappers B W, Stinebring D R, Stovall K, Swiggum J K, Taylor S R, Theureau G, Tiburzi C, Toomey L, Vallisneri M, van Straten W, Vecchio A, Wang Y, Wen L, You X P, Zhu W W & Zhu X J 2016 *MNRAS* **458**(2), 1267–1288.

Verma M K 2004 *Phys. Rep.* **401**, 229–380.

Verma M K & Bhattacharjee J K 1995 *Europhysics Letters (EPL)* **31**(4), 195–200.
URL: https://doi.org/10.1209%2F0295-5075%2F31%2F4%2F002

von Kármán T 1948 *Proceedings of the National Academy of Science* **34**, 530–539.

Wagstaff J M & Banerjee R 2016 *JCAP* **2016**(1), 002.

Wagstaff J M, Banerjee R, Schleicher D & Sigl G 2014 *PRD* **89**, 103001.

Waleffe F 1992 *Physics of Fluids A* **4**, 350–363.

Weinberg S 2008 *Cosmology* Oxford University Press.

Witten E 1984 *Phys. Rev. D* **30**, 272–285.
URL: https://link.aps.org/doi/10.1103/PhysRevD.30.272

Wolfe A M, Jorgenson R A, Robishaw T, Heiles C & Prochaska J X 2008 *Nature* **455**(7213), 638–640.

Yeung P K & Zhou Y 1997 *Phys. Rev. E* **56**, 1746–1752.
URL: https://link.aps.org/doi/10.1103/PhysRevE.56.1746

Zhou Y 2010 *Physics Reports* **488**(1), 1 – 49.
URL: http://www.sciencedirect.com/science/article/pii/S0370157309002129

Acknowledgements

This thesis was quite troubled by many and long-fought numerical problems and my difficulties in finding the right numerical approach, health problems and a burn-out, and less than five months ago, I even contemplated not to finish this thesis, and only focus on finalizing some still even now missing publications. So on many levels not just the obvious, I am grateful for having been given the opportunity and trust to work on and dedicate myself to the study of the fascinating subject of magnetohydrodynamics in the early universe, not just as it allowed me to study this interesting subject but it also laid bare many of my own personal flaws and pitfalls. These lessons are likely going to exert a strong guidance for my future path in life and my personal evolution. For the opportunity to study this subject, I wholeheartedly thank my supervisor Prof. Günter Sigl. I am also grateful to him for the opportunity to teach, particularly enjoying the practica, and being given the chance to substitute him on two lectures. Furthermore, I am grateful to be given the opportunity to finish my thesis even after all my shortcomings and all the shared meals and discussions. I also thank my secondary advisor Prof. Robi Banerjee, in particular for comments on the numerical simulation especially about informing me about hyperviscous damping. Next, I'd like to thank my part-time office companions Andrey Saveliev and Pranjal Trivedi, whom I have constantly bothered with my incomplete thoughts and ideas pretty much all the time they were present. Furthermore, Andrey Saveliev helped me in the beginning of my project and showed or told me the important bits and pieces about DESY and Hamburg. I am also very deeply grateful for all the support Pranjal Trivedi has given me, especially during my burn-out by reaching out to me and later during an extended sickness by checking up on me. Additionally, I am thankful for the comments he gave me on some parts of this thesis, even though he had barely any time available. Moreover, I want to thank my former co-PHD students Andrej Dundovic, Natacha Leite and Petar Pavlovic in particular for interesting philosophical debates and for trying to keep me grounded. In particular I enjoyed my biketrip to the north sea with Andrej even though or especially as it was quite literally a shitstorm for him. Also, I want to thank Martin Schlederer who, together with Günter, led me to study the generation of gravitational waves from MHD turbulence. Lastly, I want to thank my parents and my younger brother for all the support the haven given me, especially in the last year. The even somewhat "forcefully" picked me up during last christmas, as I was still completely anxiety stricken, poorly concentrated, sleep deprived and unable to commit myself to anything other than some as-of-yet still unfinished projects, which greatly helped in getting me out of my burn-out.

Eidesstattliche Versicherung

Hiermit erkläre ich an Eides statt, dass ich die vorliegende Dissertationsschrift selbst verfasst und keine anderen als die angegebenen Quellen und Hilfsmittel benutzt habe.

Declaration on oath

I hereby declare, on oath, that I have written the present dissertation by my own and have not used other than the acknowledged resources and aids.

Peter Niksa